Zerebrale kavernöse Malformationen: Von der Identifizierung von Strukturvarianten zur iPSC-basierten Modellierung der Pathogenese

I n a u g u r a l d i s s e r t a t i o n

zur

Erlangung des akademischen Grades eines

Doktors der Naturwissenschaften (Dr. rer. nat.)

der

Mathematisch-Naturwissenschaftlichen Fakultät

der

Universität Greifswald

vorgelegt von
Robin Alexander Pilz

Greifswald, den 21.11.2022

Dekan: Prof. Dr. Gerald Kerth

1. Gutachterin: Prof. Dr. Ute Felbor
2. Gutachter: Prof. Dr. Andreas Fischer
3. Gutachter: Prof. Dr. Malte Spielmann

Tag der Promotion: 03.05.2023

Inhaltsverzeichnis

1 Zusammenfassung

Zerebrale kavernöse Malformationen (CCMs) sind Gefäßfehlbildungen im Gehirn oder Rückenmark und können sich klinisch aufgrund einer erhöhten Blutungsbereitschaft mit Kopfschmerzen, Gefühls- und Sprachstörungen bis hin zu Krampfanfällen äußern. Sie treten sporadisch oder im Rahmen einer autosomal-dominant erblichen Form auf. Kausale Sequenzveränderungen sind dabei in den drei Genen *CCM1*, *CCM2* und *CCM3* bekannt. Die Detektionsrate für pathogene Varianten ist mit bis zu 60 % für sporadische Fälle und mit weit über 90 % für familiäre Fälle sehr hoch. Während Genpanel-Analysen sehr verlässlich Einzelnukleotidveränderungen, kleine Insertions- und Deletionsvarianten sowie Kopienzahlveränderungen detektieren können, werden komplexe Strukturvarianten oder Veränderungen in nicht-kodierenden Regionen kaum erfasst. Diese rücken jedoch für die bisher genetisch unaufgeklärten Fälle immer mehr in den Fokus des Interesses. Diese Arbeit adressiert daher zum einen die Identifizierung neuer Strukturvarianten und deren funktionale Interpretation im Kontext der CCM-Erkrankung.

Im Rahmen der vorliegenden Arbeit ist der erstmalige Nachweis einer interchromosomalen Insertion bei einem CCM-Patienten gelungen. Die unbalancierte Insertion genomischen Materials von Chromosom 1 in die kodierende Region des *CCM2*-Gens konnte durch die Verbindung von bioinformatischen Auswertestrategien der *Next Generation Sequencing*-Genpanel-Daten, molekularzytogenetischen Analysen und einer molekularen Bruchpunktkartierung genau charakterisiert werden. Die Identifikation einer weiteren Strukturvariante, einer Deletion des Transkriptionsstarts von *CCM1*, verdeutlichte die Herausforderungen bei der Bewertung von Veränderungen in nicht-kodierenden Genbereichen. Für eine eindeutige Klassifikation der Variante wurden daher funktionale Analysen durchgeführt, die auf einer CRISPR/Cas9-vermittelten Nachbildung der Deletion in iPSCs und der anschließenden Differenzierung in Endothelzellen beruhte. Damit konnte gezeigt werden, dass die Deletion zu einem Verlust der *CCM1* mRNA- und Proteinexpression führt. Zudem wurde in den differenzierten Endothelzellen eine für die CCM-Pathogenese charakteristische Deregulation von *KLF2*, *THBS1*, *NOS3* und *HEY2* beobachtet. Schließlich war es auf Basis dieser *in vitro*-Analysen möglich, die Variante entsprechend den ACMG-Richtlinien als wahrscheinlich pathogen zu bewerten und somit die molekulare CCM-Diagnose zu sichern.

Die Verbindung des CRISPR/Cas9-Systems mit iPSCs ist nicht nur für die Variantenbewertung von großem Nutzen, sondern bietet auch das Potential zum besseren Verständnis von Krankheitsmechanismen. Ein weiterer Fokus der vorliegenden Arbeit lag daher auf der Etablierung und Verwendung iPSC-basierter Zellkulturmodelle für die CCM-Modellierung. Zunächst ist es gelungen, mehrere iPSC-Linien mit einer kompletten CRISPR/Cas9-vermittelten *CCM1*-, *CCM2*- oder *CCM3*-Inaktivierung zu generieren. Diese

wurden anschließend für die Differenzierung in hBMEC-ähnliche Zellen und innovative dreidimensionale vaskuläre Organoide verwendet. In diesen Systemen konnte beispielsweise eindrücklich eine tumorähnliche Proliferation CCM3-defizienter Endothelzellen nachvollzogen werden, die nur in Kontakt mit Wildtyp-Zellen auftrat. RNA-Sequenzierungen in einem *CCM1*-basierten Knockout-Modell konnten darüber hinaus die Rolle von *CCM1* als Endothel-spezifisches Suppressorgen stärken. Die im Rahmen der Arbeit etablierten Systeme werden zukünftig für weitere Fragestellungen der CCM-Pathogenese wie der endothelialen Barrierestörung eingesetzt und stellen darüber hinaus sehr gut geeignete Plattformen für die effektive Entwicklung dringend benötigter therapeutischer Ansätze dar.

2 Einleitung

2.1 Zerebrale kavernöse Malformationen

„*Because brains and spines shouldn't bleed*“, heißt es in einem Leitspruch der seit 2002 bestehenden Organisation *Alliance to Cure Cavernous Malformation*, ursprünglich *Angioma Alliance* (Alliance to Cure Cavernous Malformation, 2022). Sie ist eine von zahlreichen internationalen Anstrengungen, die Entwicklung dringend benötigter neuer Therapieansätze für zerebrale kavernöse Malformationen (*Cerebral Cavernous Malformations*, CCMs) voranzutreiben. Diese vaskulären Fehlbildungen des zentralen Nervensystems treten mit einer Prävalenz von etwa 0,5 % in der allgemeinen Bevölkerung auf (Otten et al., 1989; Al-Shahi et al., 2003; Flemming et al., 2017), sodass allein in Deutschland mehr als 400000 Menschen betroffen sind. CCMs sind vor allem durch irregulär-strukturierte, dünnwandige und erweiterte Endothelzellkanäle gekennzeichnet, die fokal im venös-kapillären Gefäßbett des Gehirns oder Rückenmarks auftreten können. Makroskopisch erscheinen sie als maulbeerartige Strukturen mit Ausmaßen von bis zu mehreren Zentimetern (Batra et al., 2009). Als geeignetste Methode zur Visualisierung und Charakterisierung von CCMs gelten hierbei die T2*-gewichtete Gradienten-Echo- und suszeptibilitätsgewichtete Magnetresonanztomographie (MRT) (Akers et al., 2017; Spiegler et al., 2018b). In histopathologischen Untersuchungen von Kavernomen lassen sich oft intraläsionale Thrombosen und Kalzifikationen nachweisen, die auf einen verlangsamten Blutfluss innerhalb von CCMs zurückgeführt werden können (Clatterbuck et al., 2001; Batra et al., 2009). Zudem sind in ihrer Umgebung oftmals Hämosiderinablagerungen zu beobachten, die als Auswirkung von Blutungsereignissen in das umliegende Gewebe entstehen. Dies ist Folge einer gestörten Blut-Hirn-Schranke (BHS), welche durch weniger funktionale interzelluläre Verbindungen der auskleidenden Endothelzellen gekennzeichnet ist (Clatterbuck et al., 2001). Blutungen können bei betroffenen Patient*innen zu einem variablen Spektrum an Beschwerden führen. Dazu zählen wiederkehrende Kopfschmerzen, Gefühls- und Sprachstörungen, aber auch Epilepsien und Schlaganfall-ähnliche Symptome (Batra et al., 2009). Deren individuelle Ausprägung hängt hierbei vor allem von der Lokalisation der Kavernome ab. In weniger eloquenten Arealen verursachen diese häufig keine klinischen Anzeichen. So sind bis zu ca. 40 % der CCM-Patient*innen asymptomatisch (Denier et al., 2006). Läsionen im Hirnstamm führen hingegen oft zu schwerwiegenden neurologischen Komplikationen. Neben einer supportiven Behandlung ist die chirurgische Entfernung von Läsionen bisher die einzige therapeutische Option. Die Indikation einer operativen Resektion wird hierbei abhängig der Größe und Lage der Kavernome gestellt (Akers et al., 2017).

Bei der CCM-Erkrankung unterscheidet man zwischen einer sporadischen und einer autosomal-dominant erblichen Form. Die sporadische Form geht oftmals mit dem Auftreten einer einzelnen Malformation einher, während Patient*innen mit der familiären Form meist durch multiple, bereits im jungen Lebensalter auftretende Kavernome oder eine positive Familienanamnese auffallen (Labauge et al., 1998). Bei der hereditären Kavernomatose sind pathogene *Loss-of-Function*-Keimbahnvarianten in den drei Genen *CCM1* (*KRIT1*, *Online Mendelian Inheritance in Man* [OMIM]: 604214) (Laberge-le Couteulx et al., 1999; Sahoo et al., 1999), *CCM2* (OMIM: 607929) (Liquori et al., 2003; Denier et al., 2004) und *CCM3* (*PDCD10*, OMIM: 609118) (Bergametti et al., 2005) bekannt, die in heterozygotem Status vorliegen. Das Spektrum identifizierter Veränderungen umfasst vor allem *Nonsense*-Varianten, kleine Deletionen und Duplikationen (Indel), Spleißvarianten und Kopienzahlveränderungen (*Copy Number Variations*, CNV) (Spiegler et al., 2018b; Ricci et al., 2021). Abhängig vom veränderten Gen ist hierbei mit einer unvollständigen Penetranz von ca. 55-68 % auszugehen (Denier et al., 2006; Spiegler et al., 2018b). Die Prävalenz symptomatischer familiärer Fälle wird auf 1:5400-1:6200 geschätzt (Spiegler et al., 2018b). Patient*innen mit einer pathogenen *CCM3*-Variante erkranken dabei meist schon in früherem Alter und weisen ein erhöhtes Risiko für zerebrale Blutungen auf als Träger*innen einer kausalen *CCM1*- oder *CCM2*-Variante (Shenkar et al., 2015).

Die molekulargenetische Diagnostik ist für Patient*innen mit multiplen Kavernomen oder einer auffälligen Familienanamnese indiziert. Da innerhalb der *CCM*-Gene keine sicheren Bereiche einer gehäuften Mutationshäufigkeit ausgemacht werden können, werden im Rahmen der Diagnostik alle kodierenden Genbereiche einschließlich der angrenzenden Exon-Intron-Grenzen untersucht. Zur Detektion von Exon-übergreifenden Deletionen und Duplikationen wird entweder die Methode der multiplexen ligationsabhängigen Sondenamplifikation (*Multiplex Ligation-dependent Probe Amplification*, MLPA) oder auch die *Next Generation Sequencing* (NGS)-basierte CNV-Analyse herangezogen (Much et al., 2019). Die Detektionsrate für pathogene Varianten ist mit bis zu 60 % für sporadische und mit 87-98 % für familiäre CCM-Fälle sehr hoch (Spiegler et al., 2014; Spiegler et al., 2018b). Der Nachweis einer pathogenen Variante ist insbesondere auch für weitere Familienmitglieder von Bedeutung, denen in diesem Fall eine prädiktive Analyse auf die bekannte Veränderung angeboten werden kann.

Die Entstehung von CCMs kann jedoch nicht gänzlich durch das alleinige Vorliegen einer heterozygoten pathogenen Keimbahnvariante erklärt werden. Stattdessen ist bekannt, dass erst durch das Auftreten einer zweiten postzygotischen Veränderung entsprechend der Knudsonschen Zweischrittinaktivierung (Knudson, 1971) die Kavernombildung initiiert wird. Dies wird durch mehrere Studien an humanen Läsionen unterstützt (Gault et al., 2005; Akers et al., 2009; McDonald et al., 2014; Rath et al., 2020). Entsprechend konnte in Patient*innen

mit pathogener Keimbahnvariante eine immunhistochemische Negativität für das entsprechende CCM-Protein in den Endothelzellen des Kavernoms, nicht jedoch im umliegenden Gewebe, beobachtet werden (Pagenstecher et al., 2009). Analysen in speziellen Mausmodellen etablierten ferner die heute gängige Auffassung, dass eine klonale Expansion von Zellen mit kompletter Inaktivierung des jeweiligen *CCM*-Gens und eine anschließende Rekrutierung von Zellen mit erhaltener CCM-Expression zur Bildung und Progression von Kavernomen beitragen (Abb. 1) (Detter et al., 2018; Malinverno et al., 2019).

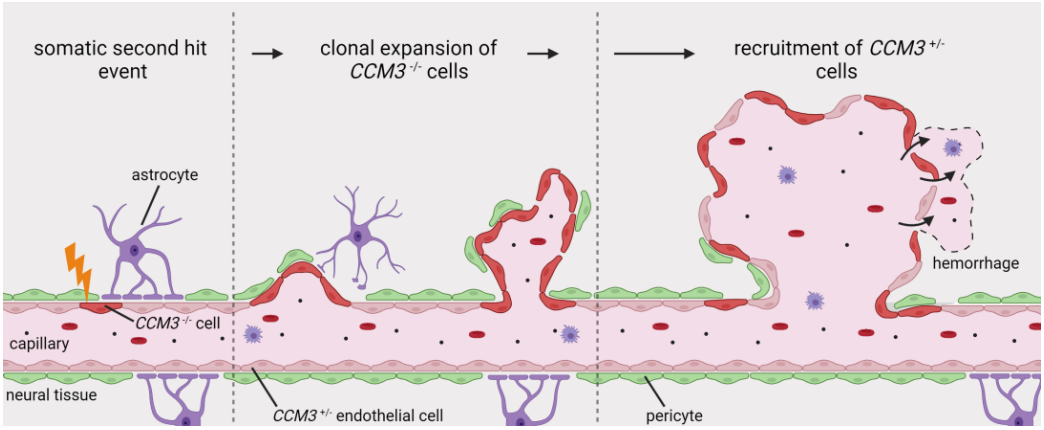

Abbildung 1 | Modell der Entstehung und Progression von CCMs. In einer Trägerin bzw. einem Träger einer pathogenen, heterozygoten *CCM3*-Keimbahnvariante wird die CCM-Bildung durch eine zweite somatische Inaktivierung in einer Endothelzelle initiiert (linker Abschnitt). Nachfolgend erfolgt eine klonale Expansion der *CCM3*$^{-/-}$-Zelle (mittlerer Abschnitt). Durch die Rekrutierung von heterozygoten Zellen kommt es zum Wachstum des Kavernoms, welches charakteristischerweise aus einem Mosaik aus *CCM3*$^{-/-}$ und *CCM3*$^{+/-}$ Zellen besteht. Eine Störung der endothelialen Barrierefunktion kann schließlich zur Blutung in das umliegende Gewebe führen (rechter Abschnitt). Abbildung stammt aus Skowronek et al. 2021.

2.2 Strukturvarianten

Die in der molekulargenetischen Diagnostik der CCM-Erkrankung eingesetzte *Short-Read*-basierte Panel-Sequenzierung zielt insbesondere auf die Identifikation von Einzelnukleotidveränderungen (*Single Nucleotide Variants*, SNVs) sowie kleinen Indel-Varianten ab. Aber auch dem möglichen Auftreten größerer CNVs, welche einen substantiellen Anteil der identifizierten pathogenen Varianten in den *CCM*-Genen ausmachen (Riant et al., 2013), wird durch die MLPA-Analyse oder NGS-basierte Methoden Rechnung getragen. Über die Häufigkeit von anderen und komplexeren SVs ist im CCM-Kontext hingegen wenig bekannt. Dabei tragen SVs im Allgemeinen nicht nur zur phänotypischen Variabilität bei, sondern können auch bei der Krankheitsentstehung eine bedeutende Rolle spielen (Feuk et al., 2006).

Der Einsatz der Gesamtgenomsequenzierung (*Whole Genome Sequencing*, WGS) in groß angelegten Populationsstudien hat eine umfängliche Charakterisierung der humanen

genetischen Variation ermöglicht. Mit Abschluss des *1000 Genomes Project*, welches die Genome von 2504 Individuen rekonstruierte, konnte gezeigt werden, dass sich ein typisches humanes Genom in vier bis fünf Millionen Stellen vom Referenzgenom unterscheidet (The 1000 Genomes Project Consortium, 2015). Den Großteil dieser Variation machen SNVs sowie kleine Indel-Varianten aus. Es treten jedoch auch größere SVs auf, die als strukturelle und quantitative chromosomale Umlagerungen von mehr als 50 Basenpaaren (bp) beschrieben werden und sowohl zytogenetisch sichtbare als auch submikroskopische Sequenzveränderungen umfassen (Spielmann et al., 2018). Auch wenn der Anteil von SVs an der genetischen Variation deutlich geringer ist als für SNVs, sind sie aufgrund ihrer Größe für den Großteil der variierenden Nukleotide zwischen humanen Genomen verantwortlich (Pang et al., 2010). Dabei können sie sowohl als CNVs in Form von Deletionen, Duplikationen und Insertionen als auch balanciert in Form von Inversionen und Translokationen vorliegen (Weischenfeldt et al., 2013). Durch die Kombination verschiedener Sequenziertechnologien und bioinformatischer Algorithmen wurde gezeigt, dass mehr als 27000 solcher SVs im humanen Genom zu finden sind (Chaisson et al., 2019). Deren Entstehung kann hierbei mechanistisch auf Rekombinations-, Replikations- sowie Reparaturmechanismen der DNA zurückgeführt werden (Weischenfeldt et al., 2013).

Die Suche nach kausalen chromosomalen Umlagerungen gewinnt bei der Diagnose seltener Erkrankungen zunehmend an Bedeutung, wobei diese einen Teil des Phänomens der fehlenden Erblichkeit (*Missing Heritability*) bei genetisch bisher ungelösten Fällen erklären können (Maroilley and Tarailo-Graovac, 2019). Tatsächlich ist ein funktional negativer Einfluss seltener SVs sogar wahrscheinlicher als für seltene SNVs (Chiang et al., 2017; Eichler, 2019). Eine schädliche Auswirkung von SVs kann sich beispielsweise infolge einer direkten Unterbrechung der Genorganisation oder von Positionseffekten äußern, welche die transkriptionale Regulation von Genen beeinflussen (Feuk et al., 2006; Spielmann et al., 2018). Im Gegensatz zu Veränderungen geringer Größe stellt die Detektion von SVs jedoch eine große Herausforderung dar. Vor allem die oft eingesetzte *Short-Read*-basierte Panel-Sequenzierung stößt hierbei an ihre Grenzen. Insbesondere Varianten, die nicht zu einer Veränderung der Kopienzahl führen oder sich in nicht-kodierenden Genbereichen befinden, können hiermit nur sehr schwer oder gar nicht erfasst werden. Neue Sequenziertechnologien und verbesserte Algorithmen sowie die Integration von Daten verschiedener Plattformen haben die Identifikation und Charakterisierung von SVs deutlich verbessert (Ho et al., 2020). Besonders der Einsatz der *Long-Read*-Sequenzierung (LRS) kann in diesem Zusammenhang entscheidende Limitationen bisheriger Ansätze überwinden (Merker et al., 2018; Sanchis-Juan et al., 2018; Mitsuhashi and Matsumoto, 2020), da durch lange Sequenzierreads die gesamte SV überspannt und die Kartierung in repetitiven Regionen verbessert werden kann (De Coster and Van Broeckhoven, 2019).

2.3 Das CRISPR/Cas9-System zur Genomeditierung

Die Möglichkeit Veränderungen genomischen Materials gezielt vornehmen zu können, hat die biologische und biomedizinische Forschung grundlegend verändert. Die Genomeditierung und im Speziellen das CRISPR/Cas-System stellt insbesondere bei der Untersuchung von Genfunktionen und der Modellierung von Krankheiten sowie der Entwicklung von therapeutischen Ansätzen ein wertvolles Werkzeug dar. Bisherige Studien zu Pathomechanismen der CCM-Erkrankung in Zellkulturmodellen basierten zumeist auf einer nur transienten Herunterregulation des *CCM*-Zielgens unter Einsatz der RNA-Interferenz-Methode (Glading et al., 2007; Stockton et al., 2010; Wüstehube et al., 2010; Zhu et al., 2010; Zhou et al., 2016). Durch komplementäre Basenpaarung kann hiermit die Genexpression inhibiert werden. Eine der *in vivo*-Situation entsprechende dauerhafte Ausschaltung des entsprechenden *CCM*-Gens kann so jedoch nicht ausreichend abgebildet werden. Stattdessen eignet sich die CRISPR/Cas-Technologie hervorragend dazu, die Langzeitinaktivierung von *CCM*-Genen zu studieren, indem stabile biallelische Varianten eingeführt werden können.

Die Generierung von Sequenzveränderungen mit Hilfe programmierbarer Nukleasen basiert auf der Einführung von DNA-Doppelstrangbrüchen, die nachfolgend durch zelleigene Mechanismen repariert werden. Neben Meganukleasen, Zinkfingernukleasen sowie transkriptionsaktivatorähnlichen Effektornukleasen zeichnet sich die CRISPR/Cas-Technologie vor allem durch die deutlich einfachere und flexiblere Verwendung aus (Chandrasegaran and Carroll, 2016). Die für dieses System charakteristische repetitive DNA-Sequenzen (*Clustered Regularly Interspaced Short Palindromic Repeats*, CRISPR) und mit diesen assoziierte Gene (*CRISPR-associated*, Cas) wurden erstmals in Prokaryoten entdeckt (Ishino et al., 1987; Mojica et al., 1995). Dort dient es als adaptives Immunsystem zur Abwehr von eindringender Fremd-DNA (Makarova et al., 2006; Barrangou et al., 2007). Durch biotechnologische Modifikationen lässt sich das CRISPR/Cas-System sowohl *in vitro* als auch *in vivo z*ur präzisen Genomeditierung in vielen verschiedenen Organismen einsetzen. Weit verbreitet ist hierbei eine Adaption des Typ II CRISPR/Cas-Systems (Klasse 2) von *Streptococcus pyogenes*. Zunächst wird hierbei nach Hybridisierung einer sequenzspezifischen CRISPR-RNA (crRNA) mit einer transaktivierenden crRNA (tracrRNA) ein Ribonukleoproteinkomplex (RNP) mit der Cas9-Nuklease gebildet. Vermehrt kommen hierbei auch einzelne RNA-Moleküle zum Einsatz, die als *single-guide* RNA die Eigenschaften von crRNA und tracrRNA vereinen (Sander and Joung, 2014). Die Cas9-Nuklease wird basierend auf einer komplementären Basenpaarung schließlich zu einer spezifischen Ziel-DNA-Sequenz geleitet. Diese weist normalerweise eine Länge von 20 bp auf liegt benachbart zu einem *protospacer adjacent motif* (PAM) der Form 5‘-NGG bzw. 5‘-NAG (N = A, T, C oder G). Die zwei Nuklease-Domänen der Cas9 spalten anschließend

die DNA, wodurch es zu einem Doppelstrangbruch kommt. Dieser wird innerhalb von Zellen über den Mechanismus der nicht-homologen Endverknüpfung (*Non-Homologous End-Joining*, NHEJ) oder der homologen Rekombination (*Homology-Directed Repair*, HDR) repariert. Im Zuge der NHEJ kann es zur Entstehung von Indel-Varianten kommen, was sich zum Beispiel bei der Generierung von Gen-Knockouts zu Nutze gemacht wird. Wenn eine zum Ziellokus homologe Spendermatrize zur Verfügung gestellt wird, ist im Sinne eines HDR auch die Einführung spezifischer Sequenzen möglich (Sander and Joung, 2014). Durch die Weiterentwicklung des Systems kann darüber hinaus eine gezielte Baseneditierung vorgenommen werden. Der Einsatz von Cas9-Nickasen erlaubt hierbei die Konvertierung einzelner Basen ohne die Erzeugung eines Doppelstrangbruchs. Des Weiteren kann die CRISPR/Cas-Technologie auch für die Regulation der Genexpression eingesetzt werden, indem katalytisch inaktivierte Cas9-Nukleasen verwendet werden. Durch die Kopplung der Nuklease mit spezifischen Effektoren lassen sich ferner epigenetische Veränderungen vornehmen (Adli, 2018). Generell gilt, dass sich das Auftreten unerwünschter Nebeneffekte an genomischen Stellen, die zu der verwendeten crRNA eine hohe Ähnlichkeit aufweisen, durch die direkte Einbringung eines RNP-Komplexes in die Zielstruktur aufgrund dessen kürzeren Halbwertszeit minimieren lässt (Kim et al., 2014).

Das CRISPR/Cas9-System konnte in der eigenen Arbeitsgruppe bereits erfolgreich zur Editierung der *CCM*-Gene in immortalisierten humanen Nabelschnurvenenendothelzellen (*Immortalized Human Umbilical Vein Endothelial Cells*, CI-huVECs), endothelialen Vorläuferzellen aus Blut (*Blood Outgrowth Endothelial Cells*, BOECs) sowie humanen zerebralen mikrovaskulären Endothelzellen (*Human Cerebral Microvascular Endothelial Cells*, hCMECs) eingesetzt werden. Dies erlaubte die nähere Charakterisierung wichtiger CCM-assoziierter Dysfunktionen in den entsprechenden Knockout-Endothelzellen, wie beispielsweise eines klonogenen Überlebensvorteils, eines gestörten angiogenen Verhaltens, der vermehrten Bildung von Aktinstressfasern, einer verringerten Fibronektin-Expression oder der Akkumulation von Von-Willebrand-Faktor (Schwefel et al., 2019; Schwefel et al., 2020; Much et al., 2021). Gegenüber primären und immortalisierten Zellen gewinnen vor allem Stammzellen zunehmend an Bedeutung bei der *in vitro*-Modellierung von Krankheiten. Durch ihre einzigartigen Eigenschaften, sich unbegrenzt vermehren und in alle drei Keimblätter differenzieren zu können, überwinden sie entscheidende Limitationen bisheriger Zellkultur-Ansätze (Grskovic et al., 2011). Die Verbindung von Stammzellen mit der CRISPR/Cas9-Technologie birgt dabei ein enormes Potential, nicht nur biologische Prozesse und Krankheitsmechanismen in komplexeren Modellen wie beispielsweise dreidimensionalen Organoiden besser zu verstehen, sondern auch innovative therapeutische Strategien zu entwickeln (Hendriks et al., 2020).

3 Zusammenfassung und Diskussion

3.1 Identifikation und Charakterisierung von Strukturvarianten als genetische Ursache der Kavernomatose

3.1.1 Identifikation einer submikroskopischen interchromosomalen Insertion im *CCM2*-Gen

Immense technologische Fortschritte im Bereich der Hochdurchsatzsequenzierung haben die Diagnostik von seltenen Erkrankungen, die zum Großteil einen genetischen Hintergrund besitzen, erheblich verbessert (Nguengang Wakap et al., 2020; Vinkšel et al., 2021). Dennoch bleiben immer noch viele Fälle ungeklärt. Für CCM-Patient*innen, bei denen trotz erfüllten Einschlusskriterien keine kausale Sequenzveränderung in der Standarddiagnostik detektiert werden konnte, wurden in der Literatur unter anderem ein bisher unbekanntes Kandidatengen (Liquori et al., 2006) und somatische Mosaike (McDonald et al., 2014) diskutiert. Durch die mittels WGS identifizierte erste große genomische Inversion im *CCM2*-Gen (Spiegler et al., 2018a) rückten jedoch auch Strukturvarianten in den Fokus des Interesses. Auch Genpanel-Analysen können Hinweise auf das Vorliegen von SVs liefern, wenn die entsprechenden Bruchpunkte innerhalb oder nahe dem kodierenden Genbereich liegen. So konnte in einem Probanden erstmals eine submikroskopisch vorliegende interchromosomale Insertion identifiziert werden (Pilz et al., 2020).

Bei dem männlichen Indexpatienten, der zum Zeitpunkt der genetischen Analyse 58 Jahre alt war, wurden in der MRT-Bildgebung zahlreiche Kavernome im Gehirn und Rückenmark nachgewiesen (Abb. 2 A, B). Vier dieser Läsionen wurden aufgrund von Blutungsereignissen bereits chirurgisch entfernt. Nach einer Hybridisierungs-basierten Anreicherung der diagnostischen Zielregionen fielen in der bioinformatischen Analyse der NGS-Daten zahlreiche fehlerhaft kartierte Sequenzierreads im *CCM2*-Gen auf. Diese sogenannten *Split Reads* konnten bemerkenswerterweise nur mittels *Sequence-Pilot*-Software (JSI medical systems), nicht jedoch unter Einsatz der Kartierungs- und Alignierungsinformationen der *MiSeq Reporter*-Software (Illumina) detektiert werden. Basierend auf ihrer Kartierung war eine Einteilung der aberranten Reads in zwei Gruppen möglich. Die Reads der ersten Gruppe konnten teilweise dem 5'-Bereich des Exons 6 von *CCM2* und außerdem dem chromosomalen Bereich 1p11.2 oder 1q21.1 zugeordnet werden. Eine Spezifikation der Kartierung auf Chromosom 1 war aufgrund bekannter Sequenzhomologien nicht möglich. Der zweite Teil der Reads wurde hingegen partiell auf den 3'-Bereich von *CCM2* Exon 6 und zudem auf den Bereich 1p12 kartiert. Diese Daten ließen eine Insertion eines 294 Kilobasenpaare (kb) großen Fragmentes von Chromosom 1 (1p12-p11.2) in die proteinkodierende Region von *CCM2* auf Chromosom 7 (7p13) vermuten (Abb. 2 C). Dies

konnte durch Fluoreszenz-*in-situ*-Hybridisierung (FISH) an Metaphase-Chromosomen von Blutlymphozyten des Patienten bestätigt werden (Abb. 2 D) (Pilz et al., 2020).

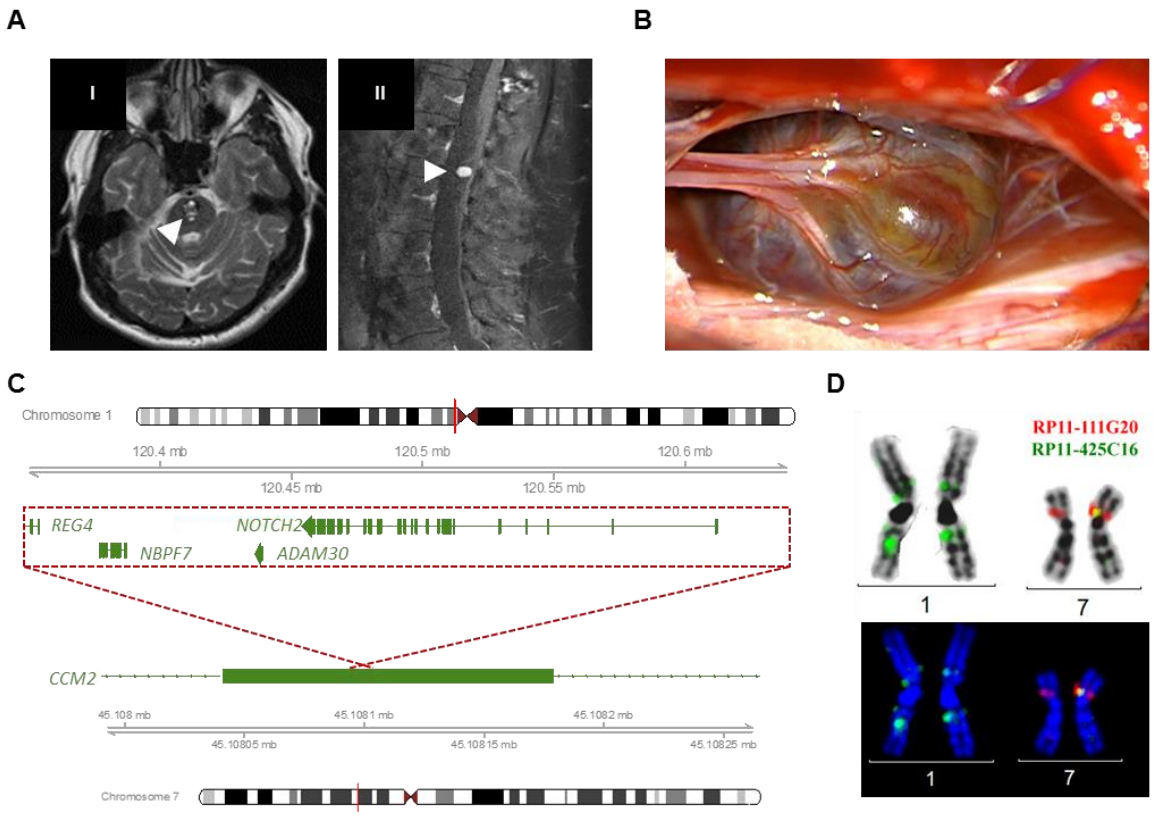

Abbildung 2 | Identifizierung einer interchromosomalen Insertion bei einem CCM-Patienten mit multiplen zerebralen und spinalen CCMs. (A) MRT-Analysen zeigen CCMs in der *Pons* (I) und der *Cauda equina* (II) des Indexpatienten (weiße Pfeile). **(B)** Intraoperative Aufnahme der kavernösen Läsion in der *Cauda equina*. **(C)** Schematische Darstellung der identifizierten Strukturvariante. Genomisches Material von Chromosom 1 lag in invertierter Orientierung inseriert im Exon 6 von *CCM2* auf Chromosom 7 vor. **(D)** Bestätigung der interchromosomalen Insertion mittels FISH-Analyse. Die BAC-Sonden RP11–425C16 (1p12; hg19: 120176963–120358983) und RP11–111G20 (7p12.3~13; hg19: 45283437–45448789) wurden verwendet. Es ist eine Kreuzhybridisierung der verwendeten Sonde RP11–425C16 in 1q21.1 bekannt. (Modifizierte) Abbildungen stammen aus Pilz et al. 2020.

Durch eine MLPA-Analyse konnten zusätzlich drei Kopien des *NOTCH2*-Gens nachgewiesen werden. Dies versicherte, dass der betreffende Bereich auf Chromosom 1 in veränderter Kopienzahl vorlag. *NOTCH2* lag neben den Genen *ADAM30*, *NBPF7* und einem Teil des *REG4*-Gens innerhalb des inserierten Fragmentes und ist das einzige dieser Gene mit einem in der Datenbank OMIM hinterlegten assoziierten Phänotyp. Der Patient zeigte jedoch weder für das Alagille- noch das Hajdu-Cheney-Syndrom typische Symptome. Durch eine Amplifikation der vermuteten Bruchpunkte mit Hilfe spezifischer Primer gelang nicht nur die Bestätigung der Insertion auf molekularer Ebene, sondern auch die genaue Bestimmung der Bruchpunkte mittels Sanger-Sequenzierung ([hg19] chr1:120347265, chr1:120641440 und chr7:45108098–45108101). Diese versicherte zum einen, dass das inserierte Fragment

in invertierter Orientierung vorlag, und zeigte zum anderen, dass dieses durch eine kleine Insertion sowie Indel-Variante flankiert war (Abb. 3) (Pilz et al., 2020).

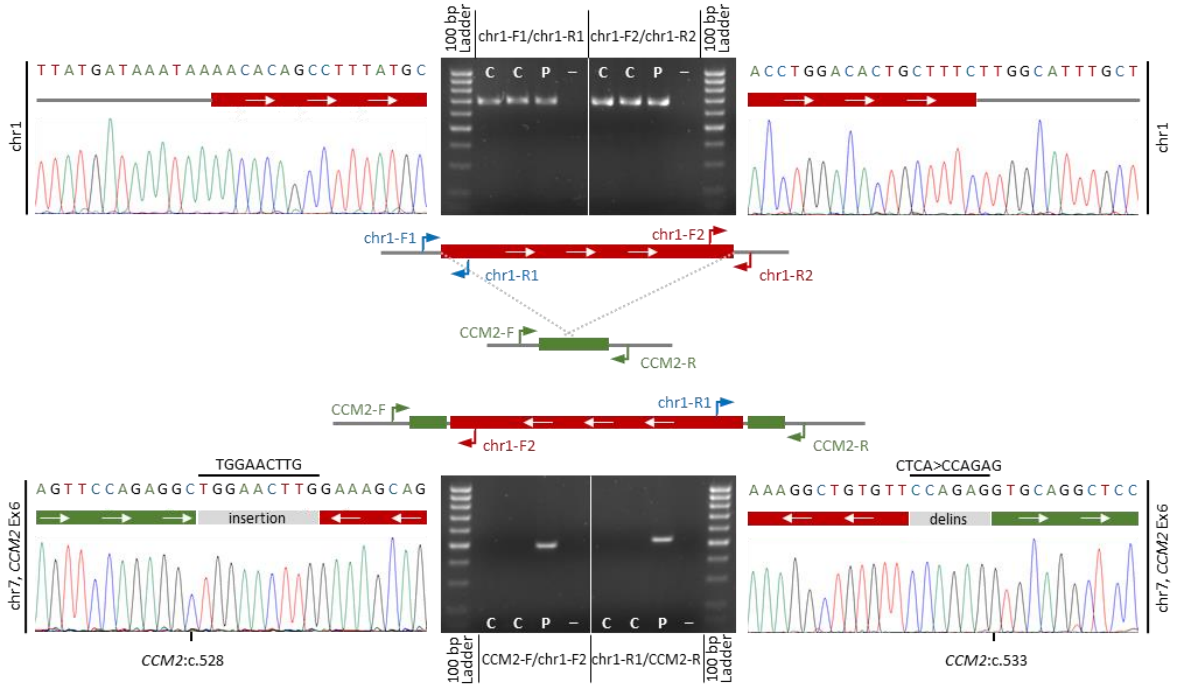

Abbildung 3 | Molekulare Charakterisierung der Bruchpunkte mittels Sanger-Sequenzierung. Im mittleren Abschnitt ist eine schematische Darstellung des Referenz- und des Insertions-Allels gezeigt. Die blauen, roten und grünen Pfeile repräsentieren die PCR- und Sequenzierungs-Primer (chr1: chr1-F1 + R1 und chr1-F2 + R2; chr7: CCM2-F + R). Die PCR-Produkte und Chromatogramme des Referenz-Allels auf Chromosom 1 (oberer Abschnitt; chr1-F1/R1 und chr1-F2/R2) sowie der invertierten Insertion auf Chromosom 7 (unterer Abschnitt; CCM2-F/chr1-F2 und chr1-R1/CCM2-R) sind dargestellt. C = gesunde Kontrolle; P = Indexpatient; – = Negativkontrolle; Ex = Exon. Abbildung stammt aus Pilz et al. 2020.

Die SV führt durch die Unterbrechung der kodierenden Region von *CCM2* sehr wahrscheinlich nicht zur Synthese eines funktionsfähigen Proteins und wurde daher als *Loss-of-Function*-Variante betrachtet. Entsprechend den ACMG (*The American College of Medical Genetics and Genomics*)-Richtlinien zur Interpretation von Sequenzvarianten (Richards et al., 2015) wurde die heterozygot vorliegende interchromosomale Insertion daher als pathogen bewertet. Die Identifizierung einer pathogenen Variante ist nicht nur zur Sicherung der Diagnose einer hereditären CCM-Erkrankung und optimalen klinischen Betreuung betroffener Patient*innen wichtig, sondern auch für die genetische Beratung von Familienangehörigen von großer Bedeutung. Insbesondere stellte sich die Frage, ob die Variante vererbt wurde oder neu aufgetreten ist (*de novo*). Weder für die Elternteile noch für andere Familienmitglieder wurden kavernöse Läsionen oder typische CCM-Symptome beschrieben. Im Fall der identifizierten SV ist das Vorliegen einer *de novo*-Veränderung demnach plausibel. Da jedoch bis zu 45 % der Träger*innen einer pathogenen *CCM2*-

Variante asymptomatisch sind (Denier et al., 2006), ist ein erblicher Fall nicht auszuschließen. Weil die Elternteile des Indexpatienten bereits verstorben waren und weitere Familienangehörige für eine genetische Untersuchung nicht zur Verfügung standen, konnte die Herkunft der identifizierten SV nicht abschließend geklärt werden.
Im Rahmen der vorliegenden Arbeit wurde untersucht, ob weitere kausale genomische Umlagerungen in anscheinend mutationsnegativen CCM-Patient*innen identifiziert werden können. Hierzu wurden die NGS-Genpanel-Daten von sieben weiteren am Institut für Humangenetik Greifswald untersuchten Proband*innen ohne eine nachgewiesene pathogene SNV, Indel-Variante oder CNV analysiert. Hierbei wurde zusätzlich die *SureCall*-Software (Agilent Technologies) eingesetzt, um auf Translokationsereignisse basierend auf dem Vorhandensein von aberranten Reads in den NGS-Daten zu prüfen. Während die Software die interchromosomale Insertion des Indexpatienten akkurat detektieren konnte, wurden für die weiteren Patient*innen keine chromosomalen Umlagerungen identifiziert (Pilz et al., 2020). Nichtsdestotrotz bekräftigt die Studie, dass schwer zu detektierende SVs als Ursache für bisher genetisch unaufgeklärte Fälle berücksichtigt werden sollten. In Zusammenschau konnte durch die vorliegende Arbeit nicht nur das in der molekulargenetischen Diagnostik der CCM-Erkrankung zu bedenkende Mutationsspektrum erweitert, sondern ebenso die Limitationen und Bedeutsamkeit spezieller bioinformatischer Werkzeuge und Filterkriterien bei der Detektion von SVs in Genpanel-Daten verdeutlicht werden.

Auch wenn es mit Genpanel- und MLPA-Analysen zwar prinzipiell möglich ist, SVs bzw. CNVs zu detektieren, bietet sich bei der Identifikation und näheren Charakterisierung dieser vor allem die *Long-Read*-Sequenzierung als Technologie der dritten Generation an (Miller et al., 2021). Sie bietet das Potential, die gesamte SV zu überspannen und deren Kartierung zu verbessern, sodass sie in einem diagnostischen Kontext gut als ergänzende Analyse zu *Short-Read*-basierten Panel-Ansätzen geeignet wäre. In der eigenen Arbeitsgruppe wurde daher basierend auf einer CRISPR/Cas9-basierten Selektion der genomischen Zielregionen (Gilpatrick et al., 2020) die LRS aller drei *CCM*-Gene auf der MinION-Plattform (Nanopore Technologies) etabliert (Skowronek et al., 2022 [unter Begutachtung]). Durch die erneute Analyse bekannter großer Deletionen in CCM Patient*innen mittels LRS gelang uns so eine exakte Bruchpunktkartierung für die Varianten, bei der Genpanel- und MLPA-Analysen hingegen sehr limitiert sind. Dies erlaubte nicht nur erstmals die akkurate Bestimmung der Deletionsgrößen, sondern auch den Entwurf Deletions-spezifischer PCR-Ansätze (Skowronek et al., 2022 [unter Begutachtung]). Diese besitzen vor allem als günstige und schnelle Alternative für prädiktive Analysen weiterer Familienangehöriger große Bedeutung. Die bisher eingesetzte MLPA-Methode für die Analyse auf bekannte familiäre CNVs ist im

Vergleich mit höherem Aufwand und einer geringeren Kosteneffizienz verbunden, wenn es zu einer oftmals zeitversetzten Untersuchung vieler Familienmitglieder kommt (Gaetzner et al., 2007; Singh et al., 2021). Ein weiterer Vorteil der LRS liegt in der Fähigkeit, komplexe Sequenzveränderungen verlässlich detektieren zu können. Dies ist insbesondere für Varianten entscheidend, die außerhalb der in der Diagnostik standardmäßig analysierten Regionen liegen oder zu keiner Veränderung der Kopienzahl führen. Mit unserem LRS-Ansatz waren wir beispielsweise in der Lage, die zuvor beschriebene interchromosomale Insertion im *CCM2*-Gen akkurat nachzuweisen (Skowronek et al., 2022 [unter Begutachtung]). Insgesamt stellt die LRS für die CCM-Diagnostik somit eine vielversprechende *second-line*-Technologie für die Entwicklung günstiger und schneller PCR-basierter Ansätze im Rahmen familiärer Analysen sowie das Screening auf komplexere SVs bei bisher unaufgeklärten Fällen dar.

3.1.2 Funktionale Bewertung einer Strukturvariante mittels CRISPR/Cas9 Genomeditierung

Der Großteil der pathogenen Varianten in den *CCM*-Genen ist in den kodierenden Genbereichen lokalisiert, sodass sich die molekulargenetische CCM-Diagnostik hauptsächlich auf diese Regionen fokussiert. Dabei sind allgemein gesehen nicht-kodierende Regionen, wie beispielsweise Promotormotive, die 3'- und 5'- untranslatierten Bereiche und intronische Sequenzen, wichtige funktionelle Bereiche, die bei der Krankheitsentstehung eine bedeutende Rolle spielen können (French and Edwards, 2020). Auch wenn Fortschritte im Bereich der Sequenziertechnologien eine effiziente Detektion solcher Veränderungen ermöglichen, ist die Bewertung von nicht-kodierenden Varianten hinsichtlich ihrer funktionalen Relevanz jedoch in der Regel schwierig. Dies spiegelt sich beispielsweise darin wider, dass diese öfter als „Variante unklarer klinischer Signifikanz“ (VUS) klassifiziert werden (Ellingford et al., 2022). Existierende Richtlinien zur Interpretation von Sequenzvarianten konzentrieren sich hauptsächlich auf die proteinkodierenden Genbereiche. Die für eine breite Anwendung konzipierten ACMG-Richtlinien zur Variantenbewertung klassifizieren Veränderungen hinsichtlich der funktionellen Relevanz als neutral, wahrscheinlich neutral, wahrscheinlich pathogen, pathogen oder als VUS, wenn zum Zeitpunkt der Bewertung die vorhandenen Daten für eine eindeutige Klassifikation nicht ausreichend sind (Richards et al., 2015). Diese ist jedoch von großer Bedeutsamkeit, da eine Einordnung der Variante als pathogen bzw. wahrscheinlich pathogen mitunter mit weitreichenden klinischen Konsequenzen verknüpft ist. Gerade für nicht-kodierende Varianten ist es oftmals notwendig, funktionale Analysen für eine eindeutige Bewertung durchzuführen (Ellingford et al., 2022). Zur *in vitro*-Modellierung solcher Varianten hat sich hierbei das CRISPR/Cas9-System als sehr nützlich erwiesen und wurde beispielsweise

schon in induzierten pluripotenten Stammzellen (*Induced Pluripotent Stem Cells*, iPSCs) genutzt, um die Pathogenität von VUS zu entschlüsseln (Garg et al., 2018; Ma et al., 2018). Im Rahmen dieser Arbeit wurde eine bisher nicht beschriebene Deletion des nicht-kodierenden Exons 1 im *CCM1*-Gen identifiziert und initial als VUS nach den ACMG-Kriterien klassifiziert. Ziel der Arbeit war es, diese Variante mit Hilfe von *in vitro* durchgeführten funktionalen Untersuchungen akkurat zu bewerten (Pilz et al., 2022a).
In den NGS-Genpanel-Daten der Indexpatientin mit multiplen Kavernomen waren keine pathogenen SNVs oder kleine Indel-Varianten identifiziert worden, jedoch eine hohe Anzahl von aberranten Reads im Intron 1 des *CCM1*-Gens aufgefallen. Die *Sequence-Pilot*- und *SureCall*-Software sowie schließlich die NGS-basierte CNV-Analyse wiesen auf eine heterozygote Deletion des Exons 1 von *CCM1* hin. Eine spezifische PCR-basierte, die betreffende Region überspannende Amplifikation resultierte schließlich in einer Wildtyp-Bande und einer etwa 400 bp kürzeren Bande für die Indexpatientin und ihren Vater. Mittels Sanger-Sequenzierung konnten die exakten Bruchpunkte der 411 bp großen Deletion bestimmt werden, die den Transkriptionsstartpunkt (TSP) aller relevanten *CCM1*-Transkripte und mehrere Transkriptionsfaktorbindestellen umfasst (Abb. 4 A, B). Da das Startkodon von *CCM1* jedoch erst in Exon 5 lokalisiert ist, betrifft die Variante nicht die kodierende Region des Gens. Zudem kann das Auftreten von alternativen TSPs nicht gänzlich ausgeschlossen werden (Mondéjar et al., 2016). Gemäß den ACMG-Richtlinien wurden für die Variante die Kriterien PM1 und PP4 als zutreffend erachtet, sodass die Deletion initial entsprechend als VUS bewertet wurde (Pilz et al., 2022a).

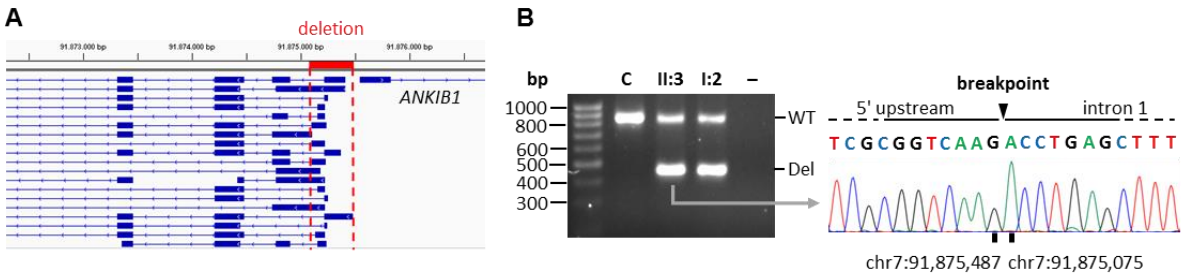

Abbildung 4 | Identifikation einer Deletion des Exons 1 von *CCM1* bei einer Patientin mit multiplen CCMs. **(A)** Die Deletion umfasst den Transkriptionsstartpunkt aller funktionell relevanten *CCM1*-Transkripte. **(B)** Eine PCR-Amplifikation der Deletionsregion resultierte in einer Wildtypbande (WT) und einer 411 bp kürzeren Deletionsbande (Del) für die Indexpatientin (II:3) und ihren Vater (I:2). Die Bruchpunkte der Deletion wurden mittels Sanger-Sequenzierung ermittelt. (Modifizierte) Abbildungen stammen aus Pilz et al. 2022a.

In der vorliegenden Arbeit sollte die CRISPR/Cas9-Technologie in einem iPSC-basierten Zellkulturmodell für die funktionale Charakterisierung der Variante verwendet werden. Um ein für *in vitro*-Analysen wichtiges Referenzsystem für die Bestimmung von Messbereichen und Grenzwerten zu etablieren (Brnich et al., 2019), wurden zunächst erstmals *CCM1*$^{-/-}$

iPSC-Zelllinien mit CRISPR/Cas9-vermittelten biallelischen *Loss-of-Function*-Varianten generiert. Hierfür wurden AICS-0023 iPSCs der *Allen Cell Collection* (Coriell Institute for Medical Research) eingesetzt. Diese weisen eine endogene Fluoreszenzmarkierung des *Tight Junction Protein 1* (ZO-1) mit grün-fluoreszierendem Protein auf. Die Transfektion der iPSCs erfolgte mit RNP-Komplexen, wobei die Zielsequenz der verwendeten *single-guide* RNA im Exon 10 von *CCM1* lag. Klonale *CCM1*$^{-/-}$ iPSC-Linien wurden dann nach serieller Verdünnung expandiert. So gelang es, eine Linie mit zwei compound-heterozygoten *Frameshift*-Varianten und eine Linie mit einer homozygoten 1 bp-Duplikation zu erzeugen. Da diese Varianten zu einer Leserasterverschiebung führen, kommt es sehr wahrscheinlich nicht zur Synthese eines funktionsfähigen Proteins. In der Tat ließen sich eine deutlich reduzierte *CCM1* mRNA-Expression sowie der Verlust des CCM1-Proteins mittels Western-Blot in diesen Zelllinien nachweisen. Aus diesen Linien mittels *STEMDiff Endothelial Differentiation Kit* (STEMCELL Technologies) differenzierte endothelzellähnliche Zellen (im Folgenden als Endothelzellen bezeichnet) exprimierten die typischen Endothelzellmarker CD31 und VE-Cadherin und zeigten eine für die CCM-Pathogenese häufig beschriebene Hochregulierung der Gene *KLF2* und *KLF4* (Zhou et al., 2016). Damit waren sie hervorragend als Referenzsystem für die Bewertung der identifizierten Deletion geeignet (Pilz et al., 2022a). Darüber hinaus wurde hiermit erstmals ein iPSC-basiertes *CCM1* Knockout-Modell der CCM-Erkrankung etabliert. Dessen besondere Bedeutung liegt vor allem in der Überwindung entscheidender Limitationen bisheriger CCM-Zellkulturmodelle. IPSCs sind nicht nur unbegrenzt verfügbar, sondern können durch ihre Differenzierungsfähigkeit die Entwicklung komplexerer dreidimensionaler und Kokultur-Systeme vorantreiben, welche die Interaktion von Endothelzellen mit anderen Zelltypen des zentralen Nervensystems in der CCM-Pathogenese besser abbilden könnten. Die Verwendung von iPSC-Zelllinien, die für CCM-relevante Zellstrukturen wie ZO-1 bereits endogen fluoreszenzmarkiert sind, eröffnet zudem spannende Anschlussmöglichkeiten im Rahmen von *Live-Cell-Imaging*-Studien oder Hochdurchsatztestungen.

Um die identifizierte Deletion in iPSCs nachzubilden, wurden zunächst in leicht zu transfizierenden HEK293T-Zellen verschiedene Paare von crRNAs getestet. Diese sollten einen genomischen Bereich ausschneiden, welcher möglichst akkurat die Deletion widerspiegelt (Abb. 5 A). Nachdem AICS-0023 iPSCs mit der optimalen crRNA-Kombination transfiziert wurden, gelang schließlich die Etablierung dreier *CCM1*$^{del/del}$ Linien mit einer biallelischen CRISPR/Cas9-induzierten Deletion (Abb. 5 B). In Übereinstimmung mit der Hypothese, dass der Verlust des TSPs pathogen ist, konnte für die Linien eine stark reduzierte *CCM1*-Expression auf RNA- und Protein-Ebene nachgewiesen werden. Interessanterweise wurde auch eine verringerte Expression des Gens *ANKIB1* beobachtet, dessen TSP in der Nähe der Deletion lokalisiert ist (Abb. 5 A). Anschließend konnten die

CCM1$^{del/del}$ iPSC-Linien erfolgreich in Endothelzellen differenziert werden (Abb. 5 C). Bemerkenswert ist, dass die Expression des *CCM1*-Transkripts für die differenzierten *CCM1*$^{del/del}$ Endothelzellen vollständig verloren gegangen war, während diese für die *CCM1*$^{-/-}$ Zellen zwar deutlich reduziert, jedoch noch vorhanden war (Abb. 5 D). Zusätzlich wurde in den differenzierten *CCM1*$^{-/-}$ und *CCM1*$^{del/del}$ Endothelzellen mittels Reverse Transkriptase-quantitativer PCR (RT-qPCR) die Expression der Gene *KLF2*, *THBS1*, *NOS3* und *HEY2* untersucht. Für diese ist eine Deregulation im Kontext der CCM1-assoziierten Kavernomatose bekannt (Wüstehube et al., 2010; Zhou et al., 2016; Lopez-Ramirez et al., 2017; Lopez-Ramirez et al., 2021). Für *THBS1* zeigte sich eine ähnliche Reduktion in *CCM1*$^{-/-}$ und *CCM1*$^{del/del}$ Zellen (Abb. 5 D). Für die Gene *KLF2*, *NOS3* und *HEY2* konnte interessanterweise ein zur *CCM1*-Expression ähnlicher Effekt beobachtet werden, wobei jeweils eine stärkere Deregulation in *CCM1*$^{del/del}$ Zellen auftrat (Abb. 5 D) (Pilz et al., 2022a). In diversen Tiermodellen konnte gezeigt werden, dass die Degradation von aberranter mRNA möglicherweise zu genetischen Kompensationsmechanismen und somit zu phänotypischen Unterschieden zwischen stabilen Mutanten und transienten Knockdowns führt (Rossi et al., 2015; El-Brolosy et al., 2019). In diesem Zusammenhang scheint die durch den Prozess der *Nonsense*-vermittelten mRNA-Degradierung ausgelöste Hochregulierung homologer Gene im Sinne einer transkriptionalen Adaption eine wichtige Rolle zu spielen (Rouf et al., 2022). Genetische Kompensationsvorgänge könnten möglicherweise auch ein Erklärungsansatz für die beobachteten Ausprägungsunterschiede der Genexpressionsderegulation zwischen den *CCM1*$^{-/-}$ und *CCM1*$^{del/del}$ Zellen sein, welcher auf dem Vorhandensein von aberranter *CCM1* mRNA in der *CCM1*$^{-/-}$ Kondition, nicht jedoch in den *CCM1*$^{del/del}$ Zellen basiert. Während Korrelationen zwischen dem Phänotyp und des zugrundeliegenden veränderten Gens für CCM etabliert sind, sind kausale Zusammenhänge zwischen der Identität der Variante in demselben Gen und der phänotypischen Ausprägung bisher nicht gezeigt (Snellings et al., 2021). Auch wenn letztlich sowohl *CCM1*$^{-/-}$ als auch *CCM1*$^{del/del}$ differenzierte Endothelzellen CCM-typische Genexpressionsunterschiede zeigten, bieten die hier etablierten Zelllinien eine gute Voraussetzung für Untersuchungen in zukünftigen Studien, ob und inwiefern sich das Vorhandensein aberranter mRNA auf die Stärke der Deregulation CCM-assoziierter molekularer Mechanismen auswirkt.

Schließlich war es auf Basis der beschriebenen funktionalen Analysen möglich, die identifizierte Deletion entsprechend den ACMG-Richtlinien als wahrscheinlich pathogen zu klassifizieren (Kriterien PS3, PM1 und PP4). Somit konnte die molekulare CCM-Diagnose für die Familie gesichert und eine genetische Analyse für weitere Risikopersonen angeboten werden. Diese Studie verdeutlicht, dass der Einsatz des CRISPR/Cas9-Systems in iPSCs sowohl zur Varianteninterpretation in funktionalen Analysen als auch für zukünftig

tiefergehende Untersuchungen der CCM-Pathogenese einen vielversprechenden Ansatz darstellt.

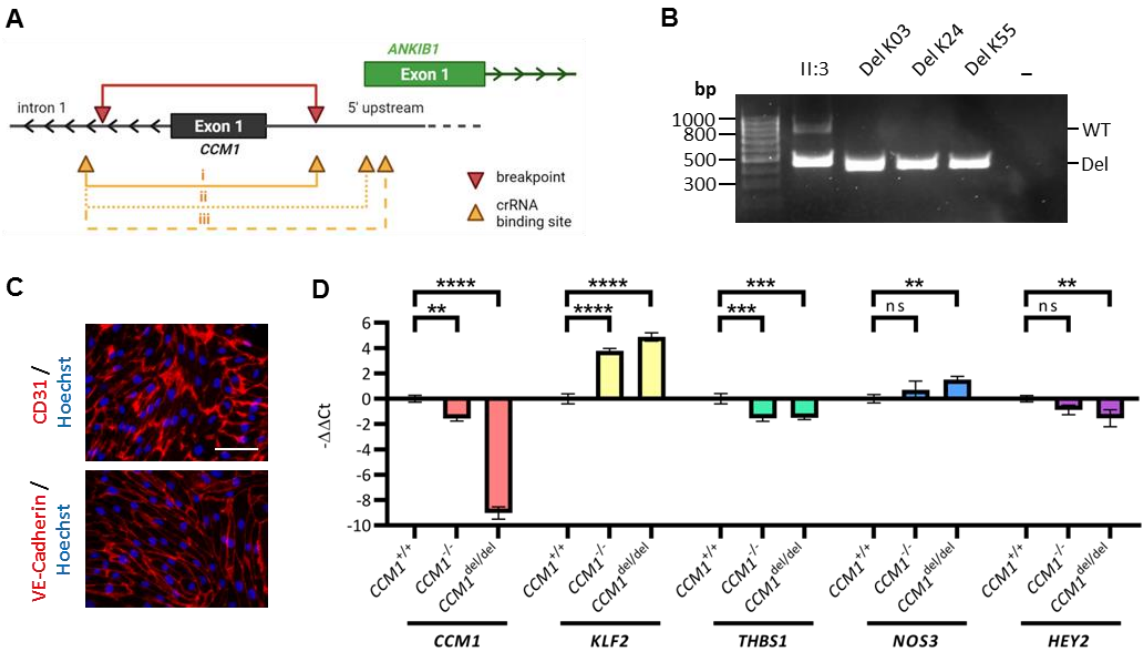

Abbildung 5 | Analyse des funktionalen Einflusses der Deletion in einem iPSC-basierten Zellkulturmodell. **(A)** Schematische Darstellung der identifizierten Deletion (rot) und der crRNA-Bindungsstellen (orange). Die drei crRNA-Kombinationen i, ii und iii wurden zur Generierung einer der identifizierten Variante ähnlichen Deletion verwendet. **(B)** PCR-Amplifikation der Deletionsregion für drei AICS-0023 iPSC-Klone mit einer biallelischen CRISPR/Cas9-induzierten Deletion nach Verwendung der crRNA-Kombination i zur Transfektion. **(C)** AICS-0023-abgeleitete *CCM1*$^{del/del}$ Endothelzellen exprimierten die Endothelzellmarker CD31 und VE-Cadherin (Maßstab: 75 µm). **(D)** RT-qPCR-Analyse für die Gene *CCM1*, *KLF2*, *THBS1*, *NOS3* und *HEY2* für differenzierte *CCM1*$^{+/+}$, *CCM1*$^{-/-}$ und *CCM1*$^{del/del}$ Endothelzellen. Für die statistische Analyse wurde eine einfache ANOVA mit multiplem Vergleichstest verwendet. ** $p < 0,01$, *** $p < 0,001$, **** $p < 0,0001$. Abbildungen und Daten stammen aus Pilz et al. 2022a.

3.2 CRISPR/Cas9- und iPSC-basierte *in vitro*-Modellierung der CCM-Erkrankung

3.2.1 RNA-Sequenzierungen in einem iPSC-basierten *CCM1* Knockout-Modell

In weiterführenden Analysen sollte der Differenzierungsprozess CCM1-defizienter iPSCs in Endothelzellen genutzt werden, um das in der CCM-Forschung noch begrenzte Wissen darüber zu erweitern, ob die zweite somatische Inaktivierung eines *CCM*-Gens unmittelbar die Entstehung von CCMs auslöst oder ob hierbei zusätzliche exogene Faktoren erforderlich sind. Dazu wurden mittels RNA-Sequenzierung die Expressionsprofile von *CCM1*$^{-/-}$ iPSCs sowie aus diesen abgeleiteten *CCM1*$^{-/-}$ differenzierten frühen mesodermalen Progenitorzellen und *CCM1*$^{-/-}$ differenzierten Endothelzellen mit der entsprechenden Wildtyp-Kondition verglichen (Abb. 6) (Pilz et al., 2022b [unter Begutachtung]).

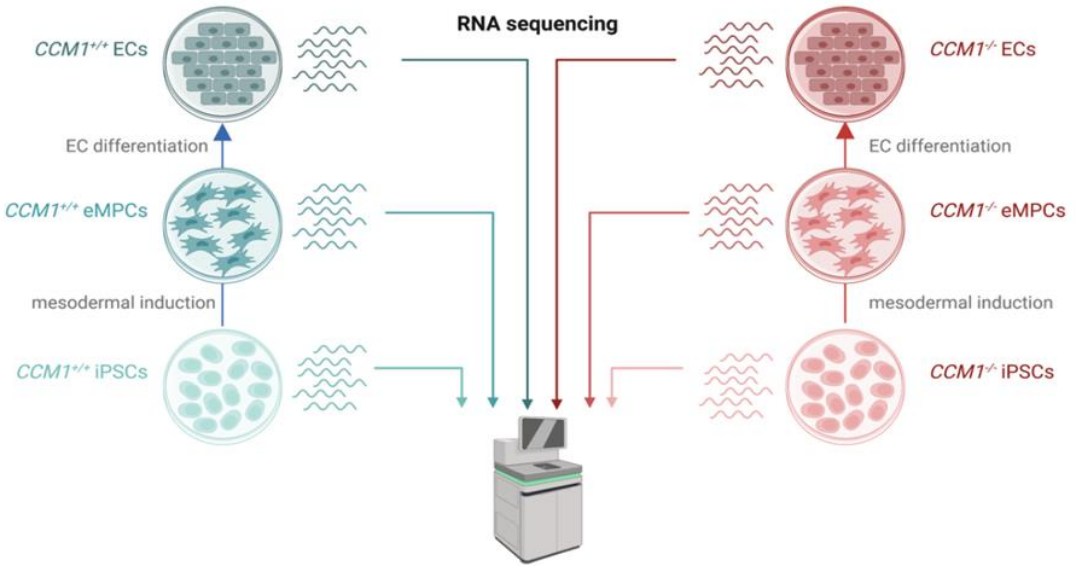

Abbildung 6 | Schematische Darstellung des experimentellen Aufbaus. Es erfolgte eine Differenzierung von *CCM1*$^{+/+}$ und *CCM1*$^{-/-}$ AICS-0023 iPSCs in frühe mesodermale Progenitorzellen (*Early Mesoderm Progenitor Cells*, eMPCs) und Endothelzellen (*Endothelial-Like Cells*, ECs). Genexpressionsunterschiede wurden mittels RNA-Sequenzierung analysiert. Abbildung stammt aus Pilz et al. 2022b [unter Begutachtung].

Die differentiell exprimierten Gene während des Differenzierungsvorgangs von *CCM1*$^{+/+}$ und *CCM1*$^{-/-}$ iPSCs zu Endothelzellen konnten erwartungsgemäß vor allem Angiogenese-assoziierten Prozessen zugeordnet werden. Größere Unterschiede waren hierbei zwischen der *CCM1*$^{-/-}$- und *CCM1*$^{+/+}$-Kondition nicht festzustellen. Beim direkten horizontalen Genotyp-Vergleich stellte sich interessanterweise heraus, dass die CCM1-Defizienz nahezu keine Auswirkung auf das Genexpressionsprofil in iPSCs hatte (Abb. 7 A). Auch in den frühen mesodermalen Progenitorzellen konnten nur minimale Genexpressionsunterschiede verzeichnet werden (Abb. 7 B). Erst in den differenzierten Endothelzellen zeigte sich eine starke Deregulation bekannter Signalwege. Dazu gehörten zum Beispiel Prozesse, welche die Angio- und Vaskulogenese betreffen, aber auch die Deregulation der Zellmotilität (Abb. 7 C-E).

Die Daten bekräftigen weiterhin die oft beschriebene Expressionsänderung von *KLF2* und *KLF4* als Marker der CCM-Pathogenese unabhängig des verwendeten Systems. In unserem Modell wurde ein Expressionsanstieg von ca. 20-fach (*KLF2*) bzw. 11-fach (*KLF4*) in den differenzierten Endothelzellen beobachtet (Pilz et al., 2022b [unter Begutachtung]). Auch andere bekannte Effekte der *CCM1*-Inaktivierung in Endothelzellen konnten in unserem System nachvollzogen werden, wie die Hochregulierung von *THBD* und die Herunterregulierung von *THBS1* (Abb. 7 D). Zusammenfassend lassen die Daten die folgenden Schlussfolgerungen zu: (1) CCM1 scheint für die endotheliale Differenzierung entbehrlich, jedoch für den Erhalt der endothelialen Quieszenz essentiell zu sein und (2) CCM1 spielt keine entscheidende Rolle in iPSCs oder frühen mesodermalen Progenitorzellen. Es erscheint somit plausibel, dass *CCM1*$^{-/-}$ Vorläuferzellen existieren,

welche erst in einer spezifischen Mikroumgebung und beim Eintritt in die endotheliale Linie ein Knockout-spezifisches Genexpressionsmuster etablieren. Die Daten lassen vermuten, dass dies nur durch exogene Faktoren wie Zytokine oder Wachstumsfaktoren ermöglicht wird, welche für die endotheliale Differenzierung verwendet werden.

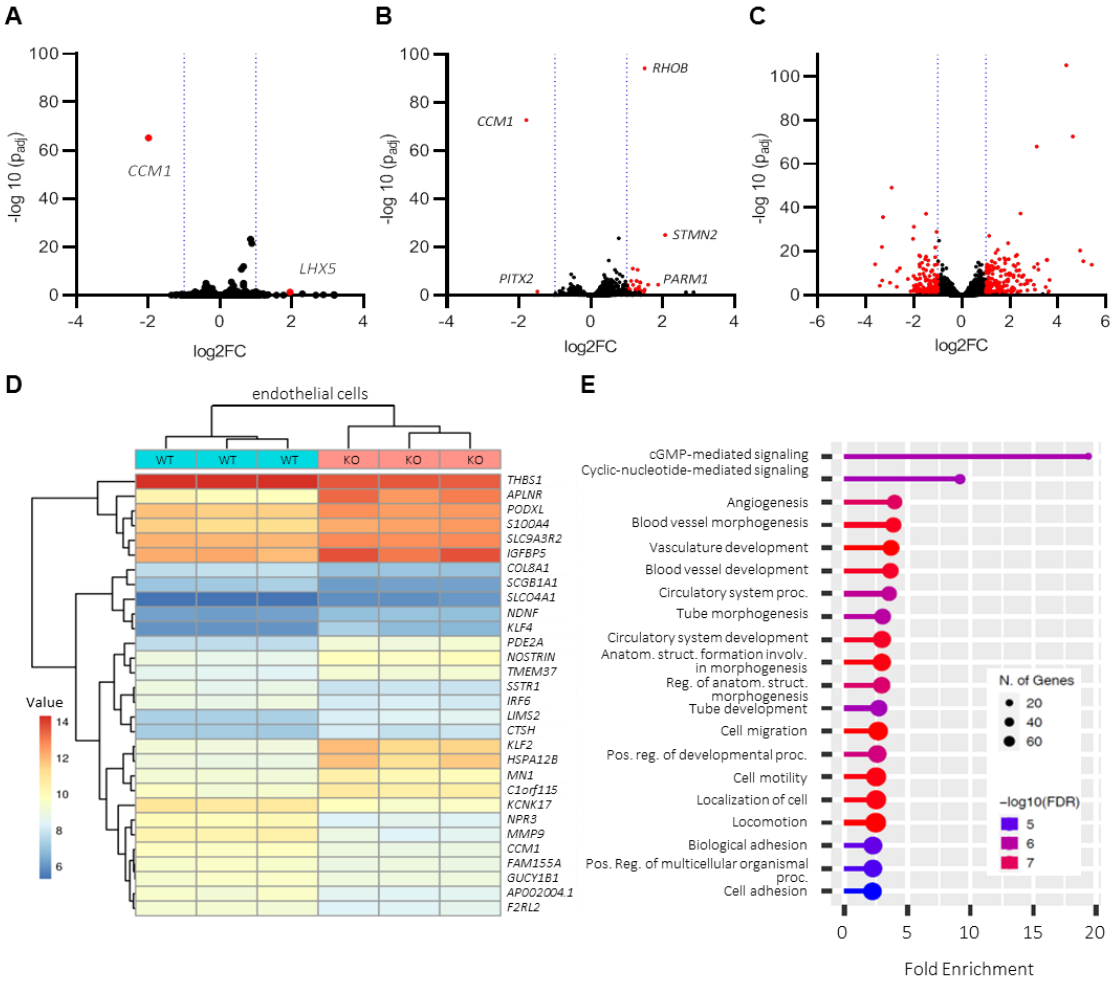

Abbildung 7 | Genexpressionsunterschiede in *CCM1*$^{-/-}$ iPSCs (A), differenzierten frühen mesodermalen Progenitorzellen (B) und differenzierten Endothelzellen (C-E) im Vergleich zur *CCM1*$^{+/+}$-Kondition. (A-C) Dargestellt sind jeweils die Volcano-Plots herunter- und hochregulierter Gene. Hierbei ist jeweils die logarithmierte relative Expressionsänderung (*log2 Fold Change,* log2FC) in Bezug zum negativen log10 adjustierten p-Wert (-log10 [p_{adj}]) abgebildet. Signifikant deregulierte Gene wurden als $p_{adj} < 0{,}05$ und $|log2FC| > 1$ definiert und sind rot markiert. **(D)** Heatmap differenziell exprimierter Gene in differenzierten *CCM1*$^{-/-}$ Endothelzellen. Es sind die regularisierten log-transformierten Readanzahlen (*Value*) für *CCM1*$^{-/-}$ (KO) und *CCM1*$^{+/+}$ (WT) Zellen gezeigt. **(E)** Anreicherungsanalyse für Genontologie-Kategorien (*GO Biological Process Enrichment Analysis*) für differenziell exprimierte Gene in differenzierten *CCM1*$^{-/-}$ Endothelzellen, dargestellt mittels *ShinyGO 0.76*-Software. *CCM1* wurde aus dieser Analyse ausgeschlossen, um eine systematische Verzerrung zu vermeiden. FDR = Falscherkennungsrate (*False Discovery Rate*). (Modifizierte) Abbildungen und Daten stammen aus Pilz et al. 2022b [unter Begutachtung].

Die Annahme, dass sich die nachgeschalteten Effekte einer *CCM1*-Inaktivierung erst in einem bestimmten Mikromilieu manifestieren und somit auch exogene Faktoren zur CCM-

Formation beitragen, wird durch weitere Studien unterstützt. So wurde beispielsweise gezeigt, dass phänotypische Effekte einer *Ccm2*-Inaktivierung in Mäusen erst in Entwicklungsstadien mit aktiver Angiogenese auftreten (Boulday et al., 2011) oder die Inhibierung der für die Angiogenese und endotheliale Differenzierung wichtigen VEGF-Signalwirkung zu einer reduzierten Anzahl von Läsionen im *Ccm1*-Mausmodell führt (DiStefano and Glading, 2020). Bei der Suche nach neuen therapeutischen Ansätzen sollten daher nicht nur die Folgen der CCM-Defizienz, sondern auch die unterstützenden Faktoren der endothelialen Dysfunktion adressiert werden.

3.2.2 Einsatz differenzierter Endothelzellen und vaskulärer Organoide bei der Untersuchung von tumorähnlichen Mechanismen der CCM-Pathogenese

In humanen CCM-Läsionen lässt sich ein Mosaikverband von Zellen mit erhaltener und vollständig verlorener CCM-Expression beobachten (Rath et al., 2020). Dies steht im Einklang mit den hochrangig publizierten Analysen in Konfetti-Mausmodellen, welche eindrücklich zeigen konnten, dass eine klonale Expansion von Endothelzellen mit einer vollständigen CCM3-Inaktivierung zur Kavernomformation beiträgt (Detter et al., 2018; Malinverno et al., 2019). Im Rahmen dieser Arbeit konnten wir in der Greifswalder Arbeitsgruppe ähnliche Beobachtungen für CI-huVECs machen, wobei CCM3-defiziente Zellen jedoch erst in Kokultur mit Wildtyp-Zellen stark erhöhte Proliferationsraten zeigten (Rath et al., 2022). Diese abnormale Proliferation schien abhängig von direkten Zell-Zell-Kontakten mit Wildtyp-Zellen zu sein, da sich zum einen die Proliferationsraten in Monokultur nicht unterschieden und sich zum anderen konditioniertes Medium nicht auf die proliferative Aktivität der Zellen auswirkte. RNA-Sequenzierungen gaben weiterhin einen interessanten Einblick in die noch unzureichend verstandene, aber für die CCM-Formation essenzielle Interaktion von Knockout- und Wildtyp-Zellen. Beispielsweise konnte aufgedeckt werden, dass Gene, die in Monokultur nach *CCM3*-Inaktivierung herunterreguliert sind, durch die Kokultur in Knockout-Zellen wieder hochreguliert wurden. Darüber hinaus konnte eine Deregulation von Chemokin- bzw. Zytokin-assoziierten Signalwegen in Wildtyp-Zellen unter Kokulturbedingungen beobachtet werden (Rath et al., 2022). Dies steht im Einklang mit anderen kürzlich publizierten Analysen, die eine wichtige Rolle von immunassoziierten Faktoren für die CCM-Pathogenese beschreiben (Yau et al., 2022).

IPSC-basierte Zellkultursysteme, welche im Rahmen der Promotionsarbeit etabliert wurden, konnten wesentlich zur Absicherung der Hypothese, dass CCM3-defiziente Endothelzellen im Mosaikverband mit Wildtyp-Zellen ein tumorähnliches Verhalten zeigen, beitragen. Einerseits konnten humane mikrovaskuläre endothelzellähnliche Zellen des Gehirns (*Human Brain Microvascular Endothelial Cells*, hBMECs) aus iPSCs mit Hilfe des Protokolls von Neal und Kolleg*innen differenziert werden (Neal et al., 2019). Für iPSC-abgeleitete hBMECs

wurde in der Literatur beschrieben, dass sie typische Merkmale der humanen BHS wie die Bildung von *Tight Junctions* oder die Transportfunktion gut abbilden können (Minami et al., 2015; Kurosawa et al., 2018; Neal et al., 2019). Zudem wurde zur weiteren Absicherung unserer Beobachtungen an der Generierung von komplexen vaskulären Organoidkulturen nach dem anspruchsvollen Protokoll von Wimmer und Kolleg*innen mitgewirkt (Wimmer et al., 2019) (Abb. 8 A). Nach der Aggregation von iPSC-Kulturen in speziellen Zellkulturplatten, welche die Adhäsion an das Zellkulturmaterial hemmen, folgte hierbei die Induktion der mesodermalen und vaskulären Differenzierung. Nachdem die Zellaggregate in eine Matrigel-Kollagen I-Matrix eingebettet wurden, wurde die Sprossung Gefäß-ähnlicher Strukturen eingeleitet. Die entstandenen vaskulären Netzwerke konnten dann aus der Matrix extrahiert werden und zu vollständigen vaskulären Organoiden mit einer Größe von etwa 1 mm kultiviert werden (Abb. 8 A). Durch den Nachweis der Expression von CD31 und PDGFRβ konnte das Vorhandensein von Endothelzellen und Perizyten veranschaulicht werden (Abb. 8 B). Konfokalmikroskopische Aufnahmen ermöglichten zudem genauere Einblicke in die Gefäßstruktur, welche die Assoziation von Endothelzellen und Perizyten in den Netzwerken illustrierten (Abb. 8 B).

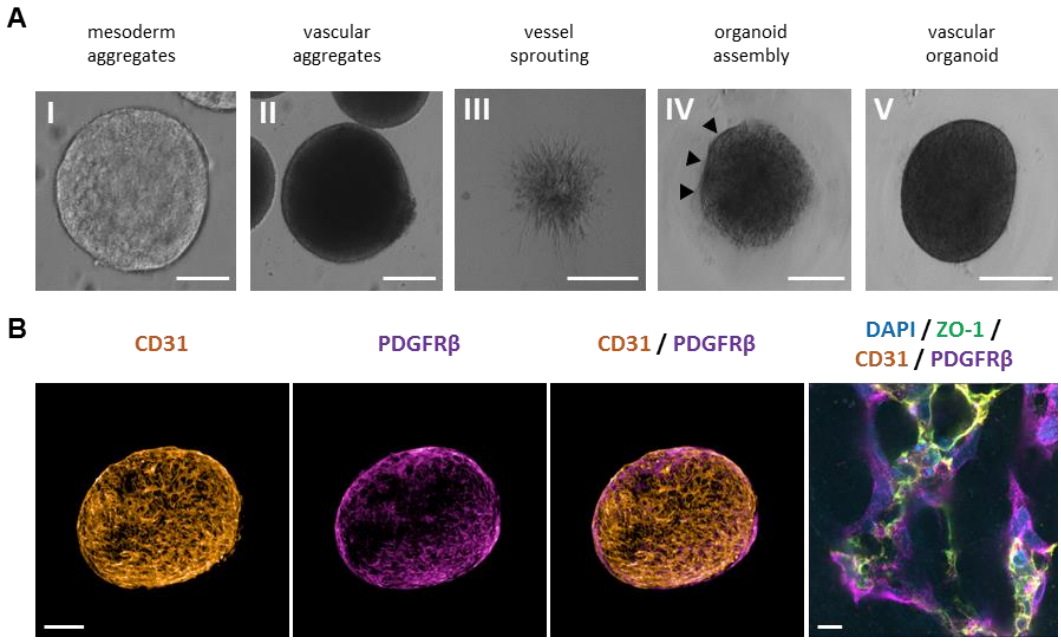

Abbildung 8 | Differenzierung von iPSCs zu vaskulären Organoiden. (A) Beispielhafte morphologische Aufnahmen im Zeitverlauf des Differenzierungsprozesses. Die schwarzen Pfeile repräsentieren die beginnende Kapselung der Organoide nach Extraktion der vaskulären Netzwerke aus einer Matrigel-Kollagen I-Matrix. Maßstab: I – 50 µm, II – 200 µm, III/IV/V – 500 µm. **(B)** Immunfluoreszenzfärbungen differenzierter Organoide für die Marker CD31 und PDGFRβ. Maßstab: linke Sektionen – 200 µm, rechte Sektion – 10 µm. Abbildungen bisher nicht veröffentlicht.

Sowohl in Kokulturen von differenzierten hBMEC-ähnlichen Zellen als auch in vaskulären Mosaik-Organoiden, bei denen Kokulturen aus *CCM3*$^{-/-}$ und *CCM3*$^{+/+}$ iPSCs als

Ausgangspunkt der Differenzierung dienten, konnte die deutlich gesteigerte Proliferation CCM3-defizienter Zellen nachvollzogen werden (Abb. 9) (Rath et al., 2022). Der Einsatz von fluoreszenzmarkierten iPSCs ermöglichte hierbei nicht nur eine effiziente Auswertestrategie, sondern erlaubte auch Einblicke in die zellulären Prozesse. So konnte festgestellt werden, dass CCM3-defiziente Zellen nicht gebündelt, sondern in einem Mosaikverband mit Wildtyp-Zellen vorliegen (Abb. 9 B, D), was auch den Beobachtungen in humanen CCM-Läsionen entspricht.

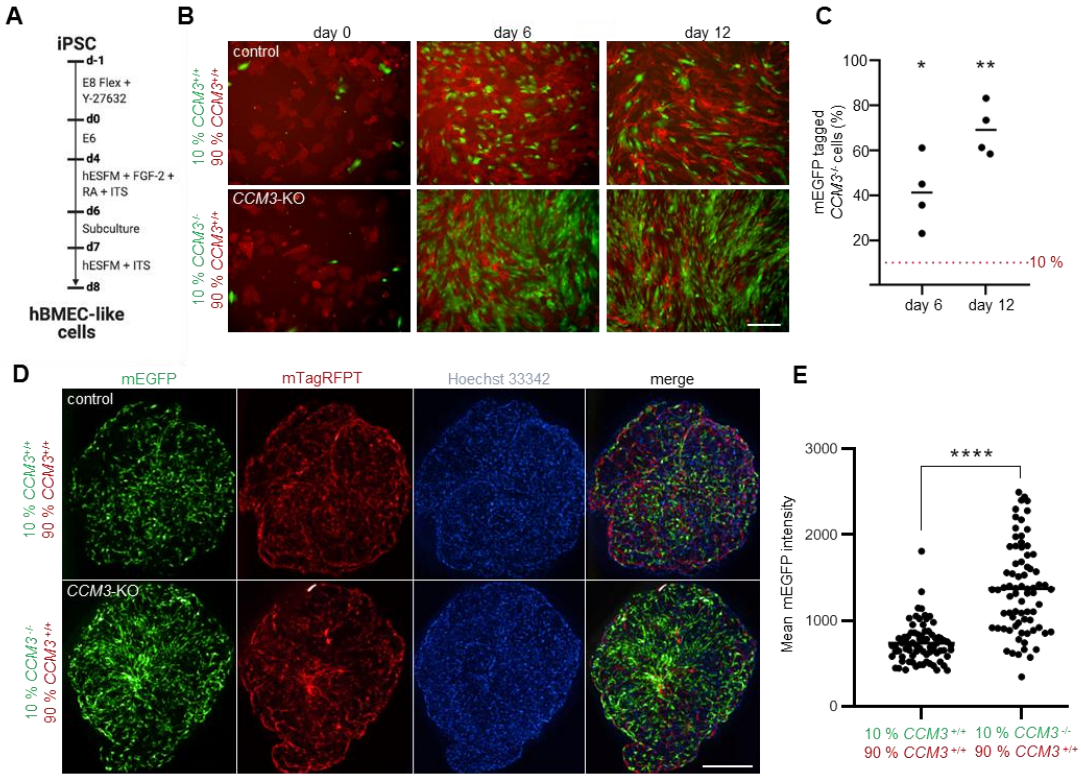

Abbildung 9 | IPSC-abgeleitete *CCM3*$^{-/-}$ Endothelzellen zeigten ein tumorähnliches proliferatives Verhalten in Kokultur mit Wildtyp-Zellen und in vaskulären Mosaikorganoiden. (A) Schematische Darstellung der Differenzierung von iPSCs in hBMEC-ähnliche Zellen nach Neal und Kolleg*innen (Neal et al., 2019). **(B)** *CCM3*$^{-/-}$ AICS-0036 (mEGFP-Markierung, Plasma, grün), *CCM3*$^{+/+}$ AICS-0036 (mEGFP-Markierung, Plasma, grün) und *CCM3*$^{+/+}$ AICS-0054 (mTagRFPT-Markierung, Membran, rot) iPSCs wurden in hBMEC-ähnliche Zellen differenziert, in einem 1:9-Verhältnis gemischt und für mehrere Tage kultiviert (Maßstab: 200 µm). **(C)** *CCM3*$^{-/-}$ hBMEC-ähnliche Zellen zeigten eine abnorme Proliferation in Kokultur mit *CCM3*$^{+/+}$ hBMEC-ähnlichen Zellen (n = 4 pro Genotyp). Ein Einstichproben-t-Test wurde zur statistischen Analyse verwendet. * $p < 0,05$, ** $p < 0,01$. **(D)** Die abnorme Proliferation von *CCM3*$^{-/-}$ Zellen wurde auch in vaskulären Mosaikorganoiden beobachtet (Maßstab: 300 µm). **(E)** Statistische Analyse von 75 Wildtyp/Wildtyp und 77 Knockout/Wildtyp Mosaikorganoiden, die in drei unabhängigen biologischen Replikaten differenziert worden sind. Es wurde ein zweiseitiger t-Test zur statistischen Analyse verwendet. **** $p < 0,0001$. Abbildungen und Daten stammen aus Rath et al. 2022.

Auch weitere Studien illustrierten, dass tumorähnliche Mechanismen in der CCM-Pathogenese eine Rolle zu spielen scheinen. Erst kürzlich wurde zum Beispiel ein Drei-Schritt-Mechanismus bei schnell wachsenden, klinisch symptomatischen CCMs postuliert, wonach zusätzlich zur kompletten Inaktivierung eines CCM-Proteins auch *Gain-of-Function*-Varianten im *PIK3CA*-Gen eine Rolle spielen (Ren et al., 2021). Das Zusammenspiel von

„vaskulärem Suppressor“ (CCM) und „vaskulärem Onkogen“ (PK3CA) erinnert hierbei an charakteristische Prozesse der Tumorgenese. Ähnlich wie der mTORC1-Inhibitor Rapamycin war mit Ponatinib auch schon der Einsatz einer für Krebstherapien eingesetzten Substanz bei der Blockierung der CCM-Initiation und -Progression im Mausmodell erfolgreich (Choi et al., 2018). Ein breites Spektrum an Nebenwirkungen limitiert jedoch die Verwendung solcher Agenzien für die Therapie von CCM-Patient*innen, weswegen die Identifikation neuer Kandidatenstoffe nach wie vor eines der primären Ziele der CCM-Forschung ist.
Dieses Ziel wurde auch in unserer Studie unter Einsatz des CI-huVEC-Kokulturansatzes verfolgt. Hierbei konnte das Molekül NSC59984 als Kandidatensubstanz identifiziert werden, welche keinen größeren Einfluss auf die Zellmorphologie oder die Lebensfähigkeit der Zellen hatte und die starke Proliferation von Knockout-Zellen in Kokultur konzentrationsabhängig inhibieren konnte (Rath et al., 2022). Auch wenn in diesem Fall ebenfalls Nebeneffekte der Substanz derzeit ihren Einsatz in der CCM-Therapie limitieren, tragen die Resultate als konzeptioneller Beweis der möglichen Inhibition der abnormalen Expansion CCM3-defizienter Endothelzellen zur Aufdeckung neuer Therapieansätze bei. Unsere Arbeiten legen nahe, dass hierbei insbesondere neue humane CRISPR/Cas9- und iPSC-basierte *in vitro*-Modelle hervorragend als Erstansatz in Hochdurchsatzstudien geeignet sind und damit die Entdeckung neuer Therapieansätze erheblich beschleunigen können.

3.2.3 CCM-Zellkulturmodelle – ein Ausblick

Im Rahmen einer Beschreibung und Bewertung der derzeit zur Verfügung stehenden Zellkulturmodelle der CCM-Erkrankung, bei der in dieser Arbeit mitgewirkt wurde, wurde die besondere Eignung CRISPR/Cas9-basierter *in vitro*-Modelle bei der Abbildung von Aspekten der endothelialen Barrierestörung und der klonalen Expansion von Endothelzellen mit CCM-Defizienz dargelegt (Skowronek et al., 2021). Neben einem auch in dieser Arbeit näher charakterisierten deutlichen Überlebensvorteil von CCM-defizienten Endothelzellen ist auch eine möglichst *in vivo*-relevante Modellierung der gestörten endothelialen Barriere von großer Bedeutung, da diese zur erhöhten Blutungsneigung der CCMs beiträgt. Eine dysfunktionale endotheliale Barriere äußert sich in Zellkulturmodellen unter anderem in gestörten Adhärenzkontakten und einer verstärkten Bildung von Aktinstressfasern. In dreidimensionalen Modellen führen gestörte Zell-Zell-Verbindungen nach Inaktivierung der *CCM*-Gene beispielsweise zu einer fehlorganisierten Sphäroidformation (Skowronek et al., 2021). Um die endotheliale Barrierestörung zukünftig genauer qualitativ und quantitativ charakterisieren zu können, konnte unter Einsatz der innovativen *OrganoPlate*-Technologie (Mimetas) im Rahmen dieser Arbeit ein dreidimensionales System etabliert werden, mit dem die Durchlässigkeit der endothelialen Barriere im CCM-Kontext effektiv untersucht werden kann. So war bereits die Kultivierung von endothelialen Kanälen aus HUVE-Zellen gegen

eine Kollagen I-Matrix in der *OrganoPlate 3-lane* (Abb. 10 A) erfolgreich. Durch das Einleiten von fluoreszierenden Dextran-Molekülen kann mittels Fluoreszenzmikroskopie beurteilt werden, ob diese in den Kanälen zurückgehalten werden oder aus diesen austreten (Abb. 10 B). Somit lässt sich das Ausmaß der Barrieredurchlässigkeit gut beobachten. Die *OrganoPlate*-Technologie wurde unter anderem schon erfolgreich verwendet, um eine funktionale BHS durch die Kokultivierung von Endothelzellen, Perizyten und Astrozyten nachzubilden (Wevers et al., 2018). Dies stellt auch für die Modellierung der CCM-Erkrankung ein hoch relevantes System dar und kann in zukünftigen Studien durch den Einsatz von iPSCs auf spezifische Fragestellungen der gestörten BHS effizient eingesetzt werden.

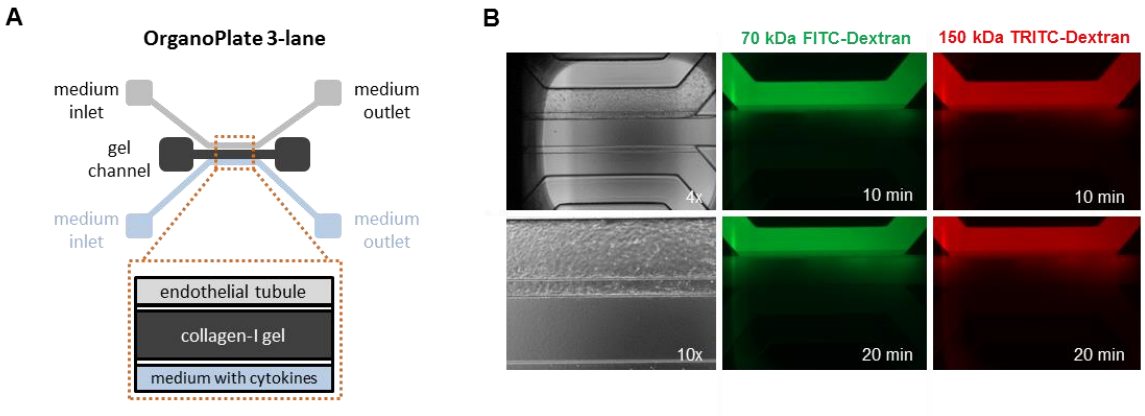

Abbildung 10 | Visualisierung der Barriereintegrität von HUVECs in der *OrganoPlate 3-lane*. (A) Schematische Darstellung des Plattensystems. **(B)** Einleitung von fluoreszierendem FITC- bzw. TRITC-Dextran mit unterschiedlichen Molekulargewichten (mittlere und rechte Sektionen) in einen endothelialen Kanal aus HUVECs (linke Sektionen). Ein Austritt der Moleküle aus dem Kanal war im untersuchten Zeitverlauf nicht zu beobachten. Abbildungen bisher nicht veröffentlicht.

Insgesamt eröffnen die im Rahmen dieser Arbeit etablierten klonalen iPSC-Linien mit einer vollständigen CRISPR/Cas9-vermittelten *CCM1*-, *CCM2*- oder *CCM3*-Inaktivierung und einer spezifischen endogenen Fluoreszenzmarkierung für CCM-relevante Zellstrukturen spannende experimentelle Anschlussmöglichkeiten. So können nicht nur faszinierende neue Einblicke in die Prozesse der CCM-Pathogenese erlangt, sondern auch die Entwicklung dringend benötigter Therapieansätze durch Hochdurchsatztestungen mit einer effektiven Auslesestrategie vorangetrieben werden.

4 Literaturverzeichnis

Adli, M. (2018). The CRISPR tool kit for genome editing and beyond. *Nat Commun* 9(1)**,** 1911. doi: 10.1038/s41467-018-04252-2.

Akers, A., Al-Shahi Salman, R., Awad, I.A., Dahlem, K., Flemming, K., Hart, B., et al. (2017). Synopsis of Guidelines for the Clinical Management of Cerebral Cavernous Malformations: Consensus Recommendations Based on Systematic Literature Review by the Angioma Alliance Scientific Advisory Board Clinical Experts Panel. *Neurosurgery* 80(5)**,** 665-680. doi: 10.1093/neuros/nyx091.

Akers, A.L., Johnson, E., Steinberg, G.K., Zabramski, J.M., and Marchuk, D.A. (2009). Biallelic somatic and germline mutations in cerebral cavernous malformations (CCMs): evidence for a two-hit mechanism of CCM pathogenesis. *Hum Mol Genet* 18(5)**,** 919-930. doi: 10.1093/hmg/ddn430.

Al-Shahi, R., Bhattacharya, J.J., Currie, D.G., Papanastassiou, V., Ritchie, V., Roberts, R.C., et al. (2003). Prospective, population-based detection of intracranial vascular malformations in adults: the Scottish Intracranial Vascular Malformation Study (SIVMS). *Stroke* 34(5)**,** 1163-1169. doi: 10.1161/01.STR.0000069018.90456.C9.

Alliance to Cure Cavernous Malformation (2022). *Role of the Alliance to Cure Cavernous Malformation – FAQ* [Online]. Available: https://www.alliancetocure.org/about-angioma-alliance/role-of-angioma-alliance-faq/ [Accessed October 2022].

Barrangou, R., Fremaux, C., Deveau, H., Richards, M., Boyaval, P., Moineau, S., et al. (2007). CRISPR provides acquired resistance against viruses in prokaryotes. *Science* 315(5819)**,** 1709-1712. doi: 10.1126/science.1138140.

Batra, S., Lin, D., Recinos, P.F., Zhang, J., and Rigamonti, D. (2009). Cavernous malformations: natural history, diagnosis and treatment. *Nat Rev Neurol* 5(12)**,** 659-670. doi: 10.1038/nrneurol.2009.177.

Bergametti, F., Denier, C., Labauge, P., Arnoult, M., Boetto, S., Clanet, M., et al. (2005). Mutations within the programmed cell death 10 gene cause cerebral cavernous malformations. *Am J Hum Genet* 76(1)**,** 42-51. doi: 10.1086/426952.

Boulday, G., Rudini, N., Maddaluno, L., Blécon, A., Arnould, M., Gaudric, A., et al. (2011). Developmental timing of CCM2 loss influences cerebral cavernous malformations in mice. *J Exp Med* 208(9)**,** 1835-1847. doi: 10.1084/jem.20110571.

Brnich, S.E., Abou Tayoun, A.N., Couch, F.J., Cutting, G.R., Greenblatt, M.S., Heinen, C.D., et al. (2019). Recommendations for application of the functional evidence PS3/BS3 criterion using the ACMG/AMP sequence variant interpretation framework. *Genome Med* 12(1)**,** 3. doi: 10.1186/s13073-019-0690-2.

Chaisson, M.J.P., Sanders, A.D., Zhao, X., Malhotra, A., Porubsky, D., Rausch, T., et al. (2019). Multi-platform discovery of haplotype-resolved structural variation in human genomes. *Nat Commun* 10(1)**,** 1784. doi: 10.1038/s41467-018-08148-z.

Chandrasegaran, S., and Carroll, D. (2016). Origins of Programmable Nucleases for Genome Engineering. *J Mol Biol* 428(5 Pt B)**,** 963-989. doi: 10.1016/j.jmb.2015.10.014.

Chiang, C., Scott, A.J., Davis, J.R., Tsang, E.K., Li, X., Kim, Y., et al. (2017). The impact of structural variation on human gene expression. *Nat Genet* 49(5)**,** 692-699. doi: 10.1038/ng.3834.

Choi, J.P., Wang, R., Yang, X., Wang, X., Wang, L., Ting, K.K., et al. (2018). Ponatinib (AP24534) inhibits MEKK3-KLF signaling and prevents formation and progression of cerebral cavernous malformations. *Sci Adv* 4(11)**,** eaau0731. doi: 10.1126/sciadv.aau0731.

Clatterbuck, R.E., Eberhart, C.G., Crain, B.J., and Rigamonti, D. (2001). Ultrastructural and immunocytochemical evidence that an incompetent blood-brain barrier is related to the pathophysiology of cavernous malformations. *J Neurol Neurosurg Psychiatry* 71(2)**,** 188-192. doi: 10.1136/jnnp.71.2.188.

De Coster, W., and Van Broeckhoven, C. (2019). Newest Methods for Detecting Structural Variations. *Trends Biotechnol* 37(9)**,** 973-982. doi: 10.1016/j.tibtech.2019.02.003.

Denier, C., Goutagny, S., Labauge, P., Krivosic, V., Arnoult, M., Cousin, A., et al. (2004). Mutations within the *MGC4607* gene cause cerebral cavernous malformations. *Am J Hum Genet* 74(2)**,** 326-337. doi: 10.1086/381718.

Denier, C., Labauge, P., Bergametti, F., Marchelli, F., Riant, F., Arnoult, M., et al. (2006). Genotype-phenotype correlations in cerebral cavernous malformations patients. *Ann Neurol* 60(5)**,** 550-556. doi: 10.1002/ana.20947.

Detter, M.R., Snellings, D.A., and Marchuk, D.A. (2018). Cerebral Cavernous Malformations Develop Through Clonal Expansion of Mutant Endothelial Cells. *Circ Res* 123(10)**,** 1143-1151. doi: 10.1161/CIRCRESAHA.118.313970.

DiStefano, P.V., and Glading, A.J. (2020). VEGF signalling enhances lesion burden in KRIT1 deficient mice. *J Cell Mol Med* 24(1)**,** 632-639. doi: 10.1111/jcmm.14773.

Eichler, E.E. (2019). Genetic Variation, Comparative Genomics, and the Diagnosis of Disease. *N Engl J Med* 381(1)**,** 64-74. doi: 10.1056/NEJMra1809315.

El-Brolosy, M.A., Kontarakis, Z., Rossi, A., Kuenne, C., Günther, S., Fukuda, N., et al. (2019). Genetic compensation triggered by mutant mRNA degradation. *Nature* 568(7751)**,** 193-197. doi: 10.1038/s41586-019-1064-z.

Ellingford, J.M., Ahn, J.W., Bagnall, R.D., Baralle, D., Barton, S., Campbell, C., et al. (2022). Recommendations for clinical interpretation of variants found in non-coding regions of the genome. *Genome Med* 14(1)**,** 73. doi: 10.1186/s13073-022-01073-3.

Feuk, L., Marshall, C.R., Wintle, R.F., and Scherer, S.W. (2006). Structural variants: changing the landscape of chromosomes and design of disease studies. *Hum Mol Genet* 15 Spec No 1**,** R57-66. doi: 10.1093/hmg/ddl057.

Flemming, K.D., Graff-Radford, J., Aakre, J., Kantarci, K., Lanzino, G., Brown, R.D., Jr., et al. (2017). Population-Based Prevalence of Cerebral Cavernous Malformations in Older Adults: Mayo Clinic Study of Aging. *JAMA Neurol* 74(7)**,** 801-805. doi: 10.1001/jamaneurol.2017.0439.

French, J.D., and Edwards, S.L. (2020). The Role of Noncoding Variants in Heritable Disease. *Trends Genet* 36(11)**,** 880-891. doi: 10.1016/j.tig.2020.07.004.

Gaetzner, S., Stahl, S., Sürücü, O., Schaafhausen, A., Halliger-Keller, B., Bertalanffy, H., et al. (2007). *CCM1* gene deletion identified by MLPA in cerebral cavernous malformation. *Neurosurg Rev* 30(2)**,** 155-159; discussion 159-160. doi: 10.1007/s10143-006-0057-1.

Garg, P., Oikonomopoulos, A., Chen, H., Li, Y., Lam, C.K., Sallam, K., et al. (2018). Genome Editing of Induced Pluripotent Stem Cells to Decipher Cardiac Channelopathy Variant. *J Am Coll Cardiol* 72(1)**,** 62-75. doi: 10.1016/j.jacc.2018.04.041.

Gault, J., Shenkar, R., Recksiek, P., and Awad, I.A. (2005). Biallelic somatic and germ line *CCM1* truncating mutations in a cerebral cavernous malformation lesion. *Stroke* 36(4)**,** 872-874. doi: 10.1161/01.STR.0000157586.20479.fd.

Gilpatrick, T., Lee, I., Graham, J.E., Raimondeau, E., Bowen, R., Heron, A., et al. (2020). Targeted nanopore sequencing with Cas9-guided adapter ligation. *Nat Biotechnol* 38(4)**,** 433-438. doi: 10.1038/s41587-020-0407-5.

Glading, A., Han, J., Stockton, R.A., and Ginsberg, M.H. (2007). KRIT-1/CCM1 is a Rap1 effector that regulates endothelial cell cell junctions. *J Cell Biol* 179(2)**,** 247-254. doi: 10.1083/jcb.200705175.

Grskovic, M., Javaherian, A., Strulovici, B., and Daley, G.Q. (2011). Induced pluripotent stem cells--opportunities for disease modelling and drug discovery. *Nat Rev Drug Discov* 10(12)**,** 915-929. doi: 10.1038/nrd3577.

Hendriks, D., Clevers, H., and Artegiani, B. (2020). CRISPR-Cas Tools and Their Application in Genetic Engineering of Human Stem Cells and Organoids. *Cell Stem Cell* 27(5)**,** 705-731. doi: 10.1016/j.stem.2020.10.014.

Ho, S.S., Urban, A.E., and Mills, R.E. (2020). Structural variation in the sequencing era. *Nat Rev Genet* 21(3)**,** 171-189. doi: 10.1038/s41576-019-0180-9.

Ishino, Y., Shinagawa, H., Makino, K., Amemura, M., and Nakata, A. (1987). Nucleotide sequence of the iap gene, responsible for alkaline phosphatase isozyme conversion in Escherichia coli, and identification of the gene product. *J Bacteriol* 169(12)**,** 5429-5433. doi: 10.1128/jb.169.12.5429-5433.1987.

Kim, S., Kim, D., Cho, S.W., Kim, J., and Kim, J.S. (2014). Highly efficient RNA-guided genome editing in human cells via delivery of purified Cas9 ribonucleoproteins. *Genome Res* 24(6)**,** 1012-1019. doi: 10.1101/gr.171322.113.

Knudson, A.G., Jr. (1971). Mutation and cancer: statistical study of retinoblastoma. *Proc Natl Acad Sci U S A* 68(4)**,** 820-823. doi: 10.1073/pnas.68.4.820.

Kurosawa, T., Tega, Y., Higuchi, K., Yamaguchi, T., Nakakura, T., Mochizuki, T., et al. (2018). Expression and Functional Characterization of Drug Transporters in Brain Microvascular Endothelial Cells Derived from Human Induced Pluripotent Stem Cells. *Mol Pharm* 15(12)**,** 5546-5555. doi: 10.1021/acs.molpharmaceut.8b00697.

Labauge, P., Laberge, S., Brunereau, L., Levy, C., and Tournier-Lasserve, E. (1998). Hereditary cerebral cavernous angiomas: clinical and genetic features in 57 French families. Société Française de Neurochirurgie. *Lancet* 352(9144)**,** 1892-1897. doi: 10.1016/s0140-6736(98)03011-6.

Laberge-le Couteulx, S., Jung, H.H., Labauge, P., Houtteville, J.P., Lescoat, C., Cecillon, M., et al. (1999). Truncating mutations in *CCM1*, encoding KRIT1, cause hereditary cavernous angiomas. *Nat Genet* 23(2)**,** 189-193. doi: 10.1038/13815.

Liquori, C.L., Berg, M.J., Siegel, A.M., Huang, E., Zawistowski, J.S., Stoffer, T., et al. (2003). Mutations in a gene encoding a novel protein containing a phosphotyrosine-binding domain cause type 2 cerebral cavernous malformations. *Am J Hum Genet* 73(6)**,** 1459-1464. doi: 10.1086/380314.

Liquori, C.L., Berg, M.J., Squitieri, F., Ottenbacher, M., Sorlie, M., Leedom, T.P., et al. (2006). Low frequency of PDCD10 mutations in a panel of CCM3 probands: potential for a fourth CCM locus. *Hum Mutat* 27(1)**,** 118. doi: 10.1002/humu.9389.

Lopez-Ramirez, M.A., Fonseca, G., Zeineddine, H.A., Girard, R., Moore, T., Pham, A., et al. (2017). Thrombospondin1 (TSP1) replacement prevents cerebral cavernous malformations. *J Exp Med* 214(11)**,** 3331-3346. doi: 10.1084/jem.20171178.

Lopez-Ramirez, M.A., Lai, C.C., Soliman, S.I., Hale, P., Pham, A., Estrada, E.J., et al. (2021). Astrocytes propel neurovascular dysfunction during cerebral cavernous malformation lesion formation. *J Clin Invest* 131(13). doi: 10.1172/JCI139570.

Ma, N., Zhang, J.Z., Itzhaki, I., Zhang, S.L., Chen, H., Haddad, F., et al. (2018). Determining the Pathogenicity of a Genomic Variant of Uncertain Significance Using CRISPR/Cas9 and Human-Induced Pluripotent Stem Cells. *Circulation* 138(23)**,** 2666-2681. doi: 10.1161/CIRCULATIONAHA.117.032273.

Makarova, K.S., Grishin, N.V., Shabalina, S.A., Wolf, Y.I., and Koonin, E.V. (2006). A putative RNA-interference-based immune system in prokaryotes: computational analysis of the predicted enzymatic machinery, functional analogies with eukaryotic RNAi, and hypothetical mechanisms of action. *Biol Direct* 1**,** 7. doi: 10.1186/1745-6150-1-7.

Malinverno, M., Maderna, C., Abu Taha, A., Corada, M., Orsenigo, F., Valentino, M., et al. (2019). Endothelial cell clonal expansion in the development of cerebral cavernous malformations. *Nat Commun* 10(1)**,** 2761. doi: 10.1038/s41467-019-10707-x.

Maroilley, T., and Tarailo-Graovac, M. (2019). Uncovering Missing Heritability in Rare Diseases. *Genes (Basel)* 10(4). doi: 10.3390/genes10040275.

McDonald, D.A., Shi, C., Shenkar, R., Gallione, C.J., Akers, A.L., Li, S., et al. (2014). Lesions from patients with sporadic cerebral cavernous malformations harbor somatic mutations in the CCM genes: evidence for a common biochemical pathway for CCM pathogenesis. *Hum Mol Genet* 23(16)**,** 4357-4370. doi: 10.1093/hmg/ddu153.

Merker, J.D., Wenger, A.M., Sneddon, T., Grove, M., Zappala, Z., Fresard, L., et al. (2018). Long-read genome sequencing identifies causal structural variation in a Mendelian disease. *Genet Med* 20(1)**,** 159-163. doi: 10.1038/gim.2017.86.

Miller, D.E., Sulovari, A., Wang, T., Loucks, H., Hoekzema, K., Munson, K.M., et al. (2021). Targeted long-read sequencing identifies missing disease-causing variation. *Am J Hum Genet* 108(8)**,** 1436-1449. doi: 10.1016/j.ajhg.2021.06.006.

Minami, H., Tashiro, K., Okada, A., Hirata, N., Yamaguchi, T., Takayama, K., et al. (2015). Generation of Brain Microvascular Endothelial-Like Cells from Human Induced Pluripotent Stem Cells by Co-Culture with C6 Glioma Cells. *PLoS One* 10(6)**,** e0128890. doi: 10.1371/journal.pone.0128890.

Mitsuhashi, S., and Matsumoto, N. (2020). Long-read sequencing for rare human genetic diseases. *J Hum Genet* 65(1)**,** 11-19. doi: 10.1038/s10038-019-0671-8.

Mojica, F.J., Ferrer, C., Juez, G., and Rodríguez-Valera, F. (1995). Long stretches of short tandem repeats are present in the largest replicons of the *Archaea Haloferax mediterranei* and *Haloferax volcanii* and could be involved in replicon partitioning. *Mol Microbiol* 17(1)**,** 85-93. doi: 10.1111/j.1365-2958.1995.mmi_17010085.x.

Mondéjar, R., Delgado, M., Solano, F., Izquierdo, G., Martinez-Mir, A., and Lucas, M. (2016). Analysis of *CCM1* expression uncovers novel minor-form exons and variable splicing patterns. *Genes Genom* 38(9)**,** 879-889. doi: 10.1007/s13258-016-0435-1.

Much, C.D., Schwefel, K., Skowronek, D., Shoubash, L., von Podewils, F., Elbracht, M., et al. (2019). Novel Pathogenic Variants in a Cassette Exon of *CCM2* in Patients With Cerebral Cavernous Malformations. *Front Neurol* 10**,** 1219. doi: 10.3389/fneur.2019.01219.

Much, C.D., Sendtner, B.S., Schwefel, K., Freund, E., Bekeschus, S., Otto, O., et al. (2021). Inactivation of Cerebral Cavernous Malformation Genes Results in Accumulation of von Willebrand Factor and Redistribution of Weibel-Palade Bodies in Endothelial Cells. *Front Mol Biosci* 8**,** 622547. doi: 10.3389/fmolb.2021.622547.

Neal, E.H., Marinelli, N.A., Shi, Y., McClatchey, P.M., Balotin, K.M., Gullett, D.R., et al. (2019). A Simplified, Fully Defined Differentiation Scheme for Producing Blood-Brain Barrier Endothelial Cells from Human iPSCs. *Stem Cell Reports* 12(6)**,** 1380-1388. doi: 10.1016/j.stemcr.2019.05.008.

Nguengang Wakap, S., Lambert, D.M., Olry, A., Rodwell, C., Gueydan, C., Lanneau, V., et al. (2020). Estimating cumulative point prevalence of rare diseases: analysis of the Orphanet database. *Eur J Hum Genet* 28(2)**,** 165-173. doi: 10.1038/s41431-019-0508-0.

Otten, P., Pizzolato, G.P., Rilliet, B., and Berney, J. (1989). 131 cases of cavernous angioma (cavernomas) of the CNS, discovered by retrospective analysis of 24,535 autopsies (in French). *Neurochirurgie* 35(2)**,** 82-83, 128-131.

Pagenstecher, A., Stahl, S., Sure, U., and Felbor, U. (2009). A two-hit mechanism causes cerebral cavernous malformations: complete inactivation of CCM1, CCM2 or CCM3 in affected endothelial cells. *Hum Mol Genet* 18(5)**,** 911-918. doi: 10.1093/hmg/ddn420.

Pang, A.W., MacDonald, J.R., Pinto, D., Wei, J., Rafiq, M.A., Conrad, D.F., et al. (2010). Towards a comprehensive structural variation map of an individual human genome. *Genome Biol* 11(5)**,** R52. doi: 10.1186/gb-2010-11-5-r52.

Pilz, R.A., Schwefel, K., Weise, A., Liehr, T., Demmer, P., Spuler, A., et al. (2020). First interchromosomal insertion in a patient with cerebral and spinal cavernous malformations. *Sci Rep* 10(1)**,** 6306. doi: 10.1038/s41598-020-63337-5.

Pilz, R.A., Skowronek, D., Hamed, M., Weise, A., Mangold, E., Radbruch, A., et al. (2022a). Using CRISPR/Cas9 genome editing in human iPSCs for deciphering the pathogenicity of a novel *CCM1* transcription start site deletion. *Front Mol Biosci* 9**,** 953048. doi: 10.3389/fmolb.2022.953048.

Pilz, R.A., Skowronek, D., Mellinger, L., Felbor, U., and Rath, M. (2022b). Endothelial differentiation of *CCM1* knockout iPSCs triggers the establishment of a specific gene expression signature. *Under Review at International Journal of Molecular Sciences*.

Rath, M., Pagenstecher, A., Hoischen, A., and Felbor, U. (2020). Postzygotic mosaicism in cerebral cavernous malformation. *J Med Genet* 57(3)**,** 212-216. doi: 10.1136/jmedgenet-2019-106182.

Rath, M., Schwefel, K., Malinverno, M., Skowronek, D., Leopoldi, A., Pilz, R.A., et al. (2022). Contact-dependent signaling triggers tumor-like proliferation of *CCM3* knockout

endothelial cells in co-culture with wild-type cells. *Cell Mol Life Sci* 79(6)**,** 340. doi: 10.1007/s00018-022-04355-6.

Ren, A.A., Snellings, D.A., Su, Y.S., Hong, C.C., Castro, M., Tang, A.T., et al. (2021). *PIK3CA* and CCM mutations fuel cavernomas through a cancer-like mechanism. *Nature* 594(7862)**,** 271-276. doi: 10.1038/s41586-021-03562-8.

Riant, F., Cecillon, M., Saugier-Veber, P., and Tournier-Lasserve, E. (2013). CCM molecular screening in a diagnosis context: novel unclassified variants leading to abnormal splicing and importance of large deletions. *Neurogenetics* 14(2)**,** 133-141. doi: 10.1007/s10048-013-0362-0.

Ricci, C., Riolo, G., and Battistini, S. (2021). Molecular genetic analysis of cerebral cavernous malformations: an update. *Vessel Plus* 5**,** 31. doi: 10.20517/2574-1209.2021.28.

Richards, S., Aziz, N., Bale, S., Bick, D., Das, S., Gastier-Foster, J., et al. (2015). Standards and guidelines for the interpretation of sequence variants: a joint consensus recommendation of the American College of Medical Genetics and Genomics and the Association for Molecular Pathology. *Genet Med* 17(5)**,** 405-424. doi: 10.1038/gim.2015.30.

Rossi, A., Kontarakis, Z., Gerri, C., Nolte, H., Hölper, S., Krüger, M., et al. (2015). Genetic compensation induced by deleterious mutations but not gene knockdowns. *Nature* 524(7564)**,** 230-233. doi: 10.1038/nature14580.

Rouf, M.A., Wen, L., Mahendra, Y., Wang, J., Zhang, K., Liang, S., et al. (2022). The recent advances and future perspectives of genetic compensation studies in the zebrafish model. *Genes & Diseases*. doi: https://doi.org/10.1016/j.gendis.2021.12.003.

Sahoo, T., Johnson, E.W., Thomas, J.W., Kuehl, P.M., Jones, T.L., Dokken, C.G., et al. (1999). Mutations in the gene encoding KRIT1, a Krev-1/rap1a binding protein, cause cerebral cavernous malformations (*CCM1*). *Hum Mol Genet* 8(12)**,** 2325-2333. doi: 10.1093/hmg/8.12.2325.

Sanchis-Juan, A., Stephens, J., French, C.E., Gleadall, N., Mégy, K., Penkett, C., et al. (2018). Complex structural variants in Mendelian disorders: identification and breakpoint resolution using short- and long-read genome sequencing. *Genome Med* 10(1)**,** 95. doi: 10.1186/s13073-018-0606-6.

Sander, J.D., and Joung, J.K. (2014). CRISPR-Cas systems for editing, regulating and targeting genomes. *Nat Biotechnol* 32(4)**,** 347-355. doi: 10.1038/nbt.2842.

Schwefel, K., Spiegler, S., Ameling, S., Much, C.D., Pilz, R.A., Otto, O., et al. (2019). Biallelic *CCM3* mutations cause a clonogenic survival advantage and endothelial cell stiffening. *J Cell Mol Med* 23(3)**,** 1771-1783. doi: 10.1111/jcmm.14075.

Schwefel, K., Spiegler, S., Kirchmaier, B.C., Dellweg, P.K.E., Much, C.D., Pané-Farré, J., et al. (2020). Fibronectin rescues aberrant phenotype of endothelial cells lacking either CCM1, CCM2 or CCM3. *FASEB J* 34(7)**,** 9018-9033. doi: 10.1096/fj.201902888R.

Shenkar, R., Shi, C., Rebeiz, T., Stockton, R.A., McDonald, D.A., Mikati, A.G., et al. (2015). Exceptional aggressiveness of cerebral cavernous malformation disease associated with *PDCD10* mutations. *Genet Med* 17(3)**,** 188-196. doi: 10.1038/gim.2014.97.

Singh, A.K., Olsen, M.F., Lavik, L.A.S., Vold, T., Drabløs, F., and Sjursen, W. (2021). Detecting copy number variation in next generation sequencing data from diagnostic gene panels. *BMC Med Genomics* 14(1)**,** 214. doi: 10.1186/s12920-021-01059-x.

Skowronek, D., Pilz, R.A., Bonde, L., Schamuhn, O.J., Feldmann, J.L., Hoffjan, S., et al. (2022). Cas9-mediated nanopore sequencing enables precise characterization of structural variants in *CCM1*, *CCM2*, and *CCM3*. *Under Review at International Journal of Molecular Sciences*.

Skowronek, D., Pilz, R.A., Schwefel, K., Much, C.D., Felbor, U., and Rath, M. (2021). Bringing CCM into a dish: cell culture models for cerebral cavernous malformations. *Med Genet* 33(3)**,** 251-259. doi: doi:10.1515/medgen-2021-2091.

Snellings, D.A., Hong, C.C., Ren, A.A., Lopez-Ramirez, M.A., Girard, R., Srinath, A., et al. (2021). Cerebral Cavernous Malformation: From Mechanism to Therapy. *Circ Res* 129(1)**,** 195-215. doi: 10.1161/CIRCRESAHA.121.318174.

Spiegler, S., Najm, J., Liu, J., Gkalympoudis, S., Schröder, W., Borck, G., et al. (2014). High mutation detection rates in cerebral cavernous malformation upon stringent inclusion criteria: one-third of probands are minors. *Mol Genet Genomic Med* 2(2)**,** 176-185. doi: 10.1002/mgg3.60.

Spiegler, S., Rath, M., Hoffjan, S., Dammann, P., Sure, U., Pagenstecher, A., et al. (2018a). First large genomic inversion in familial cerebral cavernous malformation identified by whole genome sequencing. *Neurogenetics* 19(1)**,** 55-59. doi: 10.1007/s10048-017-0531-7.

Spiegler, S., Rath, M., Paperlein, C., and Felbor, U. (2018b). Cerebral Cavernous Malformations: An Update on Prevalence, Molecular Genetic Analyses, and Genetic Counselling. *Mol Syndromol* 9(2)**,** 60-69. doi: 10.1159/000486292.

Spielmann, M., Lupiáñez, D.G., and Mundlos, S. (2018). Structural variation in the 3D genome. *Nat Rev Genet* 19(7)**,** 453-467. doi: 10.1038/s41576-018-0007-0.

Stockton, R.A., Shenkar, R., Awad, I.A., and Ginsberg, M.H. (2010). Cerebral cavernous malformations proteins inhibit Rho kinase to stabilize vascular integrity. *J Exp Med* 207(4)**,** 881-896. doi: 10.1084/jem.20091258.

The 1000 Genomes Project Consortium (2015). A global reference for human genetic variation. *Nature* 526(7571)**,** 68-74. doi: 10.1038/nature15393.

Vinkšel, M., Writzl, K., Maver, A., and Peterlin, B. (2021). Improving diagnostics of rare genetic diseases with NGS approaches. *J Community Genet* 12(2)**,** 247-256. doi: 10.1007/s12687-020-00500-5.

Weischenfeldt, J., Symmons, O., Spitz, F., and Korbel, J.O. (2013). Phenotypic impact of genomic structural variation: insights from and for human disease. *Nat Rev Genet* 14(2)**,** 125-138. doi: 10.1038/nrg3373.

Wevers, N.R., Kasi, D.G., Gray, T., Wilschut, K.J., Smith, B., van Vught, R., et al. (2018). A perfused human blood-brain barrier on-a-chip for high-throughput assessment of barrier function and antibody transport. *Fluids Barriers CNS* 15(1)**,** 23. doi: 10.1186/s12987-018-0108-3.

Wimmer, R.A., Leopoldi, A., Aichinger, M., Kerjaschki, D., and Penninger, J.M. (2019). Generation of blood vessel organoids from human pluripotent stem cells. *Nat Protoc* 14(11)**,** 3082-3100. doi: 10.1038/s41596-019-0213-z.

Wüstehube, J., Bartol, A., Liebler, S.S., Brütsch, R., Zhu, Y., Felbor, U., et al. (2010). Cerebral cavernous malformation protein CCM1 inhibits sprouting angiogenesis by activating DELTA-NOTCH signaling. *Proc Natl Acad Sci U S A* 107(28)**,** 12640-12645. doi: 10.1073/pnas.1000132107.

Yau, A.C.Y., Globisch, M.A., Onyeogaziri, F.C., Conze, L.L., Smith, R., Jauhiainen, S., et al. (2022). Inflammation and neutrophil extracellular traps in cerebral cavernous malformation. *Cell Mol Life Sci* 79(4)**,** 206. doi: 10.1007/s00018-022-04224-2.

Zhou, Z., Tang, A.T., Wong, W.Y., Bamezai, S., Goddard, L.M., Shenkar, R., et al. (2016). Cerebral cavernous malformations arise from endothelial gain of MEKK3-KLF2/4 signalling. *Nature* 532(7597)**,** 122-126. doi: 10.1038/nature17178.

Zhu, Y., Wu, Q., Xu, J.F., Miller, D., Sandalcioglu, I.E., Zhang, J.M., et al. (2010). Differential angiogenesis function of *CCM2* and *CCM3* in cerebral cavernous malformations. *Neurosurg Focus* 29(3)**,** E1. doi: 10.3171/2010.5.FOCUS1090.

5 Originalarbeiten

5.1 First interchromosomal insertion in a patient with cerebral and spinal cavernous malformations

Robin A. Pilz, Konrad Schwefel, Anja Weise, Thomas Liehr, Philipp Demmer, Andreas Spuler, Stefanie Spiegler, Eberhard Gilberg, Christian A. Hübner, Ute Felbor, Matthias Rath

Sci Rep. 2020; 10(1):6306

https://doi.org/10.1038/s41598-020-63337-5

www.nature.com/scientificreports

SCIENTIFIC REPORTS
nature research

OPEN

First interchromosomal insertion in a patient with cerebral and spinal cavernous malformations

Robin A. Pilz[1], Konrad Schwefel[1], Anja Weise[2], Thomas Liehr[2], Philipp Demmer[3], Andreas Spuler[4], Stefanie Spiegler[1], Eberhard Gilberg[1], Christian A. Hübner[2], Ute Felbor[1] & Matthias Rath[1*]

Autosomal dominant cerebral cavernous malformations (CCM) are leaky vascular lesions that can cause epileptic seizures and stroke-like symptoms. Germline mutations in either *CCM1*, *CCM2* or *CCM3* are found in the majority of patients with multiple CCMs or a positive family history. Recently, the first copy number neutral inversion in *CCM2* has been identified by whole genome sequencing in an apparently mutation-negative CCM family. We here asked the question whether further structural genomic rearrangements can be detected within NGS gene panel data of unsolved CCM cases. Hybrid capture NGS data of eight index patients without a pathogenic single nucleotide, indel or copy number variant were analyzed using two bioinformatics pipelines. In a 58-year-old male with multiple CCMs in his brain and spinal cord, we identified a 294 kb insertion within the coding sequence of *CCM2*. Fine mapping of the breakpoints, molecular cytogenetic studies, and multiplex ligation-dependent probe amplification verified that the structural variation was an inverted unbalanced insertion that originated from 1p12-p11.2. As this rearrangement disrupts exon 6 of *CCM2* on 7p13, it was classified as pathogenic. Our study demonstrates that efforts to detect structural variations in known disease genes increase the diagnostic sensitivity of genetic analyses for well-defined Mendelian disorders.

Cerebral cavernous malformations (CCM; MIM: 116860, 603284, 603285) are irregular clusters of enlarged and thin-walled vessels that can present as sporadic or autosomal dominant cerebrovascular disease. Aside from epileptic seizures and headaches, CCM patients may present with stroke-like symptoms due to chronic or acute bleeding events[1]. Pathogenic germline variants have been identified in *CCM1* (also known as *KRIT1*)[2,3], *CCM2*[4,5], and *CCM3* (*PDCD10*)[6]. The mutational spectrum primarily includes nonsense, frameshift, splice, and copy number variants (CNVs). 282 unique *CCM1*, 84 *CCM2* and 75 *CCM3* variants are classified as disease-causing in the Human Gene Mutation Database (HGMD Professional 2019.3)[7]. Depending on the inclusion criteria for genetic analyses, mutation detection rates of 87 to 98% have been reported for familial CCM cases and up to 60% for sporadic ones[8–11]. The mutation detection rate in the latter group could even be higher if patients with associated developmental venous anomalies or a history of radiotherapy to the brain were excluded[1,12]. Although pathogenic variants in a yet unknown *CCM4* candidate gene have been discussed for unresolved cases[13], we recently were able to identify the first copy number neutral inversion in *CCM2* in an apparently mutation-negative CCM family by whole genome sequencing (WGS)[14].

Disease-causing structural variants (SVs) may explain a part of the "missing heritability" in rare diseases[15]. SVs are defined as structural and quantitative chromosomal rearrangements that compromise cytogenetically visible and submicroscopic variants[16,17]. They contribute to phenotypic variation but can also cause human disease[17]. In fact, rare SVs are even more likely to be deleterious than rare single nucleotide variants (SNVs)[18,19]. Deletions, duplications, insertions, translocations, and inversions may directly disrupt the organization of a disease gene or affect its transcriptional regulation by positional effects[16,17]. Using a multi-platform WGS approach, Chaisson and colleagues have demonstrated in 2019 that more than 27,000 SVs (≥50 bp) can be found per human genome[20]. In contrast, an individual human genome harbors approximately 4,000,000 to 5,000,000 SNVs and up to 800,000

[1]Department of Human Genetics, University Medicine Greifswald, and Interfaculty Institute of Genetics and Functional Genomics, University of Greifswald, Greifswald, Germany. [2]Institute of Human Genetics, Jena University Hospital, Friedrich Schiller University, Jena, Germany. [3]Institute of Medical Diagnostics, IMD Potsdam, Potsdam, Germany. [4]Department of Neurosurgery, Helios Hospital Berlin Buch, Berlin, Germany. *email: matthias.rath@med.uni-greifswald.de

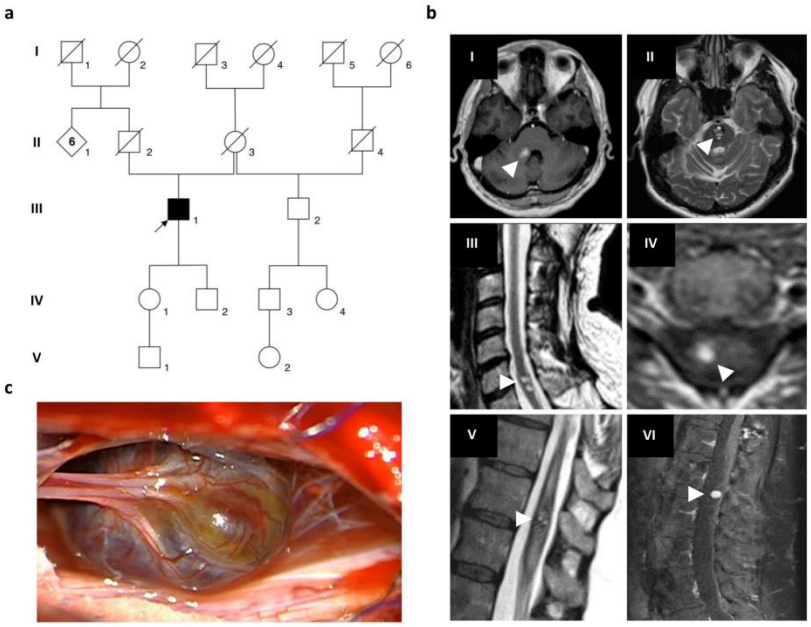

Figure 1. Multiple cerebral and spinal cavernomas in a sporadic CCM patient. (**a**) Pedigree of the CCM index case from pedigree 1 (III:1, arrow). (**b**) Repetitive magnetic resonance imaging (MRI) of the index patient's brain and spinal cord showing progression of CCM disease with two cavernous malformations in the pons (I, II), intramedullary lesions in the cervical (III, IV) and thoracic spinal cord (V) as well as a CCM in the cauda equina (VI). MRI images were acquired between 2005 and 2019. White arrowheads indicate CCMs. (**c**) Intraoperative photograph of the cauda equina cavernous malformation.

indels, which are defined as insertions or deletions with a length of up to 49 bp[18]. However, the identification of SVs remains much more challenging than SNV or indel calling in a diagnostic setting. While deletions and duplications of exonic sequences can be reliably detected with qPCR, multiplex ligation-dependent probe amplification or NGS-based CNV detection algorithms, copy number neutral SVs or deletions and duplications in non-coding regions of known disease-associated genes may escape targeted genetic approaches.

In this study, we have analyzed the hybrid capture NGS gene panel data of eight genetically unresolved CCM index patients for the presence of SVs in *CCM1*, *CCM2* or *CCM3*. An interchromosomal insertion which led to an interruption of exon 6 of the *CCM2* gene was identified in a sporadic CCM patient.

Results

Clinical findings. The male index patient III:1 (pedigree 1, Fig. 1a) was referred to genetic counselling at the age of 58 years because of multiple symptomatic CCMs. Magnetic resonance imaging (MRI) documented at least nine cavernous lesions with surrounding hemosiderin deposits in his brain and spinal cord (Fig. 1b). One brainstem cavernoma and three CCMs in his thoracic, cervical, and lumbar spine had already been resected because of acute bleeding events at the age of 44, 50, and 58, respectively (Fig. 1c, Supplementary Video S1). The index patient also reported an atrial septal defect and a traumatic L1 vertebral body fracture at the age of 55 years which had been treated with balloon kyphoplasty. On physical examination, he presented a partial loss of vibration and fine touch sensation below the level of T10 and impaired sensation of temperature on the contralateral side. In addition, he had an ataxic gait with right foot drop. The index patient's father (II:2) died of gastric cancer when he was 72 years old. Cavernous lesions or neurological symptoms that would be suggestive for CCM had not been documented for him. The mother of the index patient (II:3) passed away at the age of 90 years with no signs of CCM either. Both children (IV:1 and IV:2) are healthy, and there were no other relatives who had CCMs or reported epileptic seizures, stroke-like symptoms or chronic headaches.

Identification of an interchromosomal insertion. Gene panel sequencing of *CCM1*, *CCM2*, and *CCM3* for index patient III:1 (Fig. 1) and routine bioinformatics analyses identified no pathogenic SNV, indel or CNV. However, a high number of split reads in *CCM2* was noticed in NGS gene panel data of this proband. These deviant reads could be grouped into two clusters based on their mapping. Reads of the first group mapped with one part to the 5' half of exon 6 of *CCM2*, which is located on 7p13, and with the other part to 1p11.2 or 1q21.1. Due

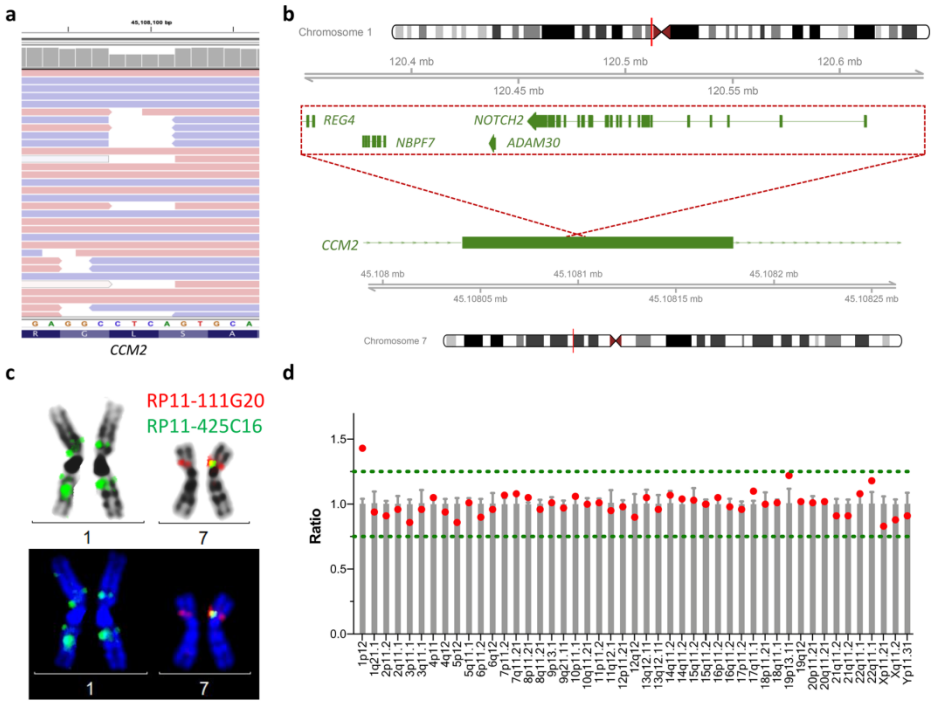

Figure 2. Identification of an unbalanced interchromosomal insertion in *CCM2*. (**a**) Read alignment of the hybrid capture NGS data of III:1. Shown is a part of exon 6 of the *CCM2* gene. The coverage plot indicated significantly reduced read depths at positions [hg19] chr7:45,108,098-45,108,101 but no reads were found that covered a deletion of 4 bp. (**b**) Schematic depiction of the identified interchromosomal insertion. Material from 1p12-p11.2 was found as an inverted insertion in exon 6 of the *CCM2* gene on 7p13. (**c**) Verification of the chromosomal rearrangement [46,XY.ish ins(7;1)(p13;1p11)(RP11-425C16+,RP11-111G2 +)] by fluorescence *in situ* hybridization. There is a known crosshybridization of the applied probe RP11–425C16 in 1q21.1, which does not need to be considered further taking into account all other data presented here. (**d**) MLPA analysis of the centromere region of chromosome 1 indicated three copies of the *NOTCH2* gene (1p12) which is part of the inserted fragment.

to known sequence homologies, aberrant mapping on chromosome 1 could not be further specified. Split reads of the second group partially mapped to the 3′ half of *CCM2* exon 6 but also to 1p12. Notably, detection of deviant reads required the SeqNext module of the Sequence Pilot tool for mapping and alignment. Using the mapping and alignment information of the MiSeq Reporter Software resulted in significantly reduced read depth at positions [hg19] chr7:45,108,098-45,108,101. However, split reads were filtered out by SeqNext and no variant was called since there were no reads that covered a heterozygous deletion of these four nucleotides (Fig. 2a).

Based on the NGS data of index patient III:1, we suspected an interchromosomal insertion from 1p12-p11.2 into the coding region of *CCM2* on 7p13 (Fig. 2b). This rearrangement was finally made visible by fluorescence *in situ* hybridization (FISH) on metaphase chromosomes from cultured blood lymphocytes of the index patient (Fig. 2c). The inserted fragment covers a genomic region of 294 kb that contains the complete *NOTCH2* (MIM: 600275), *ADAM30* (604779), and *NBPF7* (613997) genes as well as parts of *REG4* (609846). MLPA analysis with a centromere kit further indicated the presence of three copies of *NOTCH2* which is the only gene in the inserted fragment with an associated phenotype (Fig. 2d). Loss-of-function mutations and pathogenic missense variants in this gene have been reported in patients with Alagille (MIM: 610205) and Hajdu-Cheney syndrome (102500). However, the index patient did not meet the clinical diagnostic criteria of either syndrome.

Fine mapping of the breakpoints. We next amplified the breakpoints of the interchromosomal insertion for its precise molecular characterization. Sanger sequencing allowed us to fine map the breakpoints to [hg19] chr1:120,347,265, chr1:120,641,440, and chr7:45,108,098–45,108,101, respectively. It also verified that the fragment of 1p12-p11.2 was inserted in an inverted orientation on 7p13 and flanked by a small insertion and a deletion-insertion variant in which the four base pairs with reduced sequencing depths were replaced by six

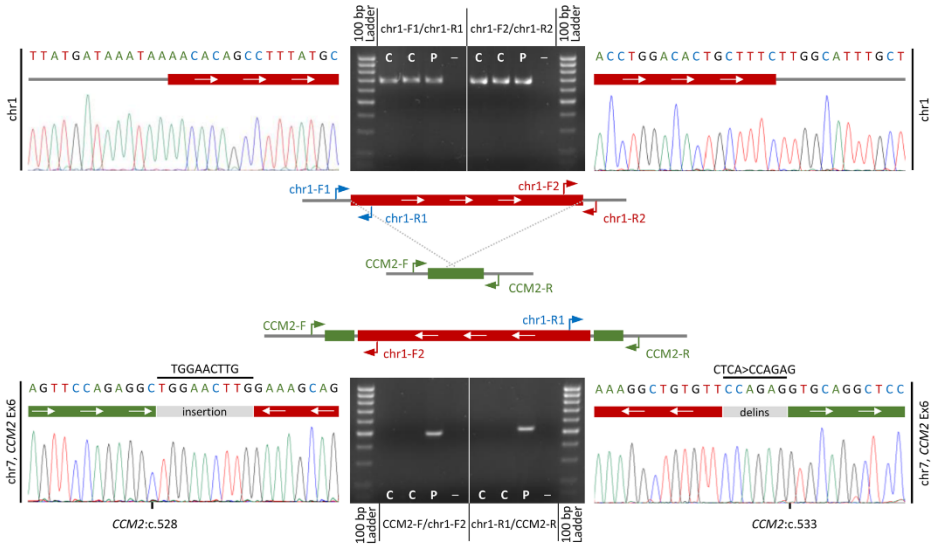

Figure 3. Fine mapping of the breakpoints by Sanger sequencing. Scheme of the normal and inverted insertion alleles (middle panel). PCR and sequencing primers (chr1: chr1-F1 + R1 and chr1-F2 + R2; chr7: CCM2-F + R) are depicted as blue, red, and green arrows, respectively. PCR products and chromatograms of the normal allele on chr1 (chr1-F1/R1 and chr1-F2/R2) are depicted in the upper panel. PCR products and chromatograms of the inverted insertion on chr7 (CCM2-F/chr1-F2 and chr1-R1/CCM2-R) are depicted in the lower panel. Fine mapping also revealed an additional small insertion and an indel variant at the breakpoints. C = healthy control; P = index patient; – = negative control; Ex = exon.

nucleotides of unknown origin (Fig. 3). While the breakpoint on 1p11.2 locates within a long interspersed nuclear element (LINE), no repeat elements were found in close proximity to the breakpoints on 1p12 or 7p13. As the heterozygous SV interrupts exon 6 of the *CCM2* gene, it was classified as pathogenic for CCM. In summary, the results of our molecular, cytogenetic, and molecular cytogenetic studies demonstrated that index patient III:1 is a heterozygous carrier of a submicroscopic, unbalanced, interchromosomal, and inverted insertion.

Screening for SVs in mutation-negative CCM patients. We finally wanted to know if SVs can also be identified in the hybrid capture NGS data of seven additional CCM patients without any pathogenic SNV, indel or CNV in *CCM1*, *CCM2* or *CCM3* that had been analyzed between 2017 and 2019 (Supplementary Table S1). Therefore, we chose the Agilent SureCall tool, which allowed us to search for translocation events based on the presence of split reads in their NGS data. The index patient III:1 from family 1 was used as a positive control. The tool precisely re-identified his SV but did not detect any further chromosomal rearrangements in the other CCM cases. Furthermore, no split reads were found by visual inspection of their NGS data.

Discussion

In this study, we have identified the first interchromosomal insertion, sometimes also referred to as interchromosomal insertional translocation (IT), in a CCM patient. Notably, current genetic analysis cannot clarify the molecular basis of CCM disease in 2 to 13% of familial cases and up to 40% of sporadic CCM patients[1]. Besides phenocopies, somatic mosaicism and pathogenic variants in an unknown *CCM4* gene or non-coding regions of *CCM1*, *CCM2* or *CCM3* have been discussed as possible explanations for these patients[21–23]. However, the identification of an interchromosomal insertion in one of eight unsolved CCM cases and the copy number neutral inversion in *CCM2*, that we have reported recently[14], demonstrate that SVs also need to be considered. It is remarkable that both rearrangements identified so far have been detected in *CCM2* which is the largest of the three CCM genes. However, future studies will have to show whether *CCM2* is more susceptible to the occurrence of SVs or whether further genomic rearrangements can be detected in *CCM1* and *CCM3* with more sensitive techniques.

ITs and other SVs have a higher prevalence than previously thought[20,24,25]. FISH confirmation and parental follow-up studies of CNVs that had been identified by clinical array comparative genomic hybridization (aCGH) analysis revealed that ITs can be found in approximately 1 of 500 patients referred to aCGH analysis[24]. This observation suggests that their prevalence might also be underestimated in patients with CCM or other inherited disorders for whom aCGH is not part of standard genetic analyses. Sophisticated bioinformatics algorithms have been developed to identify SVs from short-read NGS data based on inconsistent paired-end mapping, the

presence of split reads or changes in read depth[26,27]. While CNVs can be efficiently detected with NGS-based approaches, inversions and ITs that do not cause gain or loss in the number of *CCM1*, *CCM2* or *CCM3* alleles might be regularly missed with targeted gene panel sequencing. Furthermore, the analytical sensitivity of the available bioinformatics tools is still incomplete. Notably, only one of the two tools that were used for mapping and alignment in our current study allowed us to detect aberrant reads in the NGS data analysis for the index patient from pedigree 1.

The search for chromosomal rearrangements is becoming more and more important in genetic research projects that try to solve undiagnosed cases with rare diseases. While the detection of ITs within the coding region of a gene seems to be relatively straightforward with special bioinformatics tools and filter criteria, insertions into intronic, promotor or cis-regulatory regions that can also impair gene regulation[16] can hardly ever be detected with PCR- or hybrid capture-based target enrichment strategies and short-read sequencing. Recently, short-read WGS and a new bioinformatics pipeline revealed disease-causing SVs in 16 out of 477 patients of the Undiagnosed Diseases Network (UDN)[28]. However, third-generation sequencing technologies will probably further improve the diagnostic sensitivity for the identification of chromosomal rearrangements as the probability of spanning the whole SV and the mappability in repetitive regions are higher for long reads[29,30]. In a cohort of 1,324 undiagnosed probands with rare diseases from the NIHR BioResource research study, three cases with a complex pathogenic SV were identified by short-read WGS and a duplication-inversion-duplication event of unknown clinical significance was resolved in another proband by long-read sequencing[31]. Whole genome long-read sequencing also identified a heterozygous ~2.2 kb deletion in *PRKAR1A* which is a known disease gene for autosomal dominant Carney complex in a patient with multiple tumours for whom initial targeted *PRKAR1A* sequencing and short-read WGS had not revealed any pathogenic variant[32]. Several other examples illustrate that long-read sequencing enables effective SV calling and could help to solve undiagnosed cases[33]. Therefore, long-read WGS is a promising next step for the yet unsolved CCM cases of our cohort. These have already been checked for CNVs in *CCM1*, *CCM2*, and *CCM3* but third-generation sequencing technologies would allow the detection of CNVs and copy number neutral SVs in a genome-wide approach. Nevertheless, the combination of multiple sequencing technologies might be still necessary to achieve sufficient insertion and inversion detection sensitivities[20].

The identification of a pathogenic SNV, indel, CNV or SV is essential for genetic counselling of CCM families and always raises the question whether it is an inherited or a *de novo* variant. As both parents of the index patient from pedigree 1 died without CCMs, epileptic seizures or stroke-like symptoms, one might speculate that his SV is a *de novo* mutation. In line with this hypothesis, a recent analysis of the Genome Aggregation Database (gnomAD) Consortium suggested a *de novo* mutation rate of 0.35 SVs per generation (95% confidence interval: 0.18–0.52)[25]. Given that a significant number of SVs might have been missed with short-read WGS, this projection likely underestimates the real number of *de novo* SVs per genome. However, we can also not exclude a cryptic inherited case in pedigree 1 since the penetrance of CCM is incomplete and up to 45% of *CCM2* mutation carriers remain asymptomatic[9]. Indeed, Nowakowska and colleagues demonstrated that a significant number of apparently *de novo*, interstitial CNVs that had been found in patients with multiple congenital anomalies or mental retardation were actually the result of an unbalanced transmission of a derivative chromosome from one parent with a balanced insertional translocation[34]. Furthermore, the transmission from an obviously unaffected parent that carries the same unbalanced rearrangement as its affected child has also been reported[24]. Unfortunately, DNA samples of the index patient's parents were not available and there were no other affected family members to address the origin of the chromosomal rearrangement or to demonstrate co-segregation of the SV and CCM disease.

In conclusion, our study adds the first interchromosomal insertion to the *CCM* mutation spectrum and suggests that hard-to-detect SVs might account for more CCM cases than previously thought. Together with other literature reports of copy number neutral chromosomal rearrangements in known disease genes[14,35,36], our results support the hypothesis that efforts to detect SVs might be more promising than the search for novel candidate genes for well-defined Mendelian disorders.

Methods

Study population and ethical considerations. Genomic DNA was isolated from peripheral blood lymphocytes of all study participants with written informed consent using the NucleoSpin Blood L Kit according to the manufacturer's instructions (Macherey-Nagel, Düren, Germany). A Qubit 2.0 Fluorometer (Thermo Fisher Scientific, Waltham, USA) was used to measure DNA concentrations before NGS target enrichment. DNA purity was determined on a NanoPhotometer instrument (Implen, München, Germany). All procedures performed in this study involving human participants were in accordance with the 1964 Helsinki declaration and its later amendments.The study protocol was approved by the local ethics committee of the University Medicine Greifswald (BB 047/14) and written informed consent was obtained from index patient III:1 to publish the medical information and images that are presented here.

Target enrichment, next-generation sequencing, and bioinformatics analyses. All exons (±20 bp) of *CCM1* (Locus Reference Genomic sequence: LRG_650t1), *CCM2* (LRG_664t2), and *CCM3* (LRG_651t1) were defined as target regions for NGS gene panel analysis. A Nextera Rapid Capture Custom Enrichment Kit (Panel ID: 113402; Illumina, San Diego, USA) or an Agilent SureSelect custom library (Panel ID: 3152261, Agilent Technologies, Santa Clara, USA) and a SureSelect Reagent Kit (Agilent Technologies) were used for target enrichment and library preparation according to the manufacturers' instructions, respectively. Pre- and post-capture libraries were analyzed on a 2100 Bioanalyzer instrument (Agilent Technologies). Indexed libraries were pooled and sequenced on a MiSeq instrument (Illumina) as 2 × 150 bp paired-read runs. The MiSeq Reporter Software (Illumina) was used for demultiplexing and FASTQ file generation. Mapping and alignment

were independently performed for each sample with the MiSeq Reporter Software and the SeqNext module of the Sequence Pilot software (JSI medical systems, Ettenheim, Germany). The SeqNext module was also used in a read depth-based approach to identify CNVs in *CCM1*, *CCM2*, and *CCM3* as described previously[37]. BAM files that had been generated with the MiSeq Reporter Software were further analyzed for translocation events with the SureCall 4.1.1.5 software (Agilent Technologies), and aligned reads were grouped by the mate chromosome in the Integrative Genomics Viewer[38].

Sanger sequencing and multiplex ligation-dependent probe amplification. Specific primer pairs were designed to amplify the suspected breakpoints of a novel interchromosomal insertion identified in *CCM2*. Primer sequences are available upon request. PCR products were purified with the ExoSAP-IT Cleanup Reagent (Thermo Fisher Scientific). Sanger sequencing was performed on a SeqStudio Genetic Analyzer (Thermo Fisher Scientific) following established protocols. The SALSA MLPA P181-B1 Centromere mix 1 (MRC-Holland, Amsterdam, The Netherlands) was used according to the manufacturer's instructions to determine copy number variations of a part of the *NOTCH2* gene (MIM: 600275) which is located on chromosome 1p12 (hg19: 120,454,176–120,612,317).

Chromosome analysis and molecular cytogenetic studies. Karyotyping was performed following standard procedures on metaphases obtained from PHA stimulated blood lymphocytes. Fluorescence *in situ* hybridization (FISH) was used to confirm the interchromosomal insertion using standard protocols. The following BAC clones were used: RP11–425C16 in 1p12 (hg19: 120,176,963–120,358,983) and RP11–111G20 in 7p12.3~13 (hg19: 45,283,437–45,448,789).

Ethical approval. All procedures performed in this study involving human participants were in accordance with the ethical standards of the institutional and/or national research committee (University Medicine Greifswald; BB 047/14) and with the 1964 Helsinki declaration and its later amendments or comparable ethical standards.

Data availability

All relevant data generated or analysed during this study are included in this published article and its supplementary information files.

Received: 7 January 2020; Accepted: 30 March 2020;
Published online: 14 April 2020

References

1. Spiegler, S., Rath, M., Paperlein, C. & Felbor, U. Cerebral cavernous malformations: an update on prevalence, molecular genetic analyses, and genetic counselling. *Mol. Syndromol.* **9**, 60–69, https://doi.org/10.1159/000486292 (2018).
2. Laberge-le Couteulx, S. *et al.* Truncating mutations in *CCM1*, encoding KRIT1, cause hereditary cavernous angiomas. *Nat. Genet.* **23**, 189–193, https://doi.org/10.1038/13815 (1999).
3. Sahoo, T. *et al.* Mutations in the gene encoding KRIT1, a Krev-1/rap1a binding protein, cause cerebral cavernous malformations (*CCM1*). *Hum. Mol. Genet.* **8**, 2325–2333, https://doi.org/10.1093/hmg/8.12.2325 (1999).
4. Liquori, C. L. *et al.* Mutations in a gene encoding a novel protein containing a phosphotyrosine-binding domain cause type 2 cerebral cavernous malformations. *Am. J. Hum. Genet.* **73**, 1459–1464, https://doi.org/10.1086/380314 (2003).
5. Denier, C. *et al.* Mutations within the *MGC4607* gene cause cerebral cavernous malformations. *Am. J. Hum. Genet.* **74**, 326–337, https://doi.org/10.1086/381718 (2004).
6. Bergametti, F. *et al.* Mutations within the *programmed cell death 10* gene cause cerebral cavernous malformations. *Am. J. Hum. Genet.* **76**, 42–51, https://doi.org/10.1086/426952 (2005).
7. Stenson, P. D. *et al.* The Human Gene Mutation Database: towards a comprehensive repository of inherited mutation data for medical research, genetic diagnosis and next-generation sequencing studies. *Hum. Genet.* **136**, 665–677, https://doi.org/10.1007/s00439-017-1779-6 (2017).
8. Spiegler, S. *et al.* High mutation detection rates in cerebral cavernous malformation upon stringent inclusion criteria: one-third of probands are minors. *Mol. Genet. Genomic Med.* **2**, 176–185, https://doi.org/10.1002/mgg3.60 (2014).
9. Denier, C. *et al.* Genotype-phenotype correlations in cerebral cavernous malformations patients. *Ann. Neurol.* **60**, 550–556, https://doi.org/10.1002/ana.20947 (2006).
10. Stahl, S. *et al.* Novel *CCM1*, *CCM2*, and *CCM3* mutations in patients with cerebral cavernous malformations: in-frame deletion in *CCM2* prevents formation of a CCM1/CCM2/CCM3 protein complex. *Hum. Mutat.* **29**, 709–717, https://doi.org/10.1002/humu.20712 (2008).
11. Cigoli, M. S. *et al. PDCD10* gene mutations in multiple cerebral cavernous malformations. *PLoS One* **9**, e110438, https://doi.org/10.1371/journal.pone.0110438 (2014).
12. Akers, A. *et al.* Synopsis of guidelines for the clinical management of cerebral cavernous malformations: consensus recommendations based on systematic literature review by the Angioma Alliance Scientific Advisory Board Clinical Experts Panel. *Neurosurgery* **80**, 665–680, https://doi.org/10.1093/neuros/nyx091 (2017).
13. Liquori, C. L. *et al.* Low frequency of *PDCD10* mutations in a panel of *CCM3* probands: potential for a fourth *CCM* locus. *Hum. Mutat.* **27**, 118, https://doi.org/10.1002/humu.9389 (2006).
14. Spiegler, S. *et al.* First large genomic inversion in familial cerebral cavernous malformation identified by whole genome sequencing. *Neurogenetics* **19**, 55–59, https://doi.org/10.1007/s10048-017-0531-7 (2018).
15. Maroilley, T. & Tarailo-Graovac, M. Uncovering missing heritability in rare diseases. *Genes (Basel)* **10**, https://doi.org/10.3390/genes10040275 (2019).
16. Spielmann, M., Lupianez, D. G. & Mundlos, S. Structural variation in the 3D genome. *Nat. Rev. Genet.* **19**, 453–467, https://doi.org/10.1038/s41576-018-0007-0 (2018).
17. Feuk, L., Marshall, C. R., Wintle, R. F. & Scherer, S. W. Structural variants: changing the landscape of chromosomes and design of disease studies. *Hum. Mol. Genet.* **15**(Spec No 1), R57–66, https://doi.org/10.1093/hmg/ddl057 (2006).
18. Eichler, E. E. Genetic variation, comparative genomics, and the diagnosis of disease. *N. Engl. J. Med.* **381**, 64–74, https://doi.org/10.1056/NEJMra1809315 (2019).
19. Chiang, C. *et al.* The impact of structural variation on human gene expression. *Nat. Genet.* **49**, 692–699, https://doi.org/10.1038/ng.3834 (2017).

20. Chaisson, M. J. P. *et al.* Multi-platform discovery of haplotype-resolved structural variation in human genomes. *Nat. Commun.* **10**, 1784, https://doi.org/10.1038/s41467-018-08148-z (2019).
21. Batra, S., Lin, D., Recinos, P. F., Zhang, J. & Rigamonti, D. Cavernous malformations: natural history, diagnosis and treatment. *Nat. Rev. Neurol.* **5**, 659–670, https://doi.org/10.1038/nrneurol.2009.177 (2009).
22. Riant, F. *et al.* Deep intronic KRIT1 mutation in a family with clinically silent multiple cerebral cavernous malformations. *Clin. Genet.* **86**, 585–588, https://doi.org/10.1111/cge.12322 (2014).
23. McDonald, D. A. *et al.* Lesions from patients with sporadic cerebral cavernous malformations harbor somatic mutations in the CCM genes: evidence for a common biochemical pathway for CCM pathogenesis. *Hum. Mol. Genet.* **23**, 4357–4370, https://doi.org/10.1093/hmg/ddu153 (2014).
24. Kang, S. H. *et al.* Insertional translocation detected using FISH confirmation of array-comparative genomic hybridization (aCGH) results. *Am. J. Med. Genet. A* **152A**, 1111–1126, https://doi.org/10.1002/ajmg.a.33278 (2010).
25. Collins, R. L. *et al.* An open resource of structural variation for medical and population genetics. bioRxiv, 578674, https://doi.org/10.1101/578674 (2019).
26. Tattini, L., D'Aurizio, R. & Magi, A. Detection of genomic structural variants from next-generation sequencing data. *Front Bioeng. Biotechnol.* **3**, 92, https://doi.org/10.3389/fbioe.2015.00092 (2015).
27. Alkan, C., Coe, B. P. & Eichler, E. E. Genome structural variation discovery and genotyping. *Nat. Rev. Genet.* **12**, 363–376, https://doi.org/10.1038/nrg2958 (2011).
28. Holt, J. M. *et al.* Identification of pathogenic structural variants in rare disease patients through genome sequencing. bioRxiv, 627661, https://doi.org/10.1101/627661 (2019).
29. De Coster, W. & Van Broeckhoven, C. Newest methods for detecting structural variations. *Trends Biotechnol.* **37**, 973–982, https://doi.org/10.1016/j.tibtech.2019.02.003 (2019).
30. Mantere, T., Kersten, S. & Hoischen, A. Long-read sequencing emerging in medical genetics. *Front Genet* **10**, 426, https://doi.org/10.3389/fgene.2019.00426 (2019).
31. Sanchis-Juan, A. *et al.* Complex structural variants in Mendelian disorders: identification and breakpoint resolution using short- and long-read genome sequencing. *Genome Med.* **10**, 95, https://doi.org/10.1186/s13073-018-0606-6 (2018).
32. Merker, J. D. *et al.* Long-read genome sequencing identifies causal structural variation in a Mendelian disease. *Genet. Med.* **20**, 159–163, https://doi.org/10.1038/gim.2017.86 (2018).
33. Mitsuhashi, S. & Matsumoto, N. Long-read sequencing for rare human genetic diseases. *J. Hum. Genet.* **65**, 11–19, https://doi.org/10.1038/s10038-019-0671-8 (2020).
34. Nowakowska, B. A. *et al.* Parental insertional balanced translocations are an important cause of apparently *de novo* CNVs in patients with developmental anomalies. *Eur. J. Hum. Genet.* **20**, 166–170, https://doi.org/10.1038/ejhg.2011.157 (2012).
35. Brigida, I. *et al.* A novel genomic inversion in Wiskott-Aldrich-associated autoinflammation. *J. Allergy Clin. Immunol.* **138**, 619–622 e617, https://doi.org/10.1016/j.jaci.2016.03.007 (2016).
36. Vuillaume, M. L. *et al.* Whole genome sequencing identifies a *de novo* 2.1 Mb balanced paracentric inversion disrupting *FOXP1* and leading to severe intellectual disability. *Clin. Chim. Acta* **485**, 218–223, https://doi.org/10.1016/j.cca.2018.06.048 (2018).
37. Much, C. D. *et al.* Novel pathogenic variants in a cassette exon of *CCM2* in patients with cerebral cavernous malformations. *Front. Neurol.* **10**, 1219, https://doi.org/10.3389/fneur.2019.01219 (2019).
38. Robinson, J. T. *et al.* Integrative genomics viewer. *Nat. Biotechnol.* **29**, 24–26, https://doi.org/10.1038/nbt.1754 (2011).

Acknowledgements
This study was funded by the Deutsche Forschungsgemeinschaft (DFG, German Research Foundation, RA 2876/2–1). We would like to thank the patients for their participation in the study. Dr. W. Schröder is thanked for fruitful discussions.

Author contributions
R.A.P., U.F., and M.R. designed the study. R.A.P., K.S., S.Sp., E.G. and M.R. analyzed the NGS data. P.D. and A.S. took care for the patient and participated in interpretation of the genetic, clinical and magnetic resonance imaging data. A.W., T.L., and C.A.H. performed and analyzed the cytogenetic analyses. R.A.P., U.F., and M.R. drafted the manuscript and all authors participated in final draft revisions.

Competing interests
The authors declare no competing interests.

Additional information
Supplementary information is available for this paper at https://doi.org/10.1038/s41598-020-63337-5.

Correspondence and requests for materials should be addressed to M.R.

Reprints and permissions information is available at www.nature.com/reprints.

Publisher's note Springer Nature remains neutral with regard to jurisdictional claims in published maps and institutional affiliations.

5.2 Using CRISPR/Cas9 genome editing in human iPSCs for deciphering the pathogenicity of a novel *CCM1* transcription start site deletion

Robin A. Pilz, Dariush Skowronek, Motaz Hamed, Anja Weise, Elisabeth Mangold, Alexander Radbruch, Torsten Pietsch, Ute Felbor, Matthias Rath

Front Mol Biosci. 2022; 9:953048

https://doi.org/10.3389/fmolb.2022.953048

frontiers | Frontiers in Molecular Biosciences

TYPE Brief Research Report
PUBLISHED 25 August 2022
DOI 10.3389/fmolb.2022.953048

OPEN ACCESS

EDITED BY
Monica Ballarino,
Sapienza University of Rome, Italy

REVIEWED BY
Andrea Perrelli,
University of Rochester, United States
Surendra Kumar Prajapati,
Henry M Jackson Foundation for the Advancement of Military Medicine (HJF), United States

*CORRESPONDENCE
Matthias Rath,
matthias.rath@med.uni-greifswald.de

SPECIALTY SECTION
This article was submitted to Molecular Diagnostics and Therapeutics, a section of the journal Frontiers in Molecular Biosciences

RECEIVED 25 May 2022
ACCEPTED 09 August 2022
PUBLISHED 25 August 2022

CITATION
Pilz RA, Skowronek D, Hamed M, Weise A, Mangold E, Radbruch A, Pietsch T, Felbor U and Rath M (2022), Using CRISPR/Cas9 genome editing in human iPSCs for deciphering the pathogenicity of a novel *CCM1* transcr. *Front. Mol. Biosci.* 9:953048. doi: 10.3389/fmolb.2022.953048

Using CRISPR/Cas9 genome editing in human iPSCs for deciphering the pathogenicity of a novel *CCM1* transcription start site deletion

Robin A. Pilz[1], Dariush Skowronek[1], Motaz Hamed[2], Anja Weise[3], Elisabeth Mangold[4], Alexander Radbruch[5], Torsten Pietsch[6], Ute Felbor[1] and Matthias Rath[1]*

[1]Department of Human Genetics, University Medicine Greifswald, and Interfaculty Institute of Genetics and Functional Genomics, University of Greifswald, Greifswald, Germany, [2]Department of Neurosurgery, University Hospital Bonn, Bonn, Germany, [3]Institute of Human Genetics, Jena University Hospital, Friedrich Schiller University, Jena, Germany, [4]Institute of Human Genetics, Medical Faculty and University Hospital Bonn, University of Bonn, Bonn, Germany, [5]Department of Neuroradiology, University Hospital Bonn, Bonn, Germany, [6]Institute of Neuropathology, DGNN Brain Tumor Reference Center, University of Bonn, Bonn, Germany

Cerebral cavernous malformations are clusters of aberrant vessels that can lead to severe neurological complications. Pathogenic loss-of-function variants in the *CCM1*, *CCM2*, or *CCM3* gene are associated with the autosomal dominant form of the disease. While interpretation of variants in protein-coding regions of the genes is relatively straightforward, functional analyses are often required to evaluate the impact of non-coding variants. Because of multiple alternatively spliced transcripts and different transcription start points, interpretation of variants in the 5′ untranslated and upstream regions of *CCM1* is particularly challenging. Here, we identified a novel deletion of the non-coding exon 1 of *CCM1* in a proband with multiple CCMs which was initially classified as a variant of unknown clinical significance. Using CRISPR/Cas9 genome editing in human iPSCs, we show that the deletion leads to loss of CCM1 protein and deregulation of *KLF2*, *THBS1*, *NOS3*, and *HEY2* expression in iPSC-derived endothelial cells. Based on these results, the variant could be reclassified as likely pathogenic. Taken together, variants in regulatory regions need to be considered in genetic CCM analyses. Our study also demonstrates that modeling variants of unknown clinical significance in an iPSC-based system can help to come to a final diagnosis.

KEYWORDS

cerebral cavernous malformation, CRISPR/Cas9, induced pluripotent stem cells, transcription start site, variant of unknown clinical significance

10.3389/fmolb.2022.953048

Introduction

Cerebral cavernous malformation (CCM) is a neurovascular disorder. Based on prospective, population-based studies in Scottish and American residents (Al-Shahi et al., 2003; Flemming et al., 2017) as well as a retrospective analysis of autopsies (Otten et al., 1989), it affects approximately one in 200 people. In CCM patients, mulberry-like vascular lesions can be visualized with appropriate magnetic resonance imaging (MRI) analyses in the brain or spinal cord (Akers et al., 2017). These lesions are characterized by irregular-structured and thin-walled endothelial channels that have an increased tendency to bleed. While many CCMs remain asymptomatic, hemorrhage from CCMs can lead to severe neurological deficits. Symptoms range from sensory and speech disturbances to seizures and stroke-like events even in young patients (Batra et al., 2009; Spiegler et al., 2014). Surgical excision and symptomatic treatment remain the only therapy options for patients to date.

Besides sporadic CCMs, 6%–7% of cases are due to autosomal dominant inherited heterozygous loss-of-function germline variants in the *CCM1* (*KRIT1*; OMIM: *604214), *CCM2* (*607929), or *CCM3* gene (*PDCD10*; *609118) (Spiegler et al., 2018b). Pathogenic variants in the *CCM1* gene are the most common cause of familial CCM disease (Spiegler et al., 2014). The diverse functions of CCM1 include Rap1- and HEG1-related stabilization of endothelial cell junctions (Glading et al., 2007; Gingras et al., 2012), regulation of DELTA-NOTCH, TGF-β and BMP6 signaling (Wüstehube et al., 2010; Maddaluno et al., 2013) as well as intracellular reactive oxygen species homeostasis (Goitre et al., 2010). Loss of CCM1 is also associated with altered KLF2/KLF4 (Zhou et al., 2016), THBS1 (Lopez-Ramirez et al., 2017), NOS3 (Lopez-Ramirez et al., 2021), and HEY2 (Wüstehube et al., 2010) protein or mRNA expression. Since *CCM1* was first described as a disease gene in 1999 (Laberge-le Couteulx et al., 1999; Sahoo et al., 1999), hundreds of *CCM1* mutations have been listed in international databases. Most of the known pathogenic variants are located in the coding region of the gene, with missense and frameshift variants accounting for the largest proportion. Variants in the non-coding region mainly alter the splicing process (Spiegler et al., 2018b; Ricci et al., 2021). Very little is known about variants in non-coding regions that potentially affect *CCM1* gene expression or protein function. From a general point of view, however, the 5′ and 3′ untranslated regions (UTRs) as well as promoter, enhancer or silencer motifs play an important role in disease development (Damjanovich et al., 2011; French and Edwards, 2020; Whiffin et al., 2020; Wright et al., 2021). Although potentially disease-causing, predicting the functional impact of non-coding variants is much more difficult than of protein-coding variants. As a result of clinical DNA sequencing, "variants of unknown clinical significance" (VUS) are detected in a significant proportion of patients (Rehm et al., 2015). Remarkably, a classification as VUS is more likely for variants outside the coding region, with ~40% of coding variants versus ~60% of all UTR variants classified as VUS in ClinVar (Ellingford et al., 2022).

With the guidelines published in 2015, the American College of Medical Genetics and Genomics (ACMG) and the Association for Molecular Pathology (AMP) established a standardized criteria-based system for interpreting sequence variants (Richards et al., 2015). Because the criteria have been designed for a broad application, further general and disease-specific modifications and refinements have emerged (Harrison et al., 2019). Apart from splicing variants, existing guidelines mainly focus on coding regions which makes it very challenging to apply the criteria to variants in UTRs of genes. Although genome interaction studies, quantitative trait locus mapping, and computational predictions can be useful for interpreting non-coding variants (Zhang and Lupski, 2015), functional assays may be necessary for a reliable assessment of the pathogenicity in many cases. The CRISPR/Cas9 technology is a powerful tool to engineer such variants in model organisms. Genome editing has also recently been applied to decipher VUS pathogenicity in human induced pluripotent stem cell (iPSC)-based models (Garg et al., 2018; Ma et al., 2018).

Here, we describe the accurate classification of a novel non-coding deletion in the *CCM1* gene following after CRISPR/Cas9 editing in human iPSCs.

Materials and methods

Genetic analyses and ethical considerations

Genetic analyses were performed with written informed consent according to the German Gene Diagnostics Act and with approval of the local ethics committee of the University Medicine Greifswald (No. BB 047/14). The NucleoSpin Blood L Kit (Macherey-Nagel, Düren, Germany) was used to isolate genomic DNA. Next-generation sequencing (NGS) gene panel analysis with the target region defined as all exons (±20 bp) of *CCM1* (Locus Reference Genomic sequence: LRG_650t1), *CCM2* (LRG_664t1,t2), and *CCM3* (LRG_651t1) was performed using a hybridization capture-based approach. For target enrichment and library preparation, an Agilent SureSelect^{QXT} custom enrichment kit (Panel ID: 3152261, Agilent Technologies, Santa Clara, United States) was used. The indexed library was sequenced on a MiSeq instrument (Illumina, San Diego, United States) with 2 × 150 bp paired-read runs. FASTQ file generation was done by the MiSeq Reporter Software (Illumina). Read mapping, alignment, and variant calling was performed by the SeqNext module of the Sequence Pilot v5.1.0 software (JSI Medical Systems, Ettenheim, Germany) that was also used for

10.3389/fmolb.2022.953048

copy number variation (CNV) analyses in a read depth-based approach as described before (Much et al., 2019). To examine for translocation events, the generated FASTQ files were analyzed with the SureCall 4.2.1.10 software (Agilent Technologies). Polymerase chain reaction (PCR) was used to confirm the deletion of the *CCM1* exon 1. PCR products were separated by agarose gel electrophoresis. The band of interest was excised, purified with the Zymoclean Gel DNA Recovery Kit (Zymo Research, Irvine, United States), and analyzed by Sanger sequencing to determine the exact breakpoints of the deletion. All medical information and images presented here are published with written informed consent.

Cell culture and reagents

HEK293T cells were cultured at 37°C and 5% CO_2 in 1x Dulbecco's Modified Eagle medium (DMEM) with high glucose (Thermo Fisher Scientific, Waltham, United States) and 10% fetal bovine serum (FBS; Thermo Fisher Scientific). AICS-0023 iPSCs (Allen Cell Collection, Coriell Institute, United States) were cultured at 37°C and 5% CO_2 in Essential 8 Flex medium (Thermo Fisher Scientific) on plates coated with growth factor reduced matrigel (Corning, New York, United States) and passaged with 0.5 mM ethylenediaminetetraacetic acid (Thermo Fisher Scientific). Cell cultures were routinely checked for mycoplasma contamination by PCR. Oligonucleotides purchased from Integrated DNA Technologies and antibodies used in this study are listed in Supplementary Tables S1, S2.

CRISPR/Cas9 editing, single-cell cloning, and karyotyping

To mimic the deletion identified in the index case, two crRNA:tracrRNA:Cas9 ribonucleoprotein (RNP) complexes were combined with Lipofectamine reagent in Opti-MEM I reduced serum medium (Thermo Fisher Scientific) for co-transfection of HEK293T or AICS-0023 cells. HEK293T cells were reverse transfected with RNP complexes as described before (Schwefel et al., 2020). For the AICS-0023 iPSC line, the crRNA: tracrRNA duplexes were complexed with Cas9 protein (Integrated DNA Technologies, Coralville, United States) in Opti-MEM I and formation of transfection complexes was performed in Opti-MEM I with Lipofectamine Stem Transfection Reagent (Thermo Fisher Scientific). After detaching with StemPro Accutase (Thermo Fisher Scientific), 130,000 cells were reverse transfected in Essential 8 medium (Thermo Fisher Scientific) supplemented with 10 µM Rho-associated protein kinase (ROCK) inhibitor Y-27632 (STEMCELL Technologies, Vancouver, Canada) on growth factor reduced matrigel-coated 24-well plates. After 1 day, the medium was replaced with Essential 8 Flex medium without ROCK inhibitor. Clonal $CCM1^{del/del}$ HEK293T and AICS-0023 iPSC lines were established by seeding genome-edited cells at a density of statistically 0.5 cells/well on 96-well plates in 1x DMEM and 10% FBS or on growth factor reduced matrigel-coated 96-well plates in Essential 8 Flex medium supplemented with CloneR (STEMCELL Technologies), respectively. Genomic DNA of clonally expanded cell lines was isolated with QuickExtract DNA Extraction Solution (Lucigen, Middleton, United States). Genotypes were determined by Sanger sequencing.

For generating control $CCM1^{-/-}$ AICS-0023 iPSC lines with frameshift variants in the coding region of *CCM1*, iPSCs were transfected with a single guide RNA (sgRNA):Cas9 RNP complex with a final RNP concentration of 30 nM. Genome editing efficiency was estimated after T7 endonuclease I (T7EI) digestion of annealed PCR amplicons as described before (Schwefel et al., 2020). After single-cell cloning, Sanger sequencing was used to determine the genotypes of the lines and to evaluate sequence changes at off-target sites predicted with the CHOPCHOP tool (Labun et al., 2019). Following standard procedures, chromosome analyses for $CCM1^{-/-}$ AICS-0023 iPSC clones were performed by GTG (G-bands by trypsin using Giemsa) staining of metaphase chromosomes.

RT-qPCR, RT-PCR, and western blot

The Direct-zol RNA MiniPrep Plus Kit (Zymo Research) was used for purification of extracted RNA. Reverse transcription (RT) into cDNA was performed using the First Strand cDNA Synthesis Kit (Thermo Fisher Scientific). Transcript levels of *CCM1*, *ANKIB1*, *KLF2*, *KLF4*, *THBS1*, *NOS3*, and *HEY2* were quantified with SYBR Green-based quantitative PCR (qPCR) analyses performed on a Roche Light Cycler 480 instrument (Roche, Basel, Switzerland) or on a QuantStudio 7 Flex Real-Time PCR System (Applied Bioystems, Waltham, United States). *RPLP0* served as an endogenous control. In RT-PCR, 10 ng of transcribed cDNA were amplified in 28 (*RPLP0*) or 33 cycles (*CCM1* and *ANKIB1*). The GraphPad prism software was used for data analysis (GraphPad Software, San Diego, United States).

For western blot analyses, total protein extracted with RIPA Lysis and Extraction Buffer (Thermo Fisher Scientific) was separated on a 10% TGX Stain-Free FastCast sodium dodecyl sulfate-polyacrylamide gel (Bio-Rad, Hercules, United States) and subsequently transferred to a polyvinylidene fluoride membrane. The iBind Flex Western System (Thermo Fisher Scientific) was used for immunostaining according to the manufacturer's instructions. Stripping of the membrane was performed with ROTI Free Stripping Buffer 2.2 plus (Carl Roth, Karlsruhe, Germany). Blot documentation of Stain-Free total protein and chemiluminometric signal detection was performed using a ChemiDoc XRS+ imager. To determine

10.3389/fmolb.2022.953048

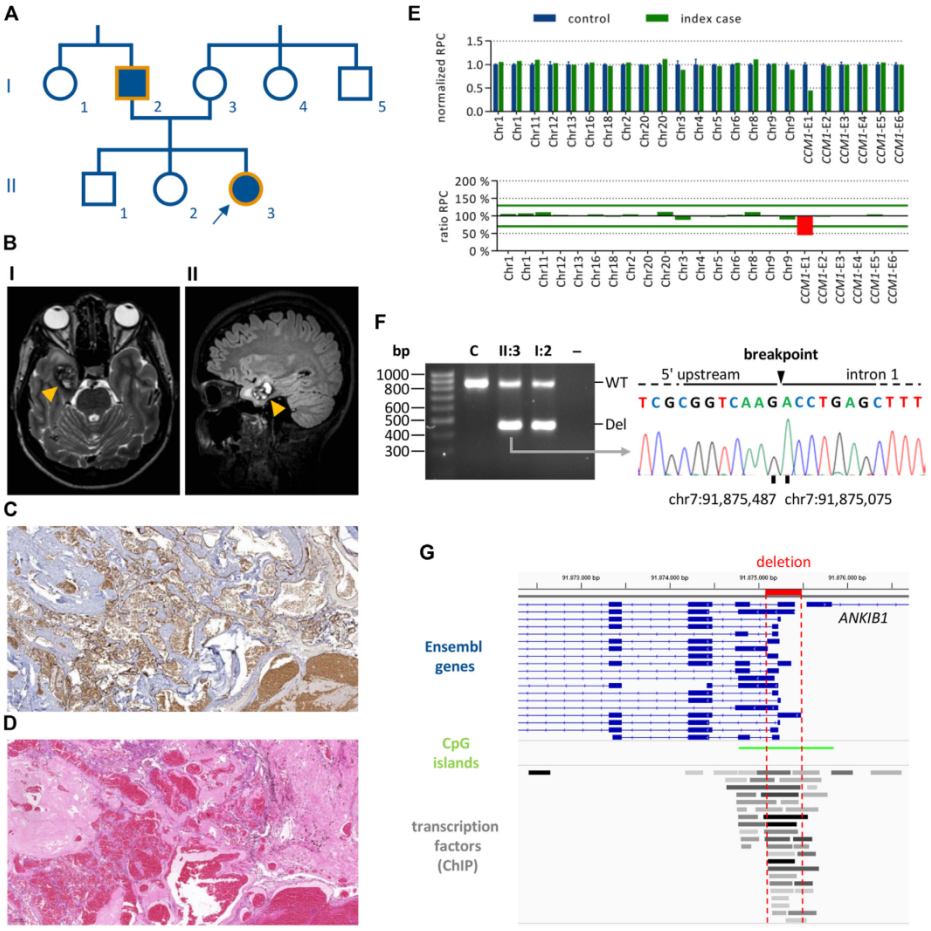

FIGURE 1
Identification of a *CCM1* exon 1 deletion in a proband with multiple CCMs. **(A)** Pedigree of the CCM index case (II:3, arrow). Filled forms indicate individuals with CCM-associated symptoms. Orange outlines indicate family members for whom genetic analyses have been performed. **(B)** Magnetic resonance imaging for the index case showing a right temporo-mesial CCM (orange arrow heads). I: T2-weighted sequence, II: FLAIR sequence. **(C,D)** Histological analyses of the CCM shown in B (x5 magnification). **(C)** CD34 staining, **(D)** HE staining. **(E)** NGS-based CNV analyses for the index case showing a heterozygous deletion of *CCM1* exon 1. **(F)** PCR amplification of the deletion region for index case II:3 and her father I:2 (WT, wild-type band; Del, deletion band; C, healthy control; –, negative control). The deletion breakpoints were determined by Sanger sequencing of the deletion band. **(G)** The deletion (highlighted in red) affects all relevant Ensembl transcripts of *CCM1*. The location of CpG islands and transcription factor binding sites are shown (ChIP, chromatin immunoprecipitation).

relative CCM1 protein expression, normalized band intensities were calculated with the ImageLab software (v5.2.1, Bio-Rad). GAPDH or total protein was used as a loading control and volume intensities of the detected protein bands were normalized to the volume intensities of the corresponding GAPDH bands or total protein fraction.

Differentiation procedures and immunofluorescent staining

Cells were fixed with 4% paraformaldehyde for 15–20 min. IPSCs were stained for pluripotency markers OCT4, SSEA4, SOX2, and TRA-1-60 using the PSC 4-Marker

10.3389/fmolb.2022.953048

Immunocytochemistry Kit (Thermo Fisher Scientific) with alternative secondary antibodies for SSEA4 and SOX2 staining. Differentiation of iPSCs into endothelial cells (ECs) was performed in 6-well-plates using the STEMdiff Endothelial Differentiation Kit (STEMCELL Technologies). Directed differentiation of iPSCs into all three germ layers was performed in 24-well-plates using the STEMdiff Trilineage Differentiation Kit (STEMCELL Technologies). The Immunofluorescence Application Solutions Kit (Cell Signaling, Danvers, United States) was used for staining of CD31, VE-Cadherin, PAX6, TUJ-1, and α-SMA. For markers Brachyury, SOX17, and FOXA2, cells were permeabilized and blocked in 0.3% Triton X-100, 1% bovine serum albumin, and 10% normal donkey serum for 45 min. Cells were incubated with primary antibodies overnight at 4°C and with secondary antibodies for 60 min at room temperature in the dark. Nuclei were stained with DAPI or Hoechst 33342 (Thermo Fisher Scientific).

Results

Clinical findings and genetic analyses

The female index case II:3 (Figure 1A) first presented in our outpatient clinic at the age of 24 with headaches and bilateral dysesthesias of the toes. Brain MRI analysis revealed a cavernoma in her right medial temporal lobe (Figure 1B) which was resected because of size progression and perifocal edema. Numerous malformed vessels, often with very severe fibrous wall thickening, and signs of recurrent bleeding events were observed in the histological analyses of the CCM tissue (Figures 1C,D). In addition to the temporo-mesial cavernoma, multiple small CCMs were identified in the left parieto-occipital lobe, the left periventricular region, the cerebellar vermis, and the head of the caudate nucleus. MRI analysis of the patient's father (I:2) also revealed hemosiderin deposits consistent with previous hemorrhages of small CCMs. Although there were no other symptomatic family members, the personal and family history of the index case suggested familial CCM disease.

NGS-based gene panel analysis did not reveal a pathogenic single nucleotide (SNV) or small indel variant but a high number of split reads in intron 1 of *CCM1*. In line with these data, NGS-based CNV detection with the SeqNext module of the Sequence Pilot software and the Agilent SureCall tool indicated a heterozygous deletion of *CCM1* exon 1 (Figure 1E). PCR amplification of the deletion region resulted in a wild-type band and an approximately 400 base pair (bp) shorter band for the index case and her father. The exact breakpoints of the 411 bp deletion were determined by Sanger sequencing (NC_000007.13: g.91875486_91875076del; Figure 1F). As shown in the Integrative Genomics Viewer (Robinson et al., 2011), the identified deletion includes the transcription start sites (TSS) of all relevant *CCM1* transcripts listed in the Ensembl database and covers several transcription factor binding sites (Figure 1G). Following the ACMG standards and guidelines for the interpretation of sequence variants (Richards et al., 2015), the deletion was classified as VUS (criteria PM1 and PP4). Notably, the PVS1 criterion was not applied because the deletion neither affects the reading frame nor canonical splice sites of the coding exons of *CCM1*.

Modeling a *CCM1* knockout in an iPSC-based cell culture system

To come to a final molecular diagnosis in our family, we decided to use CRISPR/Cas9 genome editing to rebuild the variant in an iPSC-based *in vitro* system. As a positive control for functional and molecular assays, we first generated *CCM1*$^{-/-}$ AICS-0023 iPSCs with bona fide loss-of-function variants on both alleles, mimicking the second-hit inactivation in heterozygous mutation carriers. Somatic inactivation of the remaining wild-type allele in ECs by a second mutation is described as a critical step in CCM formation (Pagenstecher et al., 2009; McDonald et al., 2014). The sgRNA target sequence used in our approach was located in exon 10, which is part of all functional *CCM1* transcripts (Figure 2A). We optimized the genome editing protocol using different sgRNA:Cas9 RNP concentrations and observed the highest indel rate of 37.4% at a concentration of 30 nM (Figure 2B). Clonal *CCM1*$^{-/-}$ iPSCs generated by limiting dilution cloning were checked for CRISPR/Cas9-induced loss-of-function variants in the target region by Sanger sequencing and NGS. Hence, we established one iPSC line with two compound heterozygous frameshift variants and one line with a homozygous 1 bp duplication (Figure 2C, Supplementary Figure S1). No sequence changes were observed at seven top off-target sites (Supplementary Figure S2). RT-qPCR and western blot analyses confirmed functional *CCM1* knockout (Figures 2D,E, Supplementary Figure S3). The *CCM1*$^{-/-}$ iPSC lines displayed a typical morphology, had a normal male karyotype (46, XY), and expressed the pluripotency markers SSEA4, OCT4, SOX2, and TRA-1-60 (Figure 2F, Supplementary Figure S1). Furthermore, they could be differentiated into ecto-, meso- and endoderm (Supplementary Figure S1).

As *CCM1* inactivation is known to induce characteristic gene expression changes in ECs, we generated iPSC-derived ECs and verified the expression of the endothelial markers CD31 and VE-Cadherin (Figure 2G). As expected, mRNA expression of *KLF2* and *KLF4* was significantly increased in iPSC-derived *CCM1*$^{-/-}$ ECs (Figure 2H). In summary, we

10.3389/fmolb.2022.953048

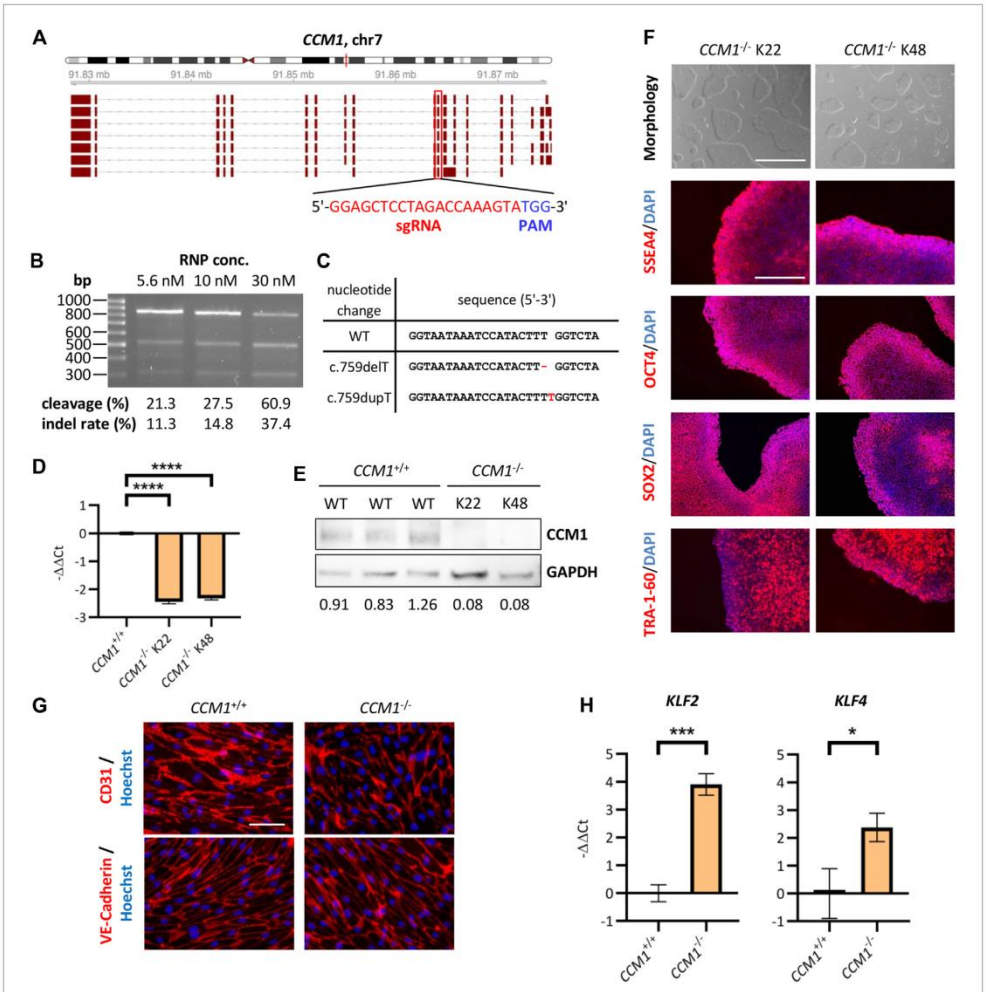

FIGURE 2
Establishment and validation of an iPSC-based *CCM1* knockout cell culture model. **(A)** Schematic depiction of the exon-intron structure of the *CCM1* gene and its relevant transcripts. The CRISPR/Cas9 target region of the sgRNA (red box) is part of all functional transcripts. **(B)** Optimization of the CRISPR/Cas9 RNP transfection showed best cleavage efficiency in the T7EI assay when using a final RNP concentration of 30 nM. **(C)** DNA sequences of the AICS-0023-derived *CCM1*$^{-/-}$ clones shown as a sequence alignment. **(D)** RT-qPCR revealed a marked reduction of *CCM1* mRNA expression in knockout lines (*CCM1*$^{+/+}$: $n = 3$, *CCM1*$^{-/-}$ K22/K48: $n = 3$ each). **(E)** Western blot analyses of clonal lines verified absence of CCM1 protein in *CCM1*$^{-/-}$ cells. Expression levels normalized to the wild-type (WT) control group are given. **(F)** Images of the morphology (scale = 1000 µm) and immunofluorescence analyses for stem cell markers SSEA4, OCT4, SOX2, and TRA-1-60 (scale = 400 µm). **(G)** AICS-0023-derived ECs expressed markers CD31 and VE-Cadherin. Representative immunofluorescent images are shown (scale = 75 µm). **(H)** AICS-0023-derived *CCM1*$^{-/-}$ ECs showed increased *KLF2* and *KLF4* mRNA expression (*CCM1*$^{+/+}$: $n = 3$, *CCM1*$^{-/-}$: $n = 3$). Data are presented as mean and standard deviation (SD). Two-tailed unpaired Student's *t* test **(D, H)** was used for statistical analyses: $^{*}p < 0.05$, $^{***}p < 0.001$, $^{****}p < 0.0001$.

10.3389/fmolb.2022.953048

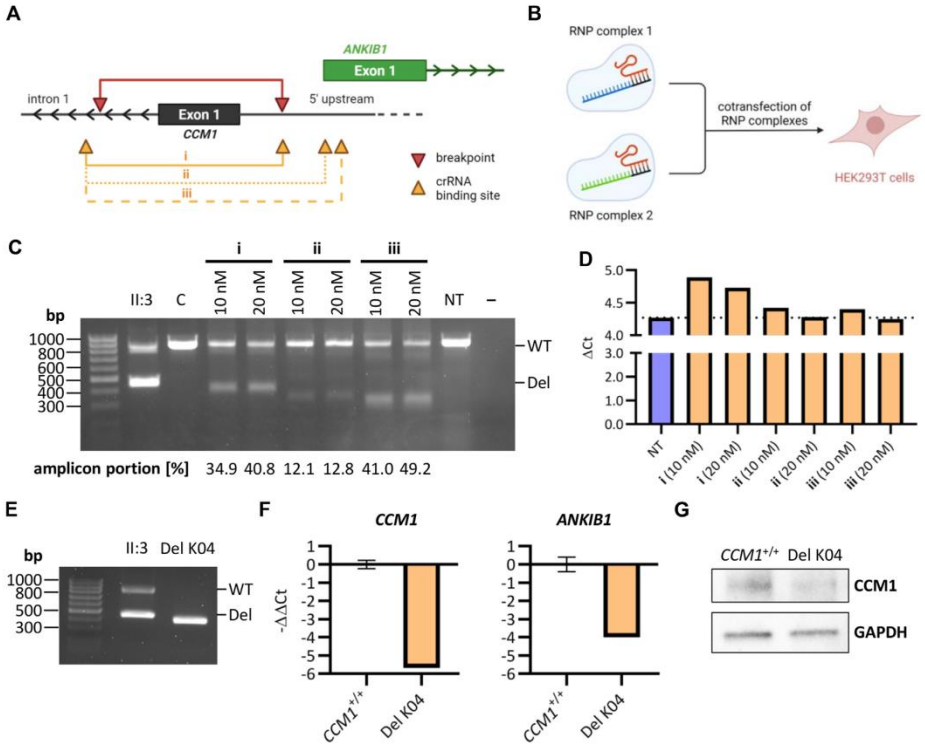

FIGURE 3
Reconstructing the identified deletion with CRISPR/Cas9 genome editing in HEK293T cells. **(A)** Schematic representation of the identified deletion in *CCM1* (red) and crRNA binding sites (orange) (Image was created with BioRender.com). The crRNA combinations i, ii, and iii were used to generate a deletion similar to the identified variant in the index case. **(B)** HEK293T cells were co-transfected with two RNP complexes for mimicking the deletion (Image was created with BioRender.com). **(C)** PCR amplification of the deletion region after co-transfection of HEK293T cells with different combinations of crRNAs and at different final RNP complex concentrations. **(D)** *CCM1* RT-qPCR for different HEK293T cell mixtures after transfection ($n = 1$ each, NT = not transfected). **(E)** PCR amplification of the deletion region for a homozygous HEK293T cell clone after using crRNA combination i for transfection. **(F)** RT-qPCR for HEK293T clone Del K04 shows a clear downregulation of *CCM1* and *ANKIB1* mRNA ($CCM1^{+/+}$: $n = 3$, Del K04: $n = 1$). **(G)** Reduction of CCM1 protein expression for HEK293T clone Del K04 is shown by western blot. Data are presented as mean and standard deviation (SD).

have hereby established an iPSC-based *CCM1* knockout model that served as a benchmark system in assessing the pathogenicity of the identified *CCM1* TSS deletion.

Using CRISPR/Cas9 editing to mimic the identified deletion in HEK293T cells

We next used easy-to-transfect and highly proliferative HEK293T cells to test the genome editing efficiencies of three crRNA combinations with binding sites near the breakpoints of the identified deletion (Figure 3A). For each combination, HEK293T cells were co-transfected with two RNP complexes at a final concentration of 10 nM or 20 nM (Figure 3B). PCR analyses indicated high efficiencies for the combinations i and iii (Figure 3C). RT-qPCR demonstrated decreased *CCM1* mRNA expression in HEK293T cells transfected with crRNA combination i (Figure 3D). The deletion induced by this combination most accurately reflects the variant identified in index case II:3 (Figure 3A). Therefore, we next established a homozygous cell clone (Del K04) from this cell mixture (Figure 3E) and verified reduced *CCM1* mRNA and protein expression in this HEK293T clone (Figures 3F,G, Supplementary Figure S3). Interestingly, we also found reduced mRNA

10.3389/fmolb.2022.953048

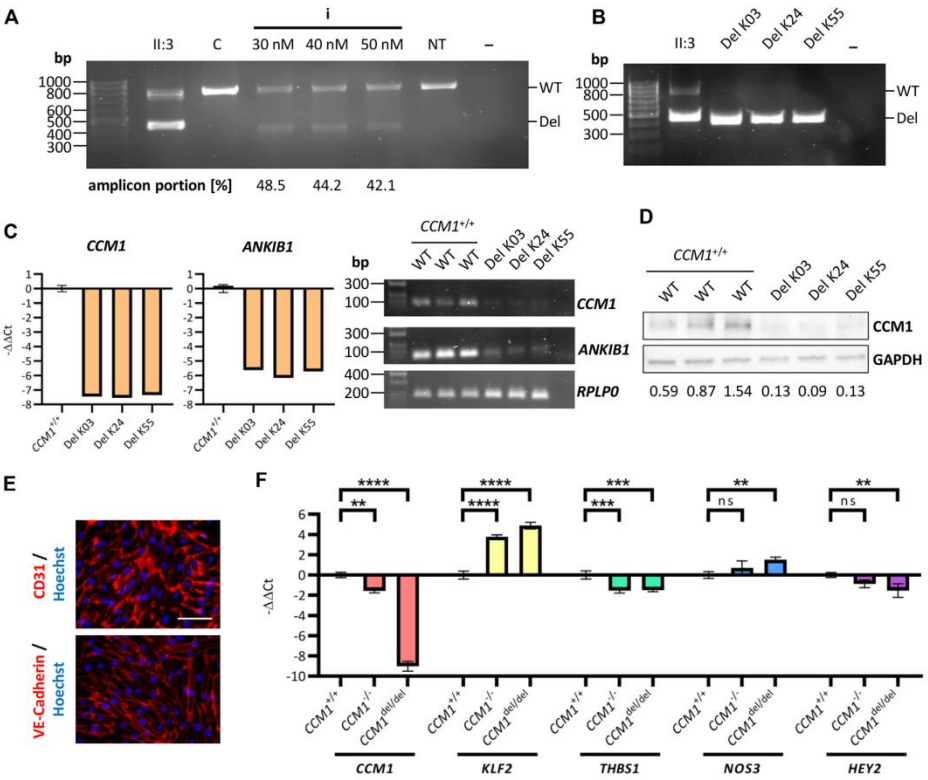

FIGURE 4
Analyzing the functional impact of the identified deletion in an iPSC-based cell culture model. **(A)** PCR amplification of the deletion region after co-transfection (crRNA combination i, Figure 3A) of AICS-0023 iPSCs at different final RNP complex concentrations. **(B)** PCR amplification of the deletion region for three AICS-0023 clones with a biallelic CRISPR/Cas9 induced deletion. **(C)** Marked reduction of *CCM1* and *ANKIB1* mRNA in $CCM1^{del/del}$ iPSC clones shown by RT-qPCR (left panels; $CCM1^{+/+}$: $n = 3$, Del K03/K24/K55: $n = 1$ each) and RT-PCR (right panel). **(D)** Western blot analysis show loss of CCM1 protein in $CCM1^{del/del}$ clones. Expression levels normalized to the wild-type (WT) control group are given. **(E)** IPSC-derived $CCM1^{del/del}$ ECs express markers CD31 and VE-Cadherin. Representative immunofluorescence images are shown (scale = 75 µm). **(F)** *CCM1*, *KLF2*, *THBS1*, *NOS3*, and *HEY2* RT-qPCR analyses for differentiated $CCM1^{+/+}$, $CCM1^{-/-}$, and $CCM1^{del/del}$ ECs. Data are presented as mean and standard deviation (SD). One-way ANOVA with multiple comparisons test **(F)** was used for statistical analyses: $^{**}p < 0.01$, $^{***}p < 0.001$, $^{****}p < 0.0001$.

expression of the *ANKIB1* gene, whose TSS is close to the deletion region (Figures 3A,F).

Gene expression analyses in iPSC-derived endothelial cells support pathogenicity of the identified deletion

Having determined the optimal crRNA combination, we finally generated AICS-0023 iPSCs with the *CCM1* TSS deletion on both alleles ($CCM1^{del/del}$). Increasing the final RNP concentration did not improve editing efficiency (Figure 4A). By single-cell cloning, three $CCM1^{del/del}$ iPSC lines could be established (Del K03, Del K24, Del K55) (Figure 4B). Consistent with the hypothesis that *CCM1* TSS deletion is pathogenic, a significantly reduced *CCM1* expression was shown by RT-qPCR and western blot analyses, respectively (Figures 4C,D, Supplementary Figure S3). *ANKIB1* mRNA expression was also reduced in $CCM1^{del/del}$ iPSCs (Figure 4C). We then differentiated the $CCM1^{del/del}$ iPSCs into ECs (Figure 4E). Interestingly, complete loss of *CCM1* mRNA expression was observed for

10.3389/fmolb.2022.953048

CCM1$^{del/del}$ ECs, whereas it was greatly reduced but still existent in *CCM1*$^{-/-}$ ECs (Figure 4F). A similar effect was observed for *KLF2*, *NOS3*, and *HEY2*, with the more pronounced dysregulation in *CCM1*$^{del/del}$ ECs (Figure 4F). We also analyzed *THBS1* expression and found equal reduction in *CCM1*$^{-/-}$ and *CCM1*$^{del/del}$ ECs (Figure 4F).

Taken together, the functional *in vitro* studies presented here provide strong evidence for the pathogenicity of the identified *CCM1* TSS deletion. Following the ACMG guideline, it can now be classified as likely pathogenic (PS3, PM1, and PP4).

Discussion

Coding variants account for the majority of pathogenic variants in the *CCM* genes. However, with the novel *CCM1* TSS deletion characterized in our study, we demonstrate that non-coding variants also need to be considered and that CRISPR/Cas9 editing in iPSCs can help with the interpretation of VUS.

Because mutational hotspots cannot be determined, genetic testing for CCM typically involves analysis of all coding exons and exon-intron boundaries of *CCM1*, *CCM2*, and *CCM3*. NGS gene panel analysis has proven superior to a stepwise approach in this context (Spiegler et al., 2018b). It allows parallel screening for SNVs, indels, and CNVs (Much et al., 2019). NGS-based CNV analyses are particularly advantageous if regions of interest such as non-coding exons are not covered by commercial multiplex ligation-dependent probe amplification kits. Nonetheless, no causative variant is identified in 2%–13% of familial CCM cases by current genetic analyses (Spiegler et al., 2018b). Apart from structural variants (Spiegler et al., 2018a; Pilz et al., 2020) and somatic mosaicism (McDonald et al., 2014), the here identified *CCM1* TSS deletion highlights that variants in regulatory regions that are not always analyzed in routine diagnostics may account for part of the missing heritability in CCM disease.

However, the clinical interpretation of variants in 5′ UTR or promoter regions is challenging. In the absence of experimental data, the identified *CCM1* TSS deletion would have been classified as VUS using the widely accepted ACMG guidelines. As the coding region of *CCM1* starts only in exon 5 (LRG_650t1), the deletion does not affect the reading frame but results in loss of the TSS. In the gnomAD structural variant database (Collins et al., 2020) with its 10,847 genome data sets no deletion only covering exon 1 is registered, but information from larger cohorts on the variant's frequency in the general population is still limited. Deletions of non-coding *CCM1* exons described in the literature so far are also considerably larger than the variant described here (Riant et al., 2013; Mondéjar et al., 2014). Furthermore, the occurrence of transcripts with alternative TSSs that may rescue the phenotype could not be excluded. Interestingly, 5′ RACE analysis revealed different TSSs and alternative splicings of the *CCM1* 5′ UTR. Intragenic TSSs were shown by quantitative transcription studies and detection of five promoter sequences by MPromDB analysis in the 5′ UTR and intragenic region of *CCM1* (Mondéjar et al., 2016). Even with consideration of further relevant recommendations for interpreting the loss-of-function variants (Abou Tayoun et al., 2018) and adaptations for single-gene copy number variants (Brandt et al., 2020) the PVS1 criterion could not be used in this case. Yet, the distinction between a pathogenic and benign variant is of great importance for accurate diagnosis, appropriate clinical management and genetic counselling of family members.

According to the ACMG guidelines, well-established *in vitro* analyses can be strong evidence of a variant's pathogenic or benign impact. Recently published recommendations aiming for a consistent clinical interpretation of non-coding variants have also highlighted the importance of functional evidence (Ellingford et al., 2022). In this context, iPSC-based disease modeling, which has developed rapidly in recent years, can be very helpful. The ability of iPSCs to differentiate into all cell types and their unlimited availability gives them an enormous advantage over primary and immortalized cell lines (Grskovic et al., 2011). Benchmarking and the use of appropriate controls, however, is a critical aspect of well-designed *in vitro* analyses to establish the range of the assay readout and to define thresholds (Brnich et al., 2019). The introduction of genetic variants into iPSCs with CRISPR/Cas9 genome editing is particularly valuable because it allows generation of isogenic lines, thereby reducing variability due to genetic background. We therefore used CRISPR/Cas9 genome editing in human iPSCs to provide functional evidence for the pathogenicity of the novel *CCM1* TSS deletion identified in our index case. The almost complete loss of *CCM1* gene expression in *CCM1*$^{del/del}$ cells was strong evidence for the pathogenicity of the variant and sufficient to classify this deletion as likely pathogenic following the ACMG guidelines. Thus, we were able to confirm the molecular CCM diagnosis for the family and can now offer genetic analysis to further at-risk relatives. We also demonstrated a reduced expression of *ANKIB1* in *CCM1*$^{del/del}$ iPSCs. However, no association can currently be established between decreased *ANKIB1* expression and the clinical phenotype of the index patient since little is known about the function of ANKIB1 so far.

Interestingly, our study led to another, rather unexpected, finding. While *CCM1* transcript levels were extremely low and thus hardly detectable in *CCM1*$^{del/del}$ iPSCs, residual *CCM1* transcript was still present in *CCM1*$^{-/-}$ knockout iPSCs with biallelic frameshift variants in the coding region of *CCM1*. We decided to study this effect in more detail and differentiated *CCM1*$^{del/del}$ and *CCM1*$^{-/-}$ iPSCs to ECs. While a very well-known consequence of *CCM1* inactivation in ECs, namely upregulation of *KLF2* (Zhou et al., 2016), was observed in both cell types, it was more pronounced in iPSC-derived *CCM1*$^{del/del}$ ECs. A similar effect was found for the expression of *NOS3* and *HEY2*. Only *THBS1* expression was equally reduced in iPSC-derived

10.3389/fmolb.2022.953048

CCM1$^{del/del}$ and *CCM1*$^{-/-}$ ECs. It has been shown in studies with different animal models that degradation of mutant mRNA is a possible trigger of genetic compensation mechanisms that may account for phenotypic differences between stable mutants and transient knockdowns (Rossi et al., 2015; El-Brolosy et al., 2019). This mechanism might also be an explanation for the more pronounced molecular consequences of the *CCM1* TSS deletion that blocks *CCM1* expression already at the transcriptional level. Thus, our *in vitro* analyses demonstrate the critical regulatory function of the region affected by the deletion. However, we were not able to directly compare homozygous *CCM1*$^{del/del}$ with heterozygous *CCM1*$^{WT/del}$ ECs, since we could not establish *CCM1*$^{WT/del}$ iPSCs. Further, possible off-target effects in iPSC-derived *CCM1*$^{del/del}$ ECs cannot be completely excluded. Yet, *CCM1* is a well-characterized disease gene and the observed molecular effects in *CCM1*$^{del/del}$ ECs correlate very well with the results from established *CCM1* knockout models.

In conclusion, our study expands the *CCM* mutation spectrum and illustrates that non-coding variants may be a cause of disease in apparently mutation-negative CCM cases. Moreover, we demonstrate that CRISPR/Cas9 editing in iPSCs represents a powerful approach for variant interpretation and can provide a promising platform for basic research or therapeutic CCM studies. Using iPSC-derived human brain microvascular endothelial-like cells and mosaic vascular organoids, we were recently able to show abnormal proliferation of *CCM3* mutant ECs in co-culture with wild-type ECs (Rath et al., 2022). In the future, novel patient-specific, co-culture or three-dimensional iPSC-based cell culture models could give further insight into CCM pathogenesis.

Data availability statement

The original contributions presented in the study are included in the article/Supplementary Material, further inquiries can be directed to the corresponding author.

Ethics statement

The studies involving human participants were reviewed and approved by the local ethics committee of the University Medicine Greifswald, Germany (No. BB 047/14). The patients/participants provided their written informed consent to participate in this study. Written informed consent was obtained from the individual(s) for the publication of any potentially identifiable images or data included in this article.

Author contributions

RP, MR, and UF designed the study. RP and DS performed the functional experiments. MR and UF supervised the experiments. RP, DS, and MR analyzed the data. MH, EM, and AR took care for the patient and provided clinical and magnetic resonance imaging data. TP performed the neuropathological analysis of tissue samples and interpreted the immunohistochemical characterization. AW performed and analyzed the cytogenetic analyses. All authors supported in data interpretation. RP, MR, and UF drafted the manuscript and all authors participated in writing.

Funding

This work was supported by the Deutsche Forschungsgemeinschaft (DFG, German Research Foundation; No. RA2876/2-2) and the German Federal Ministry of Education and Research (BMBF; No. 161L0276). MR was supported by a clinician scientist scholarship of the Gerhard Domagk program of the University Medicine Greifswald.

Acknowledgments

This research was made possible through the Allen Cell Collection, available from Coriell Institute for Medical Research. We would like to thank the patient for the participation in the study. We thank Frank Ulrich Weiß for his help with the qPCR analyses. Ole Schamuhn, Sina Ramcke, Lara Mellinger, and Lukas Zierke are thanked for their excellent technical assistance.

Conflict of interest

The authors declare that the research was conducted in the absence of any commercial or financial relationships that could be construed as a potential conflict of interest.

Publisher's note

Supplementary material

The Supplementary Material for this article can be found online at: https://www.frontiersin.org/articles/10.3389/fmolb.2022.953048/full#supplementary-material

References

Abou Tayoun, A. N., Pesaran, T., DiStefano, M. T., Oza, A., Rehm, H. L., Biesecker, L. G., et al. (2018). Recommendations for interpreting the loss of function PVS1 ACMG/AMP variant criterion. *Hum. Mutat.* 39 (11), 1517–1524. doi:10.1002/humu.23626

Akers, A., Al-Shahi Salman, R., Awad, I. A., Dahlem, K., Flemming, K., Hart, B., et al. (2017). Synopsis of guidelines for the clinical management of cerebral cavernous malformations: Consensus recommendations based on systematic literature review by the angioma alliance scientific advisory board clinical experts panel. *Neurosurgery* 80 (5), 665–680. doi:10.1093/neuros/nyx091

Al-Shahi, R., Bhattacharya, J. J., Currie, D. G., Papanastassiou, V., Ritchie, V., Roberts, R. C., et al. (2003). Prospective, population-based detection of intracranial vascular malformations in adults: the scottish intracranial vascular malformation study (SIVMS). *Stroke* 34 (5), 1163–1169. doi:10.1161/01.STR.0000069018.90456.C9

Batra, S., Lin, D., Recinos, P. F., Zhang, J., and Rigamonti, D. (2009). Cavernous malformations: natural history, diagnosis and treatment. *Nat. Rev. Neurol.* 5 (12), 659–670. doi:10.1038/nrneurol.2009.177

Brandt, T., Sack, L. M., Arjona, D., Tan, D., Mei, H., Cui, H., et al. (2020). Adapting ACMG/AMP sequence variant classification guidelines for single-gene copy number variants. *Genet. Med.* 22 (2), 336–344. doi:10.1038/s41436-019-0655-2

Brnich, S. E., Abou Tayoun, A. N., Couch, F. J., Cutting, G. R., Greenblatt, M. S., Heinen, C. D., et al. (2019). Recommendations for application of the functional evidence PS3/BS3 criterion using the ACMG/AMP sequence variant interpretation framework. *Genome Med.* 12 (1), 3. doi:10.1186/s13073-019-0690-2

Collins, R. L., Brand, H., Karczewski, K. J., Zhao, X., Alföldi, J., Francioli, L. C., et al. (2020). A structural variation reference for medical and population genetics. *Nature* 581 (7809), 444–451. doi:10.1038/s41586-020-2287-8

Damjanovich, K., Langa, C., Blanco, F. J., McDonald, J., Botella, L. M., Bernabeu, C., et al. (2011). 5'UTR mutations of *ENG* cause hereditary hemorrhagic telangiectasia. *Orphanet J. Rare Dis.* 6, 85. doi:10.1186/1750-1172-6-85

El-Brolosy, M. A., Kontarakis, Z., Rossi, A., Kuenne, C., Günther, S., Fukuda, N., et al. (2019). Genetic compensation triggered by mutant mRNA degradation. *Nature* 568 (7751), 193–197. doi:10.1038/s41586-019-1064-z

Ellingford, J. M., Ahn, J. W., Bagnall, R. D., Baralle, D., Barton, S., Campbell, C., et al. (2022). Recommendations for clinical interpretation of variants found in non-coding regions of the genome. *Genome Med.* 14 (1), 73. doi:10.1186/s13073-022-01073-3

Flemming, K. D., Graff-Radford, J., Aakre, J., Kantarci, K., Lanzino, G., Brown, R. D., Jr., et al. (2017). Population-based prevalence of cerebral cavernous malformations in older adults: mayo clinic study of aging. *JAMA Neurol.* 74 (7), 801–805. doi:10.1001/jamaneurol.2017.0439

French, J. D., and Edwards, S. L. (2020). The role of noncoding variants in heritable disease. *Trends Genet.* 36 (11), 880–891. doi:10.1016/j.tig.2020.07.004

Garg, P., Oikonomopoulos, A., Chen, H., Li, Y., Lam, C. K., Sallam, K., et al. (2018). Genome editing of induced pluripotent stem cells to decipher cardiac channelopathy variant. *J. Am. Coll. Cardiol.* 72 (1), 62–75. doi:10.1016/j.jacc.2018.04.041

Gingras, A. R., Liu, J. J., and Ginsberg, M. H. (2012). Structural basis of the junctional anchorage of the cerebral cavernous malformations complex. *J. Cell Biol.* 199 (1), 39–48. doi:10.1083/jcb.201205109

Glading, A., Han, J., Stockton, R. A., and Ginsberg, M. H. (2007). KRIT-1/CCM1 is a Rap1 effector that regulates endothelial cell cell junctions. *J. Cell Biol.* 179 (2), 247–254. doi:10.1083/jcb.200705175

Goitre, L., Balzac, F., Degani, S., Degan, P., Marchi, S., Pinton, P., et al. (2010). KRIT1 regulates the homeostasis of intracellular reactive oxygen species. *PLoS One* 5 (7), e11786. doi:10.1371/journal.pone.0011786

Grskovic, M., Javaherian, A., Strulovici, B., and Daley, G. Q. (2011). Induced pluripotent stem cells-opportunities for disease modelling and drug discovery. *Nat. Rev. Drug Discov.* 10 (12), 915–929. doi:10.1038/nrd3577

Harrison, S. M., Biesecker, L. G., and Rehm, H. L. (2019). Overview of specifications to the ACMG/AMP variant interpretation guidelines. *Curr. Protoc. Hum. Genet.* 103 (1), e93. doi:10.1002/cphg.93

Laberge-le Couteulx, S., Jung, H. H., Labauge, P., Houtteville, J. P., Lescoat, C., Cecillon, M., et al. (1999). Truncating mutations in *CCM1*, encoding KRIT1, cause hereditary cavernous angiomas. *Nat. Genet.* 23 (2), 189–193. doi:10.1038/13815

Labun, K., Montague, T. G., Krause, M., Torres Cleuren, Y. N., Tjeldnes, H., and Valen, E. (2019). CHOPCHOP v3: expanding the CRISPR web toolbox beyond genome editing. *Nucleic Acids Res.* 47 (W1), W171–W174. doi:10.1093/nar/gkz365

Lopez-Ramirez, M. A., Fonseca, G., Zeineddine, H. A., Girard, R., Moore, T., Pham, A., et al. (2017). Thrombospondin1 (TSP1) replacement prevents cerebral cavernous malformations. *J. Exp. Med.* 214 (11), 3331–3346. doi:10.1084/jem.20171178

Lopez-Ramirez, M. A., Lai, C. C., Soliman, S. I., Hale, P., Pham, A., Estrada, E. J., et al. (2021). Astrocytes propel neurovascular dysfunction during cerebral cavernous malformation lesion formation. *J. Clin. Invest.* 131 (13), 139570. doi:10.1172/JCI139570

Ma, N., Zhang, J. Z., Itzhaki, I., Zhang, S. L., Chen, H., Haddad, F., et al. (2018). Determining the pathogenicity of a genomic variant of uncertain significance using CRISPR/Cas9 and human-induced pluripotent stem cells. *Circulation* 138 (23), 2666–2681. doi:10.1161/CIRCULATIONAHA.117.032273

Maddaluno, L., Rudini, N., Cuttano, R., Bravi, L., Giampietro, C., Corada, M., et al. (2013). EndMT contributes to the onset and progression of cerebral cavernous malformations. *Nature* 498 (7455), 492–496. doi:10.1038/nature12207

McDonald, D. A., Shi, C., Shenkar, R., Gallione, C. J., Akers, A. L., Li, S., et al. (2014). Lesions from patients with sporadic cerebral cavernous malformations harbor somatic mutations in the CCM genes: evidence for a common biochemical pathway for CCM pathogenesis. *Hum. Mol. Genet.* 23 (16), 4357–4370. doi:10.1093/hmg/ddu153

Mondéjar, R., Solano, F., Rubio, R., Delgado, M., Pérez-Sempere, A., González-Meneses, A., et al. (2014). Mutation prevalence of cerebral cavernous malformation genes in Spanish patients. *PLoS One* 9 (1), e86286. doi:10.1371/journal.pone.0086286

Mondéjar, R., Delgado, M., Solano, F., Izquierdo, G., Martinez-Mir, A., and Lucas, M. (2016). Analysis of *CCM1* expression uncovers novel minor-form exons and variable splicing patterns. *Genes Genomics* 38 (9), 879–889. doi:10.1007/s13258-016-0435-1

Much, C. D., Schwefel, K., Skowronek, D., Shoubash, L., von Podewils, F., Elbracht, M., et al. (2019). Novel pathogenic variants in a cassette exon of *CCM2* in patients with cerebral cavernous malformations. *Front. Neurol.* 10, 1219. doi:10.3389/fneur.2019.01219

Otten, P., Pizzolato, G. P., Rilliet, B., and Berney, J. (1989). 131 cases of cavernous angioma (cavernomas) of the CNS, discovered by retrospective analysis of 24, 535 autopsies (in French). *Neurochirurgie* 35 (2), 82128–83131.

Pagenstecher, A., Stahl, S., Sure, U., and Felbor, U. (2009). A two-hit mechanism causes cerebral cavernous malformations: complete inactivation of CCM1, CCM2 or CCM3 in affected endothelial cells. *Hum. Mol. Genet.* 18 (5), 911–918. doi:10.1093/hmg/ddn420

Pilz, R. A., Schwefel, K., Weise, A., Liehr, T., Demmer, P., Spuler, A., et al. (2020). First interchromosomal insertion in a patient with cerebral and spinal cavernous malformations. *Sci. Rep.* 10 (1), 6306. doi:10.1038/s41598-020-63337-5

Rath, M., Schwefel, K., Malinverno, M., Skowronek, D., Leopoldi, A., Pilz, R. A., et al. (2022). Contact-dependent signaling triggers tumor-like proliferation of *CCM3* knockout endothelial cells in co-culture with wild-type cells. *Cell. Mol. Life Sci.* 79 (6), 340. doi:10.1007/s00018-022-04355-6

Rehm, H. L., Berg, J. S., Brooks, L. D., Bustamante, C. D., Evans, J. P., Landrum, M. J., et al. (2015). ClinGen- the clinical genome resource. *N. Engl. J. Med.* 372 (23), 2235–2242. doi:10.1056/NEJMsr1406261

Riant, F., Cecillon, M., Saugier-Veber, P., and Tournier-Lasserve, E. (2013). CCM molecular screening in a diagnosis context: novel unclassified variants leading to abnormal splicing and importance of large deletions. *Neurogenetics* 14 (2), 133–141. doi:10.1007/s10048-013-0362-0

Ricci, C., Riolo, G., and Battistini, S. (2021). Molecular genetic analysis of cerebral cavernous malformations: an update. *Vessel Plus* 5, 31. doi:10.20517/2574-1209.2021.28

Richards, S., Aziz, N., Bale, S., Bick, D., Das, S., Gastier-Foster, J., et al. (2015). Standards and guidelines for the interpretation of sequence variants: a joint consensus recommendation of the American College of medical genetics and genomics and the association for molecular Pathology. *Genet. Med.* 17 (5), 405–424. doi:10.1038/gim.2015.30

Robinson, J. T., Thorvaldsdóttir, H., Winckler, W., Guttman, M., Lander, E. S., Getz, G., et al. (2011). Integrative genomics viewer. *Nat. Biotechnol.* 29 (1), 24–26. doi:10.1038/nbt.1754

Rossi, A., Kontarakis, Z., Gerri, C., Nolte, H., Hölper, S., Krüger, M., et al. (2015). Genetic compensation induced by deleterious mutations but not gene knockdowns. *Nature* 524 (7564), 230–233. doi:10.1038/nature14580

Sahoo, T., Johnson, E. W., Thomas, J. W., Kuehl, P. M., Jones, T. L., Dokken, C. G., et al. (1999). Mutations in the gene encoding KRIT1, a Krev-1/rap1a binding

protein, cause cerebral cavernous malformations (*CCM1*). *Hum. Mol. Genet.* 8 (12), 2325–2333. doi:10.1093/hmg/8.12.2325

Schwefel, K., Spiegler, S., Much, C. D., Felbor, U., and Rath, M. (2020). CRISPR/Cas9-mediated generation of human endothelial cell knockout models of CCM disease. *Methods Mol. Biol.* 2152, 169–177. doi:10.1007/978-1-0716-0640-7_13

Spiegler, S., Najm, J., Liu, J., Gkalympoudis, S., Schröder, W., Borck, G., et al. (2014). High mutation detection rates in cerebral cavernous malformation upon stringent inclusion criteria: One-third of probands are minors. *Mol. Genet. Genomic Med.* 2 (2), 176–185. doi:10.1002/mgg3.60

Spiegler, S., Rath, M., Hoffjan, S., Dammann, P., Sure, U., Pagenstecher, A., et al. (2018a). First large genomic inversion in familial cerebral cavernous malformation identified by whole genome sequencing. *Neurogenetics* 19 (1), 55–59. doi:10.1007/s10048-017-0531-7

Spiegler, S., Rath, M., Paperlein, C., and Felbor, U. (2018b). Cerebral cavernous malformations: An update on prevalence, molecular genetic analyses, and genetic counselling. *Mol. Syndromol.* 9 (2), 60–69. doi:10.1159/000486292

Whiffin, N., Karczewski, K. J., Zhang, X., Chothani, S., Smith, M. J., Evans, D. G., et al. (2020). Characterising the loss-of-function impact of 5' untranslated region variants in 15, 708 individuals. *Nat. Commun.* 11 (1), 2523. doi:10.1038/s41467-019-10717-9

Wright, C. F., Quaife, N. M., Ramos-Hernández, L., Danecek, P., Ferla, M. P., Samocha, K. E., et al. (2021). Non-coding region variants upstream of *MEF2C* cause severe developmental disorder through three distinct loss-of-function mechanisms. *Am. J. Hum. Genet.* 108 (6), 1083–1094. doi:10.1016/j.ajhg.2021.04.025

Wüstehube, J., Bartol, A., Liebler, S. S., Brütsch, R., Zhu, Y., Felbor, U., et al. (2010). Cerebral cavernous malformation protein CCM1 inhibits sprouting angiogenesis by activating DELTA-NOTCH signaling. *Proc. Natl. Acad. Sci. U. S. A.* 107 (28), 12640–12645. doi:10.1073/pnas.1000132107

Zhang, F., and Lupski, J. R. (2015). Non-coding genetic variants in human disease. *Hum. Mol. Genet.* 24 (R1), R102–R110. doi:10.1093/hmg/ddv259

Zhou, Z., Tang, A. T., Wong, W. Y., Bamezai, S., Goddard, L. M., Shenkar, R., et al. (2016). Cerebral cavernous malformations arise from endothelial gain of MEKK3-KLF2/4 signalling. *Nature* 532 (7597), 122–126. doi:10.1038/nature17178

5.3 Endothelial differentiation of *CCM1* knockout iPSCs triggers the establishment of a specific gene expression signature

Robin A. Pilz*, Dariush Skowronek*, Lara Mellinger, Ute Felbor, Matthias Rath

*Diese Autoren haben gleichermaßen zur Arbeit beigetragen.

Manuskript unter Begutachtung beim *International Journal of Molecular Sciences*

Es wurde die vom Journal bereitgestellte Vorlage zur Manuskripterstellung verwendet.

International Journal of *Molecular Sciences*

MDPI

Communication

Endothelial differentiation of *CCM1* knockout iPSCs triggers the establishment of a specific gene expression signature

Robin A. Pilz[1,§], Dariush Skowronek[1,§], Lara Mellinger[1], Ute Felbor[1] and Matthias Rath[1,2,*]

[1] Department of Human Genetics, University Medicine Greifswald, and Interfaculty Institute of Genetics and Functional Genomics, University of Greifswald, 17475 Greifswald, Germany.
[2] Department of Human Medicine and Institute for Molecular Medicine, MSH Medical School Hamburg, Hamburg, Germany.
* Correspondence: Matthias.Rath@med.uni-greifswald.de; Tel.: +49 3834 865396
§ These authors contributed equally.

Abstract: Cerebral cavernous malformation (CCM) is a neurovascular disease that can lead to seizures and stroke-like symptoms. The familial form is caused by a heterozygous germline mutation in either the *CCM1*, *CCM2*, or *CCM3* gene. While the importance of a second-hit mechanism in CCM development is well established, it is still unclear whether it immediately triggers CCM development or whether additional external factors are required. We here used RNA sequencing to study differential gene expression in *CCM1* knockout induced pluripotent stem cells (*CCM1*$^{-/-}$ iPSCs), early mesoderm progenitor cells (eMPCs), and endothelial-like cells (ECs). Notably, CRISPR/Cas9-mediated inactivation of *CCM1* led to hardly any gene expression differences in iPSCs and eMPCs. However, after differentiation into ECs, we found significant deregulation of signaling pathways well known to be involved in CCM pathogenesis. These data suggest that only a microenvironment of proangiogenic cytokines and growth factors triggers the establishment of a characteristic gene expression signature upon *CCM1* inactivation. Consequently, a cellular and molecular phenotype appears to primarily occur when *CCM1*$^{-/-}$ precursor cells enter the endothelial lineage. Taken together, not only downstream consequences of *CCM1* ablation but also supporting factors must be addressed in CCM therapy development.

Keywords: Cerebral cavernous malformation; *CCM1/KRIT1*; CRISPR/Cas9 genome editing; iPSCs; iPSC-derived endothelial cells; RNA-Seq; endothelial-specific gene expression

Citation: Pilz, R.A.; Skowronek, D.; Mellinger, L.; Felbor, U.; Rath, M. Endothelial differentiation of *CCM1* knockout iPSCs triggers the establishment of a specific gene expression signature. *Int. J. Mol. Sci.* **2022**, *23*, x. https://doi.org/10.3390/xxxxx

Academic Editor: Firstname Lastname

Received: date
Accepted: date
Published: date

1. Introduction

Cerebral cavernous malformations (CCMs) are capillary-venous lesions which are primarily found in the brain and spinal cord [1]. The familial form of this neurovascular disorder is inherited in an autosomal dominant manner with incomplete penetrance. Pathogenic variants in the *CCM1* gene (also known as *KRIT1*) can be identified in nearly 50 % of patients with multiple CCMs or a positive family history [2]. Less frequently, germline mutations are detected in *CCM2* or *CCM3* (also known as *PDCD10)*. CCM lesions are associated with a significant risk of bleeding and can lead to headaches, seizures, paralysis, and other stroke-like symptoms [3]. The prevalence of symptomatic familial CCM cases is estimated to be about 1:5,400 to 1:6,200 [4]. One-third of the affected patients are minors, and no specific therapies are available yet [2].

It has long been established that a cellular recessive two-hit mechanism triggers CCM formation [5,6]. Although CCMs are benign vascular lesions, this mechanism is reminiscent of carcinogenesis. The identification of somatic *PIK3CA* mutations in human CCM tissues and the proof of clonal expansion of mutant endothelial cells in inducible CCM3 mouse models further support the concept that "cancer-like" mechanisms are involved in CCM pathogenesis [7-9]. The "cancer-like" behavior of mutant ECs, however,

is not limited to *CCM3* inactivation. Using blood outgrowth endothelial cells (BOECs), which are also referred to as endothelial colony-forming cells (ECFCs), we have previously shown that CRISPR/Cas9-induced *CCM1* ablation causes increased proliferation of mutant BOECs when co-cultured with wild-type cells [10].

Yet, it is still poorly understood whether there is a critical time window when CCM protein inactivation induces CCM formation. Interestingly, Malinverno and colleagues demonstrated that *Ccm3* inactivation in vessel-resident endothelial progenitor cells also led to their clonal expansion and CCM formation in mice [9]. Combining our recently established *CCM1* knockout induced pluripotent stem cell (iPSC) model [11], differentiation of iPSCs into endothelial-like cells (hereafter referred to as ECs), and RNA sequencing analysis, we here demonstrate that loss of *CCM1* expression leads to strong gene expression differences in ECs but not in iPSCs or early mesoderm progenitor cells (eMPCs).

Our data suggest that a second somatic mutation followed by CCM1 inactivation in endothelial precursor cells does not result in a cellular or molecular phenotype until entry of the mutant cells into the endothelial lineage.

2. Results

We have recently established a novel *CCM1* knockout iPSC model and demonstrated that *CCM1*$^{-/-}$ iPSCs can be differentiated into ECs which show upregulation of *KLF2* and *KLF4* as well as downregulation of *THBS1* [11]. These gene expression differences are well-characterized consequences of *CCM1* inactivation in ECs [12,13]. In our current study we decided to analyze the gene expression profile in *CCM1*$^{-/-}$ iPSC-derived ECs in more detail and to address the question whether CCM1 deficiency also leads to gene expression differences in iPSCs and eMPCs (Figure 1).

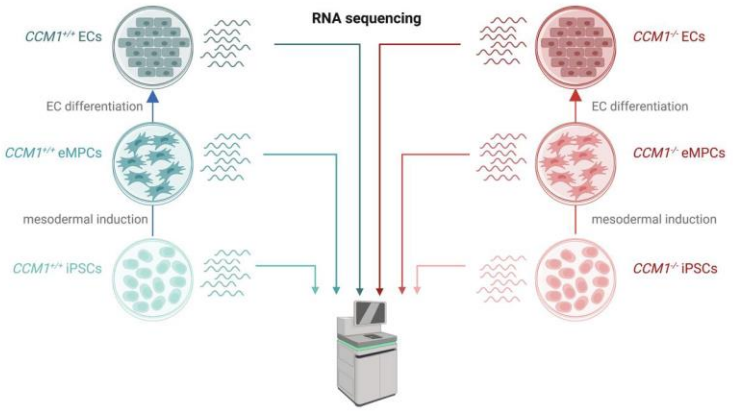

Figure 1. Experimental design of the study. *CCM1*$^{+/+}$ and *CCM1*$^{-/-}$ induced pluripotent cells (iPSCs) were differentiated into early mesoderm progenitor cells (eMPCs) and endothelial-like cells (ECs). RNA sequencing was used to study gene expression differences.

2.1. Major gene expression differences in CCM1$^{-/-}$ *iPSC-derived ECs*

Differentiation of *CCM1*$^{+/+}$ and *CCM1*$^{-/-}$ iPSCs into ECs with the STEMdiff Endothelial Differentiation Kit (Figure 2a,b) led to upregulation of 4,470 and 4,262 genes, respectively. At the same time, 4,674 and 4,468 genes were downregulated (Figure 2c,d). As expected, most of the differentially expressed genes could be assigned to angiogenesis-associated processes. No major differences could be detected between the two genotypes (Figure 2e,f; Figure S1). Furthermore, mutant and wild-type cells showed a characteristic endothelial morphology and expressed the EC markers CD31, vWF, and

VE-cadherin (Figure 2a,b). These results suggest that EC differentiation itself is not compromised by *CCM1* inactivation.

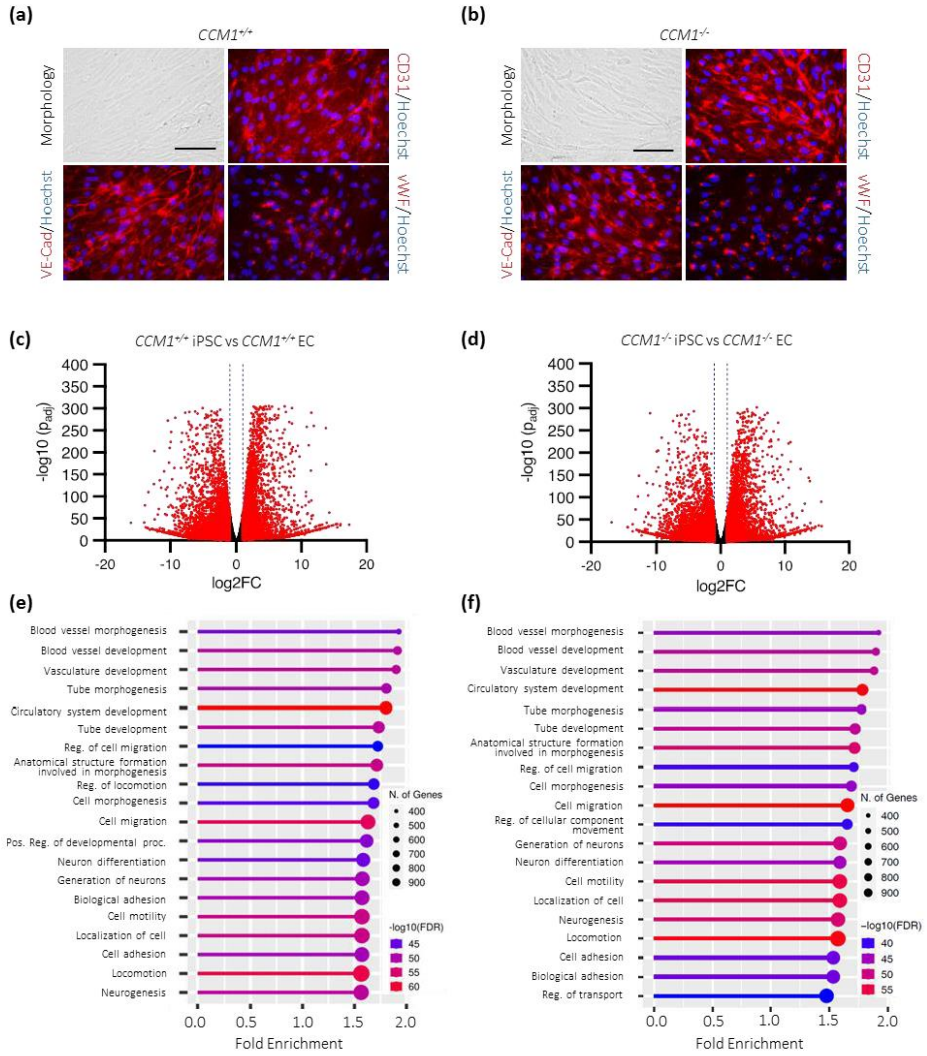

Figure 2. Targeted differentiation of iPSCs into ECs. (**a**,**b**) *CCM1*$^{+/+}$ (**a**) and *CCM1*$^{-/-}$ (**b**) iPSC-derived ECs display typical EC morphology and express EC markers CD31, VE-Cadherin, and vWF (scale = 75 µm); (**c**,**d**) Volcano plots of genes that are up- or downregulated upon differentiation of *CCM1*$^{+/+}$ (**c**) and *CCM1*$^{-/-}$ (**d**) iPSCs into ECs. The log2 fold changes (log2FC) of the normalized mean hit counts are plotted against the negative log10 adjusted p-values (-log10 (p_{adj})). Differentially expressed genes ($= p_{adj} < 0.05$ and $|log2FC| > 1$) are marked in red; (**e**,**f**) GO biological process enrichment analysis for *CCM1*$^{+/+}$ (**e**) and *CCM1*$^{-/-}$ (**f**) cells. FDR = false discovery rate. The lollipop charts were created with ShinyGO 0.76 [14]. n = 3 per genotype.

When we compared the gene expression profiles of *CCM1*$^{+/+}$ and *CCM1*$^{-/-}$ iPSC-derived ECs, we found major differences. 181 and 161 genes were significantly up- or downregulated in *CCM1*$^{-/-}$ ECs, respectively (Figure 3a). Among the most upregulated genes were *LHX6* (LIM Homeobox 6; log2FC = 5.4), *CMKLR1* (Chemerin Chemokine-Like Receptor 1; log2FC = 5.1), *APLNR* (Apelin Receptor; log2FC = 4.9), *HSPA12B* (Heat Shock Protein Family A (Hsp70) Member 12B; log2FC = 4.6), and *KLF2* (Krueppel-Like Factor 2; log2FC = 4.3). The top 10 upregulated genes also included *KLF4* (Krueppel-Like Factor 4; log2FC = 3.5). Less highly upregulated was, for example, *THBD* (Thrombomodulin; log2FC = 1.1). Strongly downregulated, on the other hand, were *TCN1* (Transcobalamin 1; log2FC = -3.6), *MT1G* (Metallothionein 1G; log2FC = -3.4), *SCGB1A1* (Secretoglobin Family 1A Member 1; log2FC = -3.3), *CRABP1* (Cellular Retinoic Acid Binding Protein 1; log2FC = -3.3), and *MMP9* (Matrix Metallopeptidase 9; log2FC = -3.3) (Figure 3b). *THBS1* (Thrombospondin 1), which has also been reported to be involved in CCM pathogenesis [13], was moderately downregulated (log2FC = -1.1).

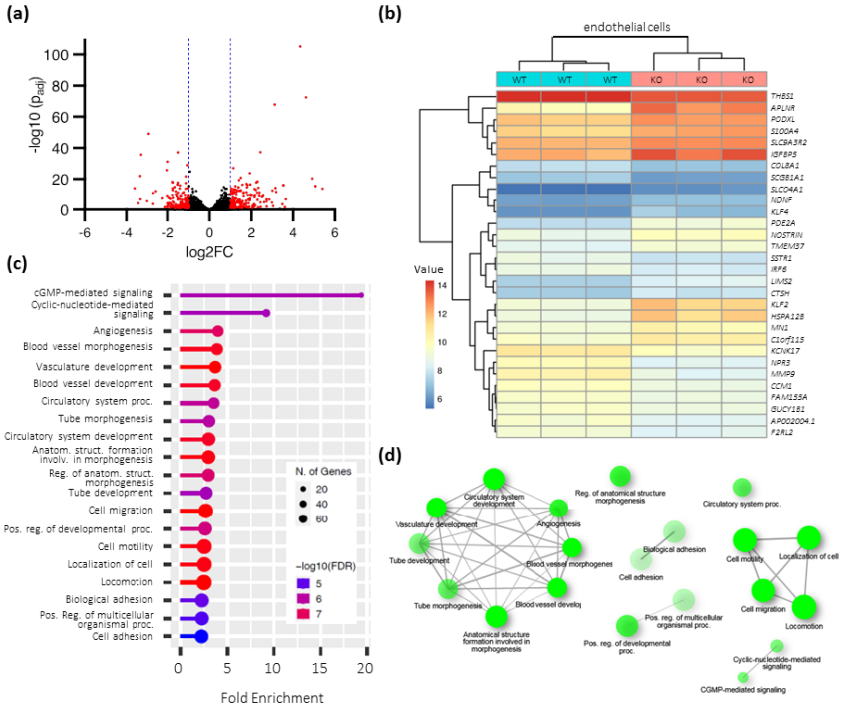

Figure 3. Gene expression differences in *CCM1*$^{-/-}$ iPSC-derived ECs. (**a**) Volcano plot of up- or downregulated genes in *CCM1*$^{-/-}$ iPSC-derived ECs. The log2 fold change (log2FC) of the normalized mean hit counts is plotted against the negative log10 adjusted p-value (-log10 (p_{adj})). Differentially expressed genes (= $p_{adj} < 0.05$ and $|log2FC| > 1$) are marked in red; (**b**) Heatmap of differentially expressed genes in *CCM1*$^{-/-}$ iPSC-derived ECs. Shown are regularized log transformed read counts (= value) for *CCM1*$^{-/-}$ (KO) and *CCM1*$^{+/+}$ (WT) iPSC-derived ECs; (**c**) GO biological process enrichment analysis for differentially expressed genes in *CCM1*$^{-/-}$ iPSC-derived ECs. To avoid a systemic bias, *CCM1* was excluded from the enrichment analysis. FDR = false discovery rate; (**d**) Enriched GO terms are visualized as network. The size of the network nodes reflects the number of genes. Lines connect related terms. The thickness of the lines reflects the percent of overlapping genes. The lollipop chart (**c**) and the network (**d**) were created with ShinyGO 0.76 [14]. n = 3 per genotype.

The deregulated genes could be assigned to different clusters of biological processes. As expected, angiogenesis-associated and vessel formation-related processes were among them. In addition, genes involved in cell motility were also deregulated (Figure 3c,d). Taken together, these data reinforce the validity of this new model and show that some key players, e.g., KLF2 or KLF4, can indeed be considered as markers of CCM pathogenesis independently of the model used.

2.2. Minor gene expression differences in CCM1$^{-/-}$ iPSC and CCM1$^{-/-}$ iPSC-derived eMPCs

We next asked whether *CCM1* inactivation also leads to a characteristic molecular phenotype in iPSCs and subjected *CCM1*$^{+/+}$ and *CCM1*$^{-/-}$ iPSCs to RNA-seq analysis. However, we could find hardly any gene expression differences (Figure 4a,b). Besides downregulation of *CCM1* gene expression (log2FC = -2.0), only *LHX5* was significantly upregulated (LIM Homeobox 5; log2FC = 1.9). Yet, the adjusted p-value for *LHX5* was only slightly below the significance level (p_{adj} = 0.045). These data suggest that *CCM1* expression is dispensable in iPSCs and that its inactivation does not result in a molecular phenotype.

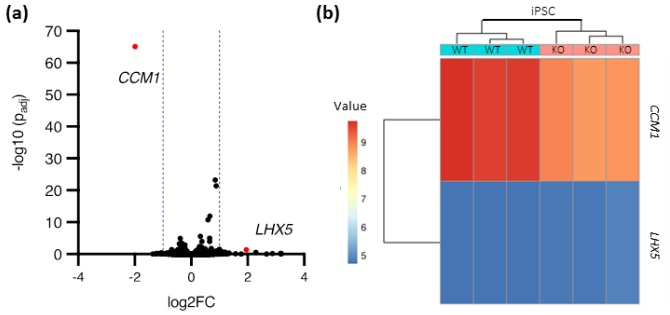

Figure 4. Gene expression differences in *CCM1*$^{-/-}$ iPSCs. (a) Volcano plot of up- or downregulated genes in *CCM1*$^{-/-}$ iPSCs. The log2 fold change (log2FC) of the normalized mean hit counts is plotted against the negative log10 adjusted p-value (-log10 (p_{adj})). Differentially expressed genes (= $p_{adj} < 0.05$ and $|log2FC| > 1$) are marked in red; (b) Heatmap of differentially expressed genes in *CCM1*$^{-/-}$ iPSCs. Shown are regularized log transformed read counts (= value) for *CCM1*$^{-/-}$ (KO) and *CCM1*$^{+/+}$ (WT) iPSCs. n = 3 per genotype.

An intermediate stage of differentiation from iPSCs to ECs with the STEMdiff Endothelial Differentiation Kit are eMPCs. Therefore, we also profiled gene expression levels for these cells by RNA-seq to characterize the effects of *CCM1* inactivation. Although we detected slightly stronger differences in these cells than in iPSCs, only 26 genes were upregulated and 2 genes were downregulated in total (Figure 5a). As expected, one of these genes was *CCM1* (log2FC = -1.8). Other deregulated genes included: *STMN2* (Stathmin 2; log2FC = 2.1), *PARM1* (Prostate Androgen-Regulated Mucin-Like Protein 1; log2FC = 1.9), *LYPD1* (LY6/PLAUR Domain Containing 1; log2FC = 1.6), *RHOB* (Ras Homolog Family Member B; log2FC = 1.5), *SLCO4A1* (Solute Carrier Organic Anion Transporter Family Member 4A1; log2FC = 1.5), and *KLF2* (Krueppel-Like Factor 2; log2FC = 1.4) (Figure 5b). Our biological process enrichment analysis found only moderate enrichment for negative regulation of microtubule polymerization and reactive oxygen species-related clusters (Figure 5c). However, we also found only moderate significance levels for eMPCs.

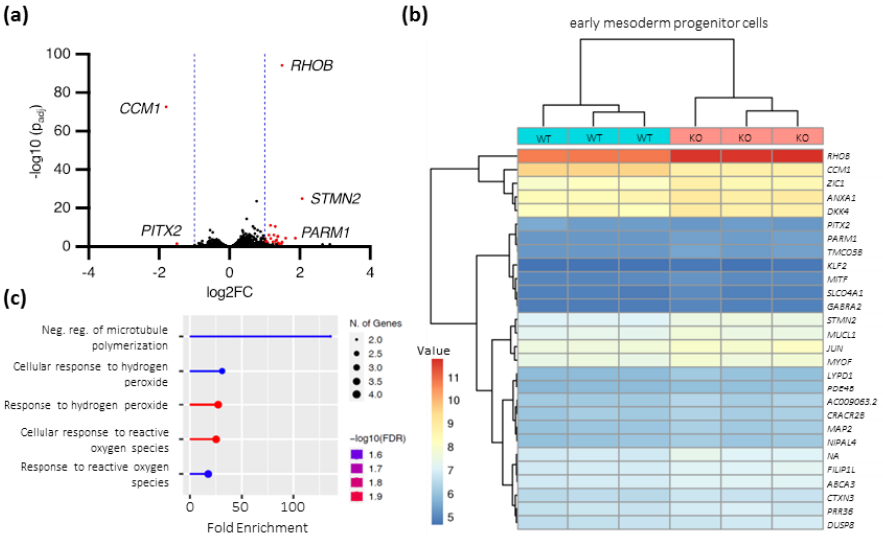

Figure 5. Gene expression differences in *CCM1*$^{-/-}$ iPSC-derived eMPCs. (**a**) Volcano plot of up- or downregulated genes in *CCM1*$^{-/-}$ iPSC-derived eMPCs. The log2 fold change (log2FC) of the normalized mean hit counts is plotted against the negative log10 adjusted p-value (-log10 (p_{adj})). Differentially expressed genes (= $p_{adj} < 0.05$ and $|log2FC| > 1$) are marked in red; (**b**) Heatmap of differentially expressed genes in *CCM1*$^{-/-}$ iPSC-derived eMPCs. Shown are regularized log transformed read counts (= value) for *CCM1*$^{-/-}$ (KO) and *CCM1*$^{+/+}$ (WT) iPSC-derived eMPCs; (**c**) GO biological process enrichment analysis for differentially expressed genes in *CCM1*$^{-/-}$ iPSC-derived eMPCs. To avoid a systemic bias, *CCM1* was excluded from the enrichment analysis. FDR = false discovery rate. The lollipop chart was created with ShinyGO 0.76 [14]. n = 3 per genotype.

3. Discussion

The results of our current study presenting comprehensive RNA sequencing data from *CCM1*$^{-/-}$ iPSCs, eMPCs, and ECs allow two conclusions: (1) CCM1 is dispensable for EC differentiation but essential for the maintenance of endothelial quiescence and (2) CCM1 apparently does not play a critical role in iPSCs and eMPCs.

Upon induction of endothelial differentiation, *CCM1*$^{-/-}$ iPSCs significantly activated signaling cascades related to blood vessel development and morphogenesis, tube formation, and cell migration. Furthermore, *CCM1*$^{-/-}$ iPSC-derived ECs showed normal morphology and expressed typical EC markers. However, when we compared *CCM1*$^{-/-}$ and *CCM1*$^{+/+}$ iPSC-derived ECs on the molecular level, we found hundreds of differentially expressed genes. Among the most upregulated transcripts in mutant ECs were *KLF2* and *KLF4*, which are crucial mediators of profound dysfunction in ECs lacking CCM1, CCM2, or CCM3 [12,15-17]. Interestingly, analyses in hCMEC/D3 cells (human cerebral microvascular endothelial cell line), HUVECs (human umbilical vein endothelial cells), and zebrafish have recently demonstrated that not only genetic *CCM1* inactivation but also inhibition of the HEG1 (heart of glass 1)-CCM1 protein complex can induce upregulation of KLF2 and KLF4 levels in ECs [18]. However, irrespective of its causes, a gain of MEKK3-KLF2/4 signaling in ECs has various consequences, e.g., deregulation of RHO/ROCK signaling, endothelial-to-mesenchymal transition (endMT), and activation of the metalloproteases ADAMTS4/5 [12,19-21]. All these mechanisms can trigger CCM formation *in vivo*. Besides induction of *KLF2/4* expression, other known effects of *CCM1* inactivation in ECs, namely deregulation of angiogenesis-related pathways, upregulation of *THBD*, or downregulation of THBS1 [13,22], could also be recapitulated in our *CCM1*

knockout iPSC-derived EC model. Based on these data, it is evident that the inactivation of *CCM1* in ECs apparently cannot be compensated and disrupts endothelial quiescence. Our RNA sequencing analysis of *CCM1*$^{-/-}$ iPSCs, eMPCs, and ECs can obviously not exclude molecular consequences of *CCM1* inactivation in other cell types. Indeed, for the *CCM3* gene, it has been reported that its inactivation in neuroglia and mural cells induces CCM-like lesions in mice [23,24]. However, our results suggest that there might be *CCM1*$^{-/-}$ precursor cells which remain silent until they come into a specific microenvironment and differentiate into endothelial cells.

Although CCM1 is ubiquitously expressed in early embryogenesis and found with high expression levels in various cell lines [25-27], its function in non-endothelial cell types remains poorly understood. Consistent with the assumption that intact CCM function is required specifically in ECs [19], we found very few gene expression differences in *CCM1* knockout eMPCs and iPSCs. In addition, the overlap of up- or downregulated genes in *CCM1*$^{-/-}$ ECs, eMPCs, and iPSCs was very small. Apart from CRISPR/Cas9-induced disruption of *CCM1* gene expression, there was no overlap between iPSCs and eMPCs or ECs, largely because only two genes were differentially expressed in *CCM1*$^{-/-}$ iPSCs anyway. However, there was also little overlap between eMPCs and ECs (Figure 6).

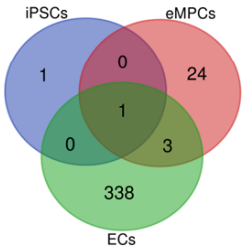

ECs ∩ eMPCs ∩ iPSC	*CCM1*$^{-/-}$ vs *CCM1*$^{+/+}$ iPSCs	*CCM1*$^{-/-}$ vs *CCM1*$^{+/+}$ eMPCs	*CCM1*$^{-/-}$ vs *CCM1*$^{+/+}$ ECs
ENSG00000001631 = *CCM1*	*log2FC = -1.99*	*log2FC = -1.80*	*log2FC = -1.49*
ECs ∩ eMPCs	*CCM1*$^{+/+}$ vs *CCM1*$^{+/+}$ iPSCs	*CCM1*$^{+/+}$ vs *CCM1*$^{+/+}$ eMPCs	*CCM1*$^{+/+}$ vs *CCM1*$^{+/+}$ ECs
ENSG00000127528 = *KLF2*	-	*log2FC = 1.41*	*log2FC = 4.35*
ENSG00000101187 = *SLCO4A1*	-	*log2FC = 1.48*	*log2FC = 3.55*
ENSG00000104435 = *STMN2*	-	*log2FC = 2.07*	*log2FC = 1.02*

Figure 6. Overlap of differential expressed genes in iPSCs, eMPCs, and ECs. Differential gene expression was defined as $p_{adj} < 0.05$ and |log2FC| > 1. iPSCs = *CCM1*$^{-/-}$ vs *CCM1*$^{+/+}$ iPSCs; eMPCs = *CCM1*$^{-/-}$ vs *CCM1*$^{+/+}$ eMPCs; ECs = *CCM1*$^{-/-}$ vs *CCM1*$^{+/+}$ ECs.

Although *KLF2* was also moderately upregulated in *CCM1*$^{-/-}$ eMPCs, the expression difference increased significantly when the cells were further differentiated into ECs. The same is true for *SLCO4A1* whose role in CCM pathogenesis is unclear so far. In contrast, the expression levels of *KLF4* and nearly all other genes that were up- or downregulated in mutant ECs were unchanged in *CCM1*$^{-/-}$ eMPCs or iPSCs. These results suggest that the establishment of a *CCM1* knockout-specific gene expression pattern is enabled by exogenous factors such as cytokines and growth factors used to induce EC differentiation. The idea that the multiple downstream effects of *CCM* gene inactivation may occur only in a specific microenvironment is not completely new. In 2011, the groups of Elisabetta Dejana and Elisabeth Tournier-Lasserve reported that EC-specific ablation of *Ccm2* in mice only led to a CCM phenotype when induced in developmental stages of active angiogenesis [28]. Furthermore, the inhibition of VEGF signaling, which is essential for angiogenesis *in vivo* and also for differentiation of iPSCs into ECs, was shown to reduce the number of CCM lesions in *Ccm1* induced endothelial cell knockout mice (*Krit1*^{ieKO}) [29,30]. This also reinforces the important role of exogenous triggers for CCM formation.

Taken together, our results suggest that in our search for new CCM therapies, we should address not only the consequences of CCM ablation but also the supporting factors for endothelial dysfunction.

4. Materials and Methods

4.1. Cell culture of induced pluripotent stem cells (iPSCs)

The *CCM1*$^{+/+}$ and *CCM1*$^{-/-}$ iPSC lines used in this study have been derived from the parental AICS-0023 iPSC line (Allen Cell Collection, Coriell Institute, USA) before [11]. IPSCs were maintained in Essential 8 Flex medium (Thermo Fisher Scientific, Waltham, USA) at 37°C and 5 % CO_2 on plates coated with growth factor reduced matrigel (Corning, New York, USA). Cultures were routinely passaged with 0.5 mM EDTA (Thermo Fisher Scientific).

4.2. Differentiation of iPSCs into eMPCs and ECs

The STEMdiff Endothelial Differentiation Kit (STEMCELL Technologies, Vancouver, Canada) was used according to the manufacturer's instructions for the differentiation of iPSCs into eMPCs and ECs. Initially, iPSCs were detached with StemPro Accutase (Thermo Fisher Scientific) and seeded at a density of 100,000 cells per 6-well in Essential 8 Flex medium supplemented with 10 µM ROCK inhibitor Y-27632 (STEMCELL Technologies). On day 7, differentiated ECs were subcultured at a density of 150,000 cells per 6-well. The cells were expanded in STEMdiff Endothelial Expansion Medium (STEMCELL Technologies) for four days, then splitted on passage #1, and cultured for additional four days. RNA was extracted for eMPCs on day 3 of the differentiation protocol and for expanded differentiated ECs at passage #1.

To check differentiated ECs for endothelial marker expression at passage #1, the Immunofluorescence Application Solutions Kit (Cell Signaling, Danvers, United States) was used for staining of CD31 (3528S, 1:800, Cell Signaling), VE-Cadherin (2500S, 1:400, Cell Signaling), and VWF (MA5-14029, 1:66, Thermo Fisher Scientific) according to the manufacturer's instructions. An anti-mouse Alexa Fluor 555 antibody (ab150114, 1:200, Abcam, Cambridge, UK) or an anti-rabbit Alexa Fluor 555 antibody (A21429, 1:500, Thermo Fisher Scientific) were used as secondary antibodies.

4.3. RNA sequencing and data analysis

The Direct-zol RNA MiniPrep Plus Kit (Zymo Research, Irvine, USA) was used for RNA purification. Concentration measurements and sample integrity control were performed with a Qubit 4.0 fluorometer (Thermo Fisher Scientific) and on a 2100 Bioanalyzer instrument (Agilent, Santa Clara, USA), respectively. RNA-library preparation by polyA selection and sequencing on an Illumina NovaSeq (Illumina) with 2x150 cycles was done by Azenta Life Sciences (Leipzig, Germany). Trimming of reads and mapping to the human reference genome assembly GRCh37 was performed with Trimmomatic v.0.36 and STAR aligner v.2.5.2b. Gene hit counts were extracted with featureCounts from the Subread package v.1.5.2.

4.4. Statistical analysis

DESeq2 was used for the analysis of differential gene expression in RNA-seq data. To generate p values and log2 fold changes the Wald test was utilized. Genes with an adjusted p value of < 0.05 and an absolute log2 fold change > 1 were considered differentially expressed between compared groups. Gene ontology analysis was performed with ShinyGO 0.76.1 [14] and an FDR cut-off of 0.05.

Supplementary Materials: The following supporting information can be downloaded at: www.mdpi.com/xxx/s1, Figure S1: Heatmaps of significantly up- or downregulated genes in targeted differentiation of *CCM1*$^{+/+}$ (**a**) and *CCM1*$^{-/-}$ (**b**) iPSCs into ECs. Shown are regularized log transformed read counts for cells. Differentially expressed genes = $p_{adj} < 0.05$ and $|\log2\ FC| > 1$. n = 3 per genotype. WT = *CCM1*$^{+/+}$ wild-type cells; KO = *CCM1*$^{-/-}$ knockout cells. (**c**) Venn diagram of the overlap of differentially expressed genes in both conditions.

Author Contributions: Conceptualization, M.R. and U.F.; formal analysis, R.A.P, D.S. and L. M.; investigation, R.A.P, D.S. and L. M.; writing—original draft preparation, M.R., R.A.P, D.S.; writing—review and editing, M.R. and U.F.; visualization, R.A.P, D.S. and L.M.; supervision, M.R. and U.F.; funding acquisition, M.R. All authors have read and agreed to the published version of the manuscript.

Funding: This research was funded by the German Research Foundation (DFG, Deutsche Forschungsgemeinschaft) [grant number RA2876/2-2], the German Federal Ministry of Education and Research (BMBF) [grant number 161L0276], and by the Research Network Molecular Medicine of the University Medicine Greifswald [FOVB-2020-01]. MR was supported by a clinician scientist scholarship of the Gerhard Domagk program of the University Medicine Greifswald.

Institutional Review Board Statement: Not applicable.

Informed Consent Statement: Not applicable.

Data Availability Statement: RNA sequencing data were uploaded to the Gene Expression Omnibus (GEO) database (record number: GSE214306). All other relevant data are published within the paper.

Acknowledgments: This research was made possible through the Allen Cell Collection, available from Coriell Institute for Medical Research. Figure 1 was created with biorender.com. We thank O. Schamuhn for his excellent technical assistance.

Conflicts of Interest: The authors declare no conflict of interest. The funders had no role in the design of the study; in the collection, analyses, or interpretation of data; in the writing of the manuscript; or in the decision to publish the results.

References

1. Haasdijk, R.A.; Cheng, C.; Maat-Kievit, A.J.; Duckers, H.J. Cerebral cavernous malformations: from molecular pathogenesis to genetic counselling and clinical management. *Eur J Hum Genet* **2012**, *20*, 134-140, doi:10.1038/ejhg.2011.155.
2. Spiegler, S.; Najm, J.; Liu, J.; Gkalympoudis, S.; Schröder, W.; Borck, G.; Brockmann, K.; Elbracht, M.; Fauth, C.; Ferbert, A.; et al. High mutation detection rates in cerebral cavernous malformation upon stringent inclusion criteria: one-third of probands are minors. *Mol Genet Genomic Med* **2014**, *2*, 176-185, doi:10.1002/mgg3.60.
3. Batra, S.; Lin, D.; Recinos, P.F.; Zhang, J.; Rigamonti, D. Cavernous malformations: natural history, diagnosis and treatment. *Nat Rev Neurol* **2009**, *5*, 659-670, doi:10.1038/nrneurol.2009.177.
4. Spiegler, S.; Rath, M.; Paperlein, C.; Felbor, U. Cerebral Cavernous Malformations: An Update on Prevalence, Molecular Genetic Analyses, and Genetic Counselling. *Mol Syndromol* **2018**, *9*, 60-69, doi:10.1159/000486292.
5. Pagenstecher, A.; Stahl, S.; Sure, U.; Felbor, U. A two-hit mechanism causes cerebral cavernous malformations: complete inactivation of CCM1, CCM2 or CCM3 in affected endothelial cells. *Hum Mol Genet* **2009**, *18*, 911-918, doi:10.1093/hmg/ddn420.
6. McDonald, D.A.; Shi, C.; Shenkar, R.; Gallione, C.J.; Akers, A.L.; Li, S.; De Castro, N.; Berg, M.J.; Corcoran, D.L.; Awad, I.A.; et al. Lesions from patients with sporadic cerebral cavernous malformations harbor somatic mutations in the CCM genes: evidence for a common biochemical pathway for CCM pathogenesis. *Hum Mol Genet* **2014**, *23*, 4357-4370, doi:10.1093/hmg/ddu153.
7. Ren, A.A.; Snellings, D.A.; Su, Y.S.; Hong, C.C.; Castro, M.; Tang, A.T.; Detter, M.R.; Hobson, N.; Girard, R.; Romanos, S.; et al. *PIK3CA* and CCM mutations fuel cavernomas through a cancer-like mechanism. *Nature* **2021**, *594*, 271-276, doi:10.1038/s41586-021-03562-8.
8. Detter, M.R.; Snellings, D.A.; Marchuk, D.A. Cerebral Cavernous Malformations Develop Through Clonal Expansion of Mutant Endothelial Cells. *Circ Res* **2018**, *123*, 1143-1151, doi:10.1161/CIRCRESAHA.118.313970.
9. Malinverno, M.; Maderna, C.; Abu Taha, A.; Corada, M.; Orsenigo, F.; Valentino, M.; Pisati, F.; Fusco, C.; Graziano, P.; Giannotta, M.; et al. Endothelial cell clonal expansion in the development of cerebral cavernous malformations. *Nat Commun* **2019**, *10*, 2761, doi:10.1038/s41467-019-10707-x.

10. Spiegler, S.; Rath, M.; Much, C.D.; Sendtner, B.S.; Felbor, U. Precise *CCM1* gene correction and inactivation in patient-derived endothelial cells: Modeling Knudson's two-hit hypothesis in vitro. *Mol Genet Genomic Med* **2019**, *7*, e00755, doi:10.1002/mgg3.755.
11. Pilz, R.A.; Skowronek, D.; Hamed, M.; Weise, A.; Mangold, E.; Radbruch, A.; Pietsch, T.; Felbor, U.; Rath, M. Using CRISPR/Cas9 genome editing in human iPSCs for deciphering the pathogenicity of a novel *CCM1* transcription start site deletion. *Front Mol Biosci* **2022**, *9*, 953048, doi:10.3389/fmolb.2022.953048.
12. Zhou, Z.; Tang, A.T.; Wong, W.Y.; Bamezai, S.; Goddard, L.M.; Shenkar, R.; Zhou, S.; Yang, J.; Wright, A.C.; Foley, M.; et al. Cerebral cavernous malformations arise from endothelial gain of MEKK3-KLF2/4 signalling. *Nature* **2016**, *532*, 122-126, doi:10.1038/nature17178.
13. Lopez-Ramirez, M.A.; Fonseca, G.; Zeineddine, H.A.; Girard, R.; Moore, T.; Pham, A.; Cao, Y.; Shenkar, R.; de Kreuk, B.J.; Lagarrigue, F.; et al. Thrombospondin1 (TSP1) replacement prevents cerebral cavernous malformations. *J Exp Med* **2017**, *214*, 3331-3346, doi:10.1084/jem.20171178.
14. Ge, S.X.; Jung, D.; Yao, R. ShinyGO: a graphical gene-set enrichment tool for animals and plants. *Bioinformatics* **2020**, *36*, 2628-2629, doi:10.1093/bioinformatics/btz931.
15. Renz, M.; Otten, C.; Faurobert, E.; Rudolph, F.; Zhu, Y.; Boulday, G.; Duchene, J.; Mickoleit, M.; Dietrich, A.C.; Ramspacher, C.; et al. Regulation of beta1 integrin-Klf2-mediated angiogenesis by CCM proteins. *Dev Cell* **2015**, *32*, 181-190, doi:10.1016/j.devcel.2014.12.016.
16. Cuttano, R.; Rudini, N.; Bravi, L.; Corada, M.; Giampietro, C.; Papa, E.; Morini, M.F.; Maddaluno, L.; Baeyens, N.; Adams, R.H.; et al. KLF4 is a key determinant in the development and progression of cerebral cavernous malformations. *EMBO Mol Med* **2016**, *8*, 6-24, doi:10.15252/emmm.201505433.
17. Zhou, Z.; Rawnsley, D.R.; Goddard, L.M.; Pan, W.; Cao, X.J.; Jakus, Z.; Zheng, H.; Yang, J.; Arthur, J.S.; Whitehead, K.J.; et al. The cerebral cavernous malformation pathway controls cardiac development via regulation of endocardial MEKK3 signaling and KLF expression. *Dev Cell* **2015**, *32*, 168-180, doi:10.1016/j.devcel.2014.12.009.
18. Lopez-Ramirez, M.A.; McCurdy, S.; Li, W.; Haynes, M.K.; Hale, P.; Francisco, K.; Oukoloff, K.; Bautista, M.; Choi, C.H.J.; Sun, H.; et al. Inhibition of the HEG1-KRIT1 interaction increases KLF4 and KLF2 expression in endothelial cells. *FASEB Bioadv* **2021**, *3*, 334-355, doi:10.1096/fba.2020-00141.
19. Snellings, D.A.; Hong, C.C.; Ren, A.A.; Lopez-Ramirez, M.A.; Girard, R.; Srinath, A.; Marchuk, D.A.; Ginsberg, M.H.; Awad, I.A.; Kahn, M.L. Cerebral Cavernous Malformation: From Mechanism to Therapy. *Circ Res* **2021**, *129*, 195-215, doi:10.1161/CIRCRESAHA.121.318174.
20. Abdelilah-Seyfried, S.; Tournier-Lasserve, E.; Derry, W.B. Blocking Signalopathic Events to Treat Cerebral Cavernous Malformations. *Trends Mol Med* **2020**, *26*, 874-887, doi:10.1016/j.molmed.2020.03.003.
21. Awad, I.A.; Polster, S.P. Cavernous angiomas: deconstructing a neurosurgical disease. *J Neurosurg* **2019**, *131*, 1-13, doi:10.3171/2019.3.JNS181724.
22. Lopez-Ramirez, M.A.; Pham, A.; Girard, R.; Wyseure, T.; Hale, P.; Yamashita, A.; Koskimäki, J.; Polster, S.; Saadat, L.; Romero, I.A.; et al. Cerebral cavernous malformations form an anticoagulant vascular domain in humans and mice. *Blood* **2019**, *133*, 193-204, doi:10.1182/blood-2018-06-856062.
23. Louvi, A.; Chen, L.; Two, A.M.; Zhang, H.; Min, W.; Günel, M. Loss of *cerebral cavernous malformation* 3 (*Ccm3*) in neuroglia leads to CCM and vascular pathology. *Proc Natl Acad Sci U S A* **2011**, *108*, 3737-3742, doi:10.1073/pnas.1012617108.
24. Wang, K.; Zhang, H.; He, Y.; Jiang, Q.; Tanaka, Y.; Park, I.H.; Pober, J.S.; Min, W.; Zhou, H.J. Mural Cell-Specific Deletion of Cerebral Cavernous Malformation 3 in the Brain Induces Cerebral Cavernous Malformations. *Arterioscler Thromb Vasc Biol* **2020**, *40*, 2171-2186, doi:10.1161/ATVBAHA.120.314586.

25. Whitehead, K.J.; Plummer, N.W.; Adams, J.A.; Marchuk, D.A.; Li, D.Y. *Ccm1* is required for arterial morphogenesis: implications for the etiology of human cavernous malformations. *Development* **2004**, *131*, 1437-1448, doi:10.1242/dev.01036.
26. Kehrer-Sawatzki, H.; Wilda, M.; Braun, V.M.; Richter, H.P.; Hameister, H. Mutation and expression analysis of the *KRIT1* gene associated with cerebral cavernous malformations (CCM1). *Acta Neuropathol* **2002**, *104*, 231-240, doi:10.1007/s00401-002-0552-6.
27. Papatheodorou, I.; Moreno, P.; Manning, J.; Fuentes, A.M.; George, N.; Fexova, S.; Fonseca, N.A.; Füllgrabe, A.; Green, M.; Huang, N.; et al. Expression Atlas update: from tissues to single cells. *Nucleic Acids Res* **2020**, *48*, D77-D83, doi:10.1093/nar/gkz947.
28. Boulday, G.; Rudini, N.; Maddaluno, L.; Blécon, A.; Arnould, M.; Gaudric, A.; Chapon, F.; Adams, R.H.; Dejana, E.; Tournier-Lasserve, E. Developmental timing of CCM2 loss influences cerebral cavernous malformations in mice. *J Exp Med* **2011**, *208*, 1835-1847, doi:10.1084/jem.20110571.
29. DiStefano, P.V.; Glading, A.J. VEGF signalling enhances lesion burden in KRIT1 deficient mice. *J Cell Mol Med* **2020**, *24*, 632-639, doi:10.1111/jcmm.14773.
30. Williams, I.M.; Wu, J.C. Generation of Endothelial Cells From Human Pluripotent Stem Cells. *Arterioscler Thromb Vasc Biol* **2019**, *39*, 1317-1329, doi:10.1161/ATVBAHA.119.312265.

Supplementary Material

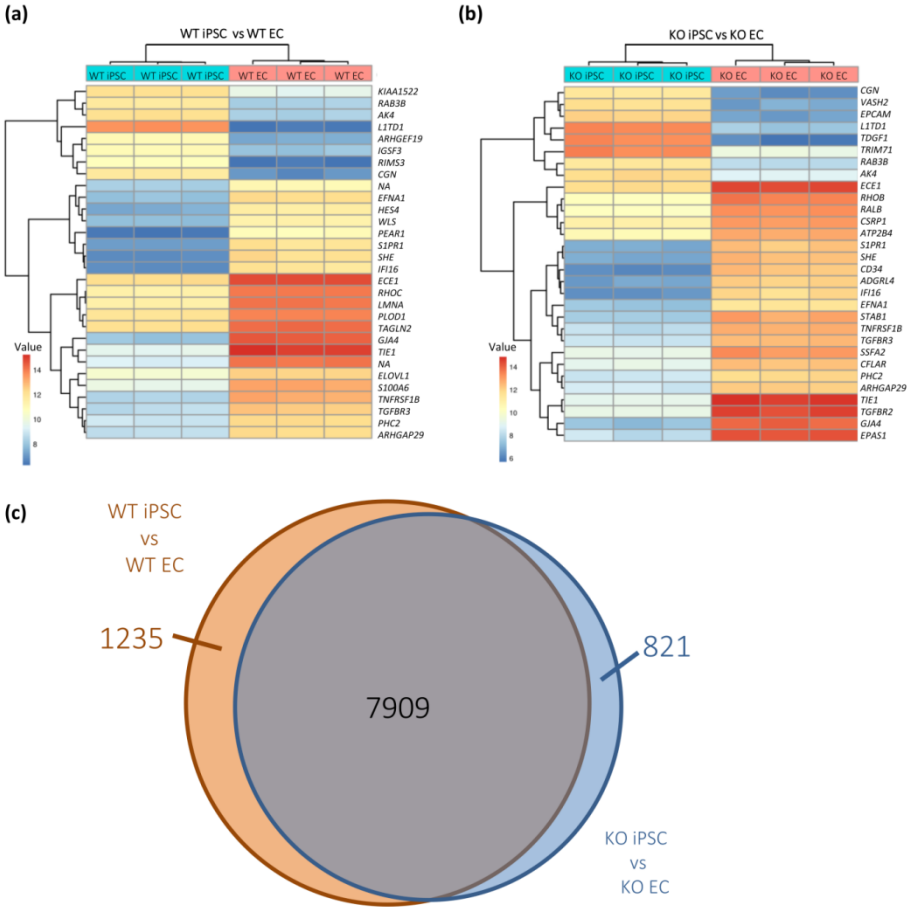

Figure S1. Heatmaps of significantly up- or downregulated genes in targeted differentiation of *CCM1*$^{+/+}$ (**a**) and *CCM1*$^{-/-}$ (**b**) iPSCs into ECs. Shown are regularized log transformed read counts for cells. Differentially expressed genes = $p_{adj} < 0.05$ and $|\log2\ FC| > 1$. n = 3 per genotype. WT = *CCM1*$^{+/+}$ wild-type cells; KO = *CCM1*$^{-/-}$ knockout cells. (**c**) Venn diagram of the overlap of differentially expressed genes in both conditions.

5.4 Bringing CCM into a dish: cell culture models for cerebral cavernous malformations

Dariush Skowronek, **Robin A. Pilz**, Konrad Schwefel, Christiane D. Much, Ute Felbor, Matthias Rath

Med Genet. 2021; 33(3):251-259

https://doi.org/10.1515/medgen-2021-2091

DE GRUYTER medizinische genetik 2021; 33(3): 251–259

Dariush Skowronek, Robin A. Pilz, Konrad Schwefel, Christiane D. Much, Ute Felbor, and Matthias Rath*

Bringing CCM into a dish: cell culture models for cerebral cavernous malformations

https://doi.org/10.1515/medgen-2021-2091
Received June 23, 2021; accepted October 21, 2021

Abstract: Cerebral cavernous malformations (CCMs) are vascular lesions that can cause severe neurological complications due to intracranial hemorrhage. Although the CCM disease genes, *CCM1*, *CCM2*, and *CCM3*, have been known for more than 15 years now, our understanding of CCM pathogenesis is still incomplete. CCM research currently focuses on three main disease mechanisms: (1) clonal expansion of endothelial cells with biallelic inactivation of *CCM1*, *CCM2*, or *CCM3*, (2) recruitment of cells with preserved CCM protein expression into the growing lesion, and (3) disruption of endothelial cell–cell junctions in CCMs. We here describe novel CRISPR/Cas9-based *in vitro* models of CCM and discuss their strengths and limitations in the context of high-throughput drug screening and repurposing approaches.

Keywords: cerebral cavernous malformations, CRISPR/Cas9 genome editing, human endothelial cells, cell junctions, spheroid sprouting

Introduction

Cerebral cavernous malformations (CCMs) are mulberry-like lesions in the microvasculature of the central nervous system (Fig. 1A,B) which are found with a prevalence of 0.5 % in the general population. They consist of densely packed, thin-walled, and leaky endothelial channels. Depending on their location and size, they can lead to a diverse spectrum of clinical signs and symptoms. While many of these vascular malformations are asymptomatic, some cause focal neurological deficits, epileptic seizures, and stroke-like symptoms due to intracranial hemorrhage. Especially brainstem lesions may lead to significant neurological complications [1]. However, CCMs can not only manifest with symptomatic hemorrhage but also with non-hemorrhagic focal neurological deficits.

Besides sporadic cases, about 6–7 % of CCMs occur in a familial form that is inherited in an autosomal dominant manner and caused by loss-of-function germline variants in *CCM1* (*KRIT1*; OMIM: *604214), *CCM2* (OMIM: *607929), or *CCM3* (*PDCD10*; OMIM: *609118) [3, 4]. Familial cases usually become symptomatic in the fourth to fifth decade of life [5]. In this context, CCMs can be a significant cause of neurologic morbidity in middle-aged adults. Genetic counseling and testing should be offered to patients with a positive family history or multiple CCMs (Fig. 1C). For patients without a positive family history, however, current best practice guidelines only recommend genetic testing if there is no associated developmental venous anomaly (DVA) and no history of brain radiation, as these features usually indicate a sporadic case [2]. Magnetic resonance imaging (MRI) with susceptibility-weighted (SWI) or gradient echo (GRE) sequences is essential for making the correct diagnosis [2, 6] (Fig. 1D). Especially small CCMs can often only be detected with these special imaging techniques. Predictive genetic testing in children is possible because the results may guide the decision to perform an MRI examination, which may require sedation in young children [2].

Although more than 20 years have passed since the first disease gene, known as *CCM1* or *KRIT1* [7, 8], was identified, there is still no specific or targeted therapy for CCM patients. While symptomatic and easily accessible lesions may be treated with neurosurgical resection, conservative management is often the only option for patients with cavernous malformations in eloquent areas. Therefore, finding new pharmaceutical targets is a primary goal of CCM research. CCM studies in mice have recently added the mTOR inhibitor rapamycin and the third-generation tyrosine kinase inhibitor ponatinib to the short list of potential novel therapies [9, 10]. Unfortunately, *in vivo* studies are time consuming, expensive, and complex. Simplified *in vitro* systems are not perfect disease models either, but they can be used to study specific aspects of CCM pathobiology in more detail. Since they are less complex, less

*Corresponding author: **Matthias Rath,** Department of Human Genetics, University Medicine Greifswald, Fleischmannstraße 43, D-17475 Greifswald, Germany; and Interfaculty Institute of Genetics and Functional Genomics, University of Greifswald, Greifswald, Germany, e-mail: matthias.rath@med.uni-greifswald.de
Dariush Skowronek, Robin A. Pilz, Konrad Schwefel, Christiane D. Much, Ute Felbor, Department of Human Genetics, University Medicine Greifswald, Greifswald, Germany; and Interfaculty Institute of Genetics and Functional Genomics, University of Greifswald, Greifswald, Germany

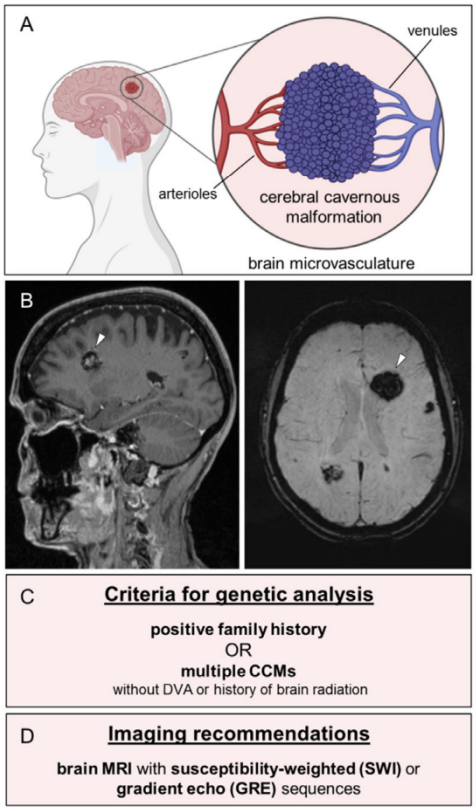

Figure 1: Clinical features of CCMs. (A) CCMs are mulberry-like vascular lesions in the microvascular bed of the central nervous system. (B) Sagittal T1-weighted (left) and axial susceptibility-weighted magnetic resonance images (right) show a large CCM (white arrowhead) and multiple smaller CCMs in both hemispheres of a patient with a pathogenic *CCM1* germline variant. (C) Criteria for genetic testing of patients with CCMs (adapted from [2]). DVA = developmental venous anomaly. (D) Recommended imaging techniques for diagnosis or follow-up of CCMs (adapted from [2]).

expensive, and compatible with the 3R principle (namely replacement, reduction, and refinement of animal experiments), they also qualify as first-line approach in high-throughput drug discovery studies. In the second or third line, *in vivo* models can then be used to validate novel drug candidates. It is important to realize that patients with sporadic CCMs could also benefit from new pharmacological treatments identified in those combined *in vitro*/*in vivo* screening assays because a substantial number of sporadic cases is caused by biallelic somatic *CCM1*, *CCM2*, or *CCM3* mutations [11, 12].

This article reviews the currently available CCM cell culture models and illustrates their strengths and limitations. In particular, we focus on our recent efforts to establish new CRISPR/Cas9-based *in vitro* models of CCM disease.

Modeling the clonal expansion of mutant endothelial cells in CCMs

In efforts to find a treatment that can block disease progression, hope rests on a better understanding of the molecular mechanisms that trigger CCM formation. In reminiscence of Knudson's two-hit model for retinoblastoma [13], DNA sequencing and immunohistochemical analyses of human CCMs demonstrated that *CCM1*, *CCM2*, or *CCM3* gene expression is completely inactivated by a germline and a second somatic mutation or by two somatic mutations in many cavernous malformations [10, 12, 14–17]. However, the vascular lesions do not only consist of mutant endothelial cells. Instead, a mosaic pattern of mutant endothelial cells and heterozygous or wild-type cells is found in CCM mouse models and human CCM tissue samples of familial and sporadic cases, respectively [17–19]. How these cells interact and whether the mosaic state is necessary for the survival of mutant cells *in vivo* is not yet understood.

Using CRISPR/Cas9 genome editing, we were recently able to study the effects of the second hit in blood outgrowth endothelial cells (BOECs) of a CCM patient with a pathogenic *CCM1* germline mutation. Signs of endothelial dysfunction, namely the disruption of intercellular junctions, the formation of actin stress fibers, and the upregulation of the transcription factor KLF2, were only observed after inactivation of the second *CCM1* allele [20, 21]. Interestingly, we were able to model a phenomenon *in vitro* that has recently been observed in CCM mouse models: clonal expansion of mutant endothelial cells [18, 19]. $CCM1^{-/-}$ BOECs and $CCM3^{-/-}$ immortalized human umbilical vein endothelial cells (CI-huVECs) demonstrated a striking survival advantage when co-cultured with $CCM1^{+/-}$ BOECs or $CCM3^{+/+}$ CI-huVECs (Fig. 2A–C), respectively [21, 22]. We also noticed resistance of $CCM1^{-/-}$ BOECs and $CCM3^{-/-}$ CI-huVECs to apoptosis, a feature reminiscent of malignant tumors. Even treatment with the broad-spectrum protein kinase inhibitor staurosporine, a potent inducer of apoptosis, only led to minimal activation of caspase-3 in CCM1- and CCM3-deficient cells [21, 22]. In a proof-of-principle approach, CRISPR/Cas9 genome editing also enabled us to study the feasibility of a targeted gene repair.

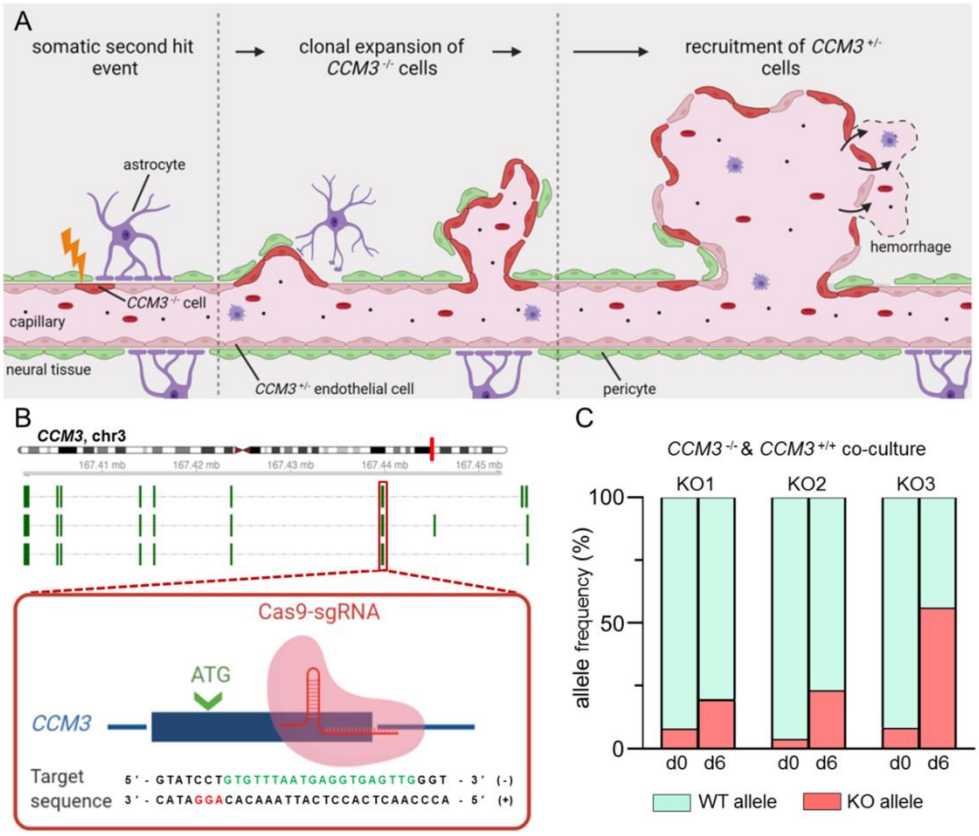

Figure 2: *CCM3* gene disruption promotes clonal expansion of endothelial cells. (A) In patients with a *CCM3* germline mutation ($CCM3^{+/-}$), a second somatic *CCM3* mutation in an endothelial cell ($CCM3^{-/-}$) initiates CCM formation. A $CCM3^{-/-}$ mutant endothelial cell undergoes clonal expansion and forms a CCM that is characterized by endothelial mosaicism of $CCM3^{-/-}$ and $CCM3^{+/-}$ endothelial cells. The impaired endothelial barrier function can lead to bleeding into the surrounding brain tissue. (B) *CCM3* knockout endothelial cells were generated with CRISPR/Cas9 genome editing. Biallelic loss-of-function variants were introduced into the first coding exon of *CCM3* (knockout [KO] clones 1 and 2: c.[87_88insAG];[87_88insAG] [p.[Phe30Serfs*5];[Phe30Serfs*5]]; KO3: c.[90dupT];[87_88insAGTTGGATAAACATGTTTATCCAACT] [p.[Asn31*];[Phe30Serfs*13]]). (C) $CCM3^{-/-}$ CI-huVECs demonstrated significant expansion in co-culture with $CCM3^{+/+}$ CI-huVECs. Knockout and wild-type (WT) allele frequencies were determined by amplicon deep sequencing after six days of co-culture.

While we were able to correct the *CCM1* germline mutation in a significant number of $CCM1^{+/-}$ BOECs *in vitro*, corrected $CCM1^{+/+}$ BOECs were replaced by highly proliferative $CCM1^{-/-}$ BOECs in co-culture [21]. In human CCM, where CRISPR/Cas9-mediated gene repair would not eradicate all mutant endothelial cells, the therapeutic benefit of such a genome editing approach would therefore be limited.

The new hypothesis that the tumor-like behavior of mutant endothelial cells represents a suitable therapeutic target has also been supported by the detection of *PIK3CA* mutations in CCMs [10]. The identification of somatic variants in this well-known oncogene suggests a three-hit mechanism in CCM pathogenesis. Following this intriguing model, only the combination of inactivating mutations in *CCM* genes acting as vascular "suppressor genes" and activating variants in vascular "oncogenes" can provoke a severe or aggressive course of CCM disease [10].

Cell culture models of the endothelial barrier dysfunction in CCMs

Apart from blocking CCM formation, restoration of an intact endothelial barrier is another primary objective in CCM therapy. As part of the blood–brain barrier (BBB), vascular endothelial cells participate in the tightly regulated exchange of ions, molecules, and cells between the blood and the brain [23]. However, no targeted therapies have yet been approved to prevent CCM bleeding and hemorrhage-associated neurological complications.

Endothelial tight and adherence junctions are indispensable to maintain BBB integrity but are highly dysfunctional in CCMs. Claudins, occludin, and junctional adhesion molecules (JAMs) are major components of endothelial tight junctions. These transmembrane proteins are linked to the actin cytoskeleton by scaffold proteins like zonula occludens protein 1 (ZO-1) (Fig. 3A). Destabilization of tight junctions and reduced expression of claudin-5, occludin, and ZO-1 have been observed in human CCM tissues [24, 25] and CCM mouse models [26–28]. These features of CCM disease can be perfectly reproduced *in vitro* [25, 28]. However, not only tight junctions but also adherens junctions are disorganized in CCMs. Using CRISPR/Cas9 genome editing, we could mimic disrup-

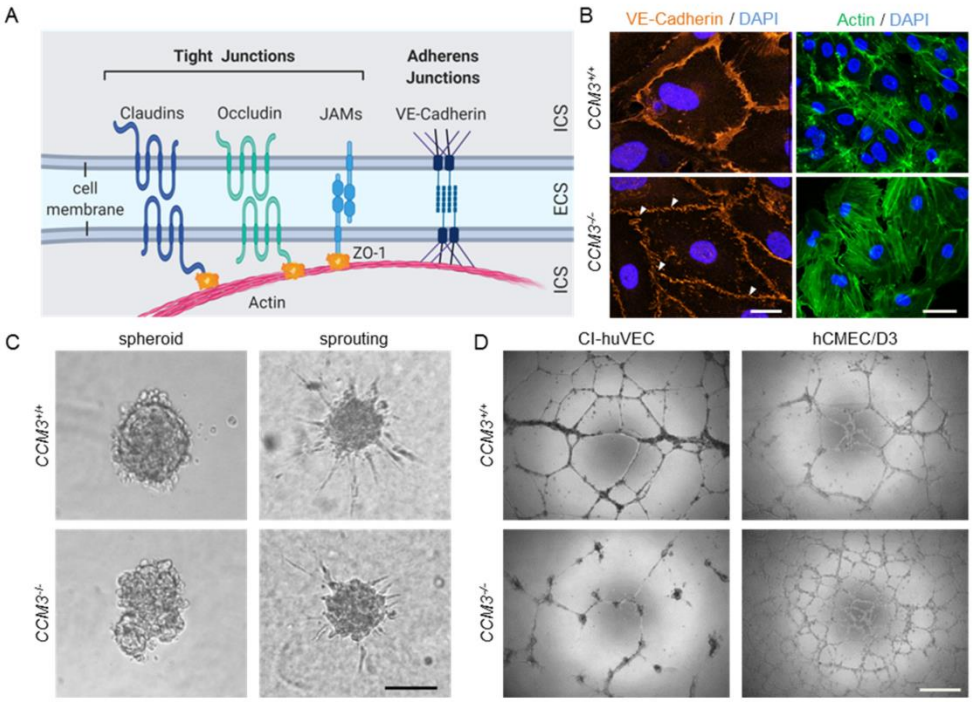

Figure 3: Disorganized cell junctions and impaired function in 3D models of angiogenesis upon *CCM3* gene inactivation. (A) Scheme of endothelial tight and adherens junctions. ICS = intracellular space. ECS = extracellular space. ZO-1 = zonula occludens protein 1. JAM = junctional adhesion molecule. (B) In contrast to wild-type CI-huVECs, *CCM3*$^{-/-}$ CI-huVECs demonstrated numerous small gaps (white arrowheads) and a less homogeneous pattern in VE-cadherin staining (red). Scale bar ≙ 20 µm. They also displayed significant actin stress fiber formation (green, phalloidin staining). Scale bar ≙ 25 µm. DAPI (blue) was used to stain cell nuclei. (C) *CCM3*$^{-/-}$ CI-huVECs demonstrated impaired spheroid formation and VEGF-induced sprouting. The number and length of sprouts formed by *CCM3*$^{-/-}$ spheroids upon stimulation with 25 ng/ml VEGF-A were significantly reduced. Scale bar ≙ 100 µm. (D) *CCM3* gene inactivation had cell type-specific effects on endothelial tube formation on Matrigel. While tubes formed by *CCM3*$^{-/-}$ CI-huVECs were unstable and had fallen apart 17 h after seeding on Matrigel, *CCM3*$^{-/-}$ hCMEC/D3 cells formed more stable meshes than hCMEC/D3 wild-type controls. Scale bar ≙ 500 µm.

tion of adherens junctions in *CCM3*$^{-/-}$ CI-huVECs (Fig. 3B) and *CCM1*$^{-/-}$ BOECs [20]. In line with previous literature reports [21, 22, 29–31], the dysfunction of endothelial cell–cell junctions was accompanied by an increased formation of actin stress fibers (Fig. 3B). These phenotypes are useful surrogate markers for the hyperpermeability and increased bleeding risk of CCMs.

Three-dimensional cell culture models in CCM research

The impaired interaction of mutant endothelial cells can also be visualized in three-dimensional (3D) cell culture models. More than 20 years ago, Thomas Korff and Hellmut G. Augustin developed a 3D spheroid formation and sprouting assay to analyze endothelial cell differentiation, cell–cell and cell–matrix interactions, and capillary sprouting [32, 33]. Using this assay, we demonstrated that CI-huVECs could only form irregular and barely demarcated spheroids upon CRISPR/Cas9-induced *CCM1*, *CCM2*, or *CCM3* gene disruption [22, 29]. Furthermore, *CCM3* gene inactivation in CI-huVECs and the immortalized human brain microvascular endothelial cell line D3 (hCMEC/D3) significantly impaired sprouting (Fig. 3C) [22]. Since transient *CCM3* knockdown and genetic *CCM3* knockout modulate this fundamental process differently [22, 26], compensatory mechanisms likely influence the angiogenic behavior of *CCM3*$^{-/-}$ endothelial cells.

Disruption of endothelial junctions after *CCM* inactivation has also been found in transwell permeability assays. Upon CCM1, CCM2, or CCM3 depletion, the permeability of HUVEC monolayers was significantly increased [31, 34]. These results demonstrate that not only an altered 3D organization and angiogenic behavior of mutant cells, but also the leaky phenotype seen in CCMs can be modeled in *in vitro* systems. However, it can be sometimes challenging to directly compare the results of different *in vitro* models. An example is endothelial tube formation of mutant endothelial cells on Matrigel, which is another widely used *in vitro* angiogenesis assay. *CCM3*$^{-/-}$ CI-huVECs form endothelial tubes that rapidly disintegrate (Fig. 3D) [22], a phenomenon that has also been reported for primary HUVECs after short hairpin RNA-mediated knockdown of *CCM1* and *CCM2* [35]. In contrast, *CCM3*$^{-/-}$ hCMEC/D3 cells were able to form stable tubes on Matrigel (Fig. 3D). The different behavior on Matrigel might be a cell type-specific effect related to the fact that CI-huVECs and hCMEC/D3 cells are derived from endothelial cells from different vascular beds. However, an effect of different culture media and supplement concentrations cannot be excluded either. A combination of different assays is therefore the best way to obtain valid results.

High-content screening in CCM drug discovery

Since drug discovery and development studies are time consuming and cost-intensive, drug repurposing approaches have become popular in recent years. In the context of CCM, endothelial barrier function and cell proliferation assays have already been used successfully in drug repurposing screens. Gibson and colleagues defined the reversion of VE-cadherin disassembly and actin stress fiber formation in *CCM2*-silenced human dermal microvascular endothelial cells as primary read-out parameters [36]. Using *in vitro* transcellular resistance analyses, dermal permeability assays in inducible endothelial-specific *Ccm2* knockout mice, and magnetic resonance imaging as secondary, tertiary, and quaternary screens, they identified tempol and cholecalciferol as promising candidates for CCM therapy [36]. Nishimura and colleagues also used a multi-step screening approach [37]. Drugs that could inhibit the proliferation of CCM3-deficient mouse astrocytes were validated in an RNAi-based *Drosophila* model and two mouse models of CCM disease. With this screening strategy, the authors identified the combination of fluvastatin and zoledronate to be effective *in vivo* and *in vitro* [37]. Finally, Otten and colleagues used *ccm2* mutant zebrafish embryos, *kri-1* (*CCM1*), and *ccm-3* ablated *C. elegans*, as well as *CCM2* knockdown HUVECs in a multi-organism-based screening approach. In downstream analyses, they validated that indirubin-3-monoxime treatment rescued VE-cadherin and actin phenotypes in *CCM1*-, *CCM2*-, and *CCM3*-silenced HUVECs [38].

Another positive example of drug repurposing in the context of CCM disease is propranolol. This pleiotropic β-blocker has recently been shown to reduce lesion burden in CCM mouse and zebrafish models [39]. A further study demonstrated that propranolol treatment also increased pericyte coverage and prevented vascular leakage in inducible endothelial-specific *Ccm3* knockout (CCM3^{iECKO}) mice [40]. After encouraging case reports on propranolol treatment in CCM patients, its effectiveness is now assessed in the Treat_CCM study, a multicenter, open-label, randomized trial [41].

Drug repurposing and discovery studies have relied on *Ccm* knockout mouse models or RNAi-based *in vitro* gene knockdown models in human endothelial cells so

far. Both have strengths and limitations. In particular, discrepancies between transient gene knockdowns and genetic knockouts, as well as the limited predictive value of some mouse studies for humans are inherent weaknesses of these studies. Because they are easy-to-handle, cost-effective, and 3R-compliant, the use of novel human CRISPR/Cas9-based *in vitro* models in primary screens may help to accelerate the process of finding effective drugs for CCM patients.

Co-culture and iPSC-based CCM models

Notably, several studies have disclosed that CCM formation and disease progression are caused by more than just endothelial dysfunction. Pericytes which interact with the abluminal side of endothelial cells and astrocytic endfeet which enclose blood vessels are also major components of the BBB and participate in CCM pathogenesis [42–44]. Wang and colleagues, for example, demonstrated that specific *Ccm3* deletion in mural cells induces a CCM phenotype in mice [44]. In particular, they found reduced cell spreading and migration of CCM3-deficient pericytes which caused impaired association with endothelial cells [44]. Additionally, a recent publication highlighted the crosstalk between endothelial cells and astrocytes in CCM lesion development. Increased endothelial NO synthase (eNOS)/nitric oxide (NO)-dependent signaling in dysfunctional endothelial cells leads to elevated levels of the astrocyte-derived angiogenesis factor VEGF, which contributes to endothelial cell junction disassembly linked to an increased risk of hemorrhage [43]. These observations provide a first explanation of why CCMs only arise in the central nervous system, although the CCM proteins are ubiquitously expressed. They also suggest that endothelial monocultures may not adequately illustrate CCM disease. *In vitro* co-culture models of endothelial cells, astrocytes, and pericytes may be more suitable. Patient-specific induced pluripotent stem cells (iPSCs) and their direct differentiation into all three cell types may allow the development of new co-culture models in the future. Co-culturing these cells in transwell or microfluidic models can improve the barrier properties and allows studying BBB dysfunction in an isogenic system [45]. Measuring the transendothelial electrical resistance (TEER) of knockout BBB co-cultures in a compound library screen may help to find a drug that can reduce the bleeding risk of CCMs. A fascinating direction of CCM disease modeling might also be the combination with a CCM xenograft model [46]. Implantation of human spheroid co-cultures into murine models might reconstruct the *in vivo* cellular environment of CCM by keeping the human origin of the affected cells.

Outlook

Although there will be no "one-stop shopping" in CCM drug discovery in the near future, we now have a broad toolkit of *in vitro* models to study CCM pathogenesis and search for new CCM therapies. In particular, CRISPR/Cas9 genome editing has become an invaluable tool to model fundamental cellular and molecular processes of CCM formation, disease progression, and endothelial barrier disruption. Targeted gene inactivations in endothelial cells, pericytes, and astrocytes will facilitate more complex 3D co-culture models of CCM. Combined with live-cell imaging and new CRISPR tools, e.g., CRISPR activation (CRISPRa) or CRISPR interference (CRISPRi), these models will help to understand the dynamics of BBB dysfunction in CCMs better. However, higher complexity is usually accompanied by lower compatibility with high-throughput drug screening assays. Therefore, future efforts to model CCM disease *in vitro* will likely go into two directions: (1) simple but high-throughput-compatible *in vitro* assays and (2) complex cell culture models to closely mimic the *in vivo* situation.

Author contributions: All authors have accepted responsibility for the entire content of this manuscript and approved its submission.

Acknowledgment: We thank the CCM patient for granting permission to publish her MRI images. Dr. rer. nat. Stefanie Spiegler is thanked for providing confocal microscopy images of VE-cadherin staining. Figures 1A, 2A, and 3A were created with BioRender.com. We apologize to all colleagues whose work has not been cited due to space limitations.

Research funding: This work was supported by the German Research Foundation (DFG RA2876/2-2), the German Federal Ministry of Education and Research (BMBF; grant number 161L0276), and the Research Association Molecular Medicine of the University Medicine Greifswald (FVMM, grant numbers FOVB-2021-07, FOVB-2020-01, FOVB-2019-01, and FOVB-2018-06). MR is supported by a scholarship from the Gerhard Domagk program of the University Medicine Greifswald.

Conflict of interest: The authors state no conflict of interest.

Informed consent: Written informed consent was obtained from the CCM patient to publish the medical information and MRI images presented here.
Ethical approval: This article does not contain any studies with human or animal subjects.

References

[1] Horne MA, Flemming KD, Su IC, Stapf C, Jeon JP, Li D, Maxwell SS, White P, Christianson TJ, Agid R, Cho W-S, Oh CW, Wu Z, Zhang J-T, Kim JE, ter Brugge K, Willinsky R, Brown RD, Murray GD, Al-Shahi Salman R. Clinical course of untreated cerebral cavernous malformations: a meta-analysis of individual patient data. Lancet Neurol. 2016;15:166–73.

[2] Akers A, Al-Shahi Salman R, Awad IA, Dahlem K, Flemming K, Hart B, Kim H, Jusue-Torres I, Kondziolka D, Lee C, Morrison L, Rigamonti D, Rebelz T, Tournier-Lasserve E, Waggoner D, Whitehead K. Synopsis of guidelines for the clinical management of cerebral cavernous malformations: consensus recommendations based on systematic literature review by the Angioma Alliance Scientific Advisory Board Clinical Experts Panel. Neurosurgery. 2017;80:665–80.

[3] Spiegler S, Rath M, Paperlein C, Felbor U. Cerebral Cavernous Malformations: An Update on Prevalence, Molecular Genetic Analyses, and Genetic Counselling. Mol Syndromol. 2018;9:60–9.

[4] Batra S, Lin D, Recinos PF, Zhang J, Rigamonti D. Cavernous malformations: natural history, diagnosis and treatment. Nat Rev Neurol. 2009;5:659–70.

[5] Denier C, Labauge P, Bergametti F, Marchelli F, Riant F, Arnoult M, Maclazek J, Vicaut E, Brunereau L, Tournier-Lasserve E, Société Française de Neurochirurgie. Genotype-phenotype correlations in cerebral cavernous malformations patients. Ann Neurol. 2006;60:550–6.

[6] Flemming KD, Lanzino G. Cerebral cavernous malformation: What a practicing clinician should know. Mayo Clin Proc. 2020;95:2005–20.

[7] Laberge-le Couteulx S, Jung HH, Labauge P, Houtteville JP, Lescoat C, Cecillon M, Marechal E, Joutel A, Bach JF, Tournier-Lasserve E. Truncating mutations in *CCM1*, encoding KRIT1, cause hereditary cavernous angiomas. Nat Genet. 1999;23:189–93.

[8] Sahoo T, Johnson EW, Thomas JW, Kuehl PM, Jones TL, Dokken CG, Touchman JW, Gallione CJ, Lee-Lin SQ, Kosofsky B, Kurth JH, Louis DN, Mettler G, Morrison L, Gil-Nagel A, Rich SS, Zabramski JM, Boguski MS, Green ED, Marchuk DA. Mutations in the gene encoding KRIT1, a Krev-1/rap1a binding protein, cause cerebral cavernous malformations (*CCM1*). Hum Mol Genet. 1999;8:2325–33.

[9] Choi JP, Wang R, Yang X, Wang X, Wang L, Ting KK, Foley M, Cogger V, Yang Z, Liu F, Han Z, Liu R, Baell J, Zheng X. Ponatinib (AP24534) inhibits MEKK3-KLF signaling and prevents formation and progression of cerebral cavernous malformations. Sci Adv. 2018;4:eaau0731.

[10] Ren AA, Snellings DA, Su YS, Hong CC, Castro M, Tang AT, Detter MR, Hobson N, Girard R, Romanos S, Lightle R, Moore T, Shenkar R, Benavides C, Beaman MM, Müller-Fielitz H, Chen M, Mericko P, Yang J, Sung DC, Lawton MT, Ruppert JM, Schwaninger M, Körbelin J, Potente M, Awad IA, Marchuk DA, Kahn ML. *PIK3CA* and CCM mutations fuel cavernomas through a cancer-like mechanism. Nature. 2021;594:271–6.

[11] Awad IA, Polster SP. Cavernous angiomas: deconstructing a neurosurgical disease. J Neurosurg. 2019;131:1–13.

[12] McDonald DA, Shi C, Shenkar R, Gallione CJ, Akers AL, Li S, De Castro N, Berg MJ, Corcoran DL, Awad IA, Marchuk DA. Lesions from patients with sporadic cerebral cavernous malformations harbor somatic mutations in the CCM genes: evidence for a common biochemical pathway for CCM pathogenesis. Hum Mol Genet. 2014;23:4357–70.

[13] Knudson AG Jr. Mutation and cancer: statistical study of retinoblastoma. Proc Natl Acad Sci USA. 1971;68:820–3.

[14] Pagenstecher A, Stahl S, Sure U, Felbor U. A two-hit mechanism causes cerebral cavernous malformations: complete inactivation of CCM1, CCM2 or CCM3 in affected endothelial cells. Hum Mol Genet. 2009;18:911–8.

[15] Gault J, Shenkar R, Recksiek P, Awad IA. Biallelic somatic and germ line *CCM1* truncating mutations in a cerebral cavernous malformation lesion. Stroke. 2005;36:872–4.

[16] Gault J, Awad IA, Recksiek P, Shenkar R, Breeze R, Handler M, Kleinschmidt-DeMasters BK. Cerebral cavernous malformations: somatic mutations in vascular endothelial cells. Neurosurgery. 2009;65:138–45.

[17] Rath M, Pagenstecher A, Hoischen A, Felbor U. Postzygotic mosaicism in cerebral cavernous malformation. J Med Genet. 2020;57:212–6.

[18] Detter MR, Snellings DA, Marchuk DA. Cerebral cavernous malformations develop through clonal expansion of mutant endothelial cells. Circ Res. 2018;123:1143–51.

[19] Malinverno M, Maderna C, Abu Taha A, Corada M, Orsenigo F, Valentino M, Pisati F, Fusco C, Graziano P, Giannotta M, Yu QC, Zeng YA, Lampugnani MG, Magnusson PU, Dejana E. Endothelial cell clonal expansion in the development of cerebral cavernous malformations. Nat Commun. 2019;10:2761.

[20] Much CD, Sendtner BS, Schwefel K, Freund E, Bekeschus S, Otto O, Pagenstecher A, Felbor U, Rath M, Spiegler S. Inactivation of Cerebral Cavernous Malformation Genes Results in Accumulation of von Willebrand Factor and Redistribution of Weibel-Palade Bodies in Endothelial Cells. Front Mol Biosci. 2021;8:622547.

[21] Spiegler S, Rath M, Much CD, Sendtner BS, Felbor U. Precise *CCM1* gene correction and inactivation in patient-derived endothelial cells: Modeling Knudson's two-hit hypothesis in vitro. Mol Genet Genomic Med. 2019;7:e00755.

[22] Schwefel K, Spiegler S, Ameling S, Much CD, Pilz RA, Otto O, Völker U, Felbor U, Rath M. Biallelic *CCM3* mutations cause a clonogenic survival advantage and endothelial cell stiffening. J Cell Mol Med. 2019;23:1771–83.

[23] Daneman R, Prat A. The blood-brain barrier. Cold Spring Harb Perspect Biol. 2015;7:a020412.

[24] Schneider H, Errede M, Ulrich NH, Virgintino D, Frei K, Bertalanffy H. Impairment of tight junctions and glucose transport in endothelial cells of human cerebral cavernous malformations. J Neuropathol Exp Neurol. 2011;70:417–29.

[25] Stamatovic SM, Sladojevic N, Keep RF, Andjelkovic AV. PDCD10 (CCM3) regulates brain endothelial barrier integrity in cerebral cavernous malformation type 3: role of CCM3-ERK1/2-cortactin

cross-talk. Acta Neuropathol. 2015;130:731–50.
[26] Zhou JH, Qin L, Zhang H, Tang W, Ji W, He Y, Liang X, Wang Z, Yuan Q, Vortmeyer A, Toomre D, Fuh G, Yan M, Kluger MS, Wu D, Min W. Endothelial exocytosis of angiopoietin-2 resulting from CCM3 deficiency contributes to cerebral cavernous malformation. Nat Med. 2016;22:1033–42.
[27] Zeineddine HA, Girard R, Saadat L, Shen L, Lightle R, Moore T, Cao Y, Hobson N, Shenkar R, Avner K, Chaudager K, Koskimäki J, Polster SP, Fam MD, Shi C, Lopez-Ramirez MA, Tang AT, Gallione C, Kahn ML, Ginsberg M, Marchuk DA, Awad IA. Phenotypic characterization of murine models of cerebral cavernous malformations. Lab Invest. 2019;99:319–30.
[28] Lopez-Ramirez MA, Fonseca G, Zeineddine HA, Girard R, Moore T, Pham A, Cao Y, Shenkar R, de Kreuk BJ, Lagarrigue F, Lawler J, Glass CK, Awad IA, Ginsberg MH. Thrombospondin1 (TSP1) replacement prevents cerebral cavernous malformations. J Exp Med. 2017;214:3331–46.
[29] Schwefel K, Spiegler S, Kirchmaier BC, Dellweg PKE, Much CD, Pané-Farré J, Strom TM, Riedel K, Felbor U, Rath M. Fibronectin rescues aberrant phenotype of endothelial cells lacking either CCM1, CCM2 or CCM3. FASEB J. 2020;34:9018–33.
[30] Glading A, Han J, Stockton RA, Ginsberg MH. KRIT-1/CCM1 is a Rap1 effector that regulates endothelial cell cell junctions. J Cell Biol. 2007;179:247–54.
[31] Shenkar R, Shi C, Rebeiz T, Stockton RA, McDonald DA, Mikati AG, Zhang L, Austin C, Akers AL, Gallione CJ, Rorrer A, Gunel M, Min W, De Souza JM, Lee C, Marchuk DA, Awad IA. Exceptional aggressiveness of cerebral cavernous malformation disease associated with *PDCD10* mutations. Genet Med. 2015;17:188–96.
[32] Korff T, Augustin HG. Integration of endothelial cells in multicellular spheroids prevents apoptosis and induces differentiation. J Cell Biol. 1998;143:1341–52.
[33] Korff T, Augustin HG. Tensional forces in fibrillar extracellular matrices control directional capillary sprouting. J Cell Sci. 1999;112:3249–58.
[34] Stockton RA, Shenkar R, Awad IA, Ginsberg MH. Cerebral cavernous malformations proteins inhibit Rho kinase to stabilize vascular integrity. J Exp Med. 2010;207:881–96.
[35] Chernaya O, Zhurikhina A, Hladyshau S, Pilcher W, Young KM, Ortner J, Andra V, Sulchek TA, Tsygankov D. Biomechanics of endothelial tubule formation differentially modulated by cerebral cavernous malformation proteins. iScience. 2018;9:347–58.
[36] Gibson CC, Zhu W, Davis CT, Bowman-Kirigin JA, Chan AC, Ling J, Walker AE, Goitre L, Delle Monache S, Retta SF, Shiu YT, Grossmann AH, Thomas KR, Donato AJ, Lesniewski LA, Whitehead KJ, Li DY. Strategy for identifying repurposed drugs for the treatment of cerebral cavernous malformation. Circulation. 2015;131:289–99.
[37] Nishimura S, Mishra-Gorur K, Park J, Surovtseva YV, Sebti SM, Levchenko A, Louvi A, Gunel M. Combined HMG-COA reductase and prenylation inhibition in treatment of CCM. Proc Natl Acad Sci USA. 2017;114:5503–8.
[38] Otten C, Knox J, Boulday G, Eymery M, Haniszewski M, Neuenschwander M, Radetzki S, Vogt I, Hähn K, De Luca C, Cardoso C, Hamad S, Igual Gil C, Roy P, Albiges-Rizo C, Faurobert E, von Kries JP, Campillos M, Tournier-Lasserve E, Derry WB, Abdelilah-Seyfried S. Systematic pharmacological screens uncover novel pathways involved in cerebral cavernous malformations. EMBO Mol Med. 2018;10:e9155.
[39] Li W, Shenkar R, Detter MR, Moore T, Benavides C, Lightle R, Girard R, Hobson N, Cao Y, Li Y, Griffin E, Gallione C, Zabramski JM, Ginsberg MH, Marchuk DA, Awad IA. Propranolol inhibits cavernous vascular malformations by β1 adrenergic receptor antagonism in animal models. J Clin Invest. 2021;131:e144893.
[40] Oldenburg J, Malinverno M, Globisch MA, Maderna C, Corada M, Orsenigo F, Conze LL, Rorsman C, Sundell V, Arce M, Smith RO, Yau ACY, Billström GH, Mägi CÖ, Beznoussenko GV, Mironov AA, Fernando D, Daniel G, Olivari D, Fumagalli F, Lampugnani MG, Dejana E, Magnusson PU. Propranolol reduces the development of lesions and rescues barrier function in cerebral cavernous malformations: A preclinical study. Stroke. 2021;52:1418–27.
[41] Lanfranconi S, Scola E, Bertani GA, Zarino B, Pallini R, d'Alessandris G, Mazzon E, Marino S, Carriero MR, Scelzo E, Faragò G, Castori M, Fusco C, Petracca A, d'Agruma L, Tassi L, d'Orio P, Lampugnani MG, Nicolis EB, Vasami A, Novelli D, Torri V, Meessen J, Al-Shahi Salman R, Dejana E, Latini R, Treat-CCM Investigators. Propranolol for familial cerebral cavernous malformation (Treat_CCM): study protocol for a randomized controlled pilot trial. Trials. 2020;21:401.
[42] Schulz GB, Wieland E, Wüstehube-Lausch J, Boulday G, Moll I, Tournier-Lasserve E, Fischer A. Cerebral cavernous malformation-1 protein controls DLL4-Notch3 signaling between the endothelium and pericytes. Stroke. 2015;46:1337–43.
[43] Lopez-Ramirez MA, Lai CC, Soliman SI, Hale P, Pham A, Estrada EJ, McCurdy S, Girard R, Verma R, Moore T, Lightle R, Hobson N, Shenkar R, Poulsen O, Haddad GG, Daneman R, Gongol B, Sun H, Lagarrigue F, Awad IA, Ginsberg MH. Astrocytes propel neurovascular dysfunction during cerebral cavernous malformation lesion formation. J Clin Invest. 2021;131:e139570.
[44] Wang K, Zhang H, He Y, Jiang Q, Tanaka Y, Park IH, Pober JS, Min W, Zhou HJ. Mural cell-specific deletion of cerebral cavernous malformation 3 in the brain induces cerebral cavernous malformations. Arterioscler Thromb Vasc Biol. 2020;40:2171–86.
[45] Appelt-Menzel A, Oerter S, Mathew S, Haferkamp U, Hartmann C, Jung M, Neuhaus W, Pless O. Human iPSC-Derived Blood-Brain Barrier Models: Valuable Tools for Preclinical Drug Discovery and Development? Curr Protoc Stem Cell Biol. 2020;55:e122.
[46] Wüstehube J, Bartol A, Liebler SS, Brütsch R, Zhu Y, Felbor U, Sure U, Augustin HG, Fischer A. Cerebral cavernous malformation protein CCM1 inhibits sprouting angiogenesis by activating DELTA-NOTCH signaling. Proc Natl Acad Sci USA. 2010;107:12640–5.

Dariush Skowronek, M.Sc. Humanbiologie
Department of Human Genetics, University Medicine Greifswald, Greifswald, Germany
Interfaculty Institute of Genetics and Functional Genomics, University of Greifswald, Greifswald, Germany

Robin A. Pilz, M.Sc. Humanbiologie
Department of Human Genetics, University Medicine Greifswald, Greifswald, Germany
Interfaculty Institute of Genetics and Functional Genomics, University of Greifswald, Greifswald, Germany

Dr. rer. nat. Konrad Schwefel
Department of Human Genetics, University Medicine Greifswald, Greifswald, Germany
Interfaculty Institute of Genetics and Functional Genomics, University of Greifswald, Greifswald, Germany

Dr. rer. nat. Christiane D. Much
Department of Human Genetics, University Medicine Greifswald, Greifswald, Germany
Interfaculty Institute of Genetics and Functional Genomics, University of Greifswald, Greifswald, Germany

Prof. Dr. med. Ute Felbor
Department of Human Genetics, University Medicine Greifswald, Greifswald, Germany
Interfaculty Institute of Genetics and Functional Genomics, University of Greifswald, Greifswald, Germany

PD Dr. med. Matthias Rath
Department of Human Genetics, University Medicine Greifswald, Fleischmannstraße 43, D-17475 Greifswald, Germany
Interfaculty Institute of Genetics and Functional Genomics, University of Greifswald, Greifswald, Germany
matthias.rath@med.uni-greifswald.de

5.5 Contact-dependent signaling triggers tumor-like proliferation of *CCM3* knockout endothelial cells in co-culture with wild-type cells

Matthias Rath*, Konrad Schwefel*, Matteo Malinverno, Dariush Skowronek, Alexandra Leopoldi, **Robin A. Pilz**, Doreen Biedenweg, Sander Bekeschus, Josef M. Penninger, Elisabetta Dejana, Ute Felbor

*Diese Autoren haben gleichermaßen zur Arbeit beigetragen.

Cell Mol Life Sci. 2022; 79(6):340

https://doi.org/10.1007/s00018-022-04355-6

Cellular and Molecular Life Sciences (2022) 79:340
https://doi.org/10.1007/s00018-022-04355-6

Cellular and Molecular Life Sciences

ORIGINAL ARTICLE

Contact-dependent signaling triggers tumor-like proliferation of *CCM3* knockout endothelial cells in co-culture with wild-type cells

Matthias Rath[1] · Konrad Schwefel[1] · Matteo Malinverno[2] · Dariush Skowronek[1] · Alexandra Leopoldi[3] · Robin A. Pilz[1] · Doreen Biedenweg[4] · Sander Bekeschus[5] · Josef M. Penninger[3,6] · Elisabetta Dejana[2,7] · Ute Felbor[1]

Received: 17 November 2021 / Revised: 21 April 2022 / Accepted: 5 May 2022 / Published online: 4 June 2022

Abstract

Cerebral cavernous malformations (CCM) are low-flow vascular lesions prone to cause severe hemorrhage-associated neurological complications. Pathogenic germline variants in *CCM1*, *CCM2*, or *CCM3* can be identified in nearly 100% of CCM patients with a positive family history. In line with the concept that tumor-like mechanisms are involved in CCM formation and growth, we here demonstrate an abnormally increased proliferation rate of CCM3-deficient endothelial cells in co-culture with wild-type cells and in mosaic human iPSC-derived vascular organoids. The observation that NSC59984, an anticancer drug, blocked the abnormal proliferation of mutant endothelial cells further supports this intriguing concept. Fluorescence-activated cell sorting and RNA sequencing revealed that co-culture induces upregulation of proangiogenic chemokine genes in wild-type endothelial cells. Furthermore, genes known to be significantly downregulated in $CCM3^{-/-}$ endothelial cell mono-cultures were upregulated back to normal levels in co-culture with wild-type cells. These results support the hypothesis that wild-type ECs facilitate the formation of a niche that promotes abnormal proliferation of mutant ECs. Thus, targeting the cancer-like features of CCMs is a promising new direction for drug development.

Keywords Cerebral cavernous malformations · CRISPR/Cas9 genome editing · Tumor-like behavior · NSC59984 · RNA sequencing · Co-culture

Matthias Rath and Konrad Schwefel contributed equally.

✉ Matthias Rath
matthias.rath@med.uni-greifswald.de

[1] Department of Human Genetics, University Medicine Greifswald and Interfaculty Institute of Genetics and Functional Genomics, University of Greifswald, Fleischmannstraße 43, 17475 Greifswald, Germany

[2] Vascular Biology Unit, FIRC Institute of Molecular Oncology Foundation (IFOM), Milan, Italy

[3] Institute of Molecular Biotechnology of the Austrian Academy of Sciences, Vienna, Austria

[4] Centre for Innovation Competence-Humoral Immune Reactions in Cardiovascular Diseases, University of Greifswald, Greifswald, Germany

[5] ZIK Plasmatis, Leibniz Institute for Plasma Science and Technology (INP), Greifswald, Germany

[6] Department of Medical Genetics, Life Sciences Institute, University of British Columbia, Vancouver, Canada

[7] Department of Immunology, Genetics and Pathology, Uppsala University, Uppsala, Sweden

Abbreviations

ADS	Amplicon deep sequencing
CCM	Cerebral cavernous malformations
CCM^{pos}	Heterozygous or wild-type ECs
CCM^{neg}	Mutant ECs
CI-huVECs	Constitutive immortalized human umbilical vein endothelial cells
EC	Endothelial cells
ECGM	Endothelial cell growth medium
FCS	Fetal calf serum
hBMEC-like cells	Human brain microvascular endothelial-like cells
hESFM	Human endothelial serum-free medium
hiPSC	Human induced pluripotent stem cell
ITGB4	Integrin β4
PFA	Paraformaldehyde
RNP	Ribonucleoprotein
SD	Standard deviation

Introduction

Cerebral cavernous malformations (CCMs), also known as cavernous haemangiomas or cavernomas, account for 10 to 15% of all vascular lesions in the central nervous system [1]. In particular, hereditary CCMs tend to cause significant neurological complications. Unfortunately, therapeutic options are still limited. Neurosurgical resection can be indicated in some cases but there is a substantial risk of early postoperative morbidity for CCMs in the brainstem or other eloquent areas [2].

CCMs can be found in a sporadic and an autosomal dominant form. The latter is associated with pathogenic germline variants in either *CCM1* (aka *KRIT1*), *CCM2,* or *CCM3* (aka *PDCD10*) [3]. Patients with familial CCMs, especially those with a pathogenic *CCM3* variant, often present at a younger age with multiple cavernomas [3–5]. The number of vascular lesions can even increase over time. Despite our growing knowledge on CCM pathogenesis, it remains unclear why CCMs almost exclusively arise in the central nervous system. Global *Ccm3* gene disruption in mice induces embryonic lethality [6]. In acute models of conditional endothelial-specific *Ccm3* inactivation, numerous CCM lesions can be found that are primarily located in the cerebellum. Chronic models lead to fewer but more randomly distributed CCMs [7]. Interestingly, specific *Ccm3* gene knockouts in astrocytes, neural cells, and brain mural cells can also induce CCM-like lesions in mice [8–10].

Genetic and immunohistochemical analyses of human cavernoma tissues have established a Knudsonian two-hit model for familial CCM disease [11–16]. Only when a somatic mutation inactivates the wild-type allele in a cell of a germline mutation carrier, CCM formation is initiated. With sophisticated transgenic *Ccm3* mouse models, recent studies have shed light on the stages of CCM genesis and demonstrated that clonal expansion of mutant endothelial cells (ECs) and recruitment of wild-type or heterozygous ECs trigger early CCM formation and later lesion growth, respectively [17, 18].

By using human-induced pluripotent stem cell (hiPSC)-derived vascular organoids and EC co-cultures, we here demonstrate that cancer-like proliferation of mutant ECs is only triggered by direct contact with wild-type ECs. The fact that the anti-cancer drug NSC59984, a small molecule known to induce constitutive phosphorylation of ERK2 and reactivate p53 signaling in cancer cells [19, 20], blocked the abnormal proliferation of CCM3-deficient ECs reinforced the hypothesis that some features of CCMs are reminiscent of tumorigenesis [17, 18]. Finally, our study reveals that wild-type ECs activate chemokine signaling pathways in co-culture and thus provides insight into the poorly understood interaction of wild-type and mutant ECs.

Materials and methods

Cell culture

Constitutive immortalized human umbilical vein endothelial cells (CI-huVECs, HK0, 240615, InSCREENeX, Braunschweig, Germany) [21] were cultured at 37 °C and 5% CO_2 in endothelial cell growth medium (ECGM, PromoCell, Heidelberg, Germany) supplemented with 10% fetal calf serum (FCS, Thermo Fisher Scientific, Waltham, MA, USA). Clonally expanded CI-huVEC lines with biallelic loss-of-function variants in the first coding exon of *CCM3* have been described before (Online Resource 1, [22, 23]). Pathogenic *TP53* variants in *CCM3*$^{-/-}$ CI-huVECs were excluded using the NEXTflex TP53 Amplicon Panel (Bioo Scientific, Austin, TX, USA). *CCM3* mutant and wild-type CI-huVECs were co-cultured in 96-well plates under standard culture conditions with the indicated mutant-to-wild-type ratios. 2500 cells were seeded per well. To investigate the role of laminin-332, 2500 *CCM3*$^{+/+}$ or *CCM3*$^{-/-}$ CI-huVECs were cultured for 6 days on 96-well plates coated with 1 µg/cm^2 human recombinant laminin-332 by Biolamina (LN332, Sunbyberg, Sweden). Wells were fixed on day 6 with 4% PFA and immunofluorescence staining was performed for laminin (1:50, sc-133178, Santa Cruz Biotechnology, Dallas, TX, USA) with goat anti-mouse, Alexa Fluor 488 secondary antibody (1:200, A-11029, Thermo Fisher Scientific).

The following endogenously tagged human iPSC lines as part of the Allen Cell Collection (Coriell Institute, Camden, NJ, USA) were used in this study: AICS-0036-006 (00003450):WTC-mEGFP-Safe harbor locus (AAVS1)-cl6 and AICS-0054-091 (00007433):WTC-mTagRFPT-CAAX-Safe harbor locus (AAVS1)-cl91. hiPSC lines were maintained at 37 °C and 5% CO_2 in Essential 8 Flex medium (Thermo Fisher Scientific) on plates coated with growth factor reduced matrigel (Corning Inc., Corning, NY, USA), passaged with 0.5 mM EDTA (Thermo Fisher Scientific), and checked for the expression of the stem cell markers OCT4, SSEA4, SOX2, and TRA-1-60 using the PSC 4-Marker Immunocytochemistry Kit (Thermo Fisher Scientific). For AICS-0036 lines, a goat anti-mouse, Alexa Fluor 555 antibody (1:500, ab150114, Abcam, Cambridge, UK) and a goat anti-rat, Alexa Fluor 555 antibody (1:500, A-21434, Thermo Fisher Scientific) were used as secondary antibodies to stain for SSEA4 and SOX2. For the AICS-0054 line, a goat anti-rabbit, Alexa Fluor 488 antibody (1:500, A-11008, Thermo Fisher Scientific) and a goat anti-mouse, Alexa Fluor 488 antibody (1:500, A-21042, Thermo Fisher Scientific) were used as secondary antibodies to stain for OCT-4 and TRA-1-60. The hPSC Genetic Analysis Kit (Stemcell Technologies) was used according to the manufacturer's instructions to exclude common chromosomal abnormalities. iPSC cultures

were regularly tested negative for mycoplasma contamination by PCR.

CRISPR/Cas9 genome editing in hiPSCs

For ribonucleoprotein (RNP)-mediated genome editing, hiPSC lines were transfected with sgRNA:Cas9 RNP-complexes with the previously described target sequence located in exon 3 of *CCM3* [23]. Briefly, 6 µM sgRNA and 6 µM *S.p.* Cas9 protein (Integrated DNA Technologies, Coralville, IA, USA) were complexed in Opti-MEM I reduced serum medium (Thermo Fisher Scientific), and transfection complexes were formed in Opti-MEM with Lipofectamine Stem Transfection Reagent (Thermo Fisher Scientific). Cells were detached with StemPro Accutase (Thermo Fisher Scientific) and reverse transfected in Essential 8 medium (Thermo Fisher Scientific) supplemented with 10 µM ROCK inhibitor Y-27632 (Stemcell Technologies, Vancouver, Canada) on growth factor reduced Matrigel-coated 24-well plates (30 nM final RNP concentration; 150,000 cells and 2.0 µl Lipofectamine Stem Transfection Reagent). After 24 h, the medium was replaced with Essential 8 Flex medium without ROCK inhibitor. To establish clonal lines, genome-edited hiPSCs were seeded at a density of 0.5 cells/well on growth factor reduced Matrigel-coated 96-well plates and cultivated with Essential 8 Flex medium supplemented with CloneR (Stemcell Technologies). The genotypes of clonally expanded lines were determined by Sanger sequencing.

Differentiation of hiPSCs to hBMEC-like cells

$CCM3^{+/+}$ AICS-0054 hiPSCs, $CCM3^{+/+}$ and $CCM3^{-/-}$ AICS-0036 hiPSCS were differentiated to human brain microvascular endothelial-like cells (hBMEC-like cells) according to the protocol of Neal and colleagues [24] with minor modifications. Briefly, 158,000 cells were seeded in Essential 8 Flex medium containing 10 µM Y-27632 on growth factor reduced Matrigel-coated 6-well plates. After 24 h, differentiation was initiated by substituting Essential 8 Flex with Essential 6 medium (Thermo Fisher Scientific). The medium was changed daily for 4 days. On day 4, the medium was switched to Human Endothelial Serum-Free Medium (hESFM, Thermo Fisher Scientific) supplemented with FGF-2 (Miltenyi Biotec, Bergisch Gladbach, Germany), retinoic acid (Sigma-Aldrich, St. Louis, MO, USA), insulin (Sigma-Aldrich), holo-transferrin (Sigma-Aldrich), and sodium selenite (Sigma-Aldrich). After 48 h, cells were replated on 24-well plates coated with collagen IV from human placenta (Sigma-Aldrich) and human plasma fibronectin (Sigma-Aldrich). 24 h later, medium was changed to hESFM supplemented with insulin, holo-transferrin, and sodium selenite until confluency was reached. Differentiated hBMEC-like cells were passaged and expanded in EndoGRO-MV medium (Merck) supplemented with 1 ng/ml FGF-2. High expression of the tight junction proteins occludin and claudin-5 was verified by immunofluorescence microscopy. Cells were fixed with 4% PFA, stained for occludin (1:100, OC-3F10, Thermo Fisher Scientific) and claudin-5 (1:50, 4C3C2, Thermo Fisher Scientific) at 4 °C overnight, and incubated with a secondary antibody (1:200, A-11029, Thermo Fisher Scientific or 1:200, ab150114, abcam) for 2 h at room temperature. HBMEC-like cells were also seeded on matrigel-coated 96-wells at a density of 20.000 cells/well in hESFM supplemented with insulin, holo-transferrin, sodium selenite, and 50 ng/ml VEGF to verify tube formation. Images were acquired after 18 h. To study the proliferation characteristics of mutant hBMEC-like cells, $CCM3^{+/+}$ AICS-0054 hBMEC-like cells and $CCM3^{+/+}$ or $CCM3^{-/-}$ AICS-0036 hBMEC-like cells were mixed in a 9:1 ratio (2500 cells per 96-well) and cultured for 6 days. On day 6, cells were fixed with 4% paraformaldehyde (PFA) or replated on 96-well plates (2500 cells per well). On day 12, the wells were fixed, and Hoechst 33342 (Thermo Fisher Scientific) staining was performed for subsequent fluorescent imaging analysis with the EVOS FL imaging system. The ratio of EGFP-tagged AICS-0036 cells compared to all cells was determined using the ImageJ software. Differentiated hBMEC-like cells were used in passages 3 and 5.

Differentiation of hiPSCs to vascular organoids

hiPSCs were differentiated to vascular organoids according to the protocol of Wimmer and colleagues [25]. To study the proliferation characteristics of mutant cells, $CCM3^{+/+}$ AICS-0054 hiPSCs and $CCM3^{+/+}$ or $CCM3^{-/-}$ AICS-0036 hiPSCS were mixed in a 9:1 ratio and differentiated to vascular organoids. Briefly, 800,000 hiPSCs were seeded in ultra-low attachment 6-well plates (Corning) in aggregation medium for 2 days until aggregates had formed. On day 0, mesodermal induction was initiated with CHIR99021 (Tocris Bioscience, Bristol, United Kingdom) and BMP-4 (Miltenyi Biotec) in N2B27 medium. Supplementation of VEGF-A (PeproTech, Inc., Rocky Hill, NJ, USA) and forskolin (Sigma-Aldrich) on day 3 induced vascular differentiation. On day 5, vascular aggregates were embedded in a collagen I-Matrigel matrix. VEGF-A, FGF-2 (Miltenyi Biotec), and FCS (Thermo Fisher Scientific) enriched StemPro-34 medium (Thermo Fisher Scientific) was added for vessel sprouting. Vascular network extraction was performed on day 10. On day 15, fully encapsulated organoids were fixed with 4% PFA, and nuclei staining was performed using Hoechst 33342 (Thermo Fisher Scientific). Fixed organoids were suspended in ibidi mounting medium (ibidi, Gräfelfing, Germany) and placed in 96-well cell imaging plates (Eppendorf AG, Hamburg, Germany). Imaging was performed using the Operetta CLS High-Content Imaging System (PerkinElmer,

Waltham, MA, USA). Data were analyzed with the Harmony High-Content Imaging and Analysis Software (version 4.9, PerkinElmer).

Fusion organoids originating from the combination and co-culture of vascular networks acquired from *CCM3*$^{+/+}$ and *CCM3*$^{-/-}$ cells were used to study the effect of NSC59984 in hiPSC derived vascular organoids. 8×10^5 AICS-0054 *CCM3*$^{+/+}$ cells, AICS-0036 *CCM3*$^{+/+}$ cells and AICS-0036 *CCM3*$^{-/-}$ cells were differentiated into vascular networks as described previously [25]. Vascular networks derived from AICS-0054 *CCM3*$^{+/+}$ hiPSCs were co-cultured with AICS-0036 *CCM3*$^{+/+}$ or AICS-0036 *CCM3*$^{-/-}$ vascular networks in the presence of 10 µM NSC59984. Medium supplemented with NSC59984 was changed every three days. On day 3 of co-culture, completely encapsulated fusion organoids were obtained and further cultivated until organoid examination on day 5 and day 10.

Clonogenic and proliferation assays

Plating efficiencies were determined following a previously published protocol [26]. In brief, *CCM3*$^{+/+}$ and *CCM3*$^{-/-}$ CI-huVEC were seeded in 6-well plates as near-perfect single cell suspensions with either 100 or 250 cells per well. Colonies were fixed and stained after eight days with a glutaraldehyde solution (G6257, Sigma-Aldrich, final concentration 6%) and crystal violet (HT901, Sigma-Aldrich, final concentration 0.5%). The plating efficiency was defined as the ratio between the number of colonies and the number of plated cells. The proliferation rate of mutant and wild-type ECs in mono-culture was quantified with the CyQuant Cell Proliferation Assay Kit (C7026, Thermo Fisher Scientific). To discriminate the proliferation rates of *CCM3*$^{+/+}$ and *CCM3*$^{-/-}$ CI-huVEC in co-culture, the CyQuant Cell Proliferation Assay results were combined with mutant allele frequencies that had been determined by amplicon deep sequencing. In detail, measured RFU from the proliferation assay experiment were converted to cell numbers using a reference standard curve (RFU vs. cell number). These numbers represent the total cell number of a replicate at a given time point in the experiment. Subsequently, total cell number was multiplied by the allele frequency of a specific genotype. Allele frequencies were calculated from amplicon deep sequencing experiments performed in parallel with the proliferation assays. Since we used *CCM3*$^{-/-}$ CI-huVEC in co-culture experiments that were either compound heterozygous or homozygous for loss-of-function alleles, the calculated allele frequency of a genotype corresponds to the proportion of cells with that genotype. For genotype-specific proliferation rates, the calculated cell number was normalized to the calculated cell number at day 0.

$$[\text{proliferation rate (in \%)}_{\text{genotype}} = \frac{\left(\text{RFU} * \text{F}_{\text{standard curve}} * \text{F}_{\text{genotype allele frequency}}\right)_{\text{day d}}}{\left(\text{RFU} * \text{F}_{\text{standard curve}} * \text{F}_{\text{genotype allele frequency}}\right)_{\text{day 0}}} * 100\%]$$

Caspase-3, caspase-8, and caspase-9 activity assays

To analyze their sensitivity to apoptosis, mutant and wild-type ECs were seeded in 96-well plates with 15,000 cells per well and treated with staurosporine (Sigma-Aldrich) 24 h later. The Caspase-3 DEVD-R110 Fluorometric HTS Assay Kit (Biotium, Fremont, CA, USA), the Cell Meter Caspase 8 Activity Apoptosis Assay Kit (AAT Bioquest, Sunnyvale, CA, USA), and the Cell Meter Caspase 9 Activity Apoptosis Assay Kit (AAT Bioquest) were used following the manufacturer's instructions.

Protein extraction, antibody arrays, western blot and ELISA analyses

For the Human Apoptosis Antibody Array (ab134001, Abcam), proteins were extracted with PeqGold TriFast reagent (Peqlab-VWR, Radnor, PA, USA) and solubilized in buffer containing 8 M Urea, 2 M Thio-Urea, and 20 mM Tris. For the Human MAPK Phosphorylation Antibody Array (ab211061, Abcam), proteins were extracted according to the manufacturer's instructions. For Western Blot analyses, proteins were extracted with PeqGold TriFast reagent or RIPA Lysis and Extraction Buffer (Thermo Fisher Scientific). A Qubit Protein Assay Kit (Thermo Fisher Scientific) or a Micro BCA Protein Assay Kit (Thermo Fisher Scientific) was used to measure protein concentrations. The Human Apoptosis Antibody Array-Membrane Kit was used according to the manufacturer's instructions to analyze the expression of apoptosis-related proteins in *CCM3*$^{+/+}$ and *CCM3*$^{-/-}$ CI-huVEC after 24 h of treatment with 0.05 µM staurosporine. The Human MAPK Phosphorylation Antibody Array Kit was used according to the manufacturer's instructions to analyze the expression of MAPK pathway markers in *CCM3*$^{+/+}$ and *CCM3*$^{-/-}$ CI-huVECs after co-culture. 600 µg of total protein was incubated for each membrane,

and chemiluminescence signals were documented with a ChemiDoc XRS+ imager (Bio-Rad, Hercules, California, USA). Densitometry data were obtained using the ImageLab software (v6.0, Bio-Rad). For CCM3 and p21 Western Blot analyses, protein samples were suspended with Laemmli Sample Buffer (Bio-Rad) and heated at 95 °C for 5 min. For p53, heat denaturation was perfomed under reducing conditions. 20 µg (p21), 30 µg (CCM3) or 40 µg (p53) of total protein were separated on a 10% TGX Stain-Free FastCast SDS-polyacrylamide gel (Bio-Rad) and subsequently transferred to PVDF membranes. The iBind Flex Western System (Thermo Fisher Scientific) was used for immunostaining according to the manufacturer's instructions. The following primary antibodies were used: Anti-PDCD10/CCM3 (1:200, ab110531, Abcam or 1:200, ab180706, Abcam), Anti-p21 (1:1000, ab109520, Abcam), Anti-p53 (1:40, sc-126, Santa Cruz Biotechnology, Dallas, TX, USA) and Anti-GAPDH (1:500, PA1-16777, Thermo Fisher Scientific). A HRP-conjugated goat anti-rabbit immunoglobulin antibody (1:400, ab205718, Abcam) or a HRP-conjugated goat anti-mouse immunoglobulin antibody (1:400, ab205719, Abcam) with Precision Protein StrepTactin-HRP Conjugate (1:2000, Bio-Rad) were used as secondary antibodies. Detection of proteins was performed using Clarity Western ECL Substrate (Bio-Rad). Stain-free total protein and colorimetric protein bands were documented using a ChemiDoc XRS+ imager. The ImageLab software was used to calculate normalized band intensities. To calculate the relative protein expression, the volume intensities of the detected protein bands were normalized to the volume intensities of the corresponding GAPDH bands. The detection of GAPDH was performed after stripping the membrane with ROTI Free Stripping Buffer 2.2 plus (Carl Roth, Karlsruhe, Germany) for 1 h at room temperature.

To examine p53 activity, the p53 Transcription Factor Assay Kit (Cayman Chemical Company, Ann Arbor, MI, USA) was used according to manufacturer's instructions. Nuclear extracts were isolated from $CCM3^{+/+}$ and $CCM3^{-/-}$ cells using the Nuclear Extraction Kit (Cayman Chemical Company). 10 µg of nuclear extracts were incubated for each well at 4 °C overnight. Signal was measured at OD_{450nm} using an Infinite M200 Plate Reader (Tecan, Männedorf, Switzerland).

Apoptosis compound library screen and amplicon deep sequencing

An apoptosis compound library with 189 small molecules was used in a high throughput screening approach [HY-L003(HY-LD-000001651); MedChem Express, Monmouth Junction, NJ, USA]. Co-cultures were treated with 10 µM of each substrate for 6 days. Compounds were added 5 h and 3 days after cell seeding. NSC59984 (IUPAC: (2E)-1-(4-Methyl-1-piperazinyl)-3-(5-nitro-2-furyl)-2-propen-1-one, HY19726, MedChem Express), isoalantolactone (IUPAC: (3aR,4aS,8aR,9aR)-8a-Methyl-3,5-bis(methylene) decahydronaphtho[2,3-b]furan-2(3H)-one, HY-N0780, MedChem Express), and GSK-872 (IUPAC: *N*-(6-propan-2-ylsulfonylquinolin-4-yl)-1,3-benzothiazol-5-amine, HY-101872, MedChem Express) were used for individual experiments with the indicated concentrations. DMSO-treatment (A994, Carl Roth) served as control. After 6 days, the fraction of mutant alleles in co-culture was analyzed by amplicon deep sequencing. In brief, the genomic target region was amplified by PCR. For NGS analysis, sequencing adapters and individual barcodes were introduced in a second PCR [22, 23]. Sequencing libraries were pooled and sequenced on a MiSeq instrument with 2×150 cycles (Illumina, San Diego, CA, USA). Data were analyzed with the SeqNext software (JSI Medical Systems, Ettenheim, Germany). The following compounds were tested for the ability to abrogate NSC59984-mediated inhibition of clonal expansion: UC2288 (Sigma-Aldrich), SCH772984 (Hycultec, Beutelsbach, Germany), and U0126-ETOH (Hycultec). Substances were supplemented 5 h and 3 days after seeding. Amplicon deep sequencing was perfomed at day 6.

Integrin antibody-array, ITGB4 qPCR and staining, FACS sorting

The β-Integrin-mediated Cell Adhesion Array Kit (ECM534, Sigma-Aldrich) was used according to the manufacturer's instructions to quantify cell surface expression of β_1, β_2, β_3, β_4, $\alpha_V\beta_5$, and $\alpha_5\beta_1$ integrins of $CCM3^{+/+}$ and $CCM3^{-/-}$ CI-huVECs. Fluorescence intensity was measured with the Qubit 4 Fluorometer (Thermo Fisher Scientific). For immunofluorescent imaging, CI-huVECS were cultured on 96-well plates until confluency was reached. Mouse anti-integrin β4 (ITGB4) antibody (1:100, MAB2059Z, Merck, Darmstadt, Germany) was added to the culture medium, and cells were incubated for 1 h at 37 °C and 5% CO_2. Cells were washed three times with culture medium and incubated for 1 h at 37 °C and 5% CO_2 with goat anti-mouse, Alexa Fluor 488 secondary antibody (1:200, A-11029, Thermo Fisher Scientific). Subsequently, cells were washed three times in culture medium and imaged with the EVOS FL imaging system (Thermo Fisher Scientific). For qPCR analysis, mRNA was transcribed into cDNA using the First Strand cDNA Synthesis Kit (Thermo Fisher Scientific). SYBR Green-based qPCR analysis was performed on a Roche Light Cycler 480 instrument (Roche, Mannheim, Germany) to validate deregulated gene expression of *ITGB4*. The gene *RPLP0* served as an endogenous control. The following primer pairs purchased from Integrated DNA Technologies were used: *ITGB4*—5′-CTACTACGAGAA

GCTTCACAC-3′ and 5′-GACCCAGTCCTCGTCTTC TG-3′; *RPLP0*—5′-TCGACAATGGCAGCATCTAC-3′ and 5′-ATCCGTCTCCACAGACAAGG-3′. For FACS sorting of co-cultured CI-huVECs, 1–2 million cells were seeded on T75-flasks in a 2:3 ratio of mutant to wild-type cells and cultured for three days. Cells were dissociated with Accutase and stained with mouse anti-integrin β4 antibody (1:200) and goat anti-mouse, Alexa Fluor 488 secondary antibody (1:200). Cells were resuspended in PBS and flow cytometry was used for sorting (BD FACSAria III Cell Sorter; BD Biosciences, Franklin Lakes, NJ, USA). The RNA of ITGB4^{high} and ITGB4^{low} fractions were extracted in TRI Reagent for fluid samples (Sigma-Aldrich). The purity of fractions was confirmed on DNA, RNA, and protein level. DNA and RNA were extracted to evaluate purity via amplicon deep sequencing and qPCR, respectively. For transcript analyses, the *CCM3* qPCR assay PrimeTime Hs.PT.58.38574999 (Integrated DNA Technologies) was used.

RNA sequencing and qPCR analyses

Extracted RNA was purified using the Direct-zol RNA MiniPrep Plus Kit (Zymo Research, Irvine, CA, USA). If necessary, isolated RNA was concentrated with the RNA Clean & Concentrator-5 Kit (Zymo Research). A Qubit 4.0 (Thermo Fisher Scientific) and the Qubit RNA BR Assay Kit (Thermo Fisher Scientific) were used to measure RNA concentrations. RNA sample integrity was controlled on a 2100 Bioanalyzer using the RNA 6000 Nano Kit (Agilent, Santa Clara, CA, USA). RNA-seq libraries were prepared via polyA selection and sequenced on an Illumina NovaSeq platform (Illumina) with 2×150 cycles by GENEWIZ (Leipzig, Germany). Reads were trimmed to remove adapter sequences using Trimmomatic v.0.36 and mapped to the Homo sapiens GRCh37 genome with STAR aligner v.2.5.2b. The software featureCounts from the Subread package v.1.5.2 was used to extract unique gene hit counts. For targeted RNA-analysis, a QIAseq Targeted Human Apoptosis and Cell Death RNA Panel (RHS-002Z, QIAGEN, Hilden, Germany) was used to prepare RNA sequencing libraries according to the manufacturer's instructions. After quality control with the High Sensitivity DNA Kit on a 2100 Bioanalyzer instrument (Agilent), the pooled libraries were sequenced on a MiSeq (Illumina) with 1×151 cycles. Differential gene expression of RNA sequencing data was carried out using the QIAseq Targeted RNA Primary and Secondary Analysis Tool (QIAGEN). The PrimeTime assays Hs.PT.58.40874346.g and Hs.PT.58.38974274 (Integrated DNA Technologies) were used to measure *CDKN1A* and *GADD45A* gene expression. The gene *RPLP0* served as an endogenous control.

Statistical analysis

The GraphPad Prism software (v.8.0.1, GraphPad Software, LA Jolla, CA, USA) was used for statistical analysis. Unless stated otherwise, all data are presented as mean and standard deviation (SD). For analyses of two or more groups, multiple t tests, one- and two-tailed Student's t test, and one- and two-way ANOVA were used. Dunnett's or Šidák's corrections were applied for multiple comparisons. P values or adjusted p values < 0.05 were regarded as statistically significant. For genome-wide RNA-seq, differential gene expression analysis was performed using DESeq2. P values and log2 fold changes were generated using the Wald test. Genes were regarded as differentially expressed between compared groups with an adjusted p value < 0.05 and an absolute log2 fold change > 1. Gene ontology analysis was performed using the GeneSCF v.1.1-p2 software combined with the goa_human GO list to cluster genes based on biological processes.

Results

CCM3 inactivation alone does not trigger EC proliferation

To compare the growth and survival characteristics of wild-type and mutant ECs, we first plated single-cell suspensions of *CCM3*$^{+/+}$ and *CCM3*$^{-/-}$ CI-huVECs, and analyzed their ability to grow into colonies. We observed a significantly higher clonogenic capacity of mutant CI-huVECs. The plating efficiency of mutant compared to wild-type ECs was actually three times higher (Fig. 1a). However, CI-huVECs in which the *CCM3* gene had been disrupted by CRISPR/Cas9 genome editing did not display significantly different proliferation rates (Fig. 1b). Next, we stimulated apoptotic cell death in *CCM3*$^{-/-}$ and *CCM3*$^{+/+}$ CI-huVECs with staurosporine and found significantly higher survival rates of mutant ECs (Online Resource 2). Two, eight, and twenty-four hours after staurosporine treatment, the activity of caspase-3, which is a major effector caspase in apoptosis, was also significantly lower in *CCM3*$^{-/-}$ CI-huVECs (Fig. 1c). Profiling the relative expression of 43 apoptosis-related proteins verified the reduced fraction of active caspase-3 but revealed no other significantly up- or downregulated targets in *CCM3*$^{-/-}$ CI-huVECs (Fig. 1d, Online Resource 3). Caspase-3 is proteolytically activated by upstream caspases of the intrinsic and extrinsic pathways of apoptosis. Our protein array did not specifically detect the active forms of caspase-8 (extrinsic pathway) and caspase-9 (intrinsic pathway). Therefore, we used specific fluorogenic indicators to measure their activities. Both were slightly reduced in mutant compared to wild-type ECs after staurosporine

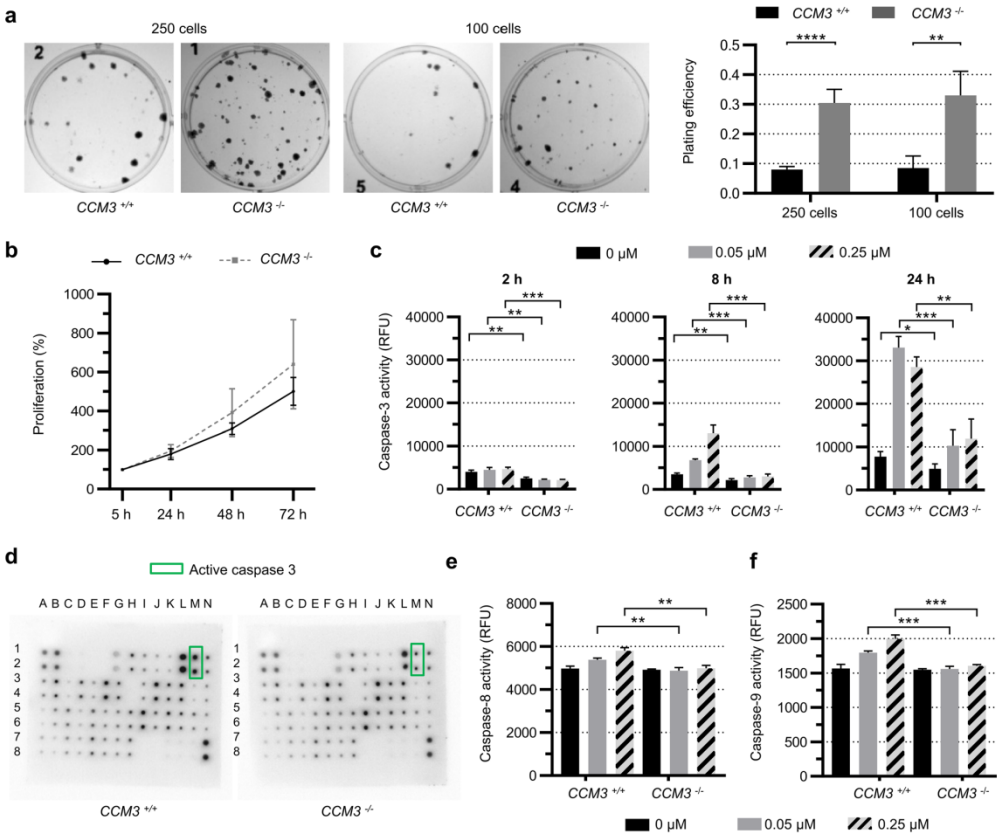

Fig. 1 Inactivation of *CCM3* gene expression in human ECs causes resistance to apoptosis and increased clonogenicity. **a** $CCM3^{-/-}$ and $CCM3^{+/+}$ CI-huVECs were seeded as (near-perfect) single-cell suspensions in 6-well plates with either 250 or 100 cells per well. Colonies were stained with crystal violet after eight days. Representative images are shown for both genotypes. The plating efficiency of $CCM3^{-/-}$ CI-huVECs was significantly increased under both seeding conditions ($n=4$ per genotype). **b** *CCM3* inactivation did not significantly enhance proliferation of CI-huVECs under standard culture conditions ($n=9$ per genotype). **c** CI-huVECs were treated with staurosporine (0.05 µM or 0.25 µM) to induce apoptotic cell death. After 2, 8, and 24 h, the caspase-3 activity was markedly reduced in $CCM3^{-/-}$ CI-huVECs ($n=3$ per genotype). **d** A human apoptosis antibody array assay verified the reduction of active caspase-3 levels in staurosporine-treated (0.05 µM, 24 h) $CCM3^{-/-}$ CI-huVECs ($n=3$ per genotype). Representative array membranes are shown for both genotypes. Green rectangles mark active caspase-3. No significant differences were found for other apoptosis markers. **e**, **f** The activities of caspase-8 (**e**) and caspase-9 (**f**) were also slightly reduced in staurosporine-treated (0.05 µM or 0.25 µM, 8 h) $CCM3^{-/-}$ CI-huVECs ($n=3$ per genotype). RFU = relative fluorescence units. Data are presented as mean and SD. Student's two-tailed *t* tests (**a–c**, **e**, **f**) were used for statistical analyses: $^{*}P<0.05$, $^{**}P<0.01$, $^{***}P<0.001$, $^{****}P<0.0001$

treatment (Fig. 1e, f). These results demonstrate that mutant ECs have a survival advantage under specific stress conditions. However, unstressed $CCM3^{-/-}$ mono-cultures do not show abnormal proliferation.

Only direct co-culture with wild-type cells stimulates abnormal proliferation of mutant ECs

To mimic the mosaic endothelial pattern in CCM tissue, in which the number of mutant ECs is usually much lower than the number of wild-type cells [15–18], we co-cultured $CCM3^{-/-}$ with $CCM3^{+/+}$ CI-huVECs in a 1:9 ratio for six days (Fig. 2a). When we combined the results of

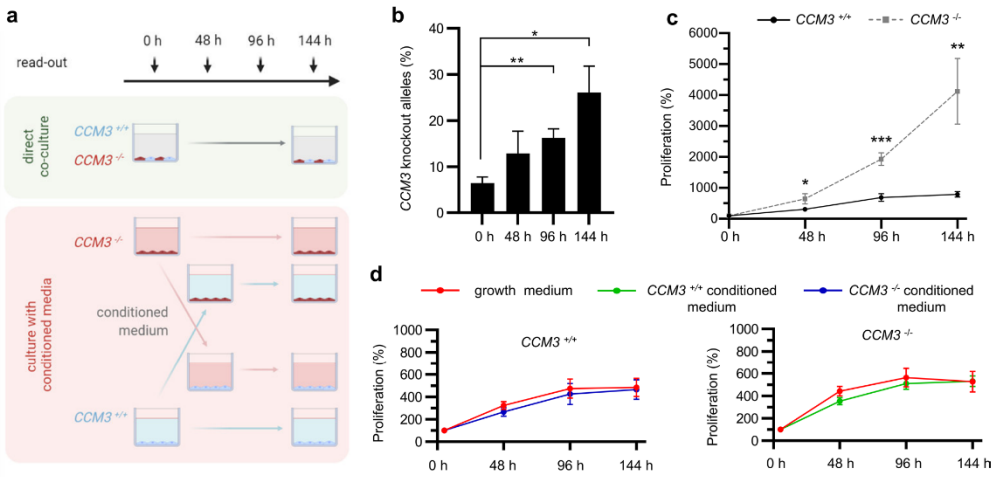

Fig. 2 *CCM3*$^{-/-}$ CI-huVECs demonstrate increased proliferative activity when directly co-cultured with *CCM3*$^{+/+}$ ECs. **a** *CCM3*$^{-/-}$ CI-huVECs were either directly co-cultured with *CCM3*$^{+/+}$ CI-huVECs or with conditioned medium of *CCM3*$^{+/+}$ CI-huVECs. In parallel, *CCM3*$^{+/+}$ CI-huVECs were cultured with conditioned medium of *CCM3*$^{-/-}$ CI-huVECs. Knockout and wild-type CI-huVECs cultured in unconditioned growth medium served as controls. Proliferation was analyzed at the indicated time points. **b**, **c** In direct co-culture, the proportion of *CCM3* knockout alleles markedly increased over time (**b**), and *CCM3*$^{-/-}$ CI-huVECs proliferated significantly more (**c**) ($n=3$ per condition). **d** *CCM3*$^{-/-}$ CI-huVECs were cultured with conditioned medium from *CCM3*$^{+/+}$ CI-huVECs and vice versa. Unconditioned growth medium was used as control. The conditioned medium alone did not influence the proliferation rate of *CCM3*$^{-/-}$ CI-huVECs ($n=3$ per condition). Data are presented as mean and SD. Student's two-tailed t tests were used for statistical analyses: $^{*}P<0.05$, $^{**}P<0.01$, $^{***}P<0.001$

fluorescence-based cell proliferation assays with amplicon deep sequencing data, we found increasing mutant allele frequencies over time (Fig. 2b) and significantly higher proliferation rates of mutant ECs compared to wild-type cells in co-culture (4124% vs. 793% after 144 h, Fig. 2c). This effect was also evident in co-cultures with very low mutant:wild-type ratios (from 5:95 to 1:99, Online Resource 4). However, it completely vanished upon reversal of this ratio (from 95:5 to 99:1, Online Resource 4). Next, we asked whether the proliferative advantage of mutant ECs in co-culture depends on cell–cell interactions or can also be triggered by paracrine signaling alone. Thus, we studied the effect of conditioned medium on the proliferation rates of *CCM3*$^{-/-}$ and *CCM3*$^{+/+}$ CI-huVECs (Fig. 2a). When we cultured mutant ECs in conditioned medium of wild-type ECs, we detected no increased proliferation. In line with this observation, the conditioned medium of mutant ECs did not affect the mitotic activity of wild-type cells (Fig. 2d). Thus, direct cell contact with *CCM3*$^{+/+}$ CI-huVECs is indispensable to trigger the proliferation of *CCM3*$^{-/-}$ ECs in co-culture.

CCM3 acts as suppressor of abnormal proliferation in vascular ECs but not in hiPSCs

We next asked whether *CCM3* gene disruption also triggers abnormal proliferation of mutant hiPSCs in co-culture with wild-type hiPSCs. To answer this question, we used CRISPR/Cas9 genome editing to inactivate *CCM3* gene expression in mEGFP-tagged AICS-0036 hiPSCs (Online Resource 5). The CCM3 knockout had neither an effect on the morphology of the hiPSC colonies nor on the expression of the pluripotency markers TRA-1-60, SOX2, OCT4, and SSEA4 (Fig. 3a). After we had excluded recurrent genomic instabilities and verified the CCM3 knockout on protein level (Fig. 3b, Online Resource 5), mEGFP-tagged *CCM3*$^{-/-}$ AICS-0036 hiPSCs and mTagRFPT-tagged *CCM3*$^{+/+}$ AICS-0054 hiPSCs were mixed in a 1:9 ratio and cultured for up to eight days. Interestingly, no abnormal proliferation of mutant hiPSCs was observed in co-culture with wild-type hiPSCs (Fig. 3c, d). To exclude a cell-type-specific effect of the striking cancer-like proliferation of *CCM3*$^{-/-}$ CI-huVECs in co-culture, we differentiated hiPSCs into human brain microvascular endothelial-like cells (hBMEC-like cells; Fig. 4a, Online Resource 6) and

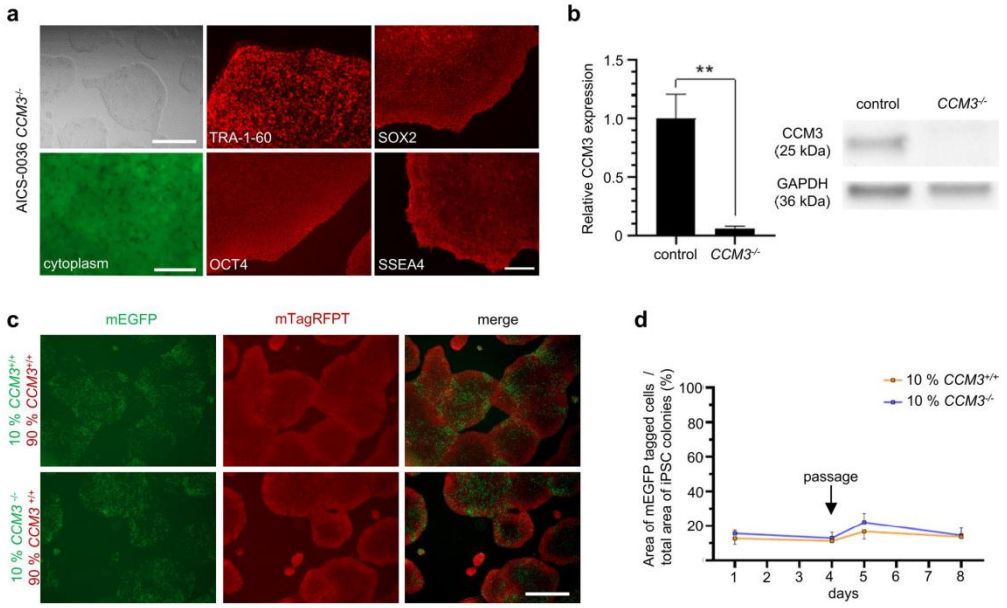

Fig. 3 CCM3-deficient hiPSCs show no abnormal proliferation in co-culture with wild-type hiPSCs. **a** *CCM3*$^{-/-}$ AICS-0036 hiPSC demonstrated typical hiPSC morphology (representative images; top left, scale bar: 500 µm) and strong expression of the pluripotency markers TRA-1–60, OCT4, SOX2, and SSEA4 (representative images; middle and right panels, scale bar: 200 µm). The mEGFP-tagged cytosol of *CCM3*$^{-/-}$ AICS-0036 hiPSC is shown in the bottom left subpanel (scale bar: 50 µm). **b** Western blot analysis verified CCM3 inactivation in *CCM3*$^{-/-}$ AICS-0036 hiPSCs. GAPDH was used as a loading control ($n=3$ per genotype). **c**, **d** *CCM3*$^{-/-}$ AICS-0036 hiPSCs were mixed with *CCM3*$^{+/+}$ AICS-0054 hiPSCs in a 1:9 ratio and co-cultured for 8 days. *CCM3*$^{+/+}$ AICS-0036 mixed with *CCM3*$^{+/+}$ AICS-0054 hiPSCs served as controls ($n=3$ per genotype). Representative images from day eight are shown in c (scale bar: 500 µm). Data are presented as mean and SD. Student's two-tailed *t* tests (**b**, **d**) were used for statistical analyses: $^{**}P<0.01$

co-cultured *CCM3*$^{-/-}$ and *CCM3*$^{+/+}$ hBMEC-like cells in a 1:9 ratio. Within 6 to 12 days, the percentage of mutant cells in co-culture increased to 41.2% (SD 15.97) and 69.0% (SD 11.42), respectively (Fig. 4b, c). No abnormal proliferation was observed in co-cultures of mEGFP-tagged *CCM3*$^{+/+}$ hBMEC-like cells and mTagRFPT-tagged *CCM3*$^{+/+}$ hBMEC-like cells (Fig. 4b).

In vivo, endothelial proliferation acts in concert with differentiation, migration, and interaction of ECs with other cell types and the extracellular matrix [27]. This complex interplay can hardly be reproduced in 2D cultures alone. Thus, we utilized hiPSC-derived vascular organoids which have been described as powerful tool to study vasculopathies in 3D cultures [28]. When we differentiated co-cultures of mutant and wild-type hiPSCs to mosaic vascular organoids (Fig. 4d), we found no apparent defects of the vascular network but a strikingly increased proliferation of mutant cells (Fig. 4e, f). Like in human CCM lesions, CCM3-deficient cells did not form clusters but were found in a mosaic pattern with wild-type cells instead. Together, these results prompted us to address the abnormal mutant cell proliferation and their interaction with wild-type cells in more detail.

Co-culture activates cytokine signaling in wild-type and cell proliferation pathways in mutant ECs

A better understanding of the interplay between mutant ECs and wild-type or heterozygous ECs in mosaic CCM lesions appears to be essential for the development of targeted therapeutic approaches. Therefore, we decided to study the gene expression profiles of *CCM3*$^{-/-}$ and *CCM3*$^{+/+}$ CI-huVECs in mono-culture and direct co-cultures. Using a ß-integrin-mediated cell adhesion array and specific immunofluorescence imaging, we identified high expression of the integrin subunit $\beta4$ (ITGB4), which is known to form a heterodimer with integrin α6, as a marker for *CCM3*$^{-/-}$ CI-huVECs (Fig. 5a, b). Consistent with published gene expression data of other groups (Online Resource 7), *ITGB4* mRNA levels were upregulated 20-fold in *CCM3*$^{-/-}$ CI-huVECs (Fig. 5c). Integrin $\alpha6\beta4$ is a specific receptor for laminin-332 and the

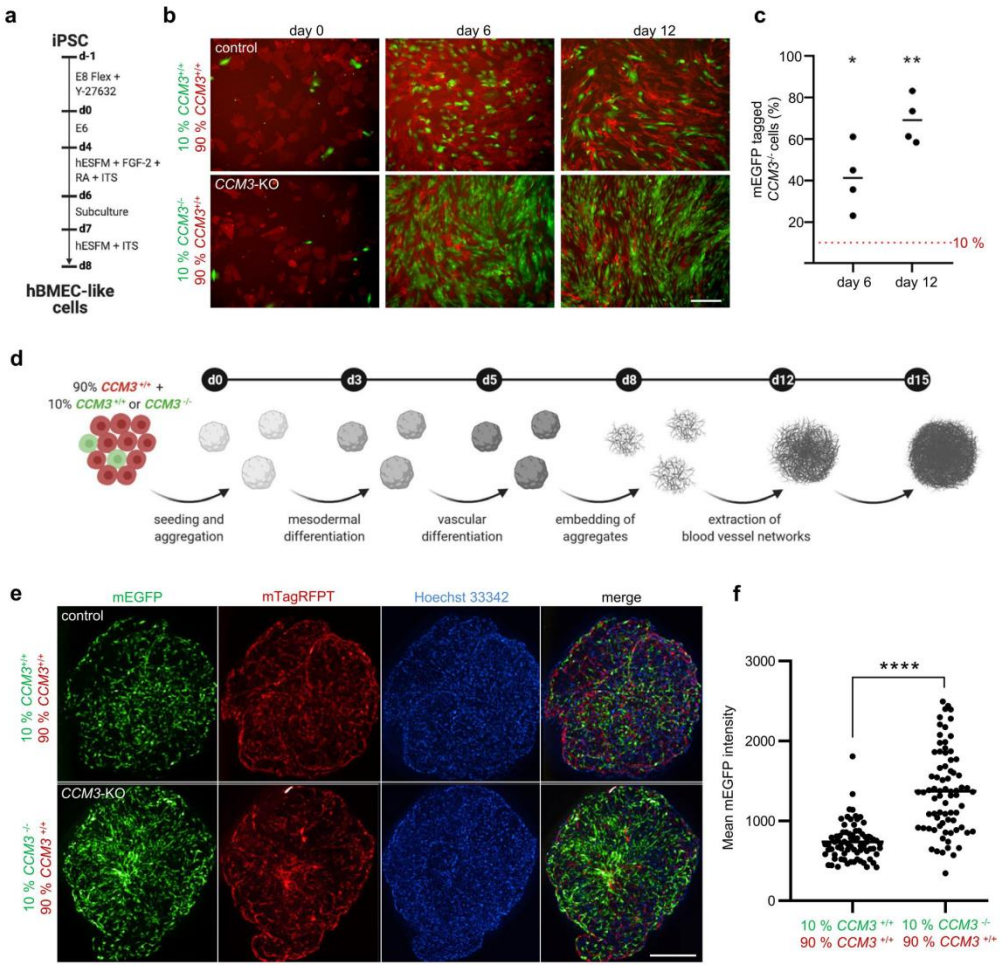

Fig. 4 Human iPSC-derived *CCM3*$^{-/-}$ ECs exhibit a tumor-like proliferative behavior in co-culture with wild-type ECs and in mosaic vascular organoids. **a–c** Brain microvascular endothelial-like cells (hBMEC-like cells) were differentiated from *CCM3*$^{-/-}$ AICS-0036 (mEGFP), *CCM3*$^{+/+}$ AICS-0036 (mEGFP), and *CCM3*$^{+/+}$ AICS-0054 (mTagRFPT) hiPCS (**a**) and mixed in a 1:9 ratio (**b**, **c**). *CCM3*$^{-/-}$ hBMEC-like cells (green) demonstrated an abnormal proliferation in co-culture with *CCM3*$^{+/+}$ hBMEC-like cells ($n=4$ per genotype; b, scale bar: 200 µm). **d** *CCM3*$^{-/-}$ AICS-0036 (mEGFP) and *CCM3*$^{+/+}$ AICS-0054 (mTagRFPT) hiPCS were mixed in a 1:9 ratio and differentiated to vascular organoids. *CCM3*$^{+/+}$ AICS-0036 mixed with *CCM3*$^{+/+}$ AICS-0054 hiPSCs served as controls. **e** Abnormal proliferation of *CCM3*$^{-/-}$ cells was observed in mosaic vascular organoids (lower left panel, scale bar: 300 µm). **f** Statistical analyses from 77 KO/WT to 75 WT/WT mosaic organoids differentiated in three independent biological replicates. Shown is the mean mEGFP fluorescence intensity. Data are presented as mean and individual data points. One sample *t* test (**c**) or Student's two-tailed *t* test (**f**) was used for statistical analyses: $^{*}P<0.05$, $^{**}P<0.01$, $^{****}P<0.0001$

ability of mutant ECs to bind exogenous laminin-332 was consequently increased (Online Resource 8). However, exogenous laminin-332 did not trigger the proliferation of *CCM3*$^{-/-}$ CI-huVECs (data not shown).

FACS sorting of co-cultured *CCM3*$^{-/-}$ and *CCM3*$^{+/+}$ CI-huVECs for ITGB4^{high} and ITGB4^{low} cells resulted in two distinct populations (Fig. 5d). Amplicon deep sequencing, qPCR and western blot analyses verified high purities

of sorted wild-type and mutant ECs, respectively (Online Resource 8). Based on these results, we set up a genome-wide gene expression profiling experiment (Fig. 5e). Focussing on $CCM3^{-/-}$ and $CCM3^{+/+}$ CI-huVECs in mono-culture, 1043 genes were found to be significantly upregulated, and 1025 were downregulated upon *CCM3* gene disruption (Fig. 5f, g, Online Resource 9). Interestingly, $CCM3^{-/-}$ CI-huVECs in direct co-culture with $CCM3^{+/+}$ CI-huVECs upregulated 99 genes and downregulated another 18 genes (Fig. 5f, g). A GO term enrichment analysis revealed deregulation of cell adhesion and proliferation pathways in $CCM3^{-/-}$ CI-huVECs under co-culture conditions (Fig. 5j). It was surprising to notice that among the upregulated genes in $CCM3^{-/-}$ CI-huVECs under co-culture conditions were especially those that were highly downregulated upon *CCM3* gene disruption (Fig. 5g, h). For example, *POSTN* gene expression, which was hardly detectable in $CCM3^{-/-}$ CI-huVECs under mono-culture conditions, was upregulated to near-normal levels in co-culture (Fig. 5h). Once in contact with wild-type ECs, mutant ECs also upregulated the expression of genes coding for other extracellular matrix components, e.g., *FBLN5* (fibulin-5) and *COL12A1* (collagen type XII alpha 1 chain). Furthermore, genes coding for cadherin superfamily members, e.g., *CDH2* (N-cadherin), *CDH4* (R-cadherin), *CDH11* (OB-cadherin), and *PCDH7* (protocadherin-7), were significantly upregulated (Online Resource 9). In $CCM3^{+/+}$ CI-huVECs, on the other hand, chemokine/cytokine-related pathways were found to be deregulated by co-culture with $CCM3^{-/-}$ CI-huVECs (Fig. 5i). In particular, wild-type ECs upregulated various chemokine genes, e.g., *CCL2* (MCP-1), *CX3CL1* (fractalkine), *CCL7* (MCP-3), *CXCL2* (MIP-2a/GRO2), *CXCL3* (MIP-2b/GRO3), and *CXCL8* (IL-8), but downregulated *POSTN* and *CDH11* in co-culture with mutant ECs (Online Resource 9). Taken together, these observations prove that mutant and wild-type ECs interact with each other and suggest that CC and CXC chemokines play a role in this complex regulatory interplay.

Compound screening identifies NSC59984 as candidate drug to block abnormal proliferation of mutant ECs

In a proof-of-concept approach, we next tested a library of 189 small compounds known to modulate apoptosis, survival, and proliferation in our CI-huVEC co-culture assay. After 6 days, the relative proportions of knockout alleles were quantified by amplicon deep sequencing (Fig. 6a). As expected, the knockout allele frequency in DMSO-treated co-cultures increased to 33.5%. Two compounds, isoalantolactone and NSC59984, suppressed the abnormal proliferation of mutant ECs by more than 80% (adjusted p value < 0.01; Fig. 6b). Knockout allele frequencies were 7.7% and 10.2%, respectively. NSC59984 had minimal effects on EC morphology and moderately reduced the viability of $CCM3^{+/+}$ and $CCM3^{-/-}$ CI-huVECs (Fig. 6c, d). Isoalantolactone induced an abnormal endothelial morphology and significant cell death. In contrast, GSK-872, which is a potent inhibitor of RIP kinase 3 (RIPK3), even enhanced mutant EC expansion (65.1%, $p_{adj} < 0.0001$; Fig. 6b, d). Interestingly, RIPK3 is a critical player in necroptosis, a regulated form of necrosis that allows programmed cell death even under apoptosis-deficient conditions [29, 30].

p21- and ERK2-independent inhibition of abnormal mutant cell proliferation by NSC59984

We decided to focus on the candidate NSC59984 in our further experiments and were able to demonstrate that it blocked the cancer-like proliferation of $CCM3^{-/-}$ CI-huVECs in a concentration-dependent manner (Fig. 7a, b). NSC59984 inhibited mutant EC expansion even at high knockout:wild-type ratios (Fig. 7c). Pre-treatment of $CCM3^{-/-}$ CI-huVECs with NSC59984 before co-culture completely abolished mutant EC expansion, and knockout alleles were hardly detectable in co-cultures after six days (Fig. 7d). Even after release from NSC59984 treatment, abnormal proliferation of $CCM3^{-/-}$ CI-huVECs was blocked for at least another 7 days (Fig. 7e). An inhibitory effect on mutant cell proliferation was also observed when we fused hiPSC-derived $CCM3^{+/+}$ and $CCM3^{-/-}$ vascular networks and treated them with NSC59984 (Fig. 7f). This is consistent with our RNA sequencing data demonstrating a cytostatic effect of NSC59984 on mutant ECs. However, there were also side-effects. For instance, we found significant deregulation of proliferation-associated pathways in wild-type ECs (Fig. 8 a, b, Online Resources 9 and 10). NSC59984 has previously been shown to reactivate p53 signalling via p73 activation and ROS-ERK2-MDM2-dependent degradation of mutant p53 in cancer cells [19, 20]. In $CCM3^{-/-}$ CI-huVECs we could neither detect a pathogenic *TP53* mutation nor significantly different p53 protein levels. Interestingly, we even found a slightly increased p53 transcription factor DNA binding activity in nuclear extracts of $CCM3^{-/-}$ CI-huVECs which indicates that there might be a downstream block of p53 signaling (Online Resource 10). NSC59984 treatment

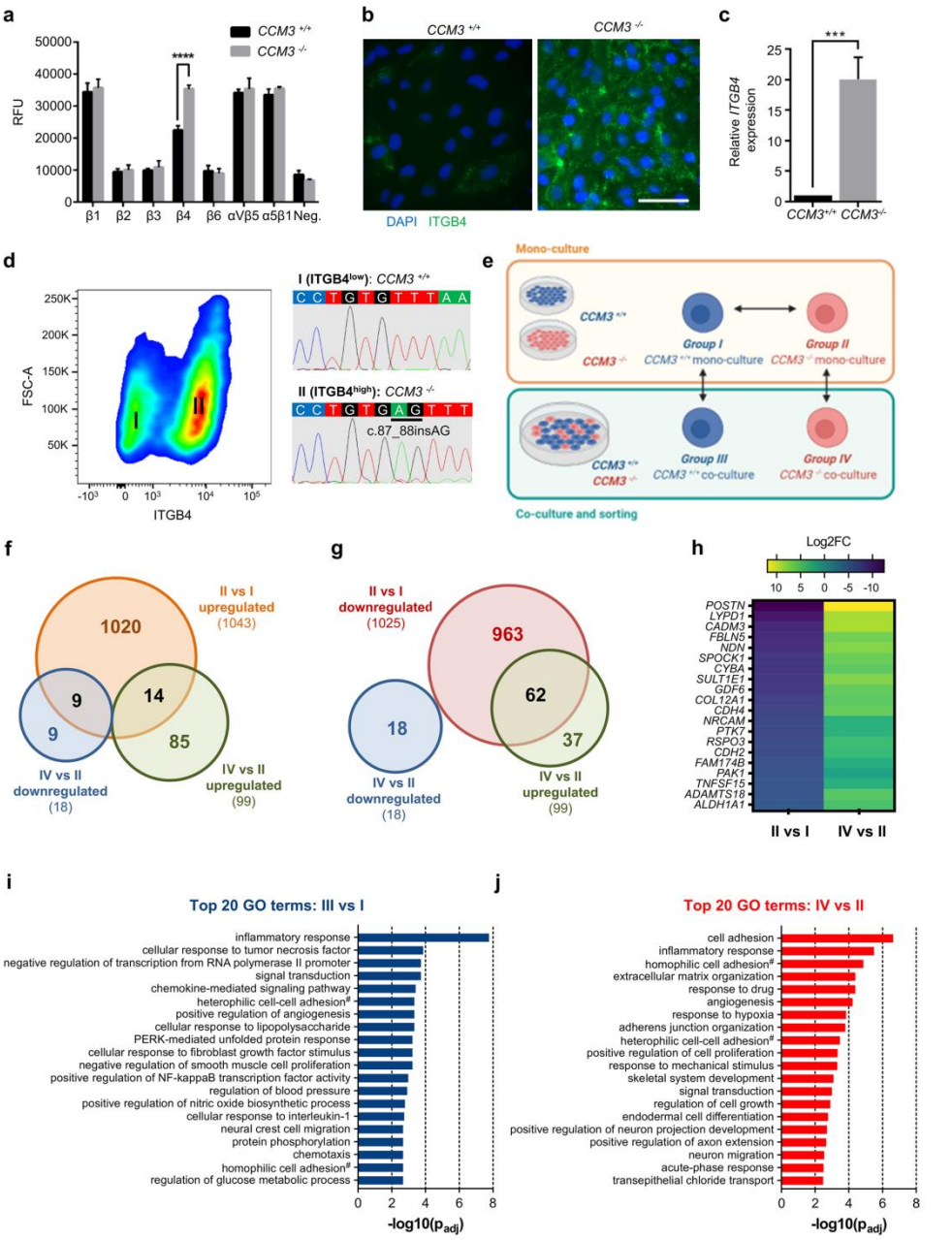
a
CCM3 +/+
CCM3 -/-
RFU
β1 β2 β3 β4 β6 αVβ5 α5β1 Neg.
b
CCM3 +/+
CCM3 -/-
DAPI ITGB4
c
Relative ITGB4 expression
CCM3+/+ CCM3-/-
d
FSC-A
ITGB4
I (ITGB4low): CCM3 +/+
II (ITGB4high): CCM3 -/-
c.87_88insAG
e
Mono-culture
Group I
Group II
Group III
Group IV
Co-culture and sorting
f
1020
II vs I upregulated (1043)
9
14
9
85
IV vs II downregulated (18)
IV vs II upregulated (99)
g
II vs I downregulated (1025)
963
62
18
37
IV vs II downregulated (18)
IV vs II upregulated (99)
h
Log2FC
POSTN
LYPD1
CADM3
FBLN5
NDN
SPOCK1
CYBA
SULT1E1
GDF6
COL12A1
CDH4
NRCAM
PTK7
RSPO3
CDH2
FAM174B
PAK1
TNFSF15
ADAMTS18
ALDH1A1
II vs I
IV vs II
i
Top 20 GO terms: III vs I
inflammatory response
cellular response to tumor necrosis factor
negative regulation of transcription from RNA polymerase II promoter
signal transduction
chemokine-mediated signaling pathway
heterophilic cell-cell adhesion#
positive regulation of angiogenesis
cellular response to lipopolysaccharide
PERK-mediated unfolded protein response
cellular response to fibroblast growth factor stimulus
negative regulation of smooth muscle cell proliferation
positive regulation of NF-kappaB transcription factor activity
regulation of blood pressure
positive regulation of nitric oxide biosynthetic process
cellular response to interleukin-1
neural crest cell migration
protein phosphorylation
chemotaxis
homophilic cell adhesion#
regulation of glucose metabolic process
-log10(padj)
j
Top 20 GO terms: IV vs II
cell adhesion
inflammatory response
homophilic cell adhesion#
extracellular matrix organization
response to drug
angiogenesis
response to hypoxia
adherens junction organization
heterophilic cell-cell adhesion#
positive regulation of cell proliferation
response to mechanical stimulus
skeletal system development
signal transduction
regulation of cell growth
endodermal cell differentiation
positive regulation of neuron projection development
positive regulation of axon extension
neuron migration
acute-phase response
transepithelial chloride transport
-log10(padj)

◂**Fig. 5** Chemokine signaling in wild-type ECs becomes deregulated in co-culture with $CCM3^{-/-}$ ECs. **a** A β-integrin-mediated cell adhesion array was used to analyse the surface expression of different integrin β subunits on $CCM3^{-/-}$ CI-huVECs ($n=3$ per group). **b**, **c** Immunofluorescence imaging and RT-qPCR analysis verified upregulation of *ITGB4* gene expression in $CCM3^{-/-}$ CI-huVECs (scale bar: 100 µm). Data are presented as mean and SD ($n=3$ per group). **d** Using high integrin beta 4 expression as marker for $CCM3^{-/-}$ CI-huVECs, mutant ECs could be efficiently sorted from mutant/wild-type co-cultures by fluorescence activated cell sorting. Sanger sequencing of sorted $ITGB4^{low}$ (I) and $ITGB4^{high}$ (II) cell populations verified high purity of $CCM3^{+/+}$ and $CCM3^{-/-}$ CI-huVECs, respectively. **e** $CCM3^{+/+}$ and $CCM3^{-/-}$ CI-huVECs were co-cultured, sorted by FACS and analyzed by RNA sequencing. $CCM3^{+/+}$ and $CCM3^{-/-}$ CI-huVEC mono-cultures served as controls. **f**, **g** Venn diagrams illustrate the overlap of genes significantly up- or downregulated in $CCM3^{-/-}$ CI-huVEC mono-cultures (group II vs group I) and genes that are significantly up- or downregulated in $CCM3^{-/-}$ CI-huVECs by co-culture with $CCM3^{+/+}$ CI-huVECs (group IV vs group II). **h** Shown is a heatmap with the 20 most downregulated genes in $CCM3^{-/-}$ CI-huVEC mono-cultures (left column; group II vs group I). The right column illustrates how co-culture with wild-type ECs affects the expression of these genes in $CCM3^{-/-}$ CI-huVECs (group IV vs group II). **i**, **j** Significantly up- or downregulated genes were also subjected to gene ontology analysis. Shown are the top 20 of significantly enriched biological process GO terms ($n=3$ per group for **e**–**j**). #via plasma membrane cell adhesion molecules. Multiple *t* tests (**a**), Student's two-tailed *t* test (**c**), and Fisher exact test (**i**, **j**) were used for statistical analyses: $^{***}P<0.001$, $^{****}P<0.0001$. p_{adj} = adjusted *p* value

of mutant ECs induced moderate upregulation of *CDKN1A* (p21), which is a target gene of p53, on mRNA level (Online Resource 10). However, p21 protein levels were unchanged and blocking p21 with UC2288 did also not revert the inhibitory effect of NSC59984 on mutant EC expansion in co-culture (Fig. 8c, Online Resource 10). We also addressed MAPK/ERK signaling in mutant ECs with protein array analyses and specific inhibitors but did not detect any significant deregulation either (Fig. 8d, Online Resource 10). Taken together, these results show that pharmacological inhibition of the abnormal proliferation of mutant ECs is possible. Nevertheless, side effects need to be addressed, and it remains to be clarified whether agents such as NSC59984 act through specific pathways in mutant ECs or have a general cytostatic effect on multiple signaling cascades.

Discussion

CCM is not a genuine malignant disease. The lesions do not metastasize or grow invasively. However, there is growing evidence that cancer-like mechanisms play an important role in CCM pathogenesis [17, 18, 31]. In line with this concept, we here demonstrate that the presence of wild-type cells upregulates mutant EC proliferation and that this tumor-like behaviour can be blocked by treatment with the anti-cancer drug NSC59984. In addition, we show that gene expression in wild-type and mutant ECs differs in mono- and co-culture.

Previously, we have shown that $CCM3^{-/-}$ ECs exhibit a reduced sensitivity to apoptotic signals in mono-culture [22]. Bringing together in vitro angiogenesis, endothelial co-culture and cell-based assays from cancer research, we now demonstrate that mutant ECs have an abnormally high clonogenic capacity but develop tumor-like growth characteristics only when co-cultured with wild-type ECs. This observation is highly relevant because mutant ECs (CCM^{neg}) coexist in a mosaic state with heterozygous or wild-type ECs (CCM^{pos}) in CCMs [15, 16]. Indeed, the number of CCM^{neg} cells within CCMs is relatively low. Despite some high-frequency mutations, somatic *CCM* variants are usually found with alternate allele frequencies of less than 15% in human CCM lesions [11–14, 16, 31]. Given that (1) only one somatic mutation has ever been identified in CCM tissues in addition to the preexisting germline variant, and (2) multiple somatic mutation events all leading to the same variant in different ECs are highly unlikely, solely expansion of the first CCM^{neg} EC can explain the endothelial mosaicism found in CCMs [16–18]. Furthermore, our finding that biallelic inactivation of *CCM3* did not induce abnormal proliferation of undifferentiated hiPSCs in co-culture with wild-type cells but specifically disturbed the balance between proliferation and cell death in vascular ECs supports the intriguing concept that *CCM* genes are not *bona fide* tumor suppressor genes but act as "*vascular suppressor genes*" [31]. This tumor-like vascular transformation seems to occur only under specific conditions and may be triggered in vivo by additional somatic gain-of-function mutations in *PIK3CA* which can act as a "*vascular oncogene*" [31].

The endothelial cell mosaicism observed in CCM tissues could also be reproduced in CRISPR'ed hiPSC-derived 3D blood vessel organoid cultures. $CCM3^{neg}$ cells were not located in clusters but found in a mosaic pattern with $CCM3^{pos}$ cells in $CCM3^{pos}$/$CCM3^{neg}$ vascular organoids. Thus, $CCM3^{neg}$ ECs apparently need contact with $CCM3^{pos}$ ECs and a supportive microenvironment. Interestingly, sophisticated in vivo studies in confetti reporter mice have also demonstrated that abnormal expansion of $CCM3^{neg}$ ECs and incorporation of CCM^{pos} ECs are essential steps in CCM genesis [17, 18]. Targeted inhibition of CCM progenitor ECs, blocking the clonal expansion of mutant ECs and inhibiting the recruitment of neighboring CCM^{pos} ECs into a growing CCM lesion have, therefore, been proposed as therapeutic approaches [32].

Our data allow an exciting insight into the poorly understood interaction of $CCM3^{pos}$ and $CCM3^{neg}$ ECs. As a marker for $CCM3^{neg}$ ECs, we used high expression levels of integrin $\beta 4$, which is known to form a heterodimer with integrin $\alpha 6$ and is primarily expressed on epithelial cells, endothelial cells, and Schwann cells [33]. Upregulation

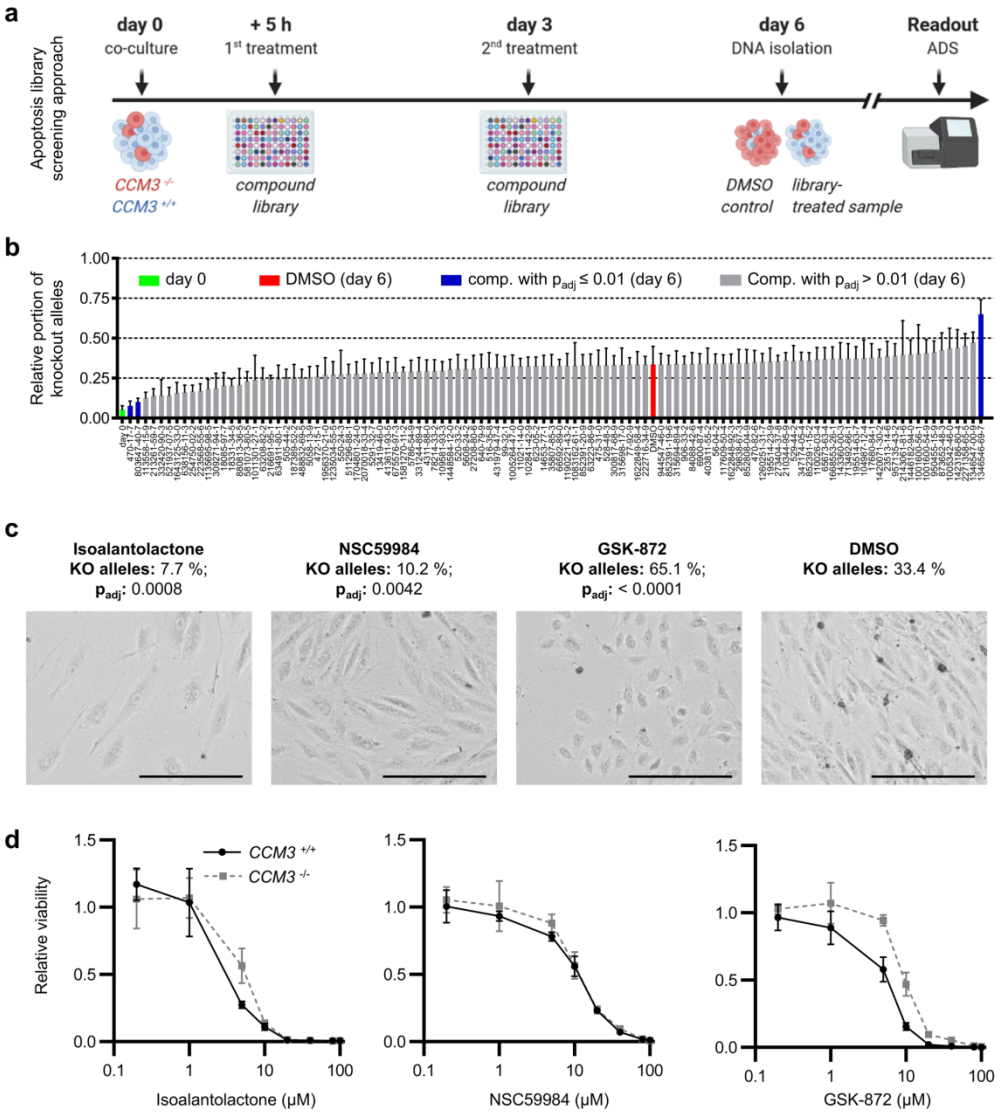

of *ITGB4* gene expression has previously been observed in human *CCM3*$^{-/-}$ CI-huVECs ([34]; GEO data set: GSE137425), mouse *Ccm1*^{ECKO} brain microvascular endothelial cells ([35]; GSE85657), and cardiac tissue of *ccm2*^{m201} mutant zebrafish embryos ([36]; GSE64753). Although its functional significance in CCM disease remains to be elucidated, it is noteworthy that ITGB4 expression is increased on various cancer cells and is thought to be involved in the regulation of cancer stem cells [37–39]. RNA-Seq analysis of FACS-sorted CCM3^{pos} ITGB4^{low} and CCM3^{neg} ITGB4^{high} ECs demonstrated that chemokine-mediated signaling pathways are induced by direct co-culture. In particular, *CCL2*, *CX3CL1*, and *CCL7* were upregulated more than fourfold in CCM3^{pos}

◂**Fig. 6** NSC59984 efficiently blocks the abnormal proliferation of $CCM3^{-/-}$ CI-huVECs in co-culture. **a** Depicted is a scheme of the apoptosis library screening approach. Co-cultures of $CCM3^{-/-}$ and $CCM3^{+/+}$ CI-huVECs were treated with 10 µM of each library compound on day 0 and day 3. DNA samples collected at day 6 were used to determine frequencies of *CCM3* knockout alleles with amplicon deep sequencing (ADS). DMSO treatment served as control. **b** NSC59984 and isoalantolactone reduced the portion of *CCM3* knockout alleles in co-culture. In contrast, GSK-872 further enhanced the abnormal proliferation of $CCM3^{-/-}$ CI-huVECs ($n=4$ per group). **c** Bright-field microscopy demonstrated that cells treated with NSC59984 had a normal EC morphology while isoalantolactone treatment induced severe morphological changes and significant cell death (10 µM of each compound; scale bar: 200 µm). After GSK-872 treatment, cells had a compact morphology that is a known feature of $CCM3^{-/-}$ CI-huVECs ($n=3$ per group). **d** No cell viability differences were observed between $CCM3^{+/+}$ and $CCM3^{-/-}$ CI-huVECs 72 h after NSC59984 or isoalantolacone treatment, whereas $CCM3^{+/+}$ CI-huVECs were more sensitive to GSK-872 treatment than mutant ECs ($n=3$ per group). *Comp.* = library compound. p_{adj} = adjusted p value. Data are presented as mean and SD. One-way ANOVA (**b**) was used for statistical analyses

ECs. These genes encode for chemokines (CCL2/MCP-1; CX3CL1/Fractalkine; CCL7/ MCP-3) that modulate the immune response but have also frequently been found to be enriched in the tumor microenvironment [40–42]. Notably, it has been demonstrated that they can orchestrate the cross-talk between cancer and stromal cells, stimulate angiogenesis, and trigger proliferation [41, 43, 44]. Additionally, the CXC chemokine genes *CXCL2*, *CXCL3*, and *CXCL8* were upregulated more than twofold. CXCL2, CXCL3, and CXCL8/IL-8 belong to the group of CXC chemokines with a Glu-Leu-Arg sequence motif (ELR^+ CXC chemokines) which are not only potent neutrophil chemoattractants but have also been reported to trigger angiogenesis and EC chemotaxis [45–47]. The results of our in vitro model are also consistent with recently published analyses in $Ccm3^{iECKO}$ mice. Using an acute, "fast progression" and a chronic, "slow progression" model of CCM, the authors demonstrated that the expression of *Ccl2*, *Cxcl2*, *Cx3cl1* and other immune-related genes was significantly upregulated in brain microvascular ECs of $Ccm3^{iECKO}$ mice [48]. In general, the proportion of cells with a *Ccm3* deletion is relatively low (< 15%) in the chronic model [48]. In the acute model, it is much higher (> 80%) but cells with *Ccm3* wild-type alleles are still present [17]. Our data now suggest that not only the mutant ECs themselves but also the wild-type ECs in contact with the mutant ECs upregulate immune-associated genes.

Taken together, these results strengthen the intriguing hypothesis that $CCM3^{pos}$ ECs contribute to the formation of a supportive niche for $CCM3^{neg}$ ECs and that the cancer-like nature of CCMs warrants testing of anti-cancer therapies. Two facts substantiate this concept: (1) NSC59984, a drug with anti-tumor activity [19], has a significant anti-proliferative effect on mutant ECs; and (2) ponatinib, a kinase inhibitor that is used to treat chronic myeloid leukemia and Ph^+ acute lymphoblastic leukemia, has been reported to stop CCM formation and lesion growth in $Ccm1^{iECKO}$ mice [49]. However, NSC59984 also induces growth arrest in wild-type ECs. Similarly, the kinase inhibitor ponatinib has a broad spectrum of side effects that would likely limit its therapeutic use in CCM, e.g., thrombocytopenia, abdominal pain, anemia, and even cardiac arrhythmias [50]. Thus, the identification of new drug candidates is required. Because of their side effects, cytotoxic agents might not be a real option for CCM patients who can have severe neurological complications but are also often asymptomatic. Modulating the microenvironment of CCMs instead would be an exciting approach. Several chemokine receptor inhibitors are currently under investigation in the context of solid tumors [51]. Our next-generation sequencing-based read-out system allows tracking mutant cell expansion in co-culture on a genetic level and will facilitate the testing of thousands

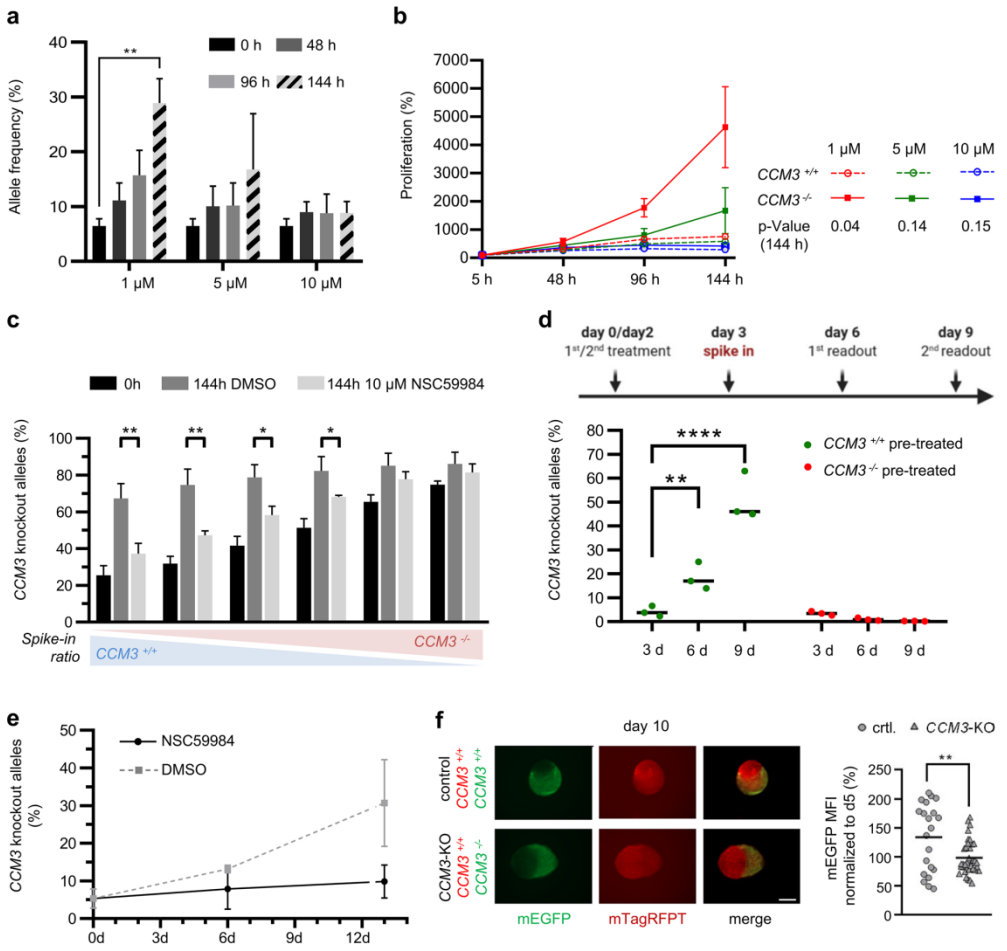

Fig. 7 NSC59984 has cytostatic effects on *CCM3*$^{-/-}$ ECs. **a**, **b** NSC59984 blocked the abnormal proliferation of *CCM3*$^{-/-}$ CI-huVECs in co-culture in a dose-dependent manner and predominantly inhibited the proliferation of mutant ECs ($n=3$ per group). **c** NSC59984 (10 µM) reduced the abnormal proliferation of mutant ECs even at high knockout:wild-type ratios [$n=3$ per group; mutant allele frequency after seeding (0 h) from left to right: 25.5%, 31.9%, 41.6%, 51.4%, 65.4% and 74.8%]. **d** *CCM3*$^{-/-}$ CI-huVECs were treated with NSC59984 prior to co-culture with untreated *CCM3*$^{+/+}$ CI-huVECs (=*CCM3*$^{-/-}$ pre-treated; red). As control, untreated *CCM3*$^{-/-}$ CI-huVECs were co-cultured with *CCM3*$^{+/+}$ CI-huVECs that had been pre-treated with NSC59984 (=*CCM3*$^{+/+}$ pre-treated; green). Pre-treatment of *CCM3*$^{-/-}$ CI-huVECs blocked their abnormal proliferation (red). In contrast, pre-treatment of *CCM3*$^{+/+}$ led to an extremely strong proliferation of mutant ECs ($n=3$ per group). **e** Endothelial mutant:wild-type co-cultures were treated with NSC59984 on day 0 and day 3, released from drug treatment on day 6, and cultured for another 7 days. NSC59984 retained its effect after treatment release. DMSO treated cultures served as control ($n=3$ per group). **f** NSC59984 inhibited mutant EC proliferation in vascular organoids. *CCM3*$^{-/-}$ AICS-0036 (mEGFP) and *CCM3*$^{+/+}$ AICS-0054 (mTagRFPT) hiPSC-derived vascular networks were fused and differentiated to vascular organoids under NSC59984 treatment for 10 days (CCM3-KO). Images were acquired on days 5 and 10. Fusions of *CCM3*$^{+/+}$ AICS-0036 and *CCM3*$^{+/+}$ AICS-0054 hiPSC-derived vascular networks served as controls (scale: 500 µm). Statistical analysis was performed for 36 KO/WT fusion organoids differentiated in three independent biological replicates. 21 WT/WT fusion organoids were used as controls. Shown is the mean mEGFP fluorescence intensity on day 10 normalized to day 5. Data are presented as mean and SD (**a**, **b**, **c**, **e**) or as mean and single data points (**d**, **f**). Multiple comparison test (Fisher's LSD; a), two-way ANOVA with multiple comparison test (**b**), multiple t-tests (**c**), two-way ANOVA with Dunnett's multiple comparison test (**d**), and Student's two-tailed *t* test (**f**) were used for statistical analyses: $*P<0.05$, $**P<0.01$, $****P<0.001$

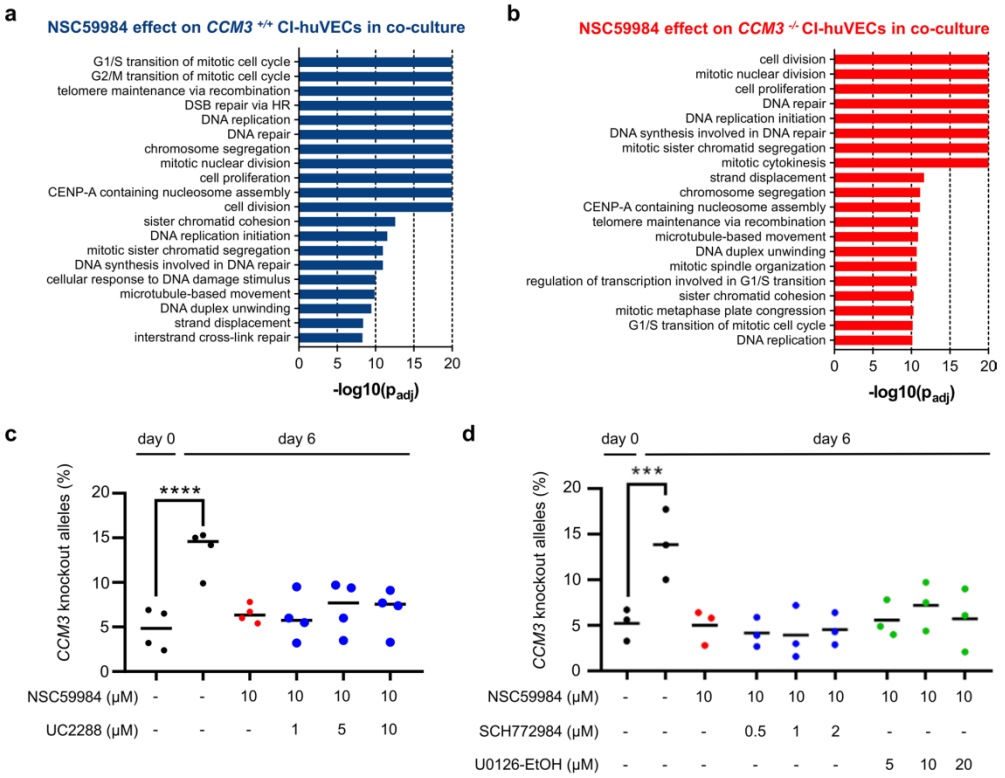

Fig. 8 p21 and ERK-independent effect of NSC59984. **a**, **b** *CCM3*$^{-/-}$ and *CCM3*$^{+/+}$ CI-huVECs were co-cultured, treated with NSC59984 (10 μM), sorted and subjected to RNA sequencing. DMSO-treated co-cultures served as controls. Shown are the top 20 of significantly enriched biological process GO terms ($n=3$ per group). **c**, **d** Co-cultures of *CCM3*$^{-/-}$ and *CCM3*$^{+/+}$ CI-huVECs were treated with NSC59984 (10 μM) and the p21 inhibitor UC2288 ($n=4$ per group; **c**), the ERK1/2 inhibitor SCH772984 or the MEK1/2 inhibitor U0126-EtOH ($n=3$ per group; **d**). Mutant allele frequencies were determined after 6 days. DMSO-treated co-cultures served as controls. Fisher exact test (**a**, **b**) and one-way ANOVA with multiple comparison test (**c**, **d**) were used for statistical analyses: ***$P<0.001$; ****$P<0.0001$. p_{adj} = adjusted p value

of potential drug candidates. Such high-throughput screens may bring drug discovery in CCM research onto the next level.

In summary, there is increasing evidence that cancer-like mechanisms promote early CCM formation and lesion growth and that these mechanisms need to be addressed with new therapeutic approaches. In this context, it is essential to focus not only on CCM^{neg} but also on CCM^{pos} cells and to clarify their role in CCM pathogenesis.

Supplementary Information The online version contains supplementary material available at https://doi.org/10.1007/s00018-022-04355-6.

Acknowledgements This work was funded by the Deutsche Forschungsgemeinschaft (DFG, German Research Foundation) [grant number RA2876/2-2], the German Federal Ministry of Education and Research (BMBF) [grant number 161L0276], and by the Research Network Molecular Medicine of the University Medicine Greifswald [FOVB-2020-01 and FOVB-2021-07]. MR was supported by a scholarship of the Gerhard Domagk program of the University Medicine Greifswald. SB was supported by the BMBF (grant numbers 03Z22DN11 and 03Z22Di1). JMP was supported by the Leducq network on vascular malformation. The Centre for Innovation Competence-Humoral Immune Reactions in Cardiovascular Diseases was supported by the BMBF (ZIK grant under agreement No.: 03Z22CN11). This research was made possible through the Allen Cell Collection, available from Coriell Institute for Medical Research. Figures 2a, 4a, 4d, 5e, 6a, and Online Resource 5a were created with biorender.com. We would like to thank S. Spiegler for fruitful discussions.

Author contributions MR, ED, and UF: designed the study and supervised the experiments; KS, MM, DS, and RAP: performed most of the functional experiments; SB and DB: performed the confocal microscopy and FACS sorting experiments; AL and JMP: contributed to the vascular organoid experiments; MR, KS, MM, DS, RAP, and SB: analyzed the data; MR, KS, DS, and RAP: prepared figures; all authors contributed to interpretation of the results; MR, KS, and UF: drafted the manuscript, and all authors contributed to writing.

Funding Open Access funding enabled and organized by Projekt DEAL. This work was funded by the Deutsche Forschungsgemeinschaft (DFG, German Research Foundation) [grant number RA2876/2-2], the German Federal Ministry of Education and Research (BMBF) [grant number 161L0276], and by the Research Network Molecular Medicine of the University Medicine Greifswald [FOVB-2020-01 and FOVB-2021-07]. MR was supported by a scholarship of the Gerhard Domagk program of the University Medicine Greifswald. SB was supported by the BMBF (grant numbers 03Z22DN11 and 03Z22Di1). JMP was supported by the Leducq network on vascular malformation. The Centre for Innovation Competence—Humoral Immune Reactions in Cardiovascular Diseases was supported by the BMBF (ZIK grant under agreement No.: 03Z22CN11).

Data availability All relevant data are included in the published article or its supplementary files.

Declarations

Conflict of interest MR, KS and UF are listed as inventors on a patent application (EP 21194373.3) related to the treatment or prevention of vascular malformations.

Ethics approval This study does not involve human participants or animal subjects.

Consent to participate This study does not involve human participants.

Consent to publish This study does not involve human participants.

References

1. Batra S, Lin D, Recinos PF, Zhang J, Rigamonti D (2009) Cavernous malformations: natural history, diagnosis and treatment. Nat Rev Neurol 5(12):659–670. https://doi.org/10.1038/nrneurol.2009.177
2. Akers A, Al-Shahi Salman R, Awad AI, Dahlem K, Flemming K, Hart B, Kim H, Jusue-Torres I, Kondziolka D, Lee C, Morrison L, Rigamonti D, Rebeiz T, Tournier-Lasserve E, Waggoner D, Whitehead K (2017) Synopsis of guidelines for the clinical management of cerebral cavernous malformations: consensus recommendations based on systematic literature review by the angioma alliance scientific advisory board clinical experts panel. Neurosurgery 80(5):665–680. https://doi.org/10.1093/neuros/nyx091
3. Spiegler S, Rath M, Paperlein C, Felbor U (2018) Cerebral cavernous malformations: an update on prevalence, molecular genetic analyses, and genetic counselling. Mol Syndromol 9(2):60–69. https://doi.org/10.1159/000486292
4. Shenkar R, Shi C, Rebeiz T, Stockton RA, McDonald DA, Mikati AG, Zhang L, Austin C, Akers AL, Gallione CJ, Rorrer A, Gunel M, Min W, De Souza JM, Lee C, Marchuk DA, Awad IA (2015) Exceptional aggressiveness of cerebral cavernous malformation disease associated with *PDCD10* mutations. Genet Med 17(3):188–196. https://doi.org/10.1038/gim.2014.97
5. Spiegler S, Najm J, Liu J, Gkalympoudis S, Schröder W, Borck G, Brockmann K, Elbracht M, Fauth C, Ferbert A, Freudenberg L, Grasshoff U, Hellenbroich Y, Henn W, Hoffjan S, Huning I, Korenke GC, Kroisel PM, Kunstmann E, Mair M, Munk-Schulenburg S, Nikoubashman O, Pauli S, Rudnik-Schoneborn S, Sudholt I, Sure U, Tinschert S, Wiednig M, Zoll B, Ginsberg MH, Felbor U (2014) High mutation detection rates in cerebral cavernous malformation upon stringent inclusion criteria: one-third of probands are minors. Mol Genet Genomic Med 2(2):176–185. https://doi.org/10.1002/mgg3.60
6. He Y, Zhang H, Yu L, Gunel M, Boggon TJ, Chen H, Min W (2010) Stabilization of VEGFR2 signaling by cerebral cavernous malformation 3 is critical for vascular development. Sci Signal 3(116):ra26. https://doi.org/10.1126/scisignal.2000722
7. Zeineddine HA, Girard R, Saadat L, Shen L, Lightle R, Moore T, Cao Y, Hobson N, Shenkar R, Avner K, Chaudager K, Koskimäki J, Polster SP, Fam MD, Shi C, Lopez-Ramirez MA, Tang AT, Gallione C, Kahn ML, Ginsberg M, Marchuk DA, Awad IA (2019) Phenotypic characterization of murine models of cerebral cavernous malformations. Lab Invest 99(3):319–330. https://doi.org/10.1038/s41374-018-0030-y
8. Louvi A, Chen L, Two AM, Zhang H, Min W, Gunel M (2011) Loss of *cerebral cavernous malformation 3* (*Ccm3*) in neuroglia leads to CCM and vascular pathology. Proc Natl Acad Sci U S A 108(9):3737–3742. https://doi.org/10.1073/pnas.1012617108
9. Wang K, Zhang H, He Y, Jiang Q, Tanaka Y, Park IH, Pober JS, Min W, Zhou HJ (2020) Mural cell-specific deletion of cerebral cavernous malformation 3 in the brain induces cerebral cavernous malformations. Arterioscler Thromb Vasc Biol 40(9):2171–2186. https://doi.org/10.1161/ATVBAHA.120.314586
10. Lopez-Ramirez MA, Lai CC, Soliman SI, Hale P, Pham A, Estrada EJ, McCurdy S, Girard R, Verma R, Moore T, Lightle R, Hobson N, Shenkar R, Poulsen O, Haddad GG, Daneman R, Gongol B, Sun H, Lagarrigue F, Awad IA, Ginsberg MH (2021) Astrocytes propel neurovascular dysfunction during cerebral cavernous malformation lesion formation. J Clin Invest. https://doi.org/10.1172/JCI139570
11. Gault J, Shenkar R, Recksiek P, Awad IA (2005) Biallelic somatic and germ line *CCM1* truncating mutations in a cerebral cavernous malformation lesion. Stroke 36(4):872–874. https://doi.org/10.1161/01.STR.0000157586.20479.fd
12. Gault J, Awad IA, Recksiek P, Shenkar R, Breeze R, Handler M, Kleinschmidt-DeMasters BK (2009) Cerebral cavernous malformations: somatic mutations in vascular endothelial cells. Neurosurgery 65(1):138–144. https://doi.org/10.1227/01.NEU.0000348049.81121.C1
13. Akers AL, Johnson E, Steinberg GK, Zabramski JM, Marchuk DA (2009) Biallelic somatic and germline mutations in cerebral

cavernous malformations (CCMs): evidence for a two-hit mechanism of CCM pathogenesis. Hum Mol Genet 18(5):919–930. https://doi.org/10.1093/hmg/ddn430
14. McDonald DA, Shi C, Shenkar R, Gallione CJ, Akers AL, Li S, De Castro N, Berg MJ, Corcoran DL, Awad IA, Marchuk DA (2014) Lesions from patients with sporadic cerebral cavernous malformations harbor somatic mutations in the CCM genes: evidence for a common biochemical pathway for CCM pathogenesis. Hum Mol Genet 23(16):4357–4370. https://doi.org/10.1093/hmg/ddu153
15. Pagenstecher A, Stahl S, Sure U, Felbor U (2009) A two-hit mechanism causes cerebral cavernous malformations: complete inactivation of CCM1, CCM2 or CCM3 in affected endothelial cells. Hum Mol Genet 18(5):911–918. https://doi.org/10.1093/hmg/ddn420
16. Rath M, Pagenstecher A, Hoischen A, Felbor U (2020) Postzygotic mosaicism in cerebral cavernous malformation. J Med Genet 57(3):212–216. https://doi.org/10.1136/jmedgenet-2019-106182
17. Malinverno M, Maderna C, Abu Taha A, Corada M, Orsenigo F, Valentino M, Pisati F, Fusco C, Graziano P, Giannotta M, Yu QC, Zeng YA, Lampugnani MG, Magnusson PU, Dejana E (2019) Endothelial cell clonal expansion in the development of cerebral cavernous malformations. Nat Commun 10(1):2761. https://doi.org/10.1038/s41467-019-10707-x
18. Detter MR, Snellings DA, Marchuk DA (2018) Cerebral cavernous malformations develop through clonal expansion of mutant endothelial cells. Circ Res 123(10):1143–1151. https://doi.org/10.1161/CIRCRESAHA.118.313970
19. Zhang S, Zhou L, Hong B, van den Heuvel AP, Prabhu VV, Warfel NA, Kline CL, Dicker DT, Kopelovich L, El-Deiry WS (2015) Small-molecule NSC59984 restores p53 pathway signaling and antitumor effects against colorectal cancer via p73 activation and degradation of mutant p53. Cancer Res 75(18):3842–3852. https://doi.org/10.1158/0008-5472.CAN-13-1079
20. Zhang S, Zhou L, El-Deiry WS (2022) Small-molecule NSC59984 induces mutant p53 degradation through a ROS-ERK2-MDM2 Axis in cancer cells. Mol Cancer Res. https://doi.org/10.1158/1541-7786.MCR-21-0149
21. Lipps C, Klein F, Wahlicht T, Seiffert V, Butueva M, Zauers J, Truschel T, Luckner M, Köster M, MacLeod R, Pezoldt J, Hühn J, Yuan Q, Müller PP, Kempf H, Zweigerdt R, Dittrich-Breiholz O, Pufe T, Beckmann R, Drescher W, Riancho J, Sanudo C, Korff T, Opalka B, Rebmann V, Göthert JR, Alves PM, Ott M, Schucht R, Hauser H, Wirth D, May T (2018) Expansion of functional personalized cells with specific transgene combinations. Nat Commun 9(1):994. https://doi.org/10.1038/s41467-018-03408-4
22. Schwefel K, Spiegler S, Ameling S, Much CD, Pilz RA, Otto O, Völker U, Felbor U, Rath M (2019) Biallelic *CCM3* mutations cause a clonogenic survival advantage and endothelial cell stiffening. J Cell Mol Med 23(3):1771–1783. https://doi.org/10.1111/jcmm.14075
23. Schwefel K, Spiegler S, Much CD, Felbor U, Rath M (2020) CRISPR/Cas9-mediated generation of human endothelial cell knockout models of CCM disease. Methods Mol Biol 2152:169–177. https://doi.org/10.1007/978-1-0716-0640-7_13
24. Neal EH, Marinelli NA, Shi Y, McClatchey PM, Balotin KM, Gullett DR, Hagerla KA, Bowman AB, Ess KC, Wikswo JP, Lippmann ES (2019) A simplified, fully defined differentiation scheme for producing blood-brain barrier endothelial cells from human iPSCs. Stem Cell Reports 12(6):1380–1388. https://doi.org/10.1016/j.stemcr.2019.05.008
25. Wimmer RA, Leopoldi A, Aichinger M, Kerjaschki D, Penninger JM (2019) Generation of blood vessel organoids from human pluripotent stem cells. Nat Protoc. https://doi.org/10.1038/s41596-019-0213-z
26. Franken NA, Rodermond HM, Stap J, Haveman J, van Bree C (2006) Clonogenic assay of cells in vitro. Nat Protoc 1(5):2315–2319. https://doi.org/10.1038/nprot.2006.339
27. Nowak-Sliwinska P, Alitalo K, Allen E, Anisimov A, Aplin AC, Auerbach R, Augustin HG, Bates DO, van Beijnum JR, Bender RHF, Bergers G, Bikfalvi A, Bischoff J, Böck BC, Brooks PC, Bussolino F, Cakir B, Carmeliet P, Castranova D, Cimpean AM, Cleaver O, Coukos G, Davis GE, De Palma M, Dimberg A, Dings RPM, Djonov V, Dudley AC, Dufton NP, Fendt SM, Ferrara N, Fruttiger M, Fukumura D, Ghesquiere B, Gong Y, Griffin RJ, Harris AL, Hughes CCW, Hultgren NW, Iruela-Arispe ML, Irving M, Jain RK, Kalluri R, Kalucka J, Kerbel RS, Kitajewski J, Klaassen I, Kleinmann HK, Koolwijk P, Kuczynski E, Kwak BR, Marien K, Melero-Martin JM, Munn LL, Nicosia RF, Noel A, Nurro J, Olsson AK, Petrova TV, Pietras K, Pili R, Pollard JW, Post MJ, Quax PHA, Rabinovich GA, Raica M, Randi AM, Ribatti D, Ruegg C, Schlingemann RO, Schulte-Merker S, Smith LEH, Song JW, Stacker SA, Stalin J, Stratman AN, Van de Velde M, van Hinsbergh VWM, Vermeulen PB, Waltenberger J, Weinstein BM, Xin H, Yetkin-Arik B, Yla-Herttuala S, Yoder MC, Griffioen AW (2018) Consensus guidelines for the use and interpretation of angiogenesis assays. Angiogenesis 21(3):425–532. https://doi.org/10.1007/s10456-018-9613-x
28. Wimmer RA, Leopoldi A, Aichinger M, Wick N, Hantusch B, Novatchkova M, Taubenschmid J, Hämmerle M, Esk C, Bagley JA, Lindenhofer D, Chen G, Boehm M, Agu CA, Yang F, Fu B, Zuber J, Knoblich JA, Kerjaschki D, Penninger JM (2019) Human blood vessel organoids as a model of diabetic vasculopathy. Nature 565(7740):505–510. https://doi.org/10.1038/s41586-018-0858-8
29. Shan B, Pan H, Najafov A, Yuan J (2018) Necroptosis in development and diseases. Genes Dev 32(5–6):327–340. https://doi.org/10.1101/gad.312561.118
30. Kim C, Pasparakis M (2014) RIP kinase 3 in necroptosis: does it take two or more to kill? Cell Death Differ 21(10):1505–1507. https://doi.org/10.1038/cdd.2014.100
31. Ren AA, Snellings DA, Su YS, Hong CC, Castro M, Tang AT, Detter MR, Hobson N, Girard R, Romanos S, Lightle R, Moore T, Shenkar R, Benavides C, Beaman MM, Müller-Fielitz H, Chen M, Mericko P, Yang J, Sung DC, Lawton MT, Ruppert JM, Schwaninger M, Körbelin J, Potente M, Awad IA, Marchuk DA, Kahn ML (2021) PIK3CA and CCM mutations fuel cavernomas through a cancer-like mechanism. Nature 594(7862):271–276. https://doi.org/10.1038/s41586-021-03562-8
32. Abdelilah-Seyfried S, Tournier-Lasserve E, Derry WB (2020) Blocking signalopathic events to treat cerebral cavernous malformations. Trends Mol Med 26(9):874–887. https://doi.org/10.1016/j.molmed.2020.03.003
33. Dusek RL, Jones JCR, Green KJ (2004) Desmosomes and Hemidesmosomes. In: Lennarz WJ, Lane MD (eds) Encyclopedia of Biological Chemistry. Elsevier, New York, pp 569–576. https://doi.org/10.1016/B0-12-443710-9/00146-0
34. Schwefel K, Spiegler S, Kirchmaier BC, Dellweg PKE, Much CD, Pane-Farre J, Strom TM, Riedel K, Felbor U, Rath M (2020) Fibronectin rescues aberrant phenotype of endothelial cells lacking either CCM1, CCM2 or CCM3. FASEB J 34(7):9018–9033. https://doi.org/10.1096/fj.201902888R
35. Lopez-Ramirez MA, Fonseca G, Zeineddine HA, Girard R, Moore T, Pham A, Cao Y, Shenkar R, de Kreuk BJ, Lagarrigue F, Lawler J, Glass CK, Awad IA, Ginsberg MH (2017) Thrombospondin1 (TSP1) replacement prevents cerebral cavernous malformations. J Exp Med 214(11):3331–3346. https://doi.org/10.1084/jem.20171178
36. Renz M, Otten C, Faurobert E, Rudolph F, Zhu Y, Boulday G, Duchene J, Mickoleit M, Dietrich AC, Ramspacher C, Steed E,

Manet-Dupe S, Benz A, Hassel D, Vermot J, Huisken J, Tournier-Lasserve E, Felbor U, Sure U, Albiges-Rizo C, Abdelilah-Seyfried S (2015) Regulation of beta1 integrin-Klf2-mediated angiogenesis by CCM proteins. Dev Cell 32(2):181–190. https://doi.org/10.1016/j.devcel.2014.12.016

37. Ruan S, Lin M, Zhu Y, Lum L, Thakur A, Jin R, Shao W, Zhang Y, Hu Y, Huang S, Hurt EM, Chang AE, Wicha MS, Li Q (2020) Integrin beta4-targeted cancer immunotherapies inhibit tumor growth and decrease metastasis. Cancer Res 80(4):771–783. https://doi.org/10.1158/0008-5472.CAN-19-1145
38. Bierie B, Pierce SE, Kroeger C, Stover DG, Pattabiraman DR, Thiru P, Liu Donaher J, Reinhardt F, Chaffer CL, Keckesova Z, Weinberg RA (2017) Integrin-beta4 identifies cancer stem cell-enriched populations of partially mesenchymal carcinoma cells. Proc Natl Acad Sci U S A 114(12):E2337–E2346. https://doi.org/10.1073/pnas.1618298114
39. Ma B, Zhang L, Zou Y, He R, Wu Q, Han C, Zhang B (2019) Reciprocal regulation of integrin beta4 and KLF4 promotes gliomagenesis through maintaining cancer stem cell traits. J Exp Clin Cancer Res 38(1):23. https://doi.org/10.1186/s13046-019-1034-1
40. Lee YS, Cho YB (2020) CCL7 Signaling in the tumor microenvironment. Adv Exp Med Biol 1231:33–43. https://doi.org/10.1007/978-3-030-36667-4_4
41. Tsuyada A, Chow A, Wu J, Somlo G, Chu P, Loera S, Luu T, Li AX, Wu X, Ye W, Chen S, Zhou W, Yu Y, Wang YZ, Ren X, Li H, Scherle P, Kuroki Y, Wang SE (2012) CCL2 mediates cross-talk between cancer cells and stromal fibroblasts that regulates breast cancer stem cells. Cancer Res 72(11):2768–2779. https://doi.org/10.1158/0008-5472.CAN-11-3567
42. Rivas-Fuentes S, Salgado-Aguayo A, Arratia-Quijada J, Gorocica-Rosete P (2021) Regulation and biological functions of the CX3CL1-CX3CR1 axis and its relevance in solid cancer: A mini-review. J Cancer 12(2):571–583. https://doi.org/10.7150/jca.47022
43. Rajaram M, Li J, Egeblad M, Powers RS (2013) System-wide analysis reveals a complex network of tumor-fibroblast interactions involved in tumorigenicity. PLoS Genet 9(9):e1003789. https://doi.org/10.1371/journal.pgen.1003789
44. Lee SJ, Namkoong S, Kim YM, Kim CK, Lee H, Ha KS, Chung HT, Kwon YG, Kim YM (2006) Fractalkine stimulates angiogenesis by activating the Raf-1/MEK/ERK- and PI3K/Akt/eNOS-dependent signal pathways. Am J Physiol Heart Circ Physiol 291(6):H2836-2846. https://doi.org/10.1152/ajpheart.00113.2006
45. Addison CL, Daniel TO, Burdick MD, Liu H, Ehlert JE, Xue YY, Buechi L, Walz A, Richmond A, Strieter RM (2000) The CXC chemokine receptor 2, CXCR2, is the putative receptor for ELR+ CXC chemokine-induced angiogenic activity. J Immunol 165(9):5269–5277. https://doi.org/10.4049/jimmunol.165.9.5269
46. Rollins BJ (1997) Chemokines. Blood 90(3):909–928
47. Strieter RM, Burdick MD, Gomperts BN, Belperio JA, Keane MP (2005) CXC chemokines in angiogenesis. Cytokine Growth Factor Rev 16(6):593–609. https://doi.org/10.1016/j.cytogfr.2005.04.007
48. Yau ACY, Globisch MA, Onyeogaziri FC, Conze LL, Smith R, Jauhiainen S, Corada M, Orsenigo F, Huang H, Herre M, Olsson AK, Malinverno M, Sundell V, Rezai Jahromi B, Niemelä M, Laakso A, Garlanda C, Mantovani A, Lampugnani MG, Dejana E, Magnusson PU (2022) Inflammation and neutrophil extracellular traps in cerebral cavernous malformation. Cell Mol Life Sci 79(4):206. https://doi.org/10.1007/s00018-022-04224-2
49. Choi JP, Wang R, Yang X, Wang X, Wang L, Ting KK, Foley M, Cogger V, Yang Z, Liu F, Han Z, Liu R, Baell J, Zheng X (2018) Ponatinib (AP24534) inhibits MEKK3-KLF signaling and prevents formation and progression of cerebral cavernous malformations. Sci Adv 4(11):eaau0731. https://doi.org/10.1126/sciadv.aau0731
50. Chan O, Talati C, Isenalumhe L, Shams S, Nodzon L, Fradley M, Sweet K, Pinilla-Ibarz J (2020) Side-effects profile and outcomes of ponatinib in the treatment of chronic myeloid leukemia. Blood Adv 4(3):530–538. https://doi.org/10.1182/bloodadvances.2019000268
51. Mollica Poeta V, Massara M, Capucetti A, Bonecchi R (2019) Chemokines and chemokine receptors: new targets for cancer immunotherapy. Front Immunol 10:379. https://doi.org/10.3389/fimmu.2019.00379

5.6 Cas9-mediated nanopore sequencing enables precise characterization of structural variants in *CCM1*, *CCM2*, and *CCM3*

Dariush Skowronek, **Robin A. Pilz**, Loisa Bonde, Ole J. Schamuhn, Janne L. Feldmann, Sabine Hoffjan, Christiane D. Much, Ute Felbor, Matthias Rath

Manuskript unter Begutachtung beim *International Journal of Molecular Sciences*

Es wurde die vom Journal bereitgestellte Vorlage zur Manuskripterstellung verwendet.

International Journal of *Molecular Sciences*

MDPI

Article

Cas9-mediated nanopore sequencing enables precise characterization of structural variants in *CCM1*, *CCM2*, and *CCM3*

Dariush Skowronek[1], Robin A. Pilz[1], Loisa Bonde[1], Ole J. Schamuhn[1], Janne L. Feldmann[1], Sabine Hoffjan[2], Christiane D. Much[1], Ute Felbor[1], Matthias Rath[1,3,*]

[1] Department of Human Genetics, University Medicine Greifswald, and Interfaculty Institute of Genetics and Functional Genomics, University of Greifswald, Greifswald, Germany
[2] Department of Human Genetics, Ruhr-University, Bochum, Germany
[3] Department of Human Medicine and Institute for Molecular Medicine, MSH Medical School Hamburg, Hamburg, Germany
* Correspondence: matthias.rath@med.uni-greifswald.de

Abstract: Deletions in the *CCM1*, *CCM2*, and *CCM3* genes are a common cause of familial cerebral cavernous malformations (CCM). In current molecular genetic laboratories, targeted next-generation sequencing or multiplex ligation-dependent probe amplification are mostly used to identify copy number variants (CNVs). However, both techniques are limited in their ability to specify the breakpoints of CNVs and identify complex structural variants (SVs). To overcome these constraints, we established a targeted Cas9-mediated nanopore sequencing approach for CNV detection with single nucleotide resolution. Using a MinION device, we achieved complete coverage for the *CCM* genes and determined the exact size of CNVs in positive controls. Long-read sequencing for a *CCM1* and *CCM2* CNV revealed that the adjacent *ANKIB1* and *NACAD* genes were also partially or completely deleted. In addition, an interchromosomal insertion and an inversion in *CCM2* were reliably re-identified by long-read sequencing. Finally, we reduced the costs of our approach by using Flongle flow cells. Fine mapping of CNV breakpoints is highly desirable as it enables fast and inexpensive PCR-based variant detection in subsequent family analyses. In conclusion, Cas9-mediated nanopore sequencing is a cost-effective and flexible tool for molecular genetic diagnostics which can be easily adapted to various target regions.

Keywords: nanopore sequencing; long-read sequencing; CRISPR/Cas9; copy number variants; cerebral cavernous malformations; structural variants

Citation: Skowronek, D.; Pilz, R.A.; Bonde, L.; Schamuhn, O.J.; Feldmann, J.L.; Much, M.D.; Felbor, U.; Rath, M. CRISPR/Cas9 mediated nanopore sequencing enables the precise identification of structural variants in *CCM1*, *CCM2*, and *CCM3*. *Int. J. Mol. Sci.* **2022**, *23*, x. https://doi.org/10.3390/xxxxx

Academic Editor: Firstname Lastname

Received: date
Accepted: date
Published: date

1. Introduction

Cerebral cavernous malformations (CCMs) are thin-walled vascular lesions in the central nervous system which are prone to hemorrhage. Depending on their location, they can cause a wide range of neurological complications such as stroke-like symptoms or seizures. The familial form of CCM, which is characterized by the presence of multiple CCMs, follows an autosomal-dominant inheritance pattern with incomplete penetrance and is caused by heterozygous germline variants in the *CCM1 (KRIT1)*, *CCM2*, or *CCM3 (PDCD10)* gene [1].

Disease-causing variants are found in more than 90 % of all familial cases [1]. Frameshift mutations account for the vast majority of pathogenic variants, followed by nonsense, splice site, and copy number variants (CNVs) [1-4]. Indeed, up to 18 % of pathogenic variants found in CCM patients are large deletions [5]. Standard diagnostic techniques for CNV detection are multiplex ligation-dependent probe amplification (MLPA) and short-read gene panel sequencing in combination with specific bioinfor-

matic pipelines. However, both methods have limitations. For example, they cannot identify the precise breakpoints of CNVs, pathogenic variants in non-coding regions and complex structural variants (SVs), e.g., inversions or interchromosomal insertions. This is particularly relevant since all these types of genetic variation have been described for CCM patients in the recent literature [6-9]. In the context of analyses for CNVs segregating within CCM families, cost-effectiveness is also an issue.

The Oxford Nanopore technology, which enables read lengths of more than 30 kb [10], has already revolutionized the sequencing landscape in biomedical research and also has the potential to overcome some limitations of current short-read sequencing-based molecular genetic diagnostics. Long-read sequencing allows bridging and precise identification of SV breakpoints, making it a reliable tool in CNV detection [11,12]. In combination with Cas9-mediated target selection, amplification-free sequencing of genomic DNA is possible [13] and has already been successfully used to identify SVs in clinically relevant genes like *BRCA1* [14]. In particular, the highly flexible and yet affordable MinION platform can be a valuable tool for almost any diagnostic lab.

In this study, we show that nanopore sequencing in combination with Cas9-mediated target selection can serve as an excellent complement to diagnostic short-read sequencing of the *CCM* genes. Detection of CNVs at single nucleotide resolution enables cost-effective and rapid PCR approaches for subsequent cascade analyses in CCM families. Furthermore, we demonstrate that even complex SVs can be reliably detected with targeted nanopore sequencing.

2. Results

2.1 Cas9-mediated nanopore sequencing confirmed a 2,552 bp deletion in CCM1

To cover the entire genomic loci of *CCM1*, *CCM2*, and *CCM3* with long reads, we first designed specific crRNAs to facilitate nanopore sequencing (Table S1). For each gene, the crRNAs were located approximately 15 kb apart from each other to avoid incomplete coverage of the target regions. Enrichment was performed in three separate reactions, allowing parallel sequencing of the three *CCM* genes in one sequencing run and ensuring that sequencing reads would not be terminated early by another CRISPR/Cas9-induced double-strand break. Whenever possible, crRNAs were designed to facilitate the same sequencing direction in a walking approach.

To validate our new crRNA-panel, we sequenced a sample with a known two-exon deletion in *CCM1*. High-molecular-weight genomic DNA was extracted, and target selection was performed by Cas9-mediated induction of double-strand breaks and ligation of sequencing adapters to cleaved ends following the Oxford nanopore protocol (Figure 1a). Long-read sequencing successfully mapped the *CCM1* deletion which started in intron 11 and ended in intron 13 with a mean sequencing coverage of 89.5x for *CCM1* (SD = 19.5; Figure 1b). In the same run, sequencing of *CCM2* and *CCM3* confirmed the absence of other SVs in the sample, while achieving a mean sequencing coverage of 71.9x (SD = 25,3) and 31.0x (SD = 18,9), respectively (Figure 1c,d). Fine-mapping revealed the exact breakpoints of the 2,552 bp deletion in *CCM1* (Figure 1e) and made it possible to design deletion-specific primers for variant confirmation by PCR and Sanger sequencing (Figure 1f; Table S2).

Because the initial sequencing depth for some areas in *CCM2* and *CCM3* was relatively low, we revised our *CCM* crRNA-panel for the following sequencing runs. The final panel combined the walking approach with the dual-cut excision approach, in which two cuts are made, one upstream and one downstream of the target region, to generate optimal coverage for *CCM1*, *CCM2*, and *CCM3* (Table S1).

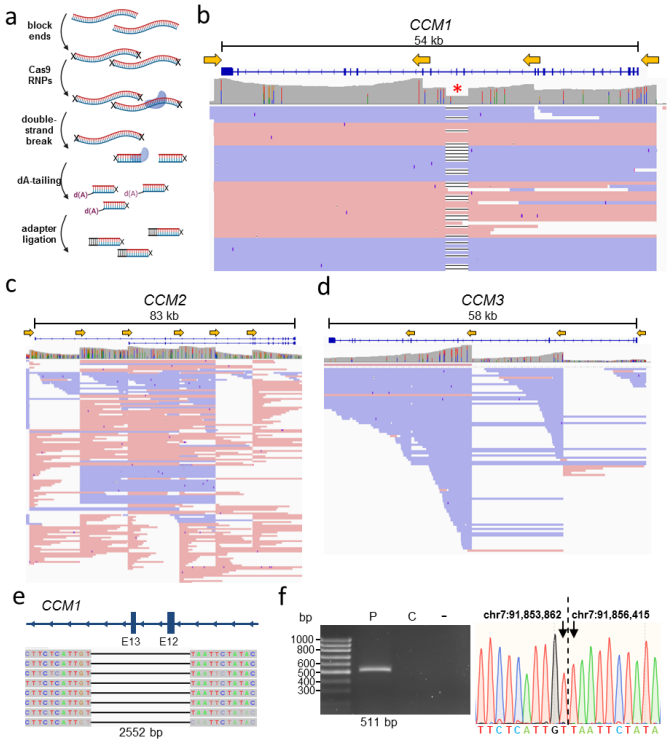

Figure 1. Cas9-targeted nanopore sequencing of the *CCM* genes precisely re-identified a two-exon deletion in *CCM1*. (a) Schematic representation of the sample preparation protocol used for Cas9-targeted nanopore sequencing. **(b)** *CCM1* sequencing data showed a two-exon deletion spanning from intron 11 to intron 13 (red star). CrRNA binding sites and sequencing orientation are symbolized by yellow arrows. The coverage with a peak at 127x is displayed in gray. An excerpt of the generated reads is shown in red and blue. **(c, d)** *CCM2* and *CCM3* long-read sequencing data. The highest coverage was 119x and 87x for *CCM2* and *CCM3*, respectively. The generated reads are shown in red and blue. **(e)** Fine-mapping revealed the exact breakpoints of the 2,552 bp deletion in *CCM1*. **(f)** Deletion-specific PCR detected a 511 bp band in the proband sample (P) and its absence in a healthy control (C) and negative control sample (-). Sanger sequencing of the extracted band confirmed the breakpoints. The genomic location is based on the GRCh37 reference genome. Read data **(b-e)** were visualized in Integrated Genomics Viewer (IGV) [15]. The Locus Reference Genomic (LRG) transcripts are shown **(b-e)**.

2.2 Targeted nanopore sequencing revealed the exact size of large deletions in familial CCM cases

Current detection methods focus on intragenic CNVs in CCM patients. For this reason, the size of variants that are partially extragenic cannot be further characterized. Therefore, we wanted to test whether our long-read sequencing approach could accurately fine-map the breakpoints of large deletions spanning gene boundaries, since this would allow the development of cost-effective PCR-based assays for familial analyses. We used a targeted approach by using crRNAs located upstream of the first deleted exon that had been previously identified by NGS or MLPA analysis.

CNV analysis by MLPA for the proband presented in Figure 2 identified a heterozygous deletion of the *CCM1* exons 2 to 6 (Figure 2a). No data could be generated for the noncoding exon 1 of *CCM1* because the commercially available MLPA kit did not contain specific probes for this region. Over the next three years, nine relatives were

tested for the presence of the variant using MLPA. We reanalyzed the DNA of the index proband by nanopore sequencing which revealed the deletion to be larger than anticipated. Fine-mapping showed that the deletion actually spans from intron 1 of the adjacent *ANKIB1* gene to intron 6 of *CCM1* (Figure 2b). These results were confirmed by deletion-specific PCR and Sanger sequencing (Figure 2c). Long-read sequencing not only enabled the design of a deletion-specific PCR assay which can be used for further familial analyses but also demonstrated partial deletion of *ANKIB1*. So far, however, little is known about the function of ANKIB1.

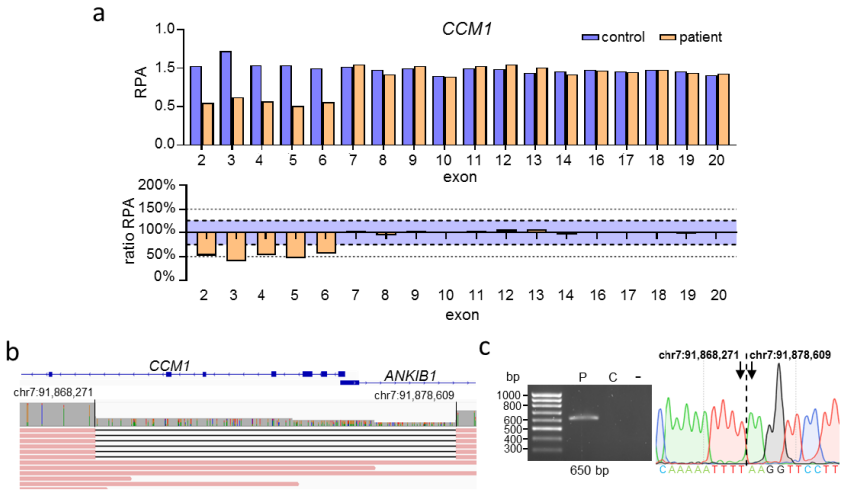

Figure 2. Nanopore sequencing of a large deletion in *CCM1* identified by MLPA revealed a partial deletion of *ANKIB1*. **(a)** MLPA revealed the heterozygous deletion of exons 2-6 of *CCM1* (RPA = relative product area). An exon is considered to be deleted or duplicated if the ratio RPA is below 75 % or above 125 %, respectively (blue area). **(b)** Subsequent nanopore sequencing showed that the deletion comprises 10,337 base pairs, spanning from *CCM1* intron 6 to *ANKIB1* intron 1. Read data was visualized in IGV [15]. **(c)** Deletion-specific PCR detected a 650 bp band in the sample of the index proband (P) and its absence in a healthy control (C) and negative control sample (-). Sanger sequencing of the extracted band confirmed the deletion breakpoints. The genomic location is based on the GRCh37 reference genome. The Locus Reference Genomic (LRG) transcript (*CCM1*) and RefSeq transcript (*ANKIB1*) are shown **(b)**.

For the proband presented in Figure 3, CNV analysis by MLPA was able to identify a multi-exon deletion in *CCM2*, spanning from exon 6 to exon 11 (Figure 3a). Nanopore sequencing revealed the true size of the deletion to be 23,777 bp, covering the complete *NACAD* gene located downstream of *CCM2* (Figure 3b). So far, the function of NACAD is unknown. A review of the CNV breakpoints in IGV suggested that this deletion originated from Alu-mediated recombination (Figure 3b). Since breakpoints were localized in these highly repetitive regions, sequence alignment was not able to confidently determine the exact distal breakpoint. Nevertheless, specific PCR primers could be designed to confirm the deletion by PCR and identify the exact breakpoints by Sanger sequencing which also revealed an additional 15 bp indel variant between the breakpoints (Figure 3c).

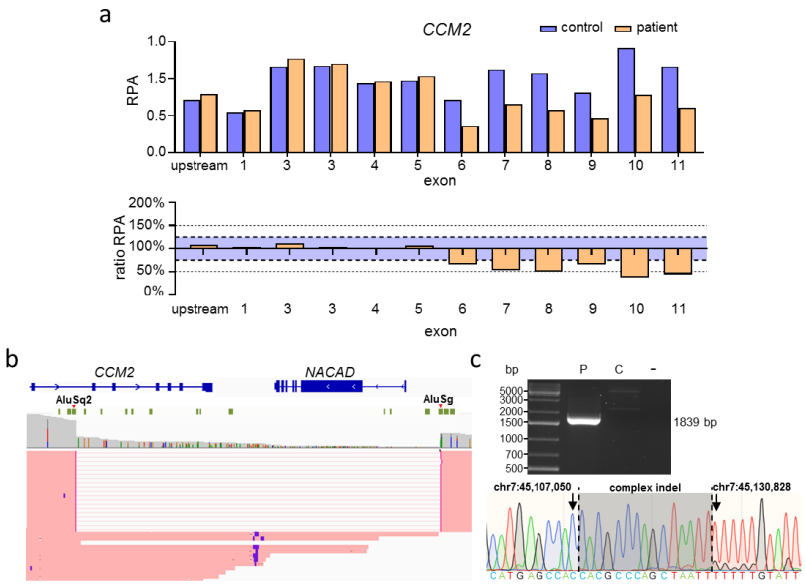

Figure 3. Nanopore sequencing of a large *CCM2* deletion suggest an Alu-mediated origin. **(a)** MLPA revealed a heterozygous deletion of exons 6-11 of *CCM2* (RPA = relative product area). An exon is considered to be deleted or duplicated if the ratio RPA is below 75 % or above 125 %, respectively (blue area). **(b)** Subsequent nanopore sequencing showed that the deletion comprises 23,777 bp, starting in intron 5 of *CCM2* and encompassing the neighboring gene *NACAD*. Deletion breakpoints are located inside of an AluSq2 and an AluSg repeat, respectively (green blocks). Read data was visualized in IGV [15]. **(c)** Deletion-specific PCR detected a 1,839 bp band in the sample of the proband (P) and its absence in a healthy control (C) and negative control sample (-). Sanger sequencing of the extracted band was able to specify the deletion breakpoints and revealed a 15 bp indel variant. The genomic location is based on the GRCh37 reference genome. The Locus Reference Genomic (LRG) transcript (*CCM2*) and RefSeq transcript (*NACAD*) are shown **(b)**.

2.3 Targeted nanopore sequencing can be used to identify complex SVs in CCM

The detection of complex SVs is hard or even impossible with short-read gene panel sequencing. Since the identification of an interchromosomal insertion and an inversion in *CCM2* [8,9] suggest that SVs must be considered as a possible cause of familial CCM disease, we wanted to test whether long-read sequencing could accurately detect these variants. Therefore, we reanalyzed a heterozygous 24 kb inversion on chromosome 7 (Figure 4a) which covers the first coding exon of *CCM2* [8] with long-read sequencing (Figure 4b). We used crRNAs that were part of our *CCM* crRNA-panel to facilitate a dual-cut excision approach covering roughly half of the coding region of *CCM2*. The crRNA located upstream of *CCM2* was within the variant boundaries of the 24 kb inverted region, whereas the downstream crRNA was located in *CCM2* intron 3. The wild-type allele was present in roughly half of all reads. Two different kinds of reads covering the inversion were present. In both cases, mapping orientation flipped after passing one of the inversion breakpoints (Figure 4b). Due to the different types of reads generated by sequencing the inversion allele, we were able to identify both breakpoints of the 24 kb inversion. This variant was discovered previously only using short-read WGS [8]. As the

variant is copy number neutral and the breakpoints lie in non-coding regions, detection via targeted panel sequencing, whole-exome sequencing, or MLPA was impossible.

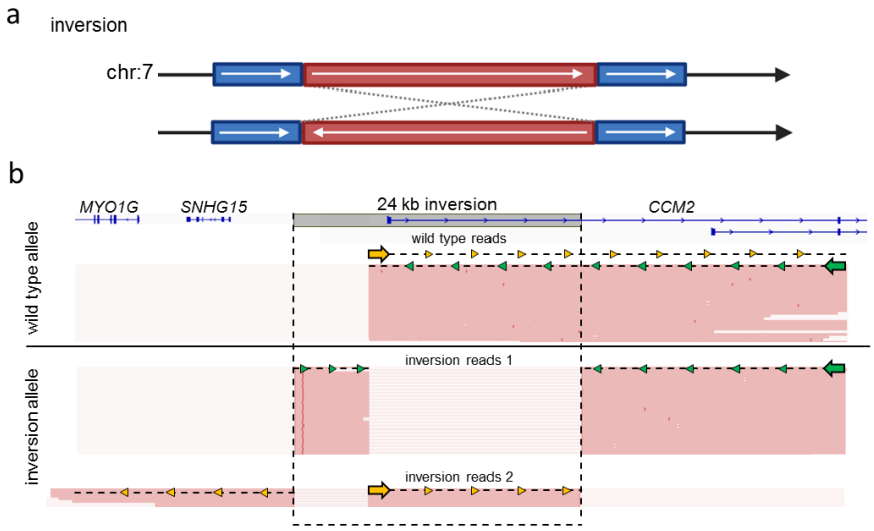

Figure 4. Nanopore sequencing confidently detected a 24 kb inversion in *CCM2*. (a) Schematic representation of the inversion in *CCM2*. **(b)** A dual-cut approach was used to re-sequence a sample with a known heterozygous 24 kb inversion in *CCM2*. CrRNAs facilitated sequencing in opposing directions. One binding site was located inside of the inversion (yellow arrow) and the other one was located downstream of the variant (green arrow). Sequencing of the wild-type allele resulted in one type of reads localized between both crRNA cut sides. Two distinct read patterns visualizing the inversion could be observed depending on which crRNA initiated sequencing of the inversion allele (inversion reads 1; inversion reads 2). Read data was visualized in IGV [15]. The Locus Reference Genomic (LRG) transcripts are shown **(b)**.

Long-read sequencing of a previously identified heterozygous interchromosomal insertion in *CCM2* (Figure 5a) [9] provided single reads with lengths of more than 20 kb. These reads spanned the breakpoint located in *CCM2* exon 6 with subsequent mapping of bases to chromosome 1 (Figure 5b). Due to read length, confident mapping of supplementary alignments on chromosome 1 was possible. In short-read sequencing data, on the other hand, the insertion was barely noticeable. Only a reduction in coverage of four bases at the breakpoint location was visible (Figure 5b). Short-read sequencing data contained some reads that were crossing the variant breakpoint but had poor alignment confidence. In our previous report, we had to use fluorescence in situ hybridization (FISH) analysis to confirm the interchromosomal insertion [9].

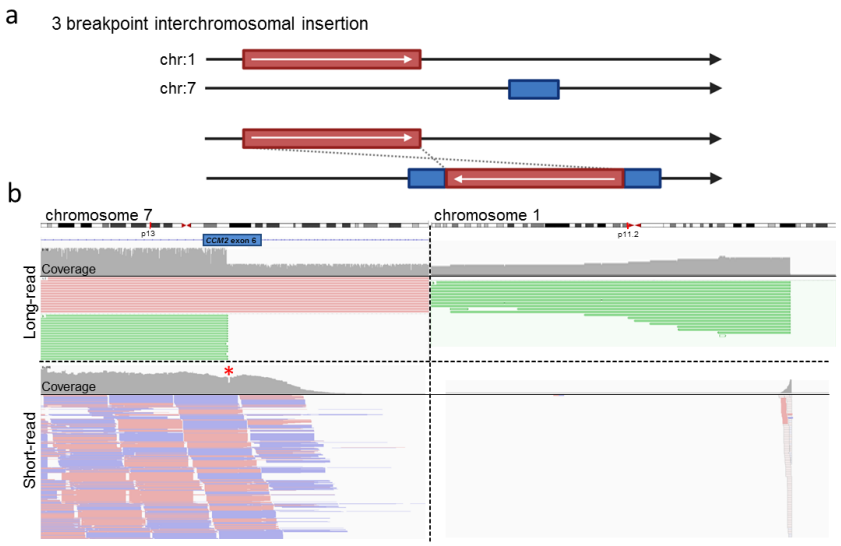

Figure 5. Nanopore sequencing confidently detected an interchromosomal insertion in *CCM2*. **(a)** Schematic representation of the interchromosomal insertion in *CCM2*. **(b)** Long-read sequencing data of a previously described heterozygous interchromosomal insertion revealed about 50 % of reads covering *CCM2* terminate in exon 6 (green). These reads all had a supplementary alignment mapping to chromosome 1. Short-read data showed consistent coverage of *CCM2* exon 6. Only a small reduction in coverage at the position of the variant breakpoint in *CCM2* could be observed (red star). Most reads bridging to chromosome 1 had an alignment confidence of 0 % (hollow reads). Read data was visualized in IGV [15].

2.4 Targeted nanopore sequencing on the Flongle flow cell is also able to determine variant breakpoints

To reduce analysis costs, we next wanted to see if Cas9-mediated nanopore sequencing was also possible on the much cheaper Flongle flow cells. In this approach, we were able to detect the exon 12 and 13 deletion in *CCM1* mentioned earlier (Figure 1) from high molecular weight DNA (Figure 6a). Additionally, we used a Flongle flow cell to re-sequence a heterozygous deletion of exons 4 and 5 in *CCM2* (Figure 6b) from medium-sized DNA typical used for routine diagnostics after size selection with the Short Read Eliminator Kit. As both variants were located intragenic and the deleted exons were previously identified, a dual-cut approach with two flanking crRNAs was used. We also tested if a single-cut approach in conjunction with Flongle sequencing was possible. Although we were able to detect the deletion in *CCM1* described in Figure 2, just one read covered the target region (Figure S1).

Consequently, Cas9-mediated Flongle sequencing can be used to characterize CNVs in CCM, but a dual-cut approach is recommended for intragenic variants. Therefore, breakpoint mapping of variants by nanopore sequencing on a Flongle flow cell as a second-line approach is the most cost-effective way to enable PCR-based assays for familial analyses.

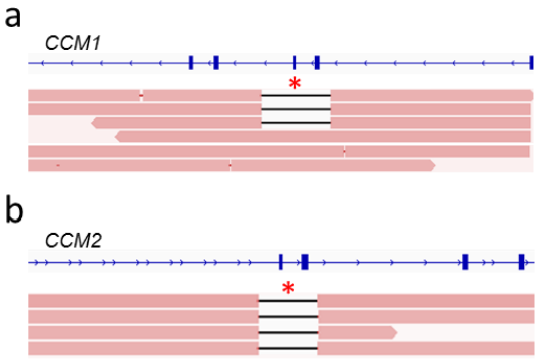

Figure 6. Sequencing on Flongle flow cells detected variant breakpoints in a shallow Cas9-mediated long-read approach. (a,b) Sequencing data from two dual-cut excision approaches sequenced on a Flongle flow cell. **(a)** Detection of the two-exon deletion (red star) of exons 12 and 13 in *CCM1* (Figure 1) with a sequencing coverage of 6x. **(b)** Re-sequencing of a heterozygous two-exon deletion (red star) of exons 3 and 4 in *CCM2* with a Flongle flow cell yielded a sequencing coverage of 4x. No wild-type reads were generated. Read data was visualized in IGV [15]. The Locus Reference Genomic (LRG) transcripts are shown **(a,b)**.

3. Discussion

In this study, we demonstrate that the implementation of Cas9-mediated long-read sequencing can significantly improve the sensitivity and accuracy of molecular genetic diagnostics for CCM patients when used as a complementary analytical approach. It allows not only fine mapping of CNV breakpoints, but also detection of complex germline SVs that can be easily missed by targeted NGS approaches.

Large deletions have been reported for all three *CCM* genes [2,16-24]. Their size ranges from a few hundred kilobases to 1.9 megabases [16,22,23]. However, the actual size of CNVs in *CCM1*, *CCM2*, or *CCM3* is often unknown because the identification methods do not allow accurate mapping of the breakpoints [16,18,23,25]. Indeed, we show here that the deletion of the first six exons of *CCM1* was much larger than initially thought and also included parts of the neighboring *ANKIB1* gene. Other studies also identified *CCM1* gene deletions with a breakpoint in *ANKIB1* [22]. Variants involving neighboring genes are also known for *CCM2* [4,17,25] and *CCM3* [20].

In molecular diagnostics, a variety of wet lab assays can be used to screen for CNVs. The MLPA technique, for example, is widely used to detect large deletions and duplications in many well-known disease genes. The resolution depends on the design of the MLPA probes and non-coding exons might not be completely covered. Microarray-based high-density comparative genomic hybridization (aCGH) offers high-throughput analyses with a minimum resolution of 500 bp [26]. However, aCGH requires special equipment and is limited in detecting small duplications [27]. Bioinformatic advances have also made it possible to detect CNVs from high-throughput short-read panel sequencing data, allowing parallel detection of SNVs, indels, and CNVs with exon-level resolution [3,28]. Nevertheless, all techniques have disadvantages regarding targeted analyses for a familial CNV. Short-read panel sequencing is rarely used to detect known familial CNVs due to its rather high costs. However, even MLPA analysis can become time-consuming and expensive if parallel analyses of multiple samples are impossible [28]. Especially in large CCM families, several relatives often need to be screened for the familial CNV at different time points [29]. For example, in one family described here (Figure 2), nine members were sequentially tested for the identified *CCM1* deletion by

MLPA. The use of less expensive and simpler assays such as allele-specific PCR for variant confirmation is therefore highly desirable. However, the exact breakpoints of a CNV must be known to establish these assays. Long-read sequencing is a very good option for this purpose. Since it would be performed only once in the index patient to map the exact breakpoints of a CNV, long-read sequencing would also be a cost-efficient option: Subsequent analyses could be done with inexpensive PCR. For predictive analyses, this can reduce the hands-on-time to a few hours, while keeping reagent costs very low. Moreover, the MinION platform can be used in any lab and has low initial investment costs [30]. Furthermore, we here demonstrate that mapping of CNV breakpoints with a Flongle flow cell is an option to further reduce the costs to less than $100 per flow cell and sample.

Breakpoint mapping by long-read sequencing not only enables the development of efficient PCR-based assays for familial analyses but can also provide insight into the origin of CNVs. Mechanisms leading to CNV formation often involve the recombination of homologous DNA sequences. Alu-repeats, for example, belong to the short interspersed nuclear elements (SINES) that largely facilitate structural variation in the genome. They are characterized as repetitive regions about 300 bp in size and contribute to almost 11 % of the human genome [31]. Because of their high homology, Alu-repeats are responsible for genomic instability. Following a double-strand break, non-allelic homologous recombination mediated by Alu-repeats can lead to deletions, duplications, and complex SVs [31]. Alu-mediated CNVs and SVs have been found in various disorders, like chronic granulomatous disease [32], limb-girdle muscular dystrophy 5 [33], and glaucoma [34]. In CCM, Alu-repeat recombination is also a known disease mechanism. Liquori and colleagues discovered a founder mutation resulting from recombination in *CCM2* between an AluSx- and an AluSg-repeat region which led to the deletion of exons 2 to 10 [4]. In our second familial case, breakpoint mapping with long-read sequencing also revealed Alu-mediated recombination as a possible cause of the identified deletion (Figure 3). Variant breakpoints were located in an AluSq2- and an AluSg-repeat, respectively.

Beyond accurate characterization of variant breakpoints, the utility of long-read sequencing as a complementary analysis to gene panel sequencing is also demonstrated by its ability to detect more complex SVs that are usually not captured by targeted short-read sequencing approaches [35]. Inversions or translocations, for example, might easily be missed when breakpoints are not located in coding regions. Unfortunately, short-read WGS, which has higher sensitivity for complex SVs, is not yet an option for routine diagnosis of monogenic diseases with well-established risk genes due to high investment costs and bioinformatics requirements. Targeted long-read sequencing, on the other hand, is relatively easy to implement and can confidently close the diagnostic gap for SVs [36]. Consistent with the experience of other groups in resolving complex structural rearrangements, our targeted long-read sequencing assay easily detected an interchromosomal insertion and a copy number-neutral inversion in the *CCM2* gene that had previously been identified in short-read approaches and elaborately validated [8,9]. Despite continuous advances in sequencing chemistry and computational compensation [37-39], however, nanopore sequencing is not yet suitable as a stand-alone diagnostic approach. In particular, the relatively high error rate of nanopore sequencing and the risk of missing whole gene deletions in Cas9-mediated targeted long-read sequencing currently limit its diagnostic power. While short-read panel sequencing remains the most cost-effective method for detecting SNVs, indels, and CNVs as a first-line approach, complementary nanopore sequencing can reduce costs and turnaround time for pathogenic familial CNVs and may also be used as second-line approach to screen for complex SVs.

Thus, we demonstrate that the implementation of long-read sequencing can be a great benefit to CCM diagnostics. Our experience also suggests that this approach can very easily be transferred to other diagnostic questions.

4. Materials and Methods

4.1. Nanopore sequencing

All study participants gave written informed consent for genetic analyses. High-molecular-weight genomic DNA was isolated from fresh blood or frozen blood samples using the Monarch HMW DNA Extraction Kit (New England BioLabs, Ipswich, MA, USA). The NucleoSpin Blood L Kit (Macherey-Nagel, Düren, Germany) was used to isolate medium-sized DNA fragments that are typically used in routine diagnostics. To eliminate short reads the Short Read Eliminator Kit (Circulomics, Baltimore, MD, USA) was used. If necessary, additional purification of genomic DNA samples was performed by magnetic bead clean-up with AMPure XP beads (Beckman Coulter, Brea, CA, USA). Target selection was performed either with the Cas9 Sequencing Kit (SQK-CS9109, Oxford Nanopore Technologies) or the Ligation sequencing Kit (SQK-CS9109, Oxford Nanopore Technologies) in combination with the following additional components: dATP Solution, NEBNext Quick Ligation Module, Quick CIP, Taq DNA Polymerase (New England BioLabs) and IDTE pH 8.0 (Integrated DNA Technologies, Coralville, IA, USA). For Cas9 cleavage, Alt-R S.p. Cas9 Nuclease V3 (Integrated DNA Technologies), Alt-R CRISPR-Cas9 tracrRNA (Integrated DNA Technologies), and Alt-R CRISPR-Cas9 crRNAs (Integrated DNA Technologies; Table S1) were used. Briefly, for targeted sequencing of a known variant, up to 5 µg of genomic DNA was used for dephosphorylation. DNA was then cleaved by RNP complexes with crRNAs located directly up- or downstream of the variant. After poly-A-tailing and AMPure XP bead purification, sequencing adapters were ligated, and sequencing was started. Long-read-sequencing was performed on a MinION device (Oxford Nanopore Technologies, Oxford, United Kingdom) equipped with R9.4.1 flow cells (Oxford Nanopore Technologies).

For combined sequencing of *CCM1*, *CCM2*, and *CCM3*, up to 15 µg of genomic DNA were divided and dephosphorylated in three separate tubes. The tubes were treated with RNP complexes originating from one of three crRNA-pools (Table S1). After poly-A-tailing, the three tubes were mixed and AMPure XP bead purification, adapter ligation, and sequencing were performed as usual. Target selection for Cas9-mediated nanopore sequencing on Flongle flow cells (Oxford Nanopore Technologies) was performed with the Cas9 sequencing kit as mentioned above. Loading of the Flongle flow cell was done with the Flongle Flow Cell Priming Kit (EXP-FSE001, Oxford Nanopore Technologies) and according to the "Loading the Flongle flow cell" section of the SQK-LSK109 sequencing protocol.

Live basecalling was performed with the MinKNOW (Oxford Nanopore Technologies) software. FASTQ files were combined with cygwin64 and alignment to the GRCh37 reference genome was carried out with the MinKNOW software utilizing the Guppy toolkit. Index files were generated with igvtools and sequencing data was visualized and evaluated in IGV 2.13.0 [15].

4.2. Multiplex ligation-dependent probe amplification, PCR, and Sanger sequencing

For copy number variation analysis by MLPA, the kits P130-A3 and P131-B1 containing probes for *CCM1*, *CCM2*, and *CCM3* were used according to the manufacturer's instructions (MRC-Holland, Amsterdam, The Netherlands). Fragment analysis was performed on a SeqStudio Genetic Analyzer (Applied Biosystems, Waltham, MA, USA) or an ABI 310 Genetic Analyzer (Applied Biosystems), and the data was analyzed with the SeqPilot software (v5.1.0, JSI Medical Systems, Ettenheim, Germany). Visualization was performed with the GraphPad Prism software (v.8.0.1, San Diego, CA, USA).

For breakpoint confirmation, variant-specific primers (Integrated DNA Technologies) were designed, and PCR reactions were carried out with the Taq DNA-Polymerase

(Thermo Fisher Scientific, Waltham, MA, USA). To amplify GC-rich regions the OneTaq DNA Polymerase (New England BioLabs) or the GC-RICH PCR-System (Roche, Basel, Switzerland) was used with GC-Rich Buffer. PCR products were evaluated on a 1.5 % agarose gel imaged on a ChemiDoc XRS+ system (BioRad, Hercules, CA, USA). Bands were cut from the gel and extracted with the Zymoclean Gel DNA Recovery Kit (Zymo Research, Irvine, CA, USA). The sequencing reaction was done with the BigDye Terminator v3.1 Cycle Sequencing Kit (Thermo Fisher Scientific). After cleanup, the samples were sequenced on a SeqStudio Genetic Analyzer. Sequencing data were evaluated with SnapGene Viewer (Dotmaticsm, Boston, MA, USA).

4.3. Illumina sequencing

Hybridization capture-based target enrichment of genomic DNA samples for *CCM1*, *CCM2*, and *CCM3* was performed using an Agilent SureSelect^{QXT} custom enrichment kit (Panel ID: 3152261, Agilent Technologies, Santa Clara, USA). Illumina sequencing was performed on an Illumina MiSeq platform with 2x150 cycles (Illumina, San Diego, USA). Basecalling and alignment to the GRCh37 reference genome were performed with the MiSeq Reporter Software v.2.6.2. Data was visualized with IGV 2.13.0 [15].

Supplementary Materials: The following supporting information can be downloaded at: www.mdpi.com/xxx/s1, Table S1: Sequencing reactions for SV screening in CCM and used crRNAs, Table S2: PCR primers for breakpoint confirmation and familial analyses, Figure S1: Sequencing of the familial *CCM1* exon 2 – 6 deletion (Figure 2) on a Flongle flow cell was able to identify the variant breakpoints. The variant was covered by one sequencing read. A single-cut approach was used. Read data was visualized in IGV [15].

Author Contributions: Conceptualization, M.R., C.D.M., and U.F.; formal analysis, D.S., L.B. and R.A.P.; investigation, D.S., L.B., J.L.F., and O.J.S.; genetic counselling, M.R., U.F. and S.H.; writing—original draft preparation, D.S., R.A.P., and L.B.; writing—review and editing, M.R. and U.F.; visualization, D.S. and L.B.; supervision, U.F. and M.R.; funding acquisition, C.D.M. and M.R. All authors have read and agreed to the published version of the manuscript.

Funding: This work was supported by the Deutsche Forschungsgemeinschaft (DFG, German Research Foundation; No. RA2876/2-2) and by the Research Network Molecular Medicine of the University Medicine Greifswald (FOVB-2022-14). MR was supported by a clinician scientist scholarship from the Gerhard Domagk program of the University Medicine Greifswald.

Institutional Review Board Statement: Informed consent was obtained from all subjects involved in the study. The study was conducted in accordance with the Declaration of Helsinki, and the protocol was approved by the Ethics Committee of the University Medicine Greifswald (BB 047/14a).

Informed Consent Statement: Informed consent was obtained from all subjects involved in the study.

Data Availability Statement: Not applicable.

Acknowledgments: Sina Ramcke is thanked for her excellent technical assistance. Figures 1a, 4a, and 5a were created with biorender.com.

Conflicts of Interest: The authors declare no conflict of interest. The funders had no role in the design of the study; in the collection, analyses, or interpretation of data; in the writing of the manuscript; or in the decision to publish the results.

References

1. Spiegler, S.; Rath, M.; Paperlein, C.; Felbor, U. Cerebral Cavernous Malformations: An Update on Prevalence, Molecular Genetic Analyses, and Genetic Counselling. *Mol Syndromol* **2018**, *9*, 60-69, doi:10.1159/000486292.
2. Felbor, U.; Gaetzner, S.; Verlaan, D.J.; Vijzelaar, R.; Rouleau, G.A.; Siegel, A.M. Large germline deletions and duplication in isolated cerebral cavernous malformation patients. *Neurogenetics* **2007**, *8*, 149-153, doi:10.1007/s10048-006-0076-7.

3. Much, C.D.; Schwefel, K.; Skowronek, D.; Shoubash, L.; von Podewils, F.; Elbracht, M.; Spiegler, S.; Kurth, I.; Flöel, A.; Schroeder, H.W.S.; et al. Novel Pathogenic Variants in a Cassette Exon of *CCM2* in Patients With Cerebral Cavernous Malformations. *Front Neurol* **2019**, *10*, 1219, doi:10.3389/fneur.2019.01219.
4. Liquori, C.L.; Berg, M.J.; Squitieri, F.; Leedom, T.P.; Ptacek, L.; Johnson, E.W.; Marchuk, D.A. Deletions in *CCM2* Are a Common Cause of Cerebral Cavernous Malformations. *Am J Hum Genet* **2007**, *80*, 69-75, doi:10.1086/510439.
5. Riant, F.; Cecillon, M.; Saugier-Veber, P.; Tournier-Lasserve, E. CCM molecular screening in a diagnosis context: novel unclassified variants leading to abnormal splicing and importance of large deletions. *Neurogenetics* **2013**, *14*, 133-141, doi:10.1007/s10048-013-0362-0.
6. Riant, F.; Odent, S.; Cecillon, M.; Pasquier, L.; de Baracé, C.; Carney, M.P.; Tournier-Lasserve, E. Deep intronic KRIT1 mutation in a family with clinically silent multiple cerebral cavernous malformations. *Clin Genet* **2014**, *86*, 585-588, doi:10.1111/cge.12322.
7. Pilz, R.A.; Skowronek, D.; Hamed, M.; Weise, A.; Mangold, E.; Radbruch, A.; Pietsch, T.; Felbor, U.; Rath, M. Using CRISPR/Cas9 genome editing in human iPSCs for deciphering the pathogenicity of a novel *CCM1* transcription start site deletion. *Front Mol Biosci* **2022**, *9*, 953048, doi:10.3389/fmolb.2022.953048.
8. Spiegler, S.; Rath, M.; Hoffjan, S.; Dammann, P.; Sure, U.; Pagenstecher, A.; Strom, T.; Felbor, U. First large genomic inversion in familial cerebral cavernous malformation identified by whole genome sequencing. *Neurogenetics* **2018**, *19*, 55-59, doi:10.1007/s10048-017-0531-7.
9. Pilz, R.A.; Schwefel, K.; Weise, A.; Liehr, T.; Demmer, P.; Spuler, A.; Spiegler, S.; Gilberg, E.; Hübner, C.A.; Felbor, U.; et al. First interchromosomal insertion in a patient with cerebral and spinal cavernous malformations. *Sci Rep-Uk* **2020**, *10*, 6306, doi:10.1038/s41598-020-63337-5.
10. Mohammadi, M.M.; Bavi, O. DNA sequencing: an overview of solid-state and biological nanopore-based methods. *Biophys Rev* **2022**, *14*, 99-110, doi:10.1007/s12551-021-00857-y.
11. Mantere, T.; Kersten, S.; Hoischen, A. Long-Read Sequencing Emerging in Medical Genetics. *Front Genet* **2019**, *10*, 426, doi:10.3389/fgene.2019.00426.
12. Sonoda, K.; Ishihara, H.; Sakazaki, H.; Suzuki, T.; Horie, M.; Ohno, S. Long-Read Sequence Confirmed a Large Deletion Including *MYH6* and *MYH7* in an Infant of Atrial Septal Defect and Atrial Arrhythmias. *Circ Genom Precis Med* **2021**, *14*, e003223, doi:10.1161/CIRCGEN.120.003223.
13. Gilpatrick, T.; Lee, I.; Graham, J.E.; Raimondeau, E.; Bowen, R.; Heron, A.; Downs, B.; Sukumar, S.; Sedlazeck, F.J.; Timp, W. Targeted nanopore sequencing with Cas9-guided adapter ligation. *Nat Biotechnol* **2020**, *38*, 433-438, doi:10.1038/s41587-020-0407-5.
14. Walsh, T.; Casadei, S.; Munson, K.M.; Eng, M.; Mandell, J.B.; Gulsuner, S.; King, M.C. CRISPR-Cas9/long-read sequencing approach to identify cryptic mutations in *BRCA1* and other tumour suppressor genes. *J Med Genet* **2021**, *58*, 850-852, doi:10.1136/jmedgenet-2020-107320.
15. Robinson, J.T.; Thorvaldsdóttir, H.; Winckler, W.; Guttman, M.; Lander, E.S.; Getz, G.; Mesirov, J.P. Integrative genomics viewer. *Nat Biotechnol* **2011**, *29*, 24-26, doi:10.1038/nbt.1754.
16. Bergametti, F.; Denier, C.; Labauge, P.; Arnoult, M.; Boetto, S.; Clanet, M.; Coubes, P.; Echenne, B.; Ibrahim, R.; Irthum, B.; et al. Mutations within the Programmed Cell Death 10 Gene Cause Cerebral Cavernous Malformations. *Am J Hum Genet* **2005**, *76*, 42-51, doi:10.1086/426952.
17. Liquori, C.L.; Penco, S.; Gault, J.; Leedom, T.P.; Tassi, L.; Esposito, T.; Awad, I.A.; Frati, L.; Johnson, E.W.; Squitieri, F.; et al. Different spectra of genomic deletions within the CCM genes between Italian and American CCM patient cohorts. *Neurogenetics* **2008**, *9*, 25-31, doi:10.1007/s10048-007-0109-x.

18. Choe, C.U.; Riant, F.; Gerloff, C.; Tournier-Lasserve, E.; Orth, M. Multiple cerebral cavernous malformations and a novel *CCM3* germline deletion in a German family. *J Neurol* **2010**, *257*, 2097-2098, doi:10.1007/s00415-010-5648-7.
19. Cigoli, M.S.; Avemaria, F.; De Benedetti, S.; Gesu, G.P.; Accorsi, L.G.; Parmigiani, S.; Corona, M.F.; Capra, V.; Mosca, A.; Giovannini, S.; et al. *PDCD10* Gene Mutations in Multiple Cerebral Cavernous Malformations. *PLoS One* **2014**, *9*, e110438, doi:10.1371/journal.pone.0110438.
20. Nardella, G.; Visci, G.; Guarnieri, V.; Castellana, S.; Biagini, T.; Bisceglia, L.; Palumbo, O.; Trivisano, M.; Vaira, C.; Scerrati, M.; et al. A single-center study on 140 patients with cerebral cavernous malformations: 28 new pathogenic variants and functional characterization of a *PDCD10* large deletion. *Hum Mutat* **2018**, *39*, 1885-1900, doi:10.1002/humu.23629.
21. Fusco, C.; Copetti, M.; Mazza, T.; Amoruso, L.; Mastroianno, S.; Nardella, G.; Guarnieri, V.; Micale, L.; D'Agruma, L.; Castori, M. Molecular diagnostic workflow, clinical interpretation of sequence variants, and data repository procedures in 140 individuals with familial cerebral cavernous malformations. *Hum Mutat* **2019**, *40*, e24-e36, doi:10.1002/humu.23851.
22. Muscarella, L.A.; Guarnieri, V.; Coco, M.; Belli, S.; Parrella, P.; Pulcrano, G.; Catapano, D.; D'Angelo, V.A.; Zelante, L.; D'Agruma, L. Small Deletion at the 7q21.2 Locus in a CCM Family Detected by Real-Time Quantitative PCR. *J Biomed Biotechnol* **2010**, 854737, doi:10.1155/2010/854737.
23. Benedetti, V.; Canzoneri, R.; Perrelli, A.; Arduino, C.; Zonta, A.; Brusco, A.; Retta, S.F. Next-Generation Sequencing Advances the Genetic Diagnosis of Cerebral Cavernous Malformation (CCM). *Antioxidants (Basel)* **2022**, *11*, 1294, doi:10.3390/antiox11071294.
24. Mondéjar, R.; Solano, F.; Rubio, R.; Delgado, M.; Pérez-Sempere, Á.; González-Meneses, A.; Vendrell, T.; Izquierdo, G.; Martinez-Mir, A.; Lucas, M. Mutation Prevalence of Cerebral Cavernous Malformation Genes in Spanish Patients. *PLoS One* **2014**, *9*, e86286, doi:10.1371/journal.pone.0086286.
25. Denier, C.; Goutagny, S.; Labauge, P.; Krivosic, V.; Arnoult, M.; Cousin, A.; Benabid, A.L.; Comoy, J.; Frerebeau, P.; Gilbert, B.; et al. Mutations within the *MGC4607* gene cause cerebral cavernous malformations. *Am J Hum Genet* **2004**, *74*, 326-337, doi:10.1086/381718.
26. Pös, O.; Radvanszky, J.; Styk, J.; Pös, Z.; Buglyó, G.; Kajsik, M.; Budis, J.; Nagy, B.; Szemes, T. Copy Number Variation: Methods and Clinical Applications. *Appl Sci* **2021**, *11*, 819, doi:10.3390/app11020819.
27. Coughlin, C.R., 2nd; Scharer, G.H.; Shaikh, T.H. Clinical impact of copy number variation analysis using high-resolution microarray technologies: advantages, limitations and concerns. *Genome Med* **2012**, *4*, 80, doi:10.1186/gm381.
28. Singh, A.K.; Olsen, M.F.; Lavik, L.A.S.; Vold, T.; Drablos, F.; Sjursen, W. Detecting copy number variation in next generation sequencing data from diagnostic gene panels. *BMC Med Genomics* **2021**, *14*, 214, doi:10.1186/s12920-021-01059-x.
29. Gaetzner, S.; Stahl, S.; Sürücü, O.; Schaafhausen, A.; Halliger-Keller, B.; Bertalanffy, H.; Sure, U.; Felbor, U. *CCM1* gene deletion identified by MLPA in cerebral cavernous malformation. *Neurosurg Rev* **2007**, *30*, 155-159; discussion 159-160, doi:10.1007/s10143-006-0057-1.
30. Brinkmann, A.; Ulm, S.L.; Uddin, S.; Förster, S.; Seifert, D.; Oehme, R.; Corty, M.; Schaade, L.; Michel, J.; Nitsche, A. AmpliCoV: Rapid Whole-Genome Sequencing Using Multiplex PCR Amplification and Real-Time Oxford Nanopore MinION Sequencing Enables Rapid Variant Identification of SARS-CoV-2. *Front Microbiol* **2021**, *12*, 651151, doi:10.3389/fmicb.2021.651151.
31. Deininger, P. Alu elements: know the SINEs. *Genome Biol* **2011**, *12*, 236, doi:10.1186/gb-2011-12-12-236.
32. Gentsch, M.; Kaczmarczyk, A.; van Leeuwen, K.; de Boer, M.; Kaus-Drobek, M.; Dagher, M.C.; Kaiser, P.; Arkwright, P.D.; Gahr, M.; Rösen-Wolff, A.; et al. Alu-repeat-induced deletions within the *NCF2* gene causing p67-*phox*-deficient chronic granulomatous disease (CGD). *Hum Mutat* **2010**, *31*, 151-158, doi:10.1002/humu.21156.

506 33. Pluta, N.; Hoffjan, S.; Zimmer, F.; Köhler, C.; Lücke, T.; Mohr, J.; Vorgerd, M.; Nguyen, H.H.P.; Atlan, D.; Wolf, B.; et al.
507 Homozygous Inversion on Chromosome 13 Involving SGCG Detected by Short Read Whole Genome Sequencing in a
508 Patient Suffering from Limb-Girdle Muscular Dystrophy. *Genes* **2022**, *13*, 1752, doi:10.3390/genes13101752.
509 34. Schilter, K.F.; Reis, L.M.; Sorokina, E.A.; Semina, E.V. Identification of an Alu-repeat-mediated deletion of *OPTN* upstream
510 region in a patient with a complex ocular phenotype. *Mol Genet Genomic Med* **2015**, *3*, 490-499, doi:10.1002/mgg3.159.
511 35. Stephens, Z.; Wang, C.; Iyer, R.K.; Kocher, J.P. Detection and visualization of complex structural variants from long reads.
512 *BMC Bioinformatics* **2018**, *19*, 508, doi:10.1186/s12859-018-2539-x.
513 36. Miller, D.E.; Sulovari, A.; Wang, T.; Loucks, H.; Hoekzema, K.; Munson, K.M.; Lewis, A.P.; Fuerte, E.P.A.; Paschal, C.R.;
514 Walsh, T.; et al. Targeted long-read sequencing identifies missing disease-causing variation. *Am J Hum Genet* **2021**, *108*,
515 1436-1449, doi:10.1016/j.ajhg.2021.06.006.
516 37. Rang, F.J.; Kloosterman, W.P.; de Ridder, J. From squiggle to basepair: computational approaches for improving nanopore
517 sequencing read accuracy. *Genome Biol* **2018**, *19*, 90, doi:10.1186/s13059-018-1462-9.
518 38. Delahaye, C.; Nicolas, J. Sequencing DNA with nanopores: Troubles and biases. *PLoS One* **2021**, *16*, e0257521,
519 doi:10.1371/journal.pone.0257521.
520 39. Xu, Z.; Mai, Y.; Liu, D.; He, W.; Lin, X.; Xu, C.; Zhang, L.; Meng, X.; Mafofo, J.; Zaher, W.A.; et al. Fast-bonito: A faster
521 deep learning based basecaller for nanopore sequencing. *Artif Intell Life Sci* **2021**, *1*, 100011, doi:10.1016/j.ailsci.2021.100011.

522

Supplementary Material

Table S1. Sequencing reactions for SV screening in CCM and crRNAs.

Reaction	Gene	No.	Name	crRNA sequence	Used in targeted sequencing
1	*CCM1*	I	CD.Cas9.RFSH5951.AA	ATTCTCGGTGTAGTGGTCAA	*CCM2* 24kb inversion (Figure 4)
		IV	CD.Cas9.KHSK6404.AA	GGTTAGACAATAATCTTGAT	*CCM1* exon 12-13 deletion (Figure 6a)
	CCM2	I	CD.Cas9.CLYJ9692.AD	GTGCCCCTAACCAATCACTT	
		IIX	CD.Cas9.NZXJ8292.AC	GGTGGGATAATCAACTACTA	*CCM2* 24kb inversion (Figure 4)
		V	CD.Cas9.HRHZ5617.AQ	TTGCAGGTCGACTCCCACGC	*CCM2* exon 4 – 5 deletion (Figure 6b)
	CCM3	III	CD.Cas9.QVBM8621.AD	TCTAAGTGGGAGAACTCCCC	
2	*CCM1*	II	Hs.Cas9.KRIT1.1.AA	ACCAGTTAGATAGTGACCAC	*CCM1* exon 12-13 deletion (Figure 6a)
	CCM2	III	CD.Cas9.GVVJ4790.AF	TCGTATGAGGCAGGTACCAT	
		VII	CD.Cas9.JXFD3882.AA	GCAAGGCCATGTTCAACCAG	*CCM2* exon 4 – 5 deletion (Figure 6b)
	CCM3	I	CD.Cas9.SFRX5440.AF	TCCAATATTCCAGAGCCACT	
		V	CD.Cas9.BVPB2717.AL	CCACCTCGTCCTCAATTAGC	
		VI	CD.Cas9.MRWC3202.AA	AATGCTATAAACGACCAAGG	
3	*CCM1*	III	CD.Cas9.KDPJ4588.AA	TGACTAATCTGGATCCTCAA	
	CCM2	IV	CD.Cas9.VXFG0396.AA	TGGGTTGAAACGTTTGGCAA	
		II	CD.Cas9.HWXB2549.AB	TAACTCTGTTCTATTGCTAC	
		VI	Hs.Cas9.CCM2.1.AB	GGTCAGTTAACGTCCATACC	*CCM2* exon 6 – 11 deletion (Figure 3); CCM2 interchromosomal insertion (Figure 5)
	CCM3	II	CD.Cas9.JJYJ9047.AL	ATAAGTACTCCGCTCTTTGA	
		IV	Hs.Cas9.PDCD10.1.AA	CACGGAGTCCCTTCTTCGTA	

For targeted sequencing of the familial *CCM1* exon 2 – 6 deletion (Figure 2), a crRNA not included in the CCM panel was used: Hs.Cas9.KRIT1.1.AC (GGAGCTCCTAGACCAAAGTA).

Table S2. PCR primers for breakpoint confirmation and familial analyses.

Gene	Variant	Forward Primer (5'-3')	Reverse Primer (5'-3')
CCM1	Exon 12 – 13 deletion (Figure 1)	GGTTAATGCCTGGAGAGGCT	GCATGGACAAACATTACCATACT
CCM1	Exon 2 – 6 deletion (Figure 2)	TGCCTTCTGTGGGCAGGTAA	AAACAACCTTGCAACAGGGTC
CCM2	Exon 6 – 11 deletion (Figure 3)	TGGCTTAGAAGGCTGGGTTG	GCCTGGCTTGCTGACCTTTC

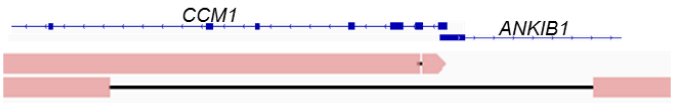

Figure S1. Sequencing of the familial *CCM1* exon 2 – 6 deletion (Figure 2) on a Flongle flow cell was able to identify the variant breakpoints. The variant was covered by one sequencing read. A single-cut approach was used. Read data was visualized in IGV [25]. The Locus Reference Genomic (LRG) transcript (*CCM1*) and RefSeq transcript (*ANKIB1*) are shown.

6 Ausweis der Eigenanteile

6.1 Robin A. Pilz, Konrad Schwefel, Anja Weise, Thomas Liehr, Philipp Demmer, Andreas Spuler, Stefanie Spiegler, Eberhard Gilberg, Christian A. Hübner, Ute Felbor, Matthias Rath (2020). First interchromosomal insertion in a patient with cerebral and spinal cavernous malformations. Sci Rep. 10(1):6306.

Anteile der Autor*innen:
RAP, UF und MR trugen zur Konzeption der Studie bei. **RAP**, KS, SSp, EG und MR analysierten die NGS-Daten. PD und AS betreuten den Patienten und trugen zur Interpretation der genetischen, klinischen und MRT-Daten bei. Die Durchführung und Analyse der zytogenetischen Untersuchungen erfolgte durch AW, TL und CAH. **RAP**, UF und MR konzipierten das Manuskript und alle Autoren beteiligten sich an Revisionen des finalen Manuskripts.

6.2 Robin A. Pilz, Dariush Skowronek, Motaz Hamed, Anja Weise, Elisabeth Mangold, Alexander Radbruch, Torsten Pietsch, Ute Felbor, Matthias Rath (2022). Using CRISPR/Cas9 genome editing in human iPSCs for deciphering the pathogenicity of a novel *CCM1* transcription start site deletion. Front Mol Biosci. 9:953048.

Anteile der Autor*innen:
RAP, MR und UF trugen zur Konzeption der Studie bei. **RAP** und DS führten die funktionalen Experimente durch. Die Betreuung der Experimente erfolgte durch MR und UF. **RAP**, DS und MR analysierten die Daten. MH, EM und AR betreuten die Patientin und stellten klinische sowie MRT-Daten bereit. TP führte die neuropathologische Analyse der Gewebeproben durch und interpretierte die immunhistochemischen Charakterisierungen. Die zytogenetischen Analysen wurden durch AW durchgeführt. Alle Autoren trugen zur Interpretation der Daten bei. **RAP**, MR und UF konzipierten das Manuskript und alle Autoren beteiligten sich am Schreibprozess.

6.3 Robin A. Pilz, Dariush Skowronek, Lara Mellinger, Ute Felbor, Matthias Rath (2022). Endothelial differentiation of *CCM1* knockout iPSCs triggers the establishment of a specific gene expression signature. Manuskript unter Begutachtung beim *International Journal of Molecular Sciences*.

Anteile der Autor*innen:
RAP und DS trugen gleichermaßen zur Arbeit bei. Für die Konzeption der Studie und die Betreuung der Experimente waren MR und UF verantwortlich. Die experimentellen und formalen Analysen sowie die Untersuchung und Visualisierung der Daten erfolgten durch **RAP**, DS und LM. Das originale Manuskript wurde durch MR, **RAP** und DS erstellt. An der Revision des finalen Manuskripts waren MR und UF beteiligt. Fördermittel wurden durch MR akquiriert.

6.4 Dariush Skowronek, **Robin A. Pilz**, Konrad Schwefel, Christiane D. Much, Ute Felbor, Matthias Rath (2021). Bringing CCM into a dish: cell culture models for cerebral cavernous malformations. Med Genet. 33(3):251-259.

Anteile der Autor*innen:
DS, **RAP**, MR und UF waren für die Konzeption des Artikels verantwortlich. Die Erstellung der Abbildungen erfolgte durch DS und **RAP**. DS, KS und CDM führten die experimentellen Analysen durch. Alle Autoren beteiligten sich am Schreibprozess.

6.5 Matthias Rath, Konrad Schwefel, Matteo Malinverno, Dariush Skowronek, Alexandra Leopoldi, **Robin A. Pilz**, Doreen Biedenweg, Sander Bekeschus, Josef M. Penninger, Elisabetta Dejana, Ute Felbor (2022). Contact-dependent signaling triggers tumor-like proliferation of *CCM3* knockout endothelial cells in co-culture with wild-type cells. Cell Mol Life Sci. 79(6):340.

Anteile der Autor*innen:
MR und KS trugen gleichermaßen zur Arbeit bei. MR, ED und UF waren für die Konzeption der Studie und die Betreuung der Experimente zuständig. Der Hauptanteil der funktionalen Experimente wurde durch KS, MM, DS und **RAP** durchgeführt. SB und DB führten die konfokalmikroskopischen und durchflusszytometrischen Experimente durch. AL und JMP trugen zu den Experimenten mit vaskulären Organoiden bei. MR, KS, MM, DS, **RAP** und SB analysierten die Daten. Die Erstellung der Abbildungen erfolgte durch MR, KS, DS und **RAP**. Alle Autoren beteiligten sich an der Interpretation der Resultate. MR, KS und UF konzipierten das Manuskript und alle Autoren beteiligten sich am Schreibprozess.

6.6 Dariush Skowronek, **Robin A. Pilz**, Loisa Bonde, Ole J. Schamuhn, Janne L. Feldmann, Sabine Hoffjan, Christiane D. Much, Ute Felbor, Matthias Rath (2022). Cas9-mediated nanopore sequencing enables precise characterization of structural variants in *CCM1*, *CCM2*, and *CCM3*. Manuskript unter Begutachtung beim *International Journal of Molecular Sciences*.

Anteile der Autor*innen:
Für die Konzeption der Studie waren MR, CDM und UF verantwortlich. Die Experimente wurden durch MR und UF betreut. Die experimentellen und formalen Analysen sowie die Untersuchung und Visualisierung der Daten erfolgten durch DS, LB, **RAP**, OJS und JLF. Die genetische Beratung bzw. die Bereitstellung der analysierten Proben wurde durch MR, UF und SH realisiert. Das originale Manuskript wurde durch DS, **RAP** und LB erstellt. An der Revision des finalen Manuskripts waren MR und UF beteiligt. Fördermittel wurden durch CDM und MR akquiriert.

Prof. Dr. med. Ute Felbor	Robin Alexander Pilz

7 Eigenständigkeitserklärung

Hiermit erkläre ich, dass diese Arbeit bisher von mir weder an der Mathematisch-Naturwissenschaftlichen Fakultät der Universität Greifswald noch einer anderen wissenschaftlichen Einrichtung zum Zwecke der Promotion eingereicht wurde. Ferner erkläre ich, dass ich diese Arbeit selbstständig verfasst und keine anderen als die darin angegebenen Hilfsmittel und Hilfen benutzt und keine Textabschnitte eines Dritten ohne Kennzeichnung übernommen habe.

_____

Robin Alexander Pilz

8 Lebenslauf

Der Lebenslauf wurde aus Datenschutzgründen entfernt.

9 Eigene Publikationen

9.1 Erstautorschaften

1. **Robin A. Pilz**, G. Christoph Korenke, Rainer Steeb, Tim M. Strom, Ute Felbor, Matthias Rath (2019). Exome sequencing identifies a recurrent *SOX2* deletion in a patient with gait ataxia and dystonia lacking major ocular malformations. J Neurol Sci. 401:34-36. DOI: 10.1016/j.jns.2019.04.007

2. **Robin A. Pilz**, Konrad Schwefel, Anja Weise, Thomas Liehr, Philipp Demmer, Andreas Spuler, Stefanie Spiegler, Eberhard Gilberg, Christian A. Hübner, Ute Felbor, Matthias Rath (2020). First interchromosomal insertion in a patient with cerebral and spinal cavernous malformations. Sci Rep. 10(1):6306. DOI: 10.1038/s41598-020-63337-5

3. **Robin A. Pilz**, Dariush Skowronek, Motaz Hamed, Anja Weise, Elisabeth Mangold, Alexander Radbruch, Torsten Pietsch, Ute Felbor, Matthias Rath (2022). Using CRISPR/Cas9 genome editing in human iPSCs for deciphering the pathogenicity of a novel *CCM1* transcription start site deletion. Front Mol Biosci. 9:953048. DOI: 10.3389/fmolb.2022.953048

4. **Robin A. Pilz***, Dariush Skowronek*, Lara Mellinger, Ute Felbor, Matthias Rath (2022). Endothelial differentiation of *CCM1* knockout iPSCs triggers the establishment of a specific gene expression signature. Manuskript unter Begutachtung beim *International Journal of Molecular Sciences*.

*Diese Autoren haben gleichermaßen zur Arbeit beigetragen.

9.2 Ko-Autorschaften

1. Konrad Schwefel, Stefanie Spiegler, Sabine Ameling, Christiane D. Much, **Robin A. Pilz**, Oliver Otto, Uwe Völker, Ute Felbor, Matthias Rath (2019). Biallelic *CCM3* mutations cause a clonogenic survival advantage and endothelial cell stiffening. J Cell Mol Med. 23(3):1771-1783. DOI: 10.1111/jcmm.14075

2. Dariush Skowronek, **Robin A. Pilz**, Konrad Schwefel, Christiane D. Much, Ute Felbor, Matthias Rath (2021). Bringing CCM into a dish: cell culture models for cerebral cavernous malformations. Med Genet. 33(3):251-259. DOI: 10.1515/medgen-2021-2091

3. Matthias Rath*, Konrad Schwefel*, Matteo Malinverno, Dariush Skowronek, Alexandra Leopoldi, **Robin A. Pilz**, Doreen Biedenweg, Sander Bekeschus, Josef M. Penninger, Elisabetta Dejana, Ute Felbor (2022). Contact-dependent signaling triggers tumor-like proliferation of *CCM3* knockout endothelial cells in co-culture with wild-type cells. Cell Mol Life Sci. 79(6):340. DOI: 10.1007/s00018-022-04355-6

*Diese Autoren haben gleichermaßen zur Arbeit beigetragen.

4. Dariush Skowronek, **Robin A. Pilz**, Loisa Bonde, Ole J. Schamuhn, Janne L. Feldmann, Sabine Hoffjan, Christiane D. Much, Ute Felbor, Matthias Rath (2022). Cas9-mediated nanopore sequencing enables precise characterization of structural variants in *CCM1*, *CCM2*, and *CCM3*. Manuskript unter Begutachtung beim *International Journal of Molecular Sciences*.

10 Vorträge und Poster

10.1 Vorträge

1. Konrad Schwefel*, Stefanie Spiegler, Sabine Ameling, Christiane D. Much, **Robin A. Pilz**, Oliver Otto, Uwe Völker, Ute Felbor, Matthias Rath. CRISPR/Cas9 vermittelte Genomeditierung von *CCM3* in humanen Endothelzellen. Vortrag, Arbeitstreffen Humangenetik Nord, Hamburg, Deutschland, November 2018

2. Konrad Schwefel, Matteo Malinverno, **Robin A. Pilz***, Dariush Skowronek, Alexandra Leopoldi, Doreen Biedenweg, Sander Bekeschus, Josef M. Penninger, Elisabetta Dejana, Ute Felbor, Matthias Rath. Tumor-like proliferation of *CCM3* knockout endothelial cells in co-culture with wild-type cells. Vortrag, Young Investigator Meeting (International Kloster Seeon Meeting “Angiogenesis”), Seeon-Seebruck, Deutschland, September 2022

*Vortragende Person

10.2 Poster

1. Stefanie Spiegler*, Konrad Schwefel, Sabine Ameling, Christiane D. Much, **Robin A. Pilz**, Oliver Otto, Uwe Völker, Ute Felbor, Matthias Rath. CRISPR/Cas9 genome editing of *CCM3* in human endothelial cells. Poster, GRC Endothelial Cell Phenotypes in Health and Disease, Lucca (Barga), Italien, Juli 2018

2. Konrad Schwefel*, Stefanie Spiegler, Sabine Ameling, Christiane D. Much, Patricia Dellweg, **Robin A. Pilz**, Oliver Otto, Uwe Völker, Ute Felbor, Matthias Rath. CRISPR/Cas9 genome editing of *CCM3* in human endothelial cells. Poster, Tag der Wissenschaft, Universitätsmedizin Greifswald, Greifswald, Deutschland, Oktober 2018

3. **Robin A. Pilz***, G. Christoph Korenke, Rainer Steeb, Tim M. Strom, Ute Felbor, Matthias Rath. Whole-exome sequencing identifies a recurrent *SOX2* deletion in a patient with global developmental delay, dystonia and ataxia in the absence of major ocular malformations. Poster, GfH-Jahrestagung, Weimar, Deutschland, März 2019

4. Konrad Schwefel*, Stefanie Spiegler, Sabine Ameling, Christiane D. Much, **Robin A. Pilz**, Oliver Otto, Uwe Völker, Ute Felbor, Matthias Rath. CRISPR/Cas9 genome editing reveals that biallelic *CCM3* mutations cause a clonogenic survival advantage and endothelial stiffening. Poster, GfH-Jahrestagung, Weimar, Deutschland, März 2019. **Ausgezeichnet mit GfH-Posterpreis 2019**

5. **Robin A. Pilz***, Konrad Schwefel, Anja Weise, Thomas Liehr, Philipp Demmer, Andreas Spuler, Stefanie Spiegler, Eberhard Gilberg, Christian A. Hübner, Ute Felbor, Matthias Rath. Structural genome variations in cerebral cavernous malformations. Poster (digital), European Human Genetics Virtual Conference (ESHG 2020.2), Juni 2020

6. Konrad Schwefel, Matteo Malinverno, **Robin A. Pilz***, Dariush Skowronek, Alexandra Leopoldi, Doreen Biedenweg, Sander Bekeschus, Josef M. Penninger, Elisabetta Dejana, Ute Felbor, Matthias Rath. Tumor-like proliferation of *CCM3* knockout endothelial cells in co-culture with wild-type cells. Poster, International Kloster Seeon Meeting “Angiogenesis”, Seeon-Seebruck, Deutschland, September 2022

*Präsentierende Person

11 Danksagung

Die Danksagung wurde aus Datenschutzgründen entfernt.